STRENGTH AND LIFETIME DISTRIBUTIONS OF UNIDIRECTIONAL FIBER COMPOSITES IN TENSION

A Dissertation

Presented to the Faculty of the Graduate School

of Cornell University

in Partial Fulfillment of the Requirements for the Degree of

Doctor of Philosophy

by

Sivasambu Mahesh

January 2002

STRENGTH AND LIFETIME DISTRIBUTIONS OF UNIDIRECTIONAL FIBER COMPOSITES IN TENSION

Sivasambu Mahesh, Ph.D.

Cornell University 2002

Quasistatic failure of highly loaded unidirectional composite materials, which consist of long aligned reinforcing fibers embedded in a matrix, is a complex stochastic process. This process is studied both in planar and three dimensional unidirectional composites by means of Monte Carlo simulation and theoretical probabilistic modeling of the composite strength and lifetime problems under tensile loads.

In Chapter 1 the random strength problem of unidirectional composites is considered. Fiber strengths are assumed Weibull or power law distributed and fibers are assumed to be arranged either linearly or in a hexagonal array to form 2D and 3D composites respectively. Failure is idealized using the chain-of-bundles model in terms of δ-bundles of length δ, which is the length-scale of fiber load transfer. Within each δ-bundle, fiber load redistribution is determined by local load-sharing models that approximate the in-plane fiber load redistribution from planar break clusters as predicted from 2D and 3D shear-lag models. As fiber strength variability is increased, it is found that the dominant failure mode in the bundle goes from one of clustered fiber breaking to one of dispersed fiber breaking up to instability. For these two cases, closed-form approximations to the composite strength distribution are developed under the local load-sharing model

and an equal load-sharing model of Daniels, respectively. The results compare favorably with simulations on bundles with up to 1500 fibers.

Chapter 2 discusses the rigorous derivation of bounds on the strength of a bundle in a planar tape when under so-called idealized local load sharing and when the fiber strengths are distributed according to a power law. The main result is established using the Chen-Stein theorem and states that if $F(x) = x^{\rho}$, $0 \leq x \leq 1$ is the strength distribution of the individual fibers, the strength distribution $G_n(x)$ of a bundle of n fibers has the lower tail behavior

$$G_n(x) \sim n x^{c_1(\rho)} \exp\left(-\frac{2c_2\rho}{x}\right).$$

In Chapter 3 we focus on the lifetime problem of unidirectional composites. The failure process involves both random time dependent fiber failure of Coleman fibers and matrix viscoelastic creep. We construct probabilistic failure models for such materials under creep loading, derive composite lifetime distributions from these models and validate them against empirical distributions obtained from Monte Carlo simulations of their failure. As in the strength problem, the dominant failure mode shifts from a clustered fiber breaking mode to a dispersed failure mode prompting the transition in the composite lifetime distribution.

Biographical Sketch

Sivasambu Mahesh was born in 1975 in Madras, India. After schooling in Kendriya Vidyalayas at Guntur, Andhra Pradesh and Minambakkam, Madras, he entered the Indian Institute of Technology at Madras(IITM) in 1992. He graduated from IITM with a Bachelor of Technology degree majoring in Naval Architecture in 1996 and began graduate school at Cornell immediately thereafter.

To the memory of

Shri Sivaraman Mahadevan

and

Shri Mahadevan Vishwanathan

Acknowledgements

I am most indebted to my advisor Prof. S. Leigh Phoenix for his patient guidance and for his enthusiasm and interest not only for this work but also for my overall graduate education. I hope I have learned from his extraordinary intuition and physical insights. I am also grateful to Prof. Chung-Yuen Hui of T&AM and Prof. Sidney Resnick of OR&IE for serving on my committee and for their advise over the years.

Special thanks are due to Dr. Irene Beyerlein of Los Alamos National Laboratory for her numerous helpful comments and suggestions and for being my mentor during a year-long visit to Los Alamos.

I am grateful to the National Science Foundation (grant no. CMS 9800413), the department of Theoretical and Applied Mechanics, Cornell University and to the Center for Materials Science, Los Alamos National Laboratory for the financial support that they provided through research and teaching assistantships.

I acknowledge the following excellent computing facilities. Part of this work made use of the CCMR Multi-User Computer Facility, an MRL Central Facility supported by the National Science Foundation under Award No. DMR-9121564. Computations for Chapter 3 were conducted using the resources of the Cornell Theory Center, which receives funding from Cornell University, New York State,

federal agencies, and corporate partners. Thanks are also given to the T&AM Computing facility at Cornell University and the computing facility of the Center for Non-Linear Studies (CNLS) at Los Alamos National Laboratory where most the simulations of Chapter 1 were run.

Finally, and most importantly, I thank my parents and sister for their advise and support. I also thank my fellow graduate students (Bhalla, Yogesh, Manoj, Madhu and others) who made my graduate school experience so enjoyable. I am also very thankful to Salil Kulkarni for helping prepare the final version of this dissertation.

Table of Contents

List of Figures

Chapter 1

Strength Distributions and Size Effects for 2D and 3D Composites with Weibull Fibers in an Elastic Matrix

1.1 Introduction

Quasistatic failure of unidirectional composite materials, which consist of long aligned reinforcing fibers embedded in a matrix, is a complex random process. This complexity stems from the occurrence of various damage events preceding formation of a catastrophic crack, possibly including fiber breakage, matrix yielding, matrix cracking, fiber-matrix interfacial debonding, and fiber pull-out. Randomness, on the other hand, arises from variability in geometric, constitutive and fracture properties of the fibers, matrix and interface. Consequently the composite

strength becomes a random quantity so that nominally identical specimens show statistical variation in their ultimate strengths.

Randomness in a constituent (fiber or matrix) property does not necessarily induce noticeable randomness in the corresponding composite property. For instance, global composite stiffness is fairly deterministic despite fluctuations in the local stiffness from material point to point as these fluctuations tend to average out over a sufficiently large volume. Composite strength, on the other hand, is largely determined by weak extremes of local strength (typically over the size scale of 5 to 100 fibers), which can lead to propagating material instabilities. Thus, local strength variability tends to persist through increasing size scale to cause strength variability at the global scale.

Analytical or numerical determination of the strength distribution of a composite structure, which reflects the full range of possible random micromechanical failure phenomena, is presently infeasible for realistic material volumes. Idealization of the local composite structure, constituent properties and stress redistribution mechanisms is therefore necessary. Sections 1.1.1–1.1.3 describe the idealizations made in this study followed by Section 1.1.4, which describes relevant literature.

1.1.1 Idealized composite structure and failure process

In idealizing the composite failure process we consider a composite consisting of a parallel array of n stiff, brittle, elastic fibers of cross sectional area A_f and length L, and embedded in a flexible, perfectly bonded, elastic matrix. Two arrays are considered: a linear array forming a 2D planar composite and a hexagonal array forming a 3D composite, as shown in Figure 1.1. We assume a high fiber-matrix stiffness ratio so that the fibers carry virtually all the tensile load. The composite

is loaded by applying a far-field, tensile stress σ to the fibers so that total tensile load is approximately $n\sigma A_{\mathrm{f}}$. The matrix acts primarily to transfer load locally from broken to intact fibers through shear. This is idealized in terms of specific fiber load-sharing models in Section 1.1.2.

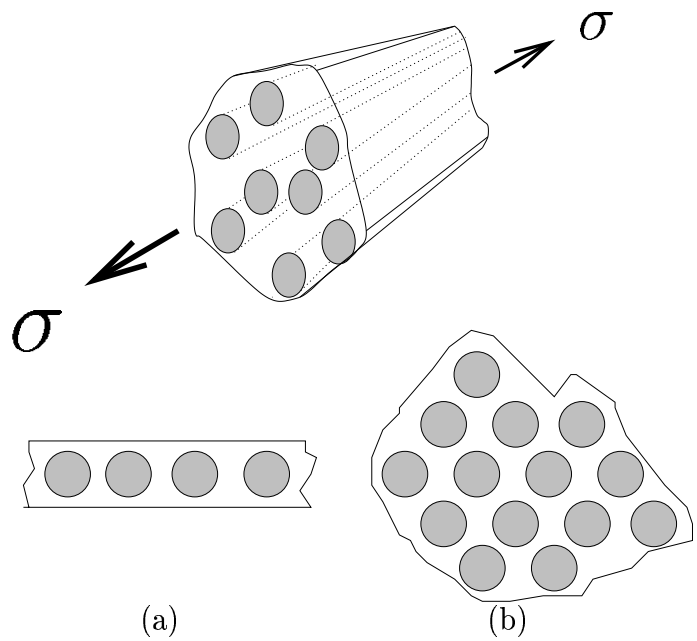

Figure 1.1: The two fiber arrays considered: (a) planar array and (b) hexagonal array. The far-field stress applied to the fibers is σ.

Variability is introduced by assuming that the fibers have random flaws distributed along them. In our main model these flaws follow Weibull-Poisson statistics. Thus, the strengths of individual fiber elements of small length δ are independent and identically distributed (i.i.d.) random variables that follow the Weibull distribution

$$F(\sigma) = 1 - \exp\left\{-\left(\sigma/\sigma_\delta\right)^\rho\right\}, \qquad \sigma \geq 0, \tag{1.1}$$

where $\rho \geq 0$ is the Weibull modulus or shape parameter and σ_δ is the Weibull scale

parameter. Accordingly the mean strength of a fiber element is $\sigma_\delta \Gamma\left(1+1/\rho\right)$ and the coefficient of variation (standard deviation/mean) is

$$\sqrt{\Gamma\left(1+2/\rho\right)/\Gamma\left(1+1/\rho\right)^2-1}.$$

Except for very small ρ the mean differs very little from σ_δ. Note also that small ρ corresponds to large variability in fiber strength and vice versa.

By this model a length effect exists whereby σ_δ is related to the fiber strength at a convenient test gage length l_0 by $\sigma_\delta = \sigma_{l_0}(l_0/\delta)^{1/\rho}$ where σ_{l_0} is the Weibull scale parameter at l_0. Later we take δ to be a characteristic length of local fiber load transfer that depends on the geometric and material constitutive parameters in the shear-lag model. Thus σ_δ becomes a normalizing parameter for composite strength.

We also consider a variation on the Weibull distribution called the power-law distribution

$$F_p(\sigma) = \begin{cases} \left(\frac{\sigma}{\sigma_\delta}\right)^\rho & \text{if } 0 \le \sigma \le \sigma_\delta, \\ 1 & \text{if } \sigma_\delta < \sigma. \end{cases} \tag{1.2}$$

Clearly as $\sigma \downarrow 0$, $F(\sigma) \sim F_p(\sigma)$. Compared to the Weibull distribution Eq. (1.1), however, $F_p(\sigma)$ limits the maximum fiber strength to σ_δ. In this work we will compare results under Eq. (1.1) and Eq. (1.2) to understand the role that exceptionally strong fibers in the Weibull distribution play in δ-bundle failure, especially when ρ is small.

When a moderate tensile stress is applied to a composite specimen, fibers fail at random and the matrix surrounding each break serves to transfer the lost fiber load to neighboring fibers through shear deformation. This stress transfer tends to occur over a certain length scale, δ, which is of the order of a few fiber

diameters. The resulting local stress concentrations may cause neighboring fibers to fail without any further increase in the applied stress. In turn, these new breaks may cause even more breaks, and so on. After the formation of a certain number of breaks, many in small transverse clusters of various sizes, the system of fiber breaks may become stable. Then a small increment in applied stress will be needed to induce new breaks, which may create even more breaks due to increased stress concentrations. Eventually, after some stress increment, the system of fiber breaks becomes unstable and failure results from a cascade of breaks (possibly with cluster linking), which forms a wandering transverse crack.

As has been common in the literature, we idealize this failure process in terms of a longitudinal partition of $m = L/\delta$ transverse slabs or short bundles of length δ, called δ-bundles. The failure process within a given δ-bundle is treated as mechanically and statistically independent of that in neighboring δ-bundles. The composite is then treated as a weakest-link arrangement of these δ-bundles; that is, the composite fails when the weakest δ-bundle fails.

Modeling the failure process in a δ-bundle requires the strength statistics of its fibers of length δ as well as a model for redistribution of stress from broken to intact elements, which we refer to as the load-sharing model. This model should closely reflect the actual micromechanics of stress transfer around approximately transverse fiber break arrays in a realistic mechanical model of the composite irrespective of partitioning it into δ-bundles. Load-sharing models of varying degrees of idealization that we use are described next. (Henceforth the fiber elements within δ-bundles will be referred to as fibers.)

1.1.2 Fiber stress redistribution and load-sharing models

The simplest load-sharing model is the *equal load-sharing* (ELS) rule which we apply separately to each δ-bundle. Under ELS, if a δ-bundle has n fibers and j fibers have failed, the load concentration factor on each surviving fiber is $\kappa_{n,j} = n/(n-j)$, while all failed fibers carry no load. ELS is a reasonable assumption for a loose bundle of fibers (no matrix) clamped uniformly at each end. However, when the fibers are embedded in a matrix, the stress tends to concentrate on the intact fibers closest to the breaks. Thus ELS is not *a priori* an accurate mechanical description of stress redistribution at a composite cross-section. Nevertheless, theoretical results under ELS will turn out to be useful in interpreting dispersed fiber failure modes in a composite.

To account for the localized nature of fiber stress redistribution, *local load-sharing* (LLS) models have been devised, the simplest of which we call the *idealized local load-sharing* (ILLS) model. In a 2D planar composite, when fibers are broken within a given δ-bundle, a surviving fiber therein is assumed to have load concentration factor $K_r = 1 + r/2$ where r is the number of contiguous failed neighbors counting on both sides. In this 1D rule, a failed fiber shifts half of its load to the closest survivor on its left and half to the one on its right; more distant survivors receive no load. In a 3D unidirectional composite with fibers arranged in a hexagonal or square array, ILLS applied to a δ-bundle becomes 2D and load redistribution to nearest survivors requires additional assumptions on assigning portions based on the local configuration of failed fibers. For a large approximately round cluster where all the lost load is redistributed onto the ring of fibers around the circumference, $K_r = 1 + D/4$ where $r \approx \pi D^2/4$, and thus, D has units yielding one fiber per unit cross-sectional area. In reality, ILLS is

too severe, i.e., the stress concentration on fibers immediately adjacent to a break cluster is lower than ILLS assumes, and the disparity increases with cluster size. Also, intact fibers more distant from the cluster experience some overloading due to longer range effects.

From a mechanics perspective, much more realistic load-sharing models for δ-bundles can be constructed from results based on shear-lag analysis of stress transfer around single transverse arrangements of fiber breaks in an infinite array of elastic fibers within an elastic matrix. Such models have been developed by [21] for 2D planar fiber arrays and by [22] for 3D hexagonal or square fiber arrays. In these models the axial fiber and matrix shear stresses can be calculated at arbitrary locations in the composite. However, we only make use of the fiber stresses calculated along the transverse plane of the breaks, which reduces the resulting load-sharing to 1D and 2D, respectively. Fibers within a δ-bundle are treated as though the calculated fiber loads apply uniformly over their full lengths δ. By these restrictions, the fiber overloading is monotonic, i.e., the load in an intact fiber will be non-decreasing during the formation of new breaks. We refer to the 1D load-sharing model derived from the 2D case as *Hedgepeth local load-sharing* (HLLS) and the 2D model from the 3D case as *Hedgepeth and Van Dyke local load-sharing* (HVLLS).

In the Monte-Carlo simulations of δ-bundle failure we work with complete numerical versions of 1D HLLS and 2D HVLLS. The stresses are calculated numerically in every intact fiber for every arrangement of breaks that occurs in the simulations. Fundamental analytical solutions to the underlying shear-lag equations are coupled to a numerical weighted superposition method to treat each configuration as for example in [6].

In developing probability models of the failure process, the above approach unfortunately results in serious analytical difficulties that require further idealizations to yield simpler rules for crucial configurations. In particular, only the stresses in intact neighbors adjacent to certain idealized, contiguous break clusters are defined. In HLLS a fiber next to an isolated group of r contiguous breaks is idealized as having load concentration factor $K_r = \sqrt{1 + \pi r/4}$. In HVLLS the load concentration on the fibers around an approximately circular cluster of diameter D is approximated as $K_r = \sqrt{1 + D/\pi}$ where again $r \approx \pi D^2/4$. The square-root feature in terms of cluster diameter indicates that these approximations are consistent with a continuum fracture mechanics viewpoint. Section 1.2 elaborates on their basis.

1.1.3 Composite strength distribution and Monte Carlo simulation approach

A key quantity of interest is the distribution function $G_n(\sigma)$ for δ-bundle strength. By the weakest link formula and chain-of-bundles assumption the strength of the composite of length $L = m\delta$ has distribution function $H_{m,n}(\sigma)$ given simply by

$$H_{m,n}(\sigma) = 1 - [1 - G_n(\sigma)]^m, \qquad \sigma \geq 0. \tag{1.3}$$

The key task is to determine $G_n(\sigma)$ in terms of $F(\sigma)$ for fiber strength and the load-sharing model for fibers in a δ-bundle.

In our model and Monte Carlo simulations we will assume periodic boundary conditions. Thus our 1D HLLS δ-bundles will form a tube, and under 2D HVLLS with hexagonal symmetry the simulation will be on a rhombus patch with doubly-periodic boundary conditions.

The Monte-Carlo algorithm for simulating failure is described in detail in [28]. In brief, to simulate the failure of a single δ-bundle, the first step is to assign numerical strength values to each fiber as sampled from the fiber strength distribution, Eq. (1.1) or Eq. (1.2). Then a load just sufficient to fail the weakest fiber is applied to the δ-bundle, and numerical stress redistribution is computed using either HLLS or HVLLS. If the new fiber stresses exceed the strengths of any other fibers then these too fail and stress redistribution for the new configuration is computed. This iterative process of fiber failures and stress redistribution is continued until either stability is reached or the δ-bundle fails catastrophically. If it becomes stable, a load increment is applied to the δ-bundle just sufficient to fail another fiber, and the above process is repeated. Eventually, at some load increment, a cascade of fiber failures occurs as the δ-bundle fails. The applied fiber stress triggering the collapse is the strength of the δ-bundle.

The Monte-Carlo algorithm involves repeating the above procedure N $(= 500)$ times for each (n, ρ) pair, yielding N individual δ-bundle strengths. The empirical strength distribution $\hat{G}_n(\sigma)$ is constructed by plotting j/N against $\sigma_{(j)}$ for $j = 1, \ldots, N$ where $\sigma_{(j)}$ is the strength of the j^{th} weakest δ-bundle of the N simulated.

1.1.4 Results and insights from previous literature

Statistical modeling of the composite failure process has a long history. Pioneering work using the chain-of-bundles framework was carried out by [16], [36] and [37], all using an ELS approach to δ-bundle failure based on work of [12] and [7]. [47], [38], [48], and [1] pursued LLS approaches to δ-bundle failure variously building on the works of [21] and [22]. These works not only initiated the discussion of dispersed versus localized cluster modes of fiber failure but also served to

uncover the enormous difficulties in performing probability calculations. Harlow and Phoenix [17, 18, 19], Smith [39, 41], Smith et al. [42] and [35] simplified LLS to ILLS to capture the essence of localized fiber stress redistribution yet allow tractable analysis. Some of the large-ρ asymptotic results were also developed by [2] and [3] under relaxation of the chain-of-bundles and ILLS assumptions. This served to point out the robustness of the chain-of-bundles assumption as a means of capturing the crucial step of transverse evolution of failure clusters up to instability.

More rigorous analytical treatments for δ-bundles under 1D ILLS have also been carried out. See for example [25], [20], [27], and [46]. Other works such as those by [29], [14], Beyerlein and Phoenix [4, 5] and [28] have used Monte Carlo simulation interpreted by approximate probability calculations to treat δ-bundle failure under more realistic HLLS and HVLLS models. A full 3D failure simulation under a special version of HVLLS for square fiber arrays and avoiding the chain-of-bundles assumption was carried out by [26]. A lattice-based variation of HVLLS that also incorporated fiber slip and pullout during failure was developed by [24]. An FEM-based, Monte Carlo model that also considered interfacial debonding was recently developed by [15]. Overviews of relevant literature have been published by [9] and [32].

The most important early work for ELS bundles (applied here to δ-bundles) was due to [12] who showed that as the number of fibers n increases, the distribution for the strength of a bundle converges to a Gaussian or normal distribution with a fixed asymptotic mean, and a standard deviation that decreases as $1/\sqrt{n}$. As [40] and [30] showed, the convergence of Daniels' Gaussian approximation to the true distribution is slow with an error approximately proportional to $n^{-1/6}$. By

developing explicit corrections to the mean and variance that were proportional to $n^{-2/3}$, they obtained dramatic improvements to the Gaussian approximation that worked well even for bundles with as few as five Weibull fibers. These accurate results will form the basis for interpreting the dispersed fiber failure mode in our Monte Carlo simulations when ρ is small.

Harlow and Phoenix [17, 18] observed numerically that 1D ILLS δ-bundles with Weibull fibers obey weakest-link scaling beyond a certain size n. In particular, their strength distribution function, $G_n(\sigma)$ behaves such that $W_n(\sigma) = 1-[1-G_n(\sigma)]^{1/n}$ rapidly becomes independent of size n, converging as $n \to \infty$ to a characteristic distribution function $W(\sigma)$. This distribution embodied the key aspects of the localized statistical failure process. [35] gave a simple formula for constructing an accurate estimate of $W(\sigma)$ when fibers have modest to small strength variability (larger ρ). Beyerlein and Phoenix [4, 5] observed from Monte Carlo simulations that δ-bundles under a full implementation of 1D HLLS also show weakest-link behavior, and they developed an expression for $W(\sigma)$ that matched very well its empirical counterpart, $\hat{W}_n(\sigma)$.

1.1.5 Outline of the paper and main results

In the next section we describe the governing equations and main results for the shear-lag models for fiber breaks in planar and hexagonal arrays of fibers. The former forms the basis for 1D HLLS and the latter for 2D HVLLS used in Sections 1.3 and 1.4. Section 1.3 summarizes the Monte-Carlo simulation results using the framework in [28], and makes connection between the dominant failure mode in a δ-bundle, i.e., cluster growth for large ρ and dispersed fiber failure for small ρ, and the behavior of its strength distribution. In Section 1.4, we study the cluster

growth failure mode and derive results for the distribution function for composite strength in terms of a characteristic distribution function $W(\sigma)$ for which we develop closed-form approximations. We also develop results under the power-law distribution for fiber strength and through comparison to those under the Weibull case, as ρ decreases, we gain insight into the effects that a few extremely strong fibers can have on the results. We also develop expressions for the critical cluster size and size effect for composite strength. Section 1.5 focuses on the dispersed failure mode observed in the HVLLS and HLLS simulations for small ρ, and uses results on ELS δ-bundles to form tight lower bounds on the failure probabilities. Section 1.6 presents some analysis giving insight into the effects of ρ on probabilities and patterns of cluster growth. The final section draws connections to other work and summarizes insights achieved in the present work.

1.2 Load-Sharing Models for δ-Bundles

We now elaborate on the basis for the local load-sharing models used in the failure of δ-bundles, earlier referred to as HLLS and HVLLS. The description covers both numerical implementation and simplifications needed for analytical probability modeling.

1.2.1 Shear-lag model for a 2D planar fiber array: basis for HLLS

The shear-lag model for a 1D transverse array of breaks in a 2D planar fiber array was first studied by [21]. In the model, fibers are assumed to deform in simple tension and the matrix deforms in simple shear. The fibers are loaded uniformly at

$z = \pm\infty$ under tensile stress σ, where z is distance along the fiber direction away from the central transverse plane where breaks are located. We let $E_{\rm f}$ be the fiber tensile modulus, and $G_{\rm m}$ be the matrix shear modulus and assume $E_{\rm f} \gg G_{\rm m}$. Each fiber has cross sectional area $A_{\rm f}$, the effective matrix width between the fibers is w, the matrix thickness (perpendicular to the plane of the fibers) is h, the center-to-center fiber spacing is d and the fiber volume fraction is $V_{\rm f}$. A simple case is to assume h is also the main fiber cross-sectional dimension. Then $A_{\rm f} \approx h^2$, $d \approx w+h$, and $A_{\rm m} \approx wh$, where $A_{\rm m}$ is the cross sectional area of the matrix between two fibers. Thus the fiber volume fraction is $V_{\rm f} = A_{\rm f}/(A_{\rm f} + A_{\rm m}) \approx h/d$. Though exact for fibers of square cross section, these relations are useful approximations for circular fibers with radius $r_{\rm f} = h/2$. To simplify the discussion, all cross-sectional dimensions will be viewed as approximate, and our primary interest will be in the effects of fiber fractures at a length scale greater than the fiber diameter.

We ignore the part of the applied load carried by the matrix in tension, as well as matrix tension effects in the stress transfer process. At the breaks we view the matrix as severed in the plane of the breaks and ignore any local singular-like stress concentrations in the fiber at a scale smaller than the fiber diameter. Many matrices locally yield rather than support such stresses. Unless $V_{\rm f}$ is small, ignoring matrix tension has little effect on stress transfer.

We let $\sigma_n(z)$ and $u_n(z)$ be the stress and displacement, respectively, in fiber n at location z along the fiber, where $-\infty < z < \infty$ and $n \in (\ldots, -2, -1, 0, 1, \ldots)$. In matrix bay n between fibers n and $n+1$, the effective shear force per unit length $q_n(z)$ is given by

$$q_n(z) = \frac{G_{\rm m} h}{w}(u_{n+1}(z) - u_n(z)). \tag{1.4}$$

The effective shear stress $\tau_n(z)$ and shear strain $\gamma_n(z)$ follow

$$\tau_n(z) = G_{\rm m}\gamma_n(z) = q_n(z)/h. \tag{1.5}$$

Hooke's law for the fiber gives

$$\sigma_n(z) = E_{\rm f}\frac{du_n(z)}{dz}, \tag{1.6}$$

and equilibrium of forces on a fiber element leads to

$$E_{\rm f}A_{\rm f}\frac{d^2u_n(z)}{dz^2} + \frac{G_{\rm m}h}{w}(u_{n+1}(z) - 2u_n(z) + u_{n-1}(z)) = 0. \tag{1.7}$$

The boundary conditions are $\sigma_n(z = \pm\infty) = \sigma$ for all fibers, $\sigma_n(0) = 0$ for the r fibers assumed to be broken on the $z = 0$ plane and $u_n(z) = 0$ for all intact fibers. We normalize the various quantities above using

$$\begin{aligned} P_n &= \sigma_n/\sigma, \\ U_n &= (u_n/\delta)(E_{\rm f}/\sigma), \\ T_n &= (h\delta/A_{\rm f})(\tau_n/\sigma), \\ \Gamma_n &= U_{n+1} - U_n = (\gamma_n G_{\rm m}/\sigma)(h\delta/A_{\rm f}), \\ \xi &= z/\delta, \end{aligned} \tag{1.8}$$

where δ is the length scale of load transfer given by

$$\delta = \sqrt{(E_{\rm f}A_{\rm f}w/(G_{\rm m}h)} = \sqrt{A_{\rm f}(E_{\rm f}/G_{\rm m})(w/h)}. \tag{1.9}$$

These normalizations yield a non-dimensional Hooke's law

$$P_n(\xi) = \frac{dU_n(\xi)}{d\xi}, \tag{1.10}$$

and a non-dimensional system of equations

$$\frac{d^2U_n(\xi)}{d\xi^2} + U_{n+1}(\xi) - 2U_n(\xi) + U_{n-1}(\xi) = 0, \tag{1.11}$$

with normalized boundary conditions

$$\begin{aligned} P_n(\pm\infty) &= 1, \quad -\infty < n < \infty \\ P_n(0) &= 0, \text{ on all } r \text{ broken fibers,} \\ U_n(0) &= 0, \text{ for all other fibers.} \end{aligned} \tag{1.12}$$

For a single break at $n = 0$ and $z = 0$ this set of equations can be solved for all z using discrete Fourier transform methods. This leads to influence functions for the effects of a single break on stress and displacements at all fiber and matrix locations. An arbitrary array of multiple breaks lying within a single plane can then be handled using a superposition of influence functions translated to the actual break locations and appropriately weighted to satisfy the boundary conditions. This operation requires numerically solving an $r \times r$ matrix equation where r is the number of breaks[1]. In the Monte Carlo simulations of δ-bundle failure, we use this method to numerically calculate the fiber loads for all break arrays that occur. A similar approach was used in [6] and Beyerlein and Phoenix [4, 5]. This constitutes the 1D load-sharing model called HLLS.

In the probability analysis for HLLS under large ρ we use accurate approximations to the load concentrations due to an isolated cluster of r contiguous fiber breaks in a single plane, or r-cluster. Specifically we want the peak load concentration factor (at the $z = 0$ plane) on the nearest neighbor, denoted K_r. We also want the load concentration factor $K_{r,s}$ on fiber number s ahead of an r-cluster. Some results due to [21] and [23] are reviewed in [6] and approximations were

[1] This method works for the more general problem in which the breaks do not lie within a single plane [6]. In that case numerical integration is required in evaluating the influence functions. In our case of aligned breaks the influence functions are simple expressions.

developed there using Stirling's formula. The approximations

$$K_r \approx \sqrt{\frac{\pi r}{4} + 1}, \tag{1.13}$$

and

$$K_{r,s} \approx K_r \sqrt{\frac{1}{\pi(s-1)+1}}, \tag{1.14}$$

are minor improvements on theirs, which are extremely accurate even for small r. For larger clusters the latter result is only useful for s within about $r/4$ of the cluster edge, at which point the stress concentration reaches the far-field value, unity, as seen in [6]. Note also that for the fiber subadjacent to the last break of a large r-cluster, the load concentration is about one-half the value on the adjacent fiber.

1.2.2 Shear-lag model for a 3D hexagonal fiber array: basis for HVLLS

In a 3D hexagonal array of fibers, as considered by [22] and shown in Figure 1.1, similar ideas apply as in the previous section. The fibers are identified by the index pair, (m, n) corresponding to axes in the transverse plane with included angle $\pi/3$ radians. All displacement and stress quantities have subscript (m, n) to replace n in the planar case and the normalizations are the same. The main change relative to the planar fiber array is that the non-dimensional differential equation for the dimensional displacement $u_{(m,n)}$ of fiber (m, n) becomes

$$\begin{aligned} \frac{d^2 U_{(m,n)}(\xi)}{d\xi^2} + \big(U_{(m+1,n)}(\xi) + U_{(m,n+1)}(\xi) + U_{(m-1,n)}(\xi) \\ + U_{(m+1,n-1)}(\xi) + U_{(m-1,n+1)}(\xi) - 6U_{(m,n)}(\xi)\big) = 0. \end{aligned} \tag{1.15}$$

Thus, six interfiber couplings exist for each fiber instead of two as in a planar array. The boundary conditions are similar to those given by Eq. (1.12) except the break

array is 2D. The numerical implementation in calculating the fiber stresses is also similar. This constitutes the 2D load-sharing model called HVLLS.

In the probability analysis for HVLLS under large ρ we use accurate approximations to the load concentrations due to an isolated cluster of r contiguous fiber breaks in a single plane, or r-cluster. We focus on the stress concentrations around a penny-shaped r-cluster. First we define an effective fiber spacing d and a dimensionless diameter D of the penny. The effective fiber spacing is chosen so that there is one fiber per unit cross-sectional area. In a hexagonal array, one fiber and matrix unit occupies area $\sqrt{3}d'^2/2$ where d' is the center-to-center fiber spacing so that $d = (\sqrt[4]{3}/\sqrt{2})d' \approx 0.9306d'$. We define D such that $r = \pi D^2/4$ so that the effective cluster diameter is Dd. The fibers surrounding the r-cluster are subjected to the "effective" stress concentration

$$K_r \approx \sqrt{\frac{D}{\pi} + 1} = \sqrt{\frac{2\sqrt{r}}{\pi^{3/2}} + 1}. \tag{1.16}$$

For the decay of the stress concentration with distance we find

$$K_{r,s} \approx \frac{K_r}{\sqrt{\pi(s-1)+1}}, \tag{1.17}$$

is a reasonable approximation, where s is the number of effective fiber spacings d (not necessarily an integer) a fiber is away from an effective cluster radius $\bar{R} = (D-1)/2$. For larger D this result is only valid for s within about $D/10$ of the edge of the cluster, beyond which the stress concentration drops very close to the far-field value, unity. See [28] and [32] for elaboration.

1.3 Failure Mechanisms in δ-bundles

We now describe certain qualitative trends observed in the Monte Carlo simulations of δ-bundle failure. The observed failure mechanisms appear to play a

fundamental role in determining the behavior of the strength distribution. The cause and effect relationship seems clearest when viewed in terms of the variability in fiber strength through ρ.

1.3.1 Small variability in fiber strength (large ρ)

For $\rho = 10$, snapshots of the damage evolution *en route* to δ-bundle failure in median ($N = 500$) 2D and 3D specimens are shown in Figures 1.2 and 1.3, respectively, where the boundary conditions are periodic. In each figure, the last stage corresponds to the pattern of breaks immediately after the formation of an unstable configuration and before collapse. We separately label the first fibers to fail after the point of instability. Since the boundary conditions are periodic a break cluster appearing at one edge (side or top) may be continued on the opposite edge.

When ρ is large (low variability in fiber strength), the tendency to form break clusters and propagate them appears to be the dominant failure mode (Figures 1.2 and 1.3). As breaks form under increasing applied load, they overload their neighbors more intensely than more distant fibers. The probability of failure of a neighbor is thus enhanced since the neighboring fibers are unlikely to be much stronger than the broken fiber. This leads to the formation of a cluster of breaks, which in turn imparts even larger stress concentrations on its neighbors and the cluster therefore propagates with increasing probability as it grows. Eventually the cluster becomes unstable and fails the composite.

As mentioned, [18] observed that the strength distribution of a composite with a cluster-forming failure mode lends itself to weakest-link scaling analysis. They found that the cumulative distribution function for the strength of a δ-bundle

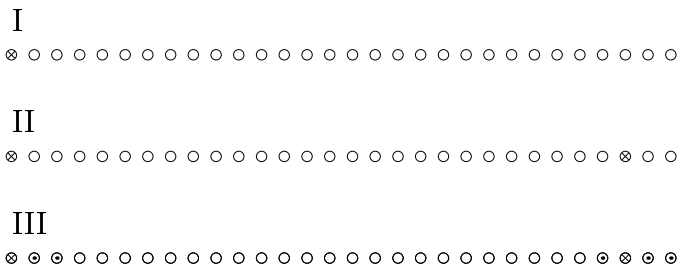

Figure 1.2: Snapshots of the failure process in median strength ($N = 50$) 1D δ-bundles with 30 Weibull fibers for $\rho = 10$ and periodic boundary conditions. $\bigcirc$ intact fibers, $\bigotimes$ broken fibers and $\bigodot$ first fibers to fail after instability.

under 1D ILLS has the form

$$G_n(\sigma) \approx 1 - [1 - W(\sigma)]^n, \qquad \sigma \geq 0, \tag{1.18}$$

when the bundle size n is larger than a certain critical size, where $W(\sigma)$ was earlier called the characteristic distribution function. The threshold for n turns out to be the critical cluster size $k(\sigma)$ for instability in the δ-bundle, being approximately defined by $K_k\sigma \approx \sigma_\delta$.

Using Weibull coordinates, we have plotted in Figure 1.4 the empirical weakest-link distributions

$$\hat{W}_n(\sigma) = 1 - [1 - \hat{G}_n(\sigma)]^{1/n}, \qquad \sigma \geq 0, \tag{1.19}$$

obtained from our Monte-Carlo failure simulations of the empirical distribution function for δ-bundle strength, $\hat{G}_n(\sigma)$, under 1D HLLS. For $\rho \geq 1$ the $\hat{W}_n(\sigma)$ curves for $n = 225$, 625 and 900 collapse onto one characteristic curve $\hat{W}(\sigma)$, but not for $\rho = 1/2$. The plotted results suggest that the cluster growth failure mode is active for $\rho \geq 1$. From the δ-bundle failure stresses observed in the simulations, rough estimates of the corresponding critical cluster sizes k are obtained from

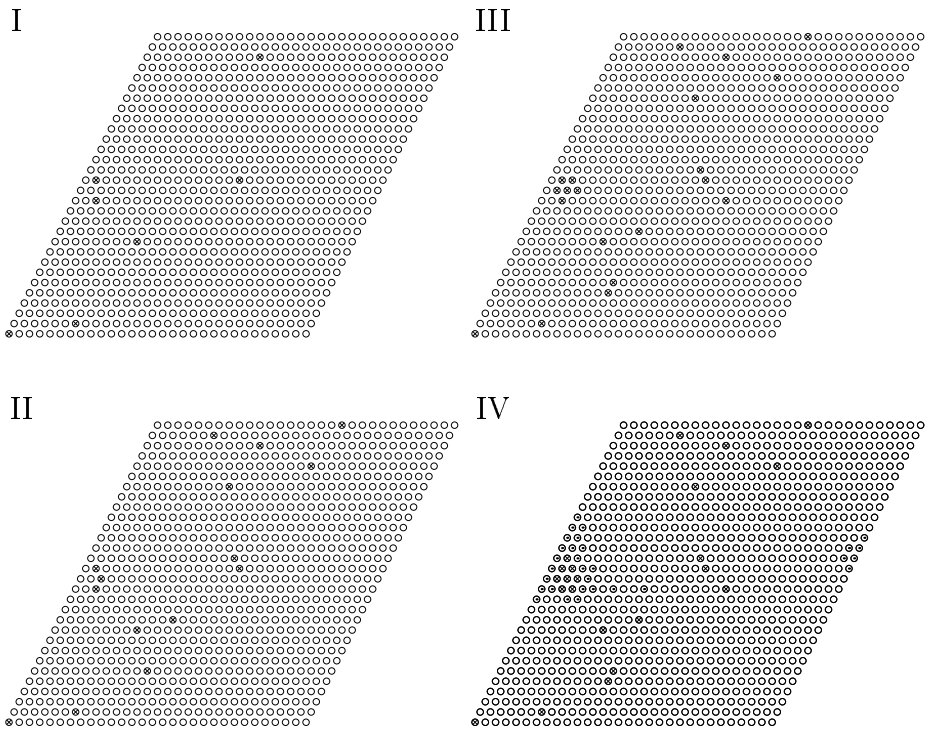

Figure 1.3: Snapshots of the failure process in median strength ($N = 500$) 2D δ-bundles with 900 Weibull fibers for $\rho = 10$ and periodic boundary conditions. $\bigcirc$ intact fibers, $\bigotimes$ broken fibers, and $\odot$ first fibers to fail after instability.

solving $K_k\sigma = \sigma_\delta$, using Eq. (1.13). In all cases k is at least an order of magnitude smaller than the size of the smallest bundle $n = 225$. For $\rho = 1$ it is less than 15 and is about 10 for $\rho = 3$. This suggests that Eq. (1.18) applies for the δ-bundle stress and size range shown, which is significant since it gives a size scaling for the strength distribution in terms of n. Figure 1.4 also shows a reversal in the weakening trend as ρ decreases from 10 to 1 to a strengthening trend as ρ decreases below 1. The latter is due to very strong fibers from the upper tail of the $\rho = 0.5$ Weibull distribution, which is examined further in Section 1.3.2.

For 2D δ-bundles under HVLLS, empirical weakest-link distributions $\hat{W}_n(\sigma)$

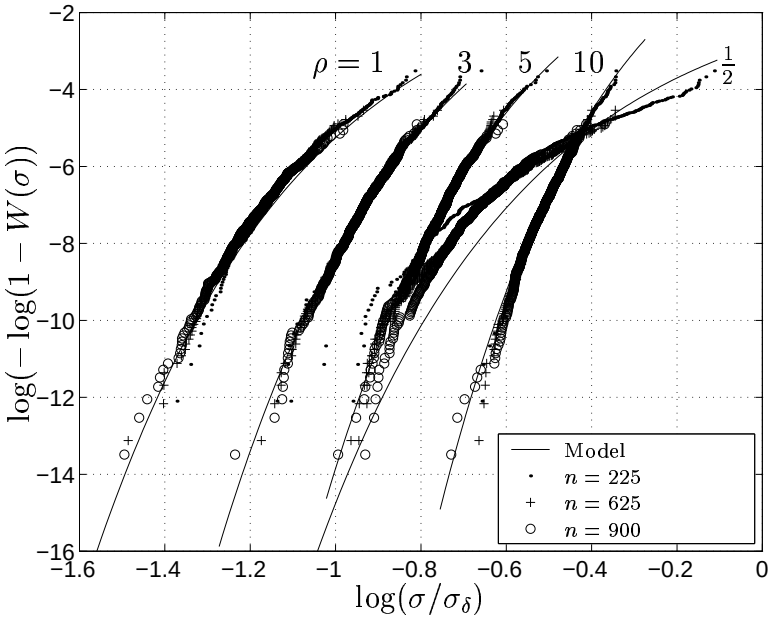

Figure 1.4: Weakest-link scaling phenomenon in 1D δ-bundles. The empirical weakest-link distributions, $\hat{W}_n(\sigma)$, for sizes $n = 225$, 625 and 900 collapse onto one master distribution, $\hat{W}(\sigma)$, for $\rho \geq 1$ but not for $\rho = 0.5$. Also shown is the characteristic distribution function, $W(\sigma)$, from the cluster growth model in Eq. (1.40).

are shown in Figure 1.5, and a similar collapse to $\hat{W}(\sigma)$ is seen for $\rho = 5$ and 10. For $\rho = 2$ and 3 the collapse is less sharp than in 1D, and it worsens rapidly as ρ is decreased further. For $0 < \rho \leq 2$, analysis of the critical cluster size k from solving $K_k\sigma = \sigma_\delta$, using Eq. (1.16), shows that k approaches the size of the smallest bundle. Thus the lack of collapse of the $\hat{W}_n(\sigma)$ curves to one master curve $\hat{W}(\sigma)$ does not necessarily imply that cluster growth dominated failure no longer dominates, an issue we revisit later.

For larger ρ, the strength distribution for δ-bundles under 2D HVLLS is governed by the lower tail of the fiber strength distribution, as is seen by considering

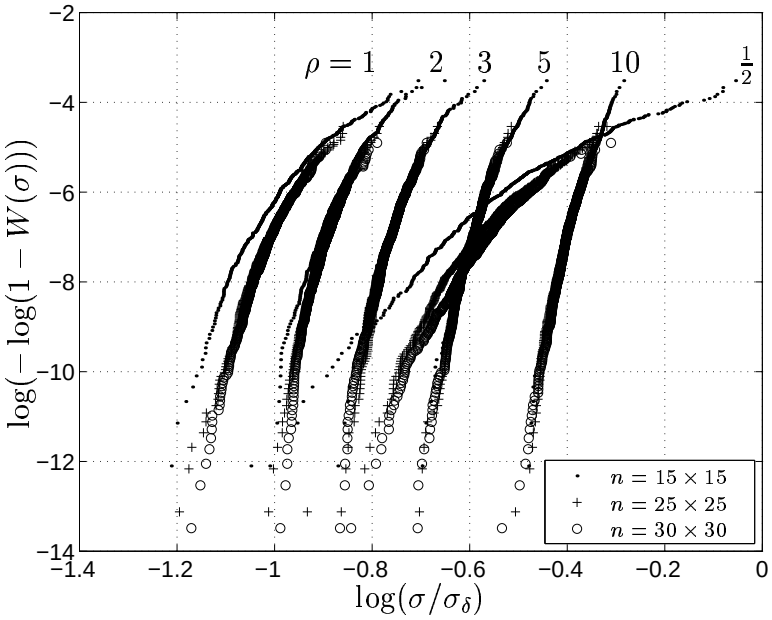

Figure 1.5: Weakest-link scaling phenomenon in 2D δ-bundles. The weakest-link distribution, $\hat{W}_n(\sigma)$, for composite sizes $n = 225$, 625 and 900 appears to converge onto one master distribution, $\hat{W}(\sigma)$, for $\rho > 1$.

two modified Weibull distributions,

$$\overline{F}(\sigma) = \begin{cases} F(\sigma) & \text{if } 0 \leq \sigma < \sigma_\delta, \\ 1 & \text{if } \sigma_\delta \leq \sigma, \end{cases} \tag{1.20}$$

and

$$\underline{F}(\sigma) = \begin{cases} 0 & \text{if } \sigma < 0, \\ 1 - 1/e & \text{if } 0 \leq \sigma < \sigma_\delta, \\ F(\sigma) & \text{if } \sigma_\delta \leq \sigma, \end{cases} \tag{1.21}$$

where $F(\sigma)$ is the original Weibull distribution, Eq. (1.1). The former reduces the strength of all fibers stronger than σ_δ to exactly σ_δ in the original Weibull distribution, and the latter weakens or pre-breaks to zero strength all fibers weaker

than σ_δ. The simulation results in Figure 1.6 show that the δ-bundle strength distribution produced by $\overline{F}(\sigma)$ agrees nearly perfectly with that due to the original Weibull $F(\sigma)$ but the same is not true of $\underline{F}(\sigma)$ where a large strength reduction occurs.

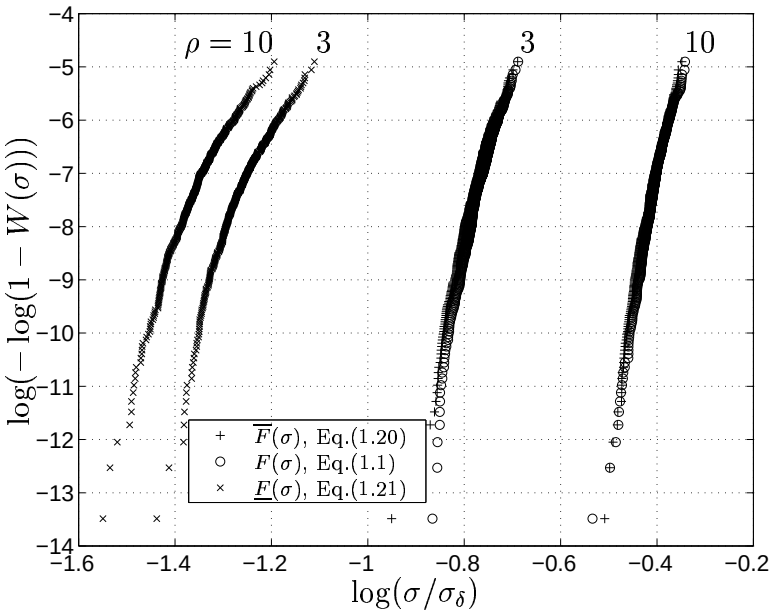

Figure 1.6: Dominance of the lower tail of the Weibull fiber strength distribution in determining δ-bundle strength for 2D HVLLS and larger ρ as seen from agreement between simulations for $\overline{F}(\sigma)$ and the original $F(\sigma)$ for $\rho = 3$ and 10.

1.3.2 Large variability in fiber strength (small ρ)

When ρ is small (large fiber variability), the cluster-driven breakdown mechanism is subdued by a dispersed failure mode in a δ-bundle. This is seen in snapshots of the fiber failure sequence in 1D HLLS and 2D HVLLS δ-bundles for $\rho = 1$, as shown in Figures 1.7 and 1.8, respectively.

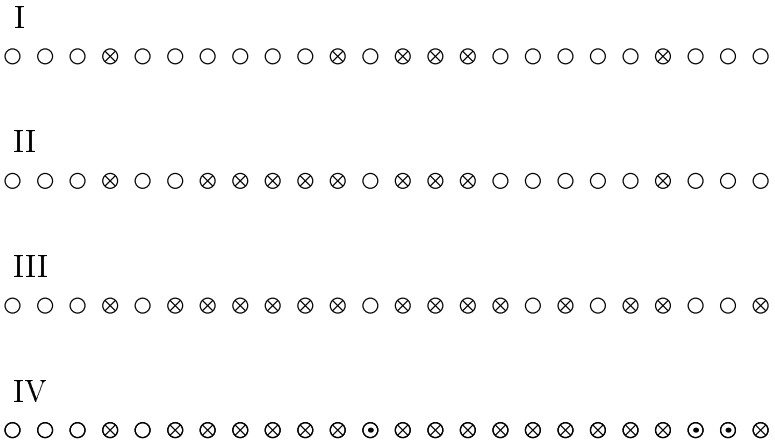

Figure 1.7: Snapshots of the failure process in a median strength ($N = 500$) 2D HLLS δ-bundle with 30 Weibull fibers and $\rho = 1$ under periodic boundary conditions. ◯ intact fibers, ⊗ broken fibers, and ⊙ first fibers to fail after instability.

A qualitative explanation for this is that the tendency to form and grow clusters is suppressed by the tendency to form breaks dispersedly, thereby undermining the ability of any one cluster to propagate. Instead, bundle failure results from the coalescence of small clusters and dispersed breaks. Thus, when the fiber strength variability is large, clusters of fiber breaks are less likely to propagate due to the presence of occasional strong fibers that impede growth. Also, many weak fibers fail under small applied loads causing the initial dispersed patterns.

Despite the dispersion of breaks in the failure mode of the 1D δ-bundles (Figure 1.7) with 30 fibers, there is convergence to a characteristic distribution $\hat{W}(\sigma)$ for sizes exceeding $n = 225$ (Figure 1.4). This suggests that fiber breakage, despite beginning dispersedly approaches clustered growth after a certain number of dispersed breaks have formed. This aspect will be revisited later.

To gain further insight into the behavior of the empirical distribution function

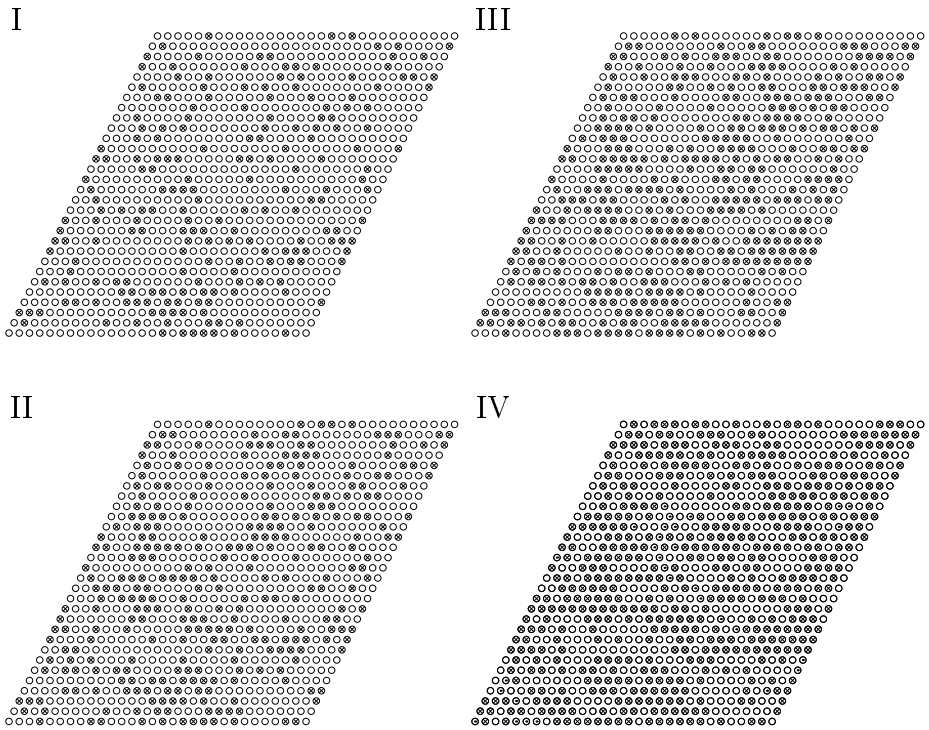

Figure 1.8: Snapshots of the failure process in a median strength ($N = 500$) 2D HVLLS δ-bundle with 900 Weibull fibers and $\rho = 1$ under periodic boundary conditions. $\bigcirc$ intact fibers, $\bigotimes$ broken fibers, and $\bigodot$ first fibers to fail after instability.

for δ-bundle strength, $\hat{G}_n(\sigma)$, for small ρ, we have plotted $\hat{G}_n(\sigma)$ in Figure 1.9 under all three types of load-sharing: 1D HLLS, 2D HVLLS and ELS (equal load-sharing) as described in Section 1.1.2. The δ-bundles all have $n = 900$ fibers, and normal (Gaussian) coordinates have been used for plotting since the strength under ELS, a truly dispersed failure mode, is very close to Gaussian (i.e., a straight line). As ρ decreases, the strength distributions for all three types of load-sharing converge. For 2D HVLLS the convergence is virtually complete for $\rho = 1$ and for 1D HLLS, the convergence improves dramatically between $\rho = 1$ and $\rho = 1/2$,

though it is not quite complete even at $\rho = 1/2$. Remarkably, as ρ decreases, the details of the load sharing mechanism diminish in importance in determining the strength distribution. Also, the ELS strength distribution acts as a lower bound on the HVLLS distribution, becoming tight as ρ becomes small. It is an open question whether ELS bundles always have lower probability of failure than LLS bundles, as ρ decreases further.

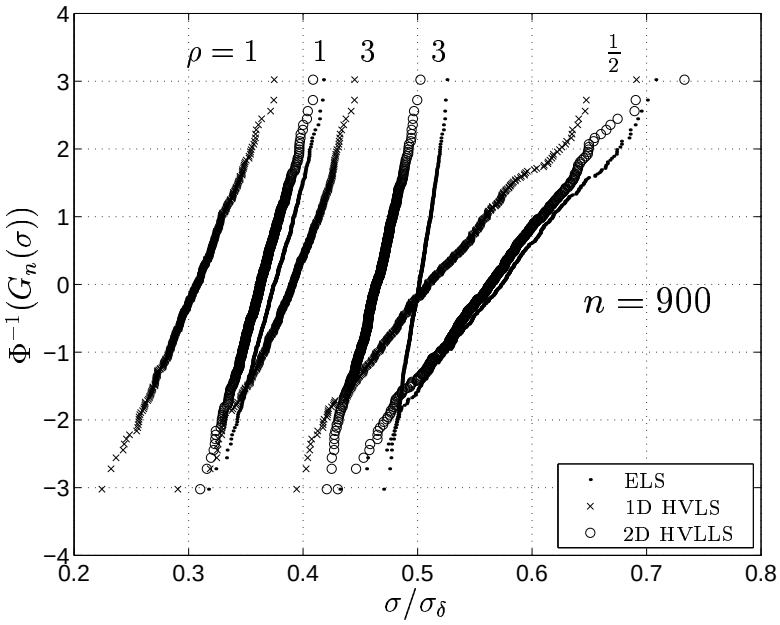

Figure 1.9: Comparison of empirical strength distributions, $\hat{G}_n(\sigma)$, for 900 fiber δ-bundles under ELS, 2D HVLLS and 1D HLLS on normal (Gaussian) probability coordinates.

Two cautionary points should be made. First, although the distributions for δ-bundle strength under HLLS and HVLLS approach those for ELS, the patterns of fiber breaks in terms of cluster sizes are not the same whereby ELS shows more dispersion. Second, if the bundle size n were increased by orders of magnitude, the reduction in variability for ELS is roughly $1/\sqrt{n}$, whereas for HVLLS and HLLS it

may be milder. In fact, HVLLS and HLLS may ultimately produce slightly weaker bundles than ELS since the scale of load-sharing over groups of fibers may be more limited than in ELS. Thus the large δ-bundle may act more like a chain of smaller δ-bundles, each roughly following ELS. We revisit this issue in Section 1.5.

For 2D HVLLS δ-bundles, when $0 < \rho \leq 1$, the strength distribution is dominated by the upper tail of the fiber strength distribution within the range of our simulations. In Figure 1.10, we compare the strength distributions produced by the upper and lower tail-modified Weibull distribution Eqs. (1.20) and (1.21) against those produced by the original Weibull distribution, Eq. (1.1). As ρ decreases, the upper tail dominance increases as the behavior becomes insensitive to the lower tail suggesting that cluster propagation is stalled by occasional strong fibers. This is the opposite to that seen in Figure 1.6 for larger ρ. Further investigation of this issue is considered in Section 1.5.

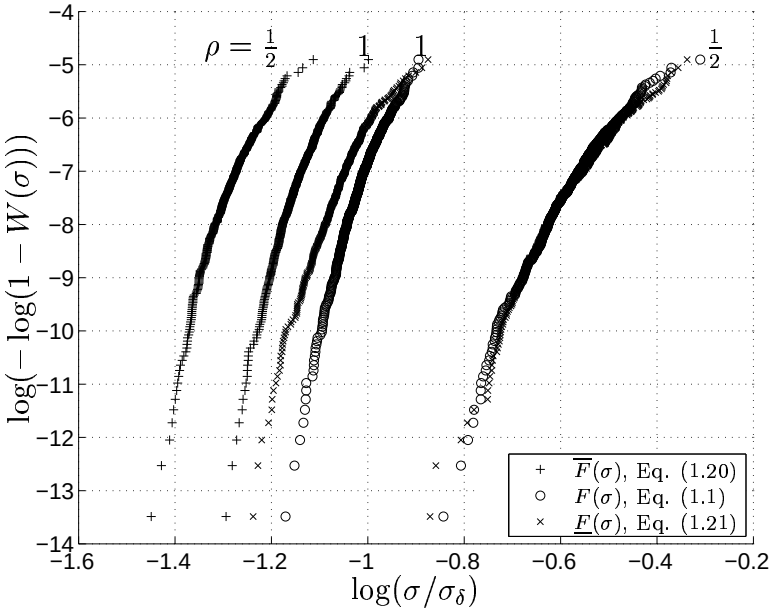

Figure 1.10: Dominance of the upper tail of the Weibull fiber strength distribution on the empirical characteristic distribution function, $\hat{W}(\sigma)$, for δ-bundles with 900 fibers and $\rho = 1$ and $1/2$. Shown are the original Weibull $F(\sigma)$, $\overline{F}(\sigma)$ with strong fibers reduced in strength, and $\underline{F}(\sigma)$ with weaker fibers reduced to zero strength.

1.4 Analysis of Composite Strength Distribution for Large ρ

We now develop closed-form analytical approximations to the characteristic distribution function $W(\sigma)$ using a cluster growth approach as originally described in [39] and [35]. The importance of this result is that the distribution function for the strength of a large composite with n fibers of length L becomes

$$\begin{aligned} H_{m,n}(\sigma) &\approx 1 - [1 - W(\sigma)]^{mn} \\ &\approx 1 - e^{-mnW(\sigma)}, \qquad \sigma \geq 0, \end{aligned} \tag{1.22}$$

where $m = L/\delta$ is the number of δ-bundles in the composite. Notably the resulting probability depends on the composite volume mn.

1.4.1 Characteristic distribution $W(\sigma)$ under 1D HLLS

To derive an approximation to $W(\sigma)$ in the case of 1D HLLS we model δ-bundle failure as a cascade of fiber failures. To begin, we approximate the probability such a cascade occurs, starting with the failure of a given fiber. The structure of such an event is that under stress σ, a given fiber fails, and its two immediate neighbors then suffer stress $K_1\sigma$, of which one fails. The pair of breaks formed causes one of the two adjacent overloaded neighbors to fail under stress $K_2\sigma$, the resulting triplet then fails one of its two overloaded neighbors under stress $K_3\sigma$, and so on until all n fibers have failed. Thus, $W(\sigma)$ is approximately

$$\begin{aligned} W_n(\sigma) &\approx F(\sigma)\{1-[1-F(K_1\sigma)]^2\}\{1-[1-F(K_2\sigma)]^2\} \quad \cdots \\ &\qquad \{1-[1-F(K_{n-1}\sigma)]^2\} \\ &= \left\{1-\exp\left[-\left(\frac{\sigma}{\sigma_\delta}\right)^\rho\right]\right\}\prod_{r=1}^{n-1}\left\{1-\exp\left[-2\left(\frac{K_r\sigma}{\sigma_\delta}\right)^\rho\right]\right\}, \end{aligned} \tag{1.23}$$

where K_r is the stress concentration on the two fibers next to an r-cluster as approximated by Eq. (1.13), and $F(\sigma)$ is given by Eq. (1.1).

Simplifying assumptions are made in writing Eq. (1.23). First, only the failure of the fibers adjacent to an r-cluster are considered. Failure of fibers further away is ignored even though such fibers are overloaded. This is justified because, as r becomes large, the fibers neighboring the cluster carry twice as much load as the fibers sub-adjacent to it, according to Eq. (1.14). Thus for large ρ, the probability of failure of a sub-adjacent fiber without the failure of the adjacent fiber is negligible. Second, the formula assumes that fibers next to the cluster are

virgin. In other words, in evaluating the probability of failure of an overloaded fiber at stress $K_r\sigma$, the event that it survived a lower stress $K_j\sigma$, $j < r$ is ignored. While the first assumption decreases the calculated probability of failure relative to the true one, the second assumption increases it. For large ρ, the errors thus committed are negligible.

While Eq. (1.23) can be used directly to estimate $W(\sigma)$ numerically for larger n, it is more illuminating to have a functional form for $W(\sigma)$ independent of n. We now derive such an approximation especially applicable in the lower tail (smaller σ/σ_δ). When $K_r\sigma \ll \sigma_\delta$ we have

$$1 - \exp\left[-2\left(\frac{K_r\sigma}{\sigma_\delta}\right)^\rho\right] \approx 2\left(\frac{K_r\sigma}{\sigma_\delta}\right)^\rho \left[1 - \left(\frac{K_r\sigma}{\sigma_\delta}\right)^\rho\right]. \tag{1.24}$$

This simplification is inaccurate when $K_r\sigma$ becomes comparable to σ_δ. In order to preserve accuracy in this range, we rewrite Eq. (1.23) as

$$\begin{aligned} W_\infty(\sigma) \approx & \left\{\left(\frac{\sigma}{\sigma_\delta}\right)^\rho \prod_{j=1}^{k(\sigma)-1}\left[2\left(\frac{K_j\sigma}{\sigma_\delta}\right)^\rho\right]\right\}\left\{\prod_{j=1}^{k(\sigma)-1}\left[1 - \left(\frac{K_j\sigma}{\sigma_\delta}\right)^\rho\right]\right\} \\ & \times \left\{\prod_{j=k(\sigma)}^{\infty}\left[1 - \exp\left(-2\left(\frac{K_j\sigma}{\sigma_\delta}\right)^\rho\right)\right]\right\} \\ \equiv & \left\{W_{k(\sigma)}(\sigma)\right\}\left\{\Psi_1(\sigma)\right\}\left\{\Psi_2(\sigma)\right\}, \end{aligned} \tag{1.25}$$

where $k(\sigma)$ is an appropriately chosen critical cluster size depending on σ, as we describe shortly. Also we have preserved the explicit dependence on k of the first quantity, which can be written as

$$W_k(\sigma) = 2^{k-1}(K_1K_2\cdots K_{k-1})^\rho \left(\frac{\sigma}{\sigma_\delta}\right)^{k\rho}. \tag{1.26}$$

Note that the third product $\Psi_2(\sigma)$, in Eq. (1.25), is carried out to ∞ instead of n since the terms in the product converge very rapidly to unity and the product itself

converges rapidly in n. Except for very small n this replacement has negligible effect and has the benefit of making $W(\sigma)$ explicitly independent of n.

One way to define $k(\sigma)$ might be to take it as the integer satisfying

$$F(K_{k-1}\sigma) < 1 - \frac{1}{e} \leq F(K_k\sigma). \tag{1.27}$$

This, however, leads to a discontinuous $W(\sigma)$ because the 2^{k-1} factor in Eq. (1.26) prevents $W(\sigma)$ from being continuous at exactly $\sigma/\sigma_\delta = 1/K_k$. Smooth transitions, however, do occur at certain values of σ where the right hand side of Eq. (1.26) has the same value for both k and $k+1$, i.e., for a transition σ such that

$$2^{k-1}(K_1K_2\cdots K_{k-1})^\rho \left(\frac{\sigma}{\sigma_\delta}\right)^{k\rho} = 2^k(K_1K_2\cdots K_k)^\rho \left(\frac{\sigma}{\sigma_\delta}\right)^{(k+1)\rho}. \tag{1.28}$$

Taking the approximation Eq. (1.13) as the equality

$$K_r = \sqrt{\frac{b+r}{b}}, \tag{1.29}$$

we then have

$$\frac{\sigma}{\sigma_\delta} = \frac{2^{-1/\rho}}{K_k} = \frac{a}{\sqrt{k+b}}, \tag{1.30}$$

where

$$a = 2^{(\rho-1)/\rho}/\pi^{1/2} \quad \text{and} \quad b = 4/\pi. \tag{1.31}$$

When σ is decreased continuously the associated k cannot increase continuously since it takes on only integer values. If we relax this requirement and also permit k to vary continuously, we may replace σ/σ_δ in Eq. (1.26) in terms of k according to Eq. (1.30). In addition, substituting for K_r using Eq. (1.29) we have $W_k(\sigma)$ only as a function of k whereby

$$W_k = \frac{a^\rho}{(k+b)^{k\rho/2}} \prod_{r=1}^{k-1} (r+b)^{\rho/2}. \tag{1.32}$$

Evaluating the product in Eq. (1.32) yields

$$\begin{aligned}\prod_{r=1}^{k-1}(r+b)^{\rho/2} &= \exp\left\{\frac{\rho}{2}\sum_{r=1}^{k-1}\log(r+b)\right\} \\ &\approx \exp\left\{\frac{\rho}{2}\int_1^k \log(u+b)du - \frac{\rho}{4}\int_1^k \frac{1}{u+b}du\right\} \\ &= \left(\frac{(b+k)^{b+k-1/2}}{(b+1)^{b+1/2}}\right)^{\rho/2}\exp\left\{-\frac{\rho(k-1)}{2}\right\},\end{aligned} \tag{1.33}$$

so that

$$W_k = C(k+b)^{\phi}\exp\left\{-\beta(k+b)\right\}, \tag{1.34}$$

where

$$\begin{aligned}\beta &= \frac{\rho}{2}, \\ \phi &= \rho\left(\frac{b}{2}-\frac{1}{4}\right), \quad \text{and} \\ C &= a^{\rho}e^{\beta(b+1)}(1+b)^{-\beta(b+1/2)}.\end{aligned} \tag{1.35}$$

To get a relationship between W_k and σ, we use Eq. (1.30) relating k to σ, and upon simplification obtain

$$W_{k(\sigma)}(\sigma) = C\left(\frac{a\sigma_\delta}{\sigma}\right)^{2\phi}\exp\left\{-\beta\left(\frac{a\sigma_\delta}{\sigma}\right)^2\right\}. \tag{1.36}$$

Next we approximate $\Psi_1(\sigma)$ in Eq. (1.25). Using Eq. (1.30) we obtain

$$\begin{aligned}\Psi_1(\sigma) &= \prod_{j=1}^{k(\sigma)}\left[1-\left(\frac{K_j\sigma}{\sigma_\delta}\right)^{\rho}\right] \\ &\approx \exp\left\{-\sum_{j=1}^{k(\sigma)}\left(\frac{K_j\sigma}{\sigma_\delta}\right)^{\rho}\right\} \\ &\approx \exp\left\{-\frac{1}{2}\int_0^{k(\sigma)}(b+u)^{\rho/2}\left(\frac{\sigma}{a\sigma_\delta}\right)^{\rho}du\right\} \\ &\approx \exp\left\{-\left(\frac{a\sigma_\delta}{\sigma}\right)^2\frac{2}{2(\rho+2)}\left[1-b^{(\rho+2)/2}\left(\frac{\sigma}{a\sigma_\delta}\right)^{\rho+2}\right]\right\}.\end{aligned} \tag{1.37}$$

Finally we evaluate $\Psi_2(\sigma)$, the third product in Eq. (1.25), which is the probability of cluster stalling. Upon using Eq. (1.30) we obtain

$$\begin{aligned}\Psi_2(\sigma) &= \prod_{j=k(\sigma)}^{\infty}\left[1-\exp\left\{-2\left(\frac{K_j\sigma}{\sigma_\delta}\right)^{\rho}\right\}\right] \\ &\approx \exp\left\{-\sum_{j=k(\sigma)}^{\infty}\exp\left\{-2\left(\frac{K_j\sigma}{\sigma_\delta}\right)^{\rho}\right\}\right\} \\ &\approx \exp\left\{-\int_{k(\sigma)}^{\infty}\exp\left\{-(b+u)^{\rho/2}\left(\frac{\sigma}{a\sigma_\delta}\right)^{\rho}\right\}du\right\} \\ &= \exp\left\{-\frac{2}{\rho}\Gamma(2/\rho,1)\left(\frac{a\sigma_\delta}{\sigma}\right)^2\right\},\end{aligned} \tag{1.38}$$

where

$$\Gamma(p,1) = \int_1^{\infty} e^{-u}u^{p-1}du \tag{1.39}$$

is the incomplete gamma function. Substituting Eqs. (1.36), (1.37) and (1.38) into Eq. (1.25), i.e., $W_\infty(\sigma) \approx W_k(\sigma)\Psi_1(\sigma)\Psi_2(\sigma)$, keeping only the dominant term in Eq. (1.37) and dropping the subscript '∞', we obtain

$$W(\sigma) \approx C\left(\frac{a\sigma_\delta}{\sigma}\right)^{2\phi}\exp\left\{-B\beta\left(\frac{a\sigma_\delta}{\sigma}\right)^2\right\}, \tag{1.40}$$

where

$$B = 1+\left(\frac{2}{\rho}\right)^2\left[\frac{\rho}{2(\rho+2)}+\Gamma(2/\rho,1)\right], \tag{1.41}$$

and all other constants are as defined in Eq. (1.31) and Eq. (1.35). Note the emergence of the quantity $\rho/2$ as an important parameter in B. As ρ decreases below 2, B begins to grow rapidly, which lowers $W(\sigma)$.

Since there are n fibers in a δ-bundle, a cascade can originate from any one of them, and these events are taken as being statistically independent. This results in the approximation Eq. (1.18), and through Eq. (1.3), to $H_{m,n}(\sigma)$ for the full composite as given by Eq. (1.22).

To investigate the success of this result we compare $W(\sigma)$ to $\hat{W}(\sigma)$, which results from the convergence of the simulated $\hat{W}_n(\sigma)$ of Eq. (1.19) with increasing n. Figure 1.4 shows $W(\sigma)$ from Eq. (1.40) together with $\hat{W}(\sigma)$ from the Monte Carlo simulations. No adjustable parameters are involved. For $\rho = 1, 3, 5$, and 10, the calculated and simulated distributions are in remarkable agreement. For $\rho = 0.5$ the agreement suddenly weakens where no n-independent $\hat{W}(\sigma)$ appears. This lack of agreement is consistent with our earlier observations in Figure 1.9 where the distribution $\hat{G}_n(\sigma)$ for δ-bundle strength was close to that for ELS, which has a dispersed fiber failure mode. The value $\rho = 2$ does not emerge as having a dominating effect. Surprisingly the model seems to apply well for $\rho = 1$, and Figure 1.4 does not rule out its application for $\rho = 1/2$. This issue is revisited in Section 1.5.

1.4.2 Size effects for critical cluster and composite strength under HLLS

We next examine the size effect for the characteristic composite strength. That is, for fixed probability of failure p, we ask how the composite strength for the pth quantile scales in terms of number of fibers n and length $L = m\delta$ where m is the number of δ-bundles in the composite. We take $p = 1 - 1/e = 0.632$, which would correspond to the Weibull scale parameter for composite strength in a Weibull approximation to $H_{m,n}(\sigma)$. We examine the dependence of the critical cluster size on n at failure probability level p, and want to know the size of the critical cluster at the point where it becomes unstable. Extending these results to the full composite is simply a matter of replacing n by mn.

We know that

$$G_n(\sigma) \approx 1 - [1 - W(\sigma)]^n \approx 1 - e^{-nW(\sigma)}. \tag{1.42}$$

Equating this further to $1 - e^{-1}$, we find that the characteristic δ-bundle strength, denoted σ_c^*, is the stress σ solving $W(\sigma) = 1/n$ where $W(\sigma)$ is given by Eq. (1.40). While this equation can be inverted asymptotically to get σ_c^*, it turns out to be useful to think also in terms of a critical cluster size k^* associated with failure probability p. This is obtained by setting $W_k = 1/n$ in Eq. (1.34), that is, k^* must solve

$$(k^* + b)^{-\phi} e^{\beta(k^*+b)} = nC, \tag{1.43}$$

which is an implicit relation between k^* and n.

To obtain an explicit relation between k^* and n, we observe that

$$-\phi \log(k^* + b) + \beta(k^* + b) = \log(nC). \tag{1.44}$$

Substituting $k^* + b = (1 + \epsilon)\log(nC)/\beta$ and using $\log(1 + \epsilon) \approx \epsilon$ gives the critical cluster size k^* for a δ-bundle approximately as

$$k^* + b = (1 + \epsilon)\frac{\log(nC)}{\beta}, \tag{1.45}$$

where

$$\epsilon \approx \frac{\phi\,\{\log[\log(nC)] - \log(\beta)\}}{\log(nC) - \phi}, \tag{1.46}$$

and log is the Napierian logarithm. To obtain an integer valued k^*, one must round up the k^* from Eq. (1.45) to the next largest integer. To obtain k^* for the full composite simply replace n by mn in Eq. (1.45).

To obtain the characteristic strength σ_c^* of a δ-bundle we first use Eq. (1.30) to recast Eq. (1.45) in terms of σ, yielding the critical stress

$$\sigma^* = a\sigma_\delta \sqrt{\frac{\beta}{\log(nC)(1 + \epsilon)}}. \tag{1.47}$$

This expression, however, does not account for the crack stalling probability $\Psi_2(\sigma)$. It can be interpreted as the stress associated with *formation* of a cluster of critical size k^* where the probability of further propagation becomes likely but not guaranteed to be catastrophic. Including $\Psi_2(\sigma)$ as well yields the characteristic δ-bundle strength

$$\sigma_c^* = a\sigma_\delta \sqrt{\frac{B\beta}{\log(nC)(1+\epsilon(B\beta))}}, \tag{1.48}$$

where $\epsilon(B\beta)$ is given by Eq. (1.46) with β replaced by $B\beta$. Again, to obtain the characteristic composite strength, replace n by mn in Eq. (1.48).

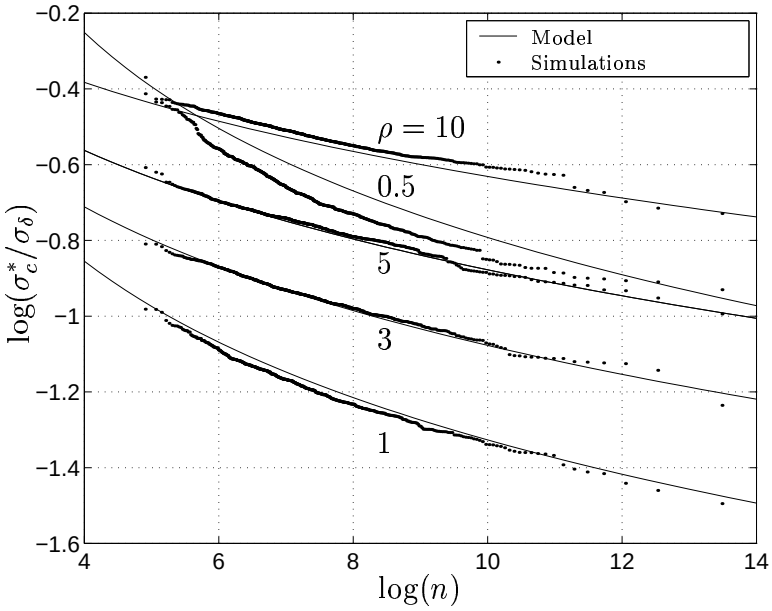

Figure 1.11: Comparison of Eq. (1.47) with size effect predicted from the simulated empirical strength distributions of a 900-fiber δ-bundle under 1D HLLS.

Figure 1.11 shows plots of the characteristic strength σ_c^* versus δ-bundle size n based on Eq. (1.48). The agreement is good even for $\rho = 1/2$, which did not show failure by cluster growth over this range of n.

1.4.3 Characteristic distribution $W(\sigma)$ under 2D HVLLS

The approach taken to approximate $W(\sigma)$ for 2D HVLLS is identical to that used in 1D HLLS except that the possible geometries of break clusters introduce additional complexities. We model the cascade event defining $W(\sigma)$ as the formation of a break cluster at stress σ that goes unstable. The diameter D of a tight circular cluster of r breaks was defined earlier as $\pi D^2/4 = r$. The circumference of the circle, $\pi D = \sqrt{4\pi r}$ is approximately the number of intact fibers surrounding this r-cluster. Let N_r be the number of these neighbors that are severely overloaded. The first step is the failure of a given fiber in the δ-bundle under σ, followed by the failure of one of its $N_1 = 6$ equally overloaded neighbors under stress $K_1\sigma$. The resulting pair of fiber breaks has eight intact neighbors of which only $N_2 = 2$ are severely overloaded under stress $K_2\sigma$. The next likely event is the failure of one of these, to form a break triplet with $N_3 = 3$ severely overloaded neighbors, of which one fails, and so on. The critical event is thus the evolution of a growing "tight" r-cluster (Figure 1.12), with each added break being the failure of one of the N_r severely overloaded fibers surrounding it.

As in the 1D case, we write this as

$$\begin{aligned} W_n(\sigma) \approx\ & F(\sigma)\{1-[1-F(K_1\sigma)]^{N_1}\} \\ & \times \{1-[1-F(K_2\sigma)]^{N_2}\} \cdots \{1-[1-F(K_{n-1}\sigma)]^{N_{n-1}}\}, \end{aligned} \tag{1.49}$$

where K_r is the stress concentration on the N_r most severely overloaded neighbors of a tight r-cluster. We introduce a two-parameter, power law to account for the actual number of neighbors at high risk,

$$N_r = \eta r^{\gamma}, \tag{1.50}$$

with parameters η and γ satisfying $\eta > 0$ and $0 < \gamma \leq 1/2$. This power form for N_r

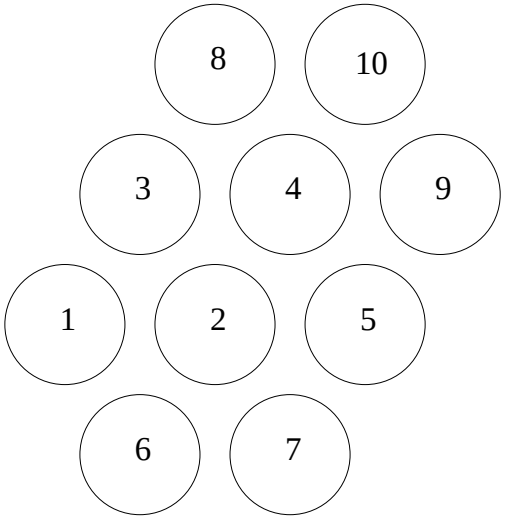

i	K_i
1	1.0000
2	1.1046
3	1.2337
4	1.2828
5	1.3205
6	1.3644
7	1.5889
8	1.4107
9	1.4596
10	1.6163

Figure 1.12: One possible sequence of tight cluster growth to 10 fiber breaks in a hexagonal fiber array. The numbers $(1, 2, \ldots, 10)$ indicate break sequence. Also included are the associated stress concentrations computed under HVLLS.

is essential for $W_n(\sigma)$ in Eq. (1.49) to agree with the simulated $\hat{W}(\sigma)$ distribution as ρ becomes small. Observe that if $\eta = \sqrt{4\pi} \approx 3.55$ and $\gamma = 1/2$, then N_r is simply the total number of intact fibers surrounding a circular r-cluster.

Applying approximations as in Section 1.4.1 we rewrite Eq. (1.49) as

$$\begin{aligned} W_\infty(\sigma) \approx & \left\{ \left(\frac{\sigma}{\sigma_\delta}\right)^\rho \prod_{j=1}^{k(\sigma)-1} \left[N_j \left(\frac{K_j\sigma}{\sigma_\delta}\right)^\rho \right] \right\} \left\{ \prod_{j=1}^{k(\sigma)-1} \left[1 - \frac{N_j}{2} \left(\frac{K_j\sigma}{\sigma_\delta}\right)^\rho \right] \right\} \\ & \times \left\{ \prod_{j=k(\sigma)}^{\infty} \left[1 - \exp\left(-N_j \left(\frac{K_j\sigma}{\sigma_\delta}\right)^\rho \right) \right] \right\} \qquad (1.51) \\ \equiv & \left\{ W_{k(\sigma)}(\sigma) \right\} \left\{ \Psi_1(\sigma) \right\} \left\{ \Psi_2(\sigma) \right\}. \end{aligned}$$

Again the explicit dependence on k in the first product $W_{k(\sigma)}(\sigma)$ is retained, and it may be written as

$$W_k(\sigma) = N_1 N_2 \cdots N_{k-1} (K_1 K_2 \cdots K_{k-1})^\rho \left(\frac{\sigma}{\sigma_\delta}\right)^{k\rho}. \qquad (1.52)$$

As in the case of 1D, we relate σ to k by setting $W_k(\sigma) = W_{k+1}(\sigma)$. Doing so and recalling Eq. (1.16) for K_r, which we rewrite as

$$K_r = \sqrt{\frac{\sqrt{r}+b}{b}}, \tag{1.53}$$

we obtain

$$\frac{\sigma}{\sigma_\delta} = ak^{-\gamma/\rho}(\sqrt{k}+b)^{-1/2}, \tag{1.54}$$

where

$$a = \sqrt{b}/\eta^{1/\rho} \quad \text{and} \quad b = \pi^{3/2}/2. \tag{1.55}$$

Using Eqs. (1.50), (1.53) and (1.54) in Eq. (1.52) and simplifying we obtain

$$W_k = \frac{[(k-1)!]^\gamma \prod_{j=0}^{k-1}(\sqrt{j}+b)^{\rho/2}}{\eta k^{k\gamma}(\sqrt{k}+b)^{k\rho/2}}. \tag{1.56}$$

We can evaluate Eq. (1.56) as follows: By Stirling's formula,

$$(k-1)! \approx \sqrt{2\pi}k^{k-1/2}e^{-k}. \tag{1.57}$$

Also,

$$\begin{aligned}
\prod_{j=0}^{k-1}(\sqrt{j}+b) &= \exp\left\{\sum_{j=0}^{k-1}\log(\sqrt{j}+b)\right\} \\
&\approx \exp\left\{\int_{u=0}^{k}\log(\sqrt{u}+b)du - \int_{u=0}^{k}\frac{1}{2}\frac{d\log(\sqrt{x}+b)}{dx}dx\right\} \\
&= (\sqrt{k}+b)^{k-b^2-1/2}b^{(b^2+1/2)} \\
&\quad \times \exp\left\{-\frac{1}{2}(\sqrt{k}+b)^2 + 2b(\sqrt{k}+b) - \frac{3b^2}{2}\right\}.
\end{aligned} \tag{1.58}$$

Using these two approximations in Eq. (1.56) and noting that

$$k^{-\gamma/2} = (\sqrt{k}+b)^{-\gamma}\left[1 - \frac{b}{\sqrt{k}+b}\right]^{-\gamma} \approx (\sqrt{k}+b)^{-\gamma}, \tag{1.59}$$

while

$$\exp\{\gamma k\} = \exp\{\gamma[(\sqrt{k}+b)^2 - 2b(\sqrt{k}+b) + b^2]\}, \tag{1.60}$$

we may reduce Eq. (1.56) to

$$W_k = C(\sqrt{k}+b)^{-\varphi} \exp\left\{-\beta_1\left(\sqrt{k}+b-\frac{\beta_2}{2\beta_1}\right)^2\right\}, \tag{1.61}$$

where

$$\begin{aligned} C &= \frac{(2\pi)^{\frac{\gamma}{2}}}{\eta} b^{(\rho/2)(b^2+1/2)} \exp\left\{-b^2\left(\frac{3\rho}{4}+\gamma\right)+\frac{\beta_2^2}{4\beta_1}\right\}, \\ \varphi &= \gamma + (\rho/2)(b^2+\frac{1}{2}), \\ \beta_1 &= \frac{\rho+4\gamma}{4}, \quad \text{and} \\ \beta_2 &= b(\rho+2\gamma). \end{aligned} \tag{1.62}$$

To get an expression in terms of σ, we first write Eq. (1.54) as

$$\frac{\sigma}{a\sigma_\delta} = (\sqrt{k}+b)^{-2\beta_1/\rho} \left[1-\frac{b}{\sqrt{k}+b}\right]^{-2\gamma/\rho}, \tag{1.63}$$

which can approximately be inverted to give

$$\sqrt{k}+b \approx \left(\frac{\sigma}{a\sigma_\delta}\right)^{-\rho/(2\beta_1)} + \frac{b\gamma}{\beta_1} + \frac{b^2\gamma}{2\beta_1^2}(\beta_1-\gamma)\left(\frac{\sigma}{a\sigma_\delta}\right)^{\rho/(2\beta_1)}. \tag{1.64}$$

Dropping the last term leads to

$$\frac{\sigma}{a\sigma_\delta} = \left(\sqrt{k}+b-\frac{b\gamma}{\beta_1}\right)^{-2\beta_1/\rho}, \tag{1.65}$$

which for given σ results in a slightly lower value of k as compared to Eq. (1.64). Substituting Eq. (1.64) into Eq. (1.61) for W_k gives

$$W_{k(\sigma)}(\sigma) = C\Omega_1(\sigma)\left(\frac{\sigma}{a\sigma_\delta}\right)^{\varphi\rho/(2\beta_1)} \exp\left\{-\beta_1\Theta_1(\sigma)\left(\frac{a\sigma_\delta}{\sigma}\right)^{\rho/\beta_1}\right\}, \tag{1.66}$$

where

$$\Omega_1(\sigma) = \left[1+\frac{b\gamma}{\beta_1}\left(\frac{\sigma}{a\sigma_\delta}\right)^{\rho/(2\beta_1)} + \frac{b^2\gamma}{2\beta_1^2}(\beta_1-\gamma)\left(\frac{\sigma}{a\sigma_\delta}\right)^{\rho/\beta_1}\right]^{-\varphi}, \tag{1.67}$$

and

$$\Theta_1(\sigma) = \left[1 - \frac{b\rho}{2\beta_1}\left(\frac{\sigma}{a\sigma_\delta}\right)^{\rho/(2\beta_1)} + \frac{b^2\gamma}{2\beta_1^2}\left(\beta_1 - \gamma\right)\left(\frac{\sigma}{a\sigma_\delta}\right)^{\rho/\beta_1}\right]^2. \tag{1.68}$$

Next we approximate the second product $\Psi_1(\sigma)$ in Eq. (1.51) as

$$\begin{aligned}
\Psi_1(\sigma) &= \prod_{j=0}^{k(\sigma)-1}\left[1 - \frac{N_j}{2}\left(\frac{K_j\sigma}{\sigma_\delta}\right)^\rho\right] \\
&\approx \exp\left\{-\sum_{j=0}^{k(\sigma)-1}\frac{N_j}{2}\left(\frac{K_j\sigma}{\sigma_\delta}\right)^\rho\right\} \\
&\approx \exp\left\{-\frac{1}{2}\left(\frac{\sigma}{a\sigma_\delta}\right)^\rho\int_0^{k(\sigma)} u^\gamma(\sqrt{u}+b)^{\rho/2}du\right\} \\
&\approx \exp\left\{-\frac{1}{2(\beta_1+1)}\Theta_2(\sigma)\left(\frac{a\sigma_\delta}{\sigma}\right)^{\frac{\rho}{\beta_1}}\right\},
\end{aligned} \tag{1.69}$$

where the last step involves applying Eq. (1.64) and keeping only the dominant terms, and where

$$\Theta_2(\sigma) = 1 - \frac{b\rho(\beta_1+1)}{2\beta_1(2\beta_1+1)}\left(\frac{\sigma}{a\sigma_\delta}\right)^{\frac{\rho}{2\beta_1}}. \tag{1.70}$$

Finally we evaluate the third product $\Psi_2(\sigma)$ in Eq. (1.51) as

$$\begin{aligned}
\Psi_2(\sigma) &= \prod_{j=k(\sigma)}^{\infty} 1 - \exp\left(-N_j\left(\frac{K_j\sigma}{\sigma_\delta}\right)^\rho\right) \\
&\approx \exp\left\{-\sum_{j=k(\sigma)}^{\infty}\exp\left\{N_j\left(\frac{K_j\sigma}{\sigma_\delta}\right)^\rho\right\}\right\} \\
&\approx \exp\left\{-\int_{k(\sigma)}^{\infty}\exp\left\{-u^\gamma(\sqrt{u}+b)^{\rho/2}\left(\frac{\sigma}{a\sigma_\delta}\right)^\rho\right\}du\right\} \\
&\approx \exp\left\{-\frac{1}{\beta_1}\Gamma\left(\frac{1}{\beta_1},1\right)\Theta_3(\sigma)\left(\frac{a\sigma_\delta}{\sigma}\right)^{\rho/\beta_1}\right\},
\end{aligned} \tag{1.71}$$

where

$$\Theta_3(\sigma) = 1 - \frac{b\rho}{4\beta_1}\frac{\Gamma\left(\frac{1}{2\beta_1},1\right)}{\Gamma\left(\frac{1}{\beta_1},1\right)}\left(\frac{\sigma}{a\sigma_\delta}\right)^{\rho/(2\beta_1)}. \tag{1.72}$$

Multiplying $W_k(\sigma)$, $\Psi_1(\sigma)$, and $\Psi_2(\sigma)$ in Eq. (1.51) and dropping the subscript '∞' finally gives our main result

$$W(\sigma) = C\Omega_1(\sigma)\left(\frac{\sigma}{a\sigma_\delta}\right)^{\varphi\rho/(2\beta_1)} \exp\left\{-\Omega_2(\sigma)\left(\frac{a\sigma_\delta}{\sigma}\right)^{\rho/\beta_1}\right\}, \tag{1.73}$$

where

$$\Omega_2(\sigma) = \beta_1\Theta_1(\sigma) + \frac{\Omega_1^{-\frac{1}{\varphi}}}{2}\Theta_2(\sigma) + \Gamma\left(\frac{1}{\beta_1}, 1\right)\frac{\Theta_3(\sigma)}{\beta_1}. \tag{1.74}$$

Figure 1.13 compares two versions of $W(\sigma)$ in Eq. (1.73) against $\hat{W}(\sigma)$ from the Monte Carlo simulations, for $\rho = 1, 2, 3, 5$, and 10. The dashed lines (Model 1) assume $\gamma = 1/2$ and $\eta = \sqrt{4\pi} = 3.55$ as is the case in Eq. (1.50) if we assume all fibers in the first ring around the cluster are equally at risk of failure. The solid lines (Model 2) assume γ and η values corresponding to the respective ρ values as shown in the table within the figure. The fit in the dashed line case, which is excellent for $\rho = 20$ (not shown) and quite good for $\rho = 10$, rapidly deteriorates for $\rho \leq 5$. However, except for $\rho = 1$ the agreement is excellent when γ and η are adjusted as shown in the table. This suggests that the growth in the number of neighbors to the cluster at high risk of failure must be retarded after the first three or four breaks. For $\rho \leq 3$ it was retarded completely by setting $\gamma = 0$ and $\eta = 6$ so that the number of neighbors remained fixed at 6 regardless of the cluster size.

Many approximations were made in deriving $W(\sigma)$ in Eq. (1.73), but using the root equation, Eq. (1.49), does not improve the agreement with the simulations. Furthermore we have assumed the clusters are round, when in reality they will become increasingly irregular as ρ is decreased. Thus for moderate ρ, i.e., $2 < \rho < 10$, this irregularity may mean that relatively fewer of the neighbors should be viewed as highly stressed, perhaps only those that protrude the most into the cluster. The emergence of powers of γ less than $1/2$ for smaller ρ may also

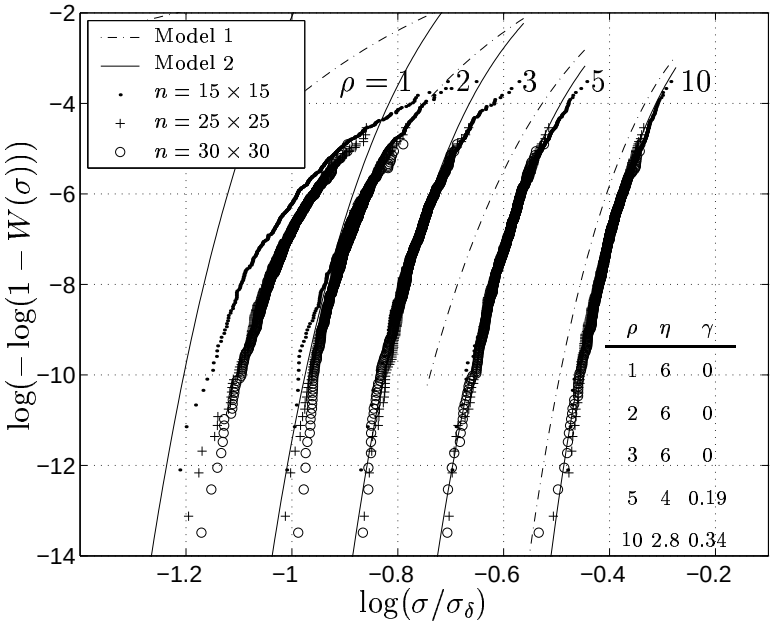

Figure 1.13: Comparison of the theoretical $W(\sigma)$ from the cluster growth model under 2D HVLLS and Weibull fibers with the empirical version $\hat{W}(\sigma)$ obtained from simulations. Model 1 assumes $\eta = \sqrt{4\pi}$ and $\gamma = 0.5$ for all ρ. In Model 2, the parameters η and γ are adjusted for each ρ to provide the best fit as shown in the table. Results corresponding to $\rho = 0.5$ are not shown because the plots of $W(\sigma)$ for both models lie off scale.

mean that the cluster roughness around the perimeter has fractal character as it grows and this somehow determines the effective number of neighbors at risk. In Section 1.6 we will suggest another possible explanation for the adjustment involving decreasing the value of γ in Eq. (1.50) for N_r. Note also that the parameter $\beta_1 = (\rho + 4\gamma)/4$ plays a role in the behavior of $W(\sigma)$ through $\Omega_2(\sigma)$, Eq. (1.74), as ρ and γ diminish. Curiously, when $\gamma = 0$ we have $\beta_1 = \rho/4$ suggesting that the value $\rho = 4$ has special significance, as is also pursued further in Section 1.6. We find that $\Omega_2(\sigma)$ starts to increase rapidly when ρ diminishes below 4 reflecting an

increased cluster stalling probability. This has the effect of decreasing $W(\sigma)$, and thus, the probability of failure, though the effect is not strong enough to explain the behavior of the simulations for small ρ in Figure 1.13.

The weakness of the fit for $\rho = 1$ is consistent with the earlier observation in Figure 1.9 that once ρ decreases below about 2, the δ-bundle failure distribution develops strong Gaussian character as seen under ELS, which is truly a dispersed failure mode.

1.4.4 Size effect for critical cluster and composite strength under HVLLS

We now derive formulas for the variation of the critical cluster size k^* with the size n of δ-bundles under 2D HVLLS and at failure probability level $p = 1 - 1/e$. We then derive the dependence of the characteristic δ-bundle strength σ_c^* on n. Converting this result to apply to the full composite only requires replacing n by mn.

The first step is to set $W_k = 1/n$ or, using Eq. (1.61), we have

$$C\left(\sqrt{k}+b\right)^{\varphi}\exp\left\{\beta_1\left(\sqrt{k}+b-\frac{\beta_2}{2\beta_1}\right)^2\right\} = nC. \tag{1.75}$$

For moderate k^*, we note that $\sqrt{k^*}+b$ is close to $\beta_2/2\beta_1$, which makes the exponential function in Eq. (1.75) amenable to a power series expansion. Asymptotic inversion leads to

$$\log\left(\sqrt{k^*}+b\right) = \frac{\log(nC)+log(\omega_1)}{\varphi}, \tag{1.76}$$

where the correction term $\log(\omega_1)$ grows slowly with $\log(nC)$ following

$$\log(\omega_1) = \frac{-\frac{\beta_2^2}{4\beta_1}\left[\frac{\log(nC)}{\varphi}-\log\left(\frac{\beta_2}{2\beta_1}\right)\right]^2}{1+\frac{\beta_2^2}{4\beta_1\varphi}\left[\frac{\log(nC)}{\varphi}-\log\left(\frac{\beta_2}{2\beta_1}\right)\right]}. \tag{1.77}$$

The correction term ω_1, while small, can have a major effect on the resulting k^*. The above formula for k^* works for a wide range of n (e.g. $n < 10^9$). However, for larger n, an expansion arises of the form

$$\sqrt{k^*} + b = \left(\sqrt{\frac{\log(nC)}{\beta_1}} + \frac{\beta_2}{2\beta_1} \right) (1 - \omega_2), \tag{1.78}$$

where the correction term ω_2 is

$$\omega_2 = \frac{\varphi \log\left(\sqrt{\frac{\log(nC)}{\beta_1}} + \frac{\beta_2}{2\beta_1} \right)}{\varphi + 2\log(nC) + \frac{\beta_2}{\beta_1}\sqrt{\frac{\log(nC)}{\beta_1}}}. \tag{1.79}$$

For astronomical n such as $n > 10^{25}$ we have

$$\sqrt{k^*} + b = \sqrt{\frac{\log(nC)}{\beta_1}}. \tag{1.80}$$

Substituting for k^* in terms of σ^* we estimate the size effect for the stress when the critical cluster forms. From Eqs. (1.65) and (1.76) we get

$$\sigma^* \approx a\sigma_\delta \left((nC\omega_1)^{1/\varphi} - \frac{b\gamma}{\beta_1} \right)^{-2\beta_1/\rho}. \tag{1.81}$$

For extremely large n, Eqs. (1.65) and (1.78) lead to

$$\sigma^* \approx a\sigma_\delta \left(\left(\sqrt{\frac{\log(nC)}{\beta_1}} + \frac{\beta_2}{2\beta_1} \right) (1 - \omega_2) - \frac{b\gamma}{\beta_1} \right)^{-2\beta_1/\rho}. \tag{1.82}$$

Finally, as $n \to \infty$, this behaves as

$$\sigma^* = a\sigma_\delta \left(\frac{\beta_1}{\log(nC)} \right)^{\beta_1/\rho}. \tag{1.83}$$

To obtain the characteristic stress for composite failure, σ_c^*, we must account for $\Psi_1(\sigma)$ and $\Psi_2(\sigma)$ leading to complex expressions. We estimate the main effect by noting that $\Omega_2(\sigma) \to B$ as $\sigma \to 0$ where

$$B = 1 + \frac{1}{2\beta_1(\beta_1 + 1)} + \frac{1}{\beta_1^2}\Gamma\left(\frac{1}{\beta_1}, 1 \right). \tag{1.84}$$

Thus for large n we may obtain σ_c^* from σ^* upon replacing $\log(nC)/\beta_1$ by $\log(nC)/(B\beta_1)$ in Eqs. (1.82) and (1.83). For smaller n, of the order used in our simulations, and larger values of ρ we can still use Eq. (1.81) for σ_c^*. For smaller ρ, say $\rho \leq 5$ where B differs appreciably from one, Eqs. (1.82) and (1.83) may be applied but are likely to be very conservative as $B\beta_1$ is a poor reflection of the full effect of $\Omega_2(\sigma)$ in Eq. (1.73).

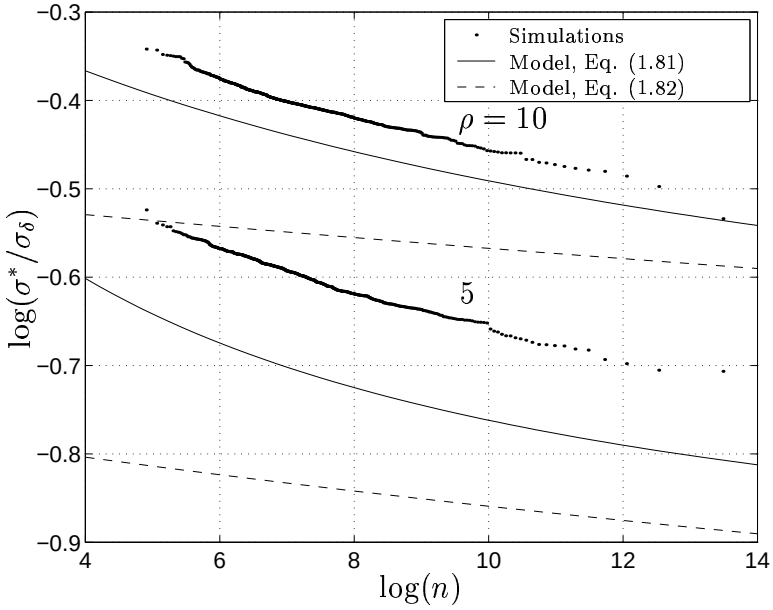

Figure 1.14: Comparison of the size effect predicted by the cluster growth model, Eqs. (1.81) and (1.82), with that derived from a $\hat{W}(\sigma)$ interpretation of the empirical strength distributions of a 900 fiber δ-bundle under 2D HVLLS.

Figure 1.14 shows a plot of σ_c^* given by Eq. (1.81) against the size effect predicted using simulations from the δ-bundles of size $n = 900$ as though they posses weakest link character in terms of $\hat{W}(\sigma)$, as is supported by Figure 1.13. The size range covered is $100 < n < 1,000,000$, which is the relevant range for Eq. (1.81). Clearly the formula works well for $\rho = 10$ and reasonably well for $\rho = 5$, but

breaks down for smaller ρ, because of the above mentioned lack of treatment of the cluster stalling probability in the derivation. For extremely large n, Eq. (1.82) with the $B\beta_1$ modification shows the anticipated poorer performance. One one hand, discrepancies in Figure 1.14 may be due approximation errors, but on the other hand this could also serves to point out that composites of the size that can presently be treated by Monte Carlo simulation may not reveal the true size effect as might be relevant in applications.

1.4.5 Power-law fiber strength and δ-bundle behavior

In Section 1.4.1, we observed for 1D HLLS that the tight cluster growth model accurately predicts the empirical strength distribution for $\rho \geq 1$, but not for $\rho < 1$. In 2D HVLLS, when the fiber strength is Weibull, Eq. (1.1), the tight cluster growth mode does not seem to apply to $\rho < 2$ as seen in Figure 1.13. These departures may be due to non-tightness of cluster growth, or to the presence of occasional strong fibers, or both.

To resolve this we consider a cluster growth failure model for a δ-bundle with fiber strength that follows a power-law distribution, $F_p(\sigma)$, given by Eq. (1.2). Using $F_p(\sigma)$ in the arguments to develop Eq. (1.51), we have

$$\begin{aligned} W_\infty(\sigma) &\approx \left\{ \left(\frac{\sigma}{\sigma_\delta}\right)^\rho \prod_{j=1}^{k(\sigma)-1} \left[N_j \left(\frac{K_j\sigma}{\sigma_\delta}\right)^\rho \right] \right\} \\ &\quad \times \left\{ \prod_{j=k(\sigma)}^{k_m(\sigma)} \left[1 - \left(1 - \left(\frac{K_j\sigma}{\sigma_\delta}\right)^\rho \right)^{N_j} \right] \right\} \\ &\equiv \left\{ W_{k(\sigma)}(\sigma) \right\} \left\{ \Psi_2(\sigma) \right\}, \end{aligned} \tag{1.85}$$

where $k_m(\sigma)$ is such that $K_{k_m(\sigma)}\sigma/\sigma_\delta = 1$. Here $W_{k(\sigma)}(\sigma)$ is still given by Eq. (1.66),

but the factor $\Psi_2(\sigma)$ is different and is approximated as

$$\Psi_2(\sigma) = \exp\left\{-\frac{4b^2}{\rho}\Theta_2(\sigma)\left(\frac{\sigma_\delta}{\sigma}\right)^\rho\right\} \tag{1.86}$$

where

$$\begin{aligned}\Theta_2(\sigma) = {} & B\left(\eta k^\gamma(\sigma)+1, \frac{4}{\rho}\right)\left\{1 - I_{\left(\sqrt{\frac{k(\sigma)+1}{b}}\sigma\right)^\rho}\left(\eta k^\gamma(\sigma)+1, \frac{4}{\rho}\right)\right\} \\ & - \left(\frac{\sigma}{\sigma_\delta}\right)^2 B\left(\eta k^\gamma(\sigma)+1, \frac{2}{\rho}\right)\left\{1 - I_{\left(\sqrt{\frac{k(\sigma)+1}{b}}\sigma\right)^\rho}\left(\eta k^\gamma(\sigma)+1, \frac{2}{\rho}\right)\right\}\end{aligned} \tag{1.87}$$

where $B(a,b) = \int_0^1 t^{a-1}(1-t)^{b-1}dt$ is the beta function and $I_p(a,b) = \int_p^1 t^{a-1}(1-t)^{b-1}dt/B(a,b)$ is the incomplete beta function. The critical cluster size $k(\sigma)$ is

$$k(\sigma) \approx \left\{\left(\frac{\sigma}{a\sigma_\delta}\right)^{-\frac{\rho}{2\beta_1}} - \frac{b\rho}{4\beta_1} + \frac{b^2\rho\gamma}{8\beta_1^2}\left(\frac{\sigma}{a\sigma_\delta}\right)^{\frac{\rho}{2\beta_1}}\right\}^2. \tag{1.88}$$

Figure 1.15 shows $W_\infty(\sigma)$ from Eq. (1.85) together with the $\hat{W}(\sigma)$ distributions obtained through Monte Carlo simulation, assuming the power-law distribution $F_p(\sigma)$ for fiber strength. For all three sizes shown, the theoretical and empirical distributions agree even at $\rho = 1$, whereas in Figure 1.13 assuming Weibull fibers they began to diverge at $\rho = 2$. Apparently, as ρ decreases in the Weibull case, the stalling probability of a growing cluster is increased by occasional strong fibers thus promoting dispersed breaking, but this does not occur under the power-law version of $F_p(\sigma)$, which has no fibers with strength exceeding σ_δ. Surprisingly, even at $\rho = 0.5$, reasonable agreement of the cluster growth model with the simulations occurs under $F_p(\sigma)$.

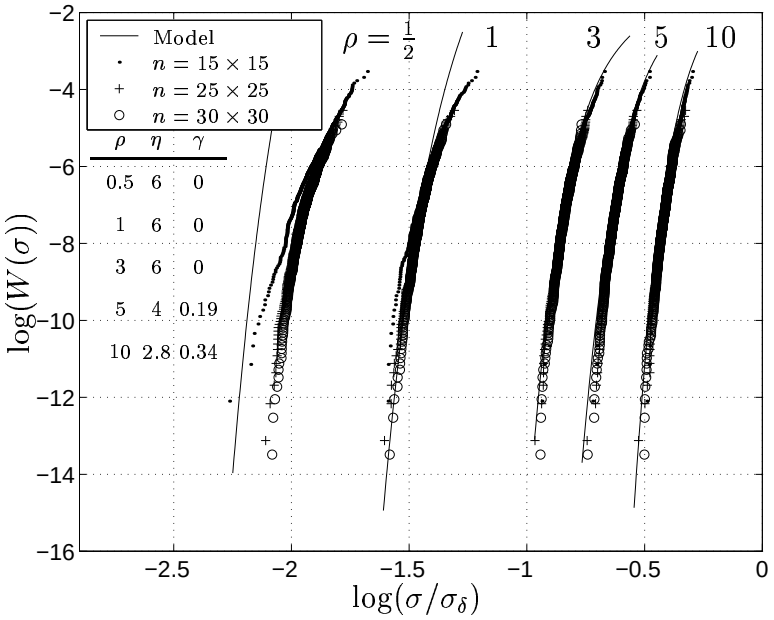

Figure 1.15: Comparison of the characteristic distribution function $W(\sigma)$ from the cluster growth model under 2D HVLLS and power-law fiber strength $F_p(\sigma)$ with the empirical version $\hat{W}(\sigma)$ obtained from Monte-Carlo simulations. The values of (η, γ) used here are identical to those in Figure 1.13 for Model 2.

1.5 Analysis of Composite Strength Distribution for Small ρ

In the case of dispersed fiber failure in a δ-bundle, it is reasonable to conjecture that for small enough ρ the details of the fiber load-sharing model are not important provided that the model conserves load. Thus we consider behavior under the equal load-sharing rule, or ELS, where the stress concentration factor for each intact fiber in an n-fiber δ-bundle with j broken fibers is $\kappa_{n,j} = n/(n-j)$, as described in Section 1.1.2. [12] showed that if the strengths of individual fibers are independent and identically distributed according to an arbitrary distribution function $B(\sigma)$,

and certain conditions are met such as $\lim_{\sigma\uparrow\infty}\sigma(1-B(\sigma))=0$ and the peak in the maximum of this function is unique, then the strength distribution $G_n(\sigma)$ of a δ-bundle asymptotically converges, as $n\to\infty$, to the normal or Gaussian form $\Phi((\sigma-\mu_n^*)/s_n^*)$ where

$$\mu_n^*=\mu^*=\sigma_\tau(1-B(\sigma_\tau)), \tag{1.89}$$

and

$$s_n^*=\sigma_\tau n^{-1/2}\sqrt{nB(\sigma_\tau)(1-B(\sigma_\tau))}, \tag{1.90}$$

and where σ_τ gives $\sigma(1-B(\sigma))$ its maximum value. Here $\Phi(\cdot)$ denotes the standard Gaussian distribution.

$$\Phi(z)=\frac{1}{\sqrt{2\pi}}\int_{-\infty}^{z}e^{-u^2/2}du. \tag{1.91}$$

As mentioned in Section 1.1.4, [40] gave a correction to the asymptotic mean to speed up convergence to the asymptotic limit. Applying Daniels' formula with Smith's correction to the Weibull fiber case, one obtains a very accurate prediction of the true strength distribution, even for quite small n. The parameters of the resulting normal strength distribution are then the asymptotic mean

$$\mu_n^*=\sigma_\delta(\rho e)^{-1/\rho}\left\{1+0.996n^{-2/3}\left(e^{2/\rho}/\rho\right)^{1/3}\right\}, \tag{1.92}$$

and the asymptotic standard deviation

$$s_n^*=\sigma_\delta n^{-1/2}\rho^{-1/\rho}\sqrt{e^{-1/\rho}(1-e^{-1/\rho})}. \tag{1.93}$$

In Subsection 1.3.2 we observed from Monte Carlo simulations that, when $\rho\downarrow 0$ and the variability in fiber strength increases, the δ-bundle strength distributions under both HLLS and HVLLS converge to the Gaussian or normal form of ELS, for the bundle sizes n considered. Two reasons were cited: The first was the tendency for small clusters to stall from the dominance of strong fibers from the Weibull

upper tail, and the second was increasing numbers of very weak fibers causing many more scattered clusters. The question arises as to whether this behavior persists as n increases by orders of magnitude.

We conjecture that, no matter how small the value of ρ and no matter how much initial dispersed fiber failure, if a δ-bundle is large enough final failure will eventually be locally initiated and a cluster will eventually propagate catastrophically to fail the rest of the surviving fibers. That is, unlike ELS, wherein material damage truly accrues globally, we conjecture that in HLLS and HVLLS there is a ρ-dependent size scale within which damage initiates and propagates. This must remain a conjecture because we are unable to simulate δ-bundles much beyond $n = 900$, yet under 2D HVLLS and $\rho = 0.5$ the critical cluster size is probably greater than 900 fibers. Nevertheless evidence for this assertion is seen from simulations on large 1D HLLS δ-bundles.

For 1D HLLS, Figure 1.16 shows the evolution of fiber breaks that occur in the median strength (out of $N = 500$) δ-bundle with $n = 900$ fibers and for $\rho = 0.5$, 1, and 10. For $\rho = 0.5$ a cluster does not initiate, as the fiber failures are largely dispersed to the very end. This happens even though the bundle size $n = 900$ is much larger than the critical cluster size. The final load increment occurs when 90% of the fibers have already failed. For $\rho = 1$, however, although breaks are initially dispersed up to the failure of slightly less than half of the fibers, the remaining fibers fail as a sharply growing cluster. For $\rho = 10$ there are just a few initial dispersed breaks, but then a sharply growing, catastrophic cluster develops near fiber number 600.

For $\rho = 1/2$, Figure 1.17 shows the break evolution sequence for the weakest and median among $N = 100$ δ-bundles with $n = 1500$ fibers. The weakest speci-

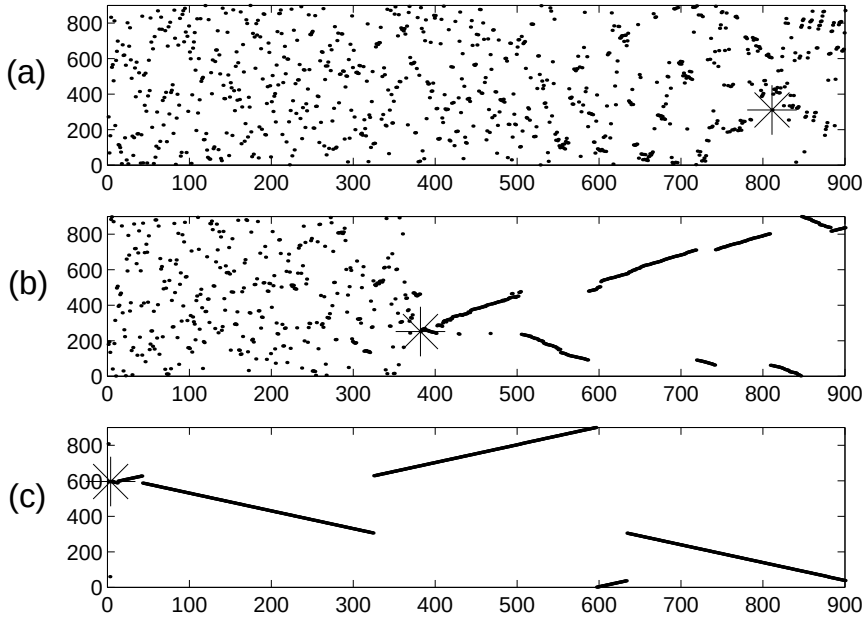

Figure 1.16: Fiber break sequence in median strength (among 500 simulations) 900-fiber δ-bundles under 1D HLLS with (a) $\rho = 0.5$, (b) $\rho = 1$ and (c) $\rho = 10$. A dot is plotted at coordinates (N_x, N_y) if fiber number N_y is the N_x-th to fail. The first fiber to fail with the last load increment is labeled $*$. The strengths of these specimen are 0.5089 for the $\rho = 0.5$ specimen, 0.3075 for $\rho = 1$, and 0.5964 for $\rho = 10$.

men develops a cascading cluster after about two-thirds of the fibers have failed. However, it develops considerable dispersion at the cluster edge and eventually stalls. Further load increments lead to additional dispersed failures followed by a final cascading cluster from a new location when only one-tenth of the fibers remain. The median 1500 fiber specimen, however, initiates cluster growth after about four-fifths of the fibers have failed and this cluster propagates without stalling until the composite fails.

Comparing with Figure 1.16, the conclusion from Figure 1.17 is that for small

ρ the cluster growth mode may not dominate until the δ-bundle reaches a certain large size well beyond the critical cluster size. Even then the network is drastically diluted by the dispersed failure mode. As it weakens with increasing size, however, we conjecture that the cluster growth mode will increasingly dominate, at least in 1D HLLS bundles.

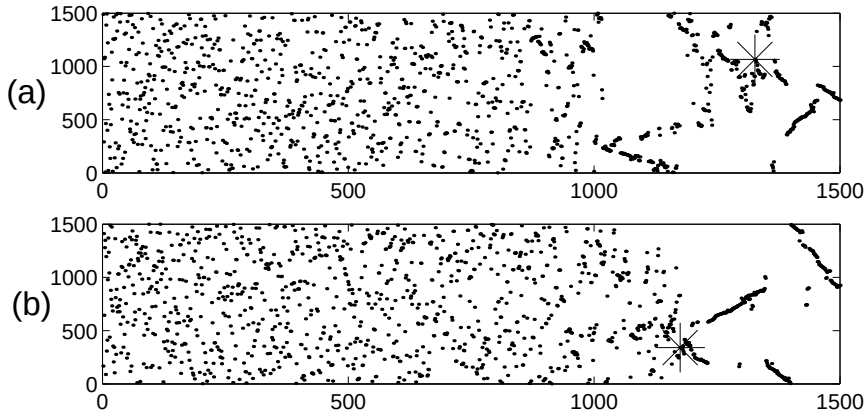

Figure 1.17: Fiber break sequence in a 1500 fiber δ-bundle under HLLS for $\rho = 0.5$: (a) weakest (lower tail) and (b) median specimen among 100 simulations. The strength of the weakest specimen is 0.3872 and of the median specimen is 0.5053. The first fiber to break with the last load increment is labeled $*$.

Although clusters may eventually form, there remains considerable dispersion and diluting of the number of intact fibers under ELS-like behavior. Thus the localized nature of the load-sharing rule is finally superimposed onto a diluted set of fibers following ELS failure statistics. One possibility for the breakdown mechanism is that local patches begin to break down following the statistics of a scale limited version of ELS, and if a patch is beyond critical size it propagates catastrophically. The statistics of the weakest ELS-like patch determines the strength distribution of the δ-bundle. A second possibility is that broad dilu-

tion of the number of surviving fibers occurs due to ELS-like behavior and local cluster growth eventually develops under a revised local load sharing mechanism on the randomly diluted set of survivors. Along these lines a 1D model under a tapered local load-sharing rule was recently developed by Phoenix and Beyerlein [33] where a weakest-link model with a characteristic distribution function $W(\sigma)$ was derived of the form given by Eq. (1.40) for 1D HLLS. In their work a nontrivial exponent arose from the local combinatorics of the dilution playing a role similar to the values of (η, γ) in Figures 1.13 and 1.15.

A model consistent with the first scenario is that failure initiates following an ELS-like failure mechanism in a patch of $\tilde{n}$ fibers smaller than n when sufficiently large. The strength of this patch has Gaussian character, and δ-bundle failure corresponds to the failure of the weakest of the $\tilde{m} = n/\tilde{n}$, $\tilde{n}$-fiber patches. That is,

$$G_n(\sigma) = 1 - \{1 - \Phi[(\sigma - \mu^*_{\tilde{n}})/s^*_{\tilde{n}})]\}^{\tilde{m}}, \tag{1.94}$$

where $\Phi(\cdot)$ denotes the standard normal distribution and $\mu^*_{\tilde{n}}$ and $\sigma^*_{\tilde{n}}$ are defined in Eqs. (1.92) and (1.93). For small σ, we may replace $\Phi(\cdot)$ with

$$\tilde{\Phi}(z) = \frac{1}{\sqrt{2\pi}\ |z|} \exp(-z^2/2), \tag{1.95}$$

which is the asymptotic form of the lower tail of the standard normal distribution. Likewise, that for the composite, $H_{m,n}(\sigma)$, is simply the above result with $\tilde{m}$ replaced by $m\tilde{m}$. Use of this result in other composite settings is found in [34]. The parameters of the Gaussian weakest-link distribution are given by the Smith corrected, Daniels formula Eq. (1.92) and (1.93).

In Figure 1.18, for $\rho = 1$, 2, 3, and 5 we have plotted the strength distribution of the smallest sized δ-bundle $(n_1 \times n_1)$ to which weak-link scaled distributions for

larger bundles collapse. This minimum δ-bundle size approximately corresponds to the critical cluster size defined previously. We also show the distributions of larger bundles of size $(n_2 \times n_2)$ or $(n_3 \times n_3)$ weak-linked to the size $(n_1 \times n_1)$. Note that as ρ is decreased, the weak-linked distributions become increasingly Gaussian (indicated by the straightness of the strength distribution on normal coordinates) and are better approximated by the ELS asymptotic distribution, though a shift exists for $\rho \geq 1$.

In the case $\rho = 0.5$, despite the excellent agreement of the 900-fiber, weak-linked strength distribution with the 625-fiber, weak-linked distribution, it turns out that they do not agree with a 2500-fiber, weak-linked δ-bundle strength distribution (of which limited results were generated but are not shown). This suggests that the smallest catastrophic failure event of the bundle occurs over more than 625 or perhaps even 900 fibers. The same may also hold in the $\rho = 1$ case. However, for $\rho \geq 2$, the maximum simulation cell size of $n = 30 \times 30$ seems to be adequate to contain the catastrophic failure event.

In the cases $\rho \leq 1$ it is unclear if the upper-tail, strong fiber dominance will continue for much larger bundles (with smaller strengths). Unfortunately, simulating such bundles is presently computationally infeasible. If it is so that the weakest link involves strong fibers and ELS dispersed failure over limited scale, Eq. (1.94) will hold for the δ-bundle strength distribution. If not, the weakest link mechanism will revert to the cluster growth model, though with dispersed fiber breaking ahead of the cluster tip, and Eq. (1.73) may hold when modified to account for the extensive dilution by fiber breaks.

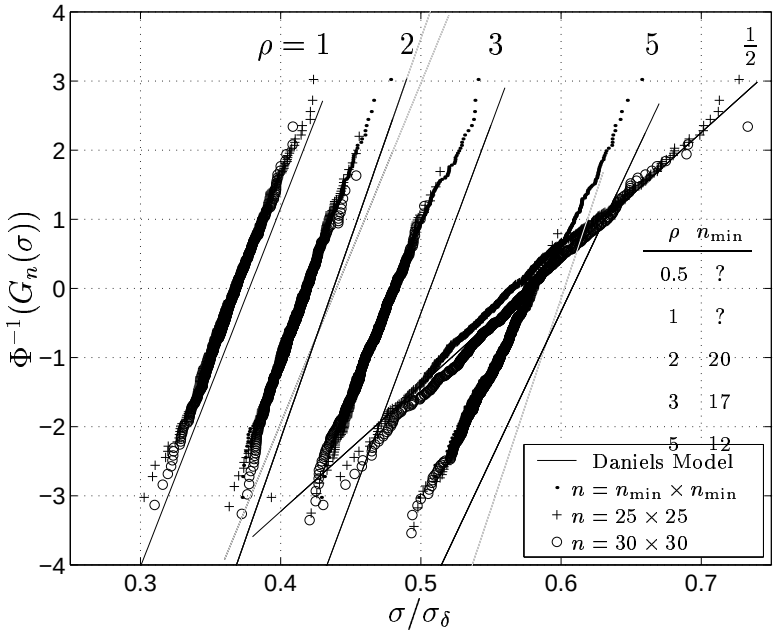

Figure 1.18: Comparison of $\Phi((\sigma - \mu_n^*)/s_n^*)$ given by Daniels' formula for ELS δ-bundles, Eq. (1.95), with weak-linked strength distributions obtained from simulations. Strength distributions for sizes $n = 625$ and 900 are weak-linked to size $n_{\min}^2$ as listed in the figure. For $\rho = 2$, 3, and 5, the distributions of $n = 625$ and 900 δ-bundles when weak-linked to size $n_{\min}^2$ appear to collapse into the strength distribution of a δ-bundle with $n_{\min}^2$ fibers chosen to be the smallest with this property. For $\rho = 0.5$ and 1 no such collapse is observed. For $\rho = 0.5$ the agreement of the strength distribution of the $n = 625$ δ-bundle and the $n = 900$ δ-bundle weak-linked to size 625 is spurious. Such agreement is not observed for a 2500 fiber δ-bundle weak-linked to size 625.

1.6 Analysis of Effect of ρ on Statistical Failure Mode

We have seen that δ-bundle failure for both 1D HLLS and 2D HVLLS shows a transition from a break cluster growth mode to a dispersed fiber failure mode somewhere in the neighborhood of $\rho = 1$ to 2. We now investigate certain statistical aspects of cluster growth that may suggest the potential for such a transition. While the stress concentrations on the neighbors of an r-cluster increase their probabilities of failure, the extent appears to depend on ρ thus influencing the onset of instability.

1.6.1 Effect of ρ on Tendency for Cluster Stalling

To investigate the effect of decreasing ρ on r-cluster growth, we add one break to form an $(r+1)$-cluster and let $\Delta(r, n')$ be the mean number of additional fibers among its n' nearest intact neighbors that will fail due to the increased load from the break, assuming all fibers have survived the previous load. We let the applied fiber stress σ be small enough that the fiber failure probability $F(K_r\sigma)$ from Eq. (1.1) is well approximated by $F(K_r\sigma) \approx (K_r\sigma/\sigma_\delta)^\rho$ in the case of Weibull fibers and is exact in the case of power-law fibers. Then,

$$\Delta(r, n') \approx n'(K_{r+1}^\rho - K_r^\rho)\,(\sigma/\sigma_\delta)^\rho\,. \tag{1.96}$$

Since $K_{r+1} > K_r > 1$, we see that $K_{r+1}^\rho - K_r^\rho$ is an increasing function of ρ so that for fixed n' and σ, $\Delta(r, n')$ increases with ρ. Thus, when ρ is small the addition of a fiber break to an r-cluster causes fewer neighbors to fail due to overloads.

We may specialize Eq. (1.96) to the case of a penny-shaped r-cluster in a 2D

planar fracture surface. In this case, $n' = 2\sqrt{\pi r}$ and we get using Eq. (1.16)

$$\begin{aligned}\Delta(r, 2\sqrt{\pi r}) &\approx 2\sqrt{\pi r}\left\{\left(1+\frac{2\sqrt{r+1}}{\pi^{3/2}}\right)^{\rho/2} - \left(1+\frac{2\sqrt{r}}{\pi^{3/2}}\right)^{\rho/2}\right\}\left(\frac{\sigma}{\sigma_\delta}\right)^{\rho}, \\ &\approx C_\rho r^{\frac{\rho}{4}-\frac{1}{2}}\left(\frac{\sigma}{\sigma_\delta}\right)^{\rho} \quad \text{for large } r.\end{aligned} \tag{1.97}$$

Thus the number of breaks around a large cluster tends to increases with r for $\rho > 2$ but decreases with r for $\rho < 2$ where the cluster will tend to stall.

This argument, however, does not account for the fact that the addition of a single break at the cluster edge will expose a few fibers in its vicinity to a much larger jump in stress of the order of from $(1/2)K_r\sigma/\sigma_\delta$ to $K_{r+1}\sigma/\sigma_\delta$, and the associated probability of failure for each of these is of order $(K_{r+1}\sigma/\sigma_\delta)^\rho$, which does not show this transition to an expected decrease as ρ decreases. This aspect of the problem may explain the need for Eq. (1.50), and the values of N_r based on the values η and γ given in Figures 1.13 and 1.15 seem reasonable in this light.

1.6.2 Effect of ρ on Break Dispersion Near Cluster Edge

Another important aspect to consider as ρ decreases is the location of new breaks due to an r-cluster introduced into a δ-bundle. Figure 1.19 shows a simulation of the fiber failures that immediately occur due to the presence of a penny-shaped cluster of $r = 239$ breaks introduced into a 2D δ-bundle under the numerical version HVLLS. In each of the four cases, the fiber strengths were derived from the same set of uniformly distributed random numbers U_i, so the Weibull strength of the j-th fiber in each case is $(-\log(U_j))^{1/\rho}$. The applied stress σ was chosen in each of the four cases so that the probability of failure of a fiber adjacent to the cluster edge was about 1/2, i.e., $(K_{239}\sigma/\sigma_\delta)^\rho \approx 0.69$, where $K_{239} = 2.56$ from Eq. (1.16). These breaks would typically cause even more breaks without a change

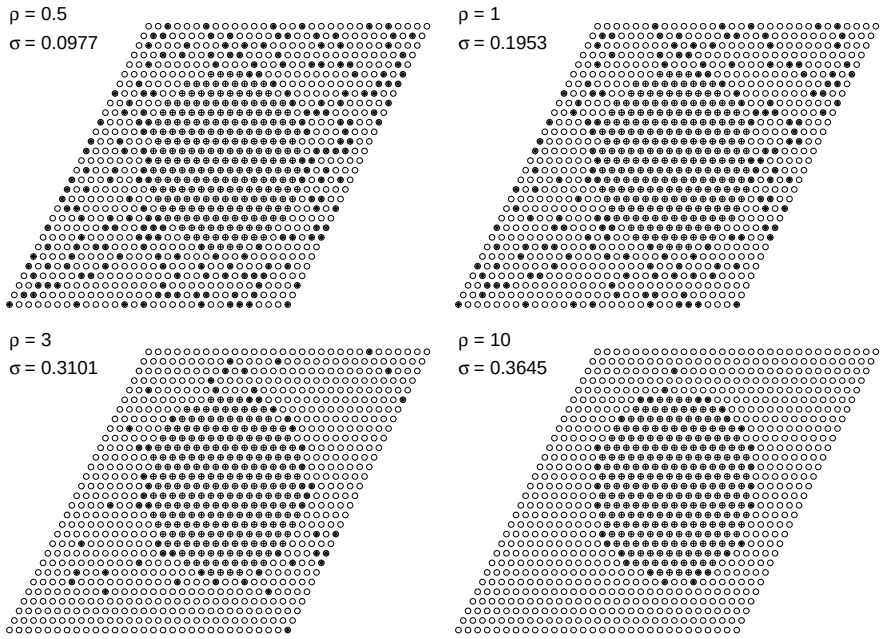

Figure 1.19: Transition from dispersed fiber failure to cluster enlargement around an initial, tight 239-break cluster, which occurs as ρ increases.

in applied load, but these secondary breaks are not shown. Observe that for the same approximate number of fiber failures in the ring around the cluster, serving to extend it, an increasing number of fibers fail away from the cluster as ρ is decreased. Many of the ones appearing for $\rho = 1/2, 1$ and 3 would have occurred anyway under the applied stress σ/σ_δ with probability $F(\sigma)$ given by Eq. (1.1). Nevertheless, as ρ decreases, dispersive effects at the edge begin to appear.

To understand these dispersive effects, we may evaluate the probability of failure of a fiber at distance s away from an r-cluster. Its probability of failure is $(K_{r,s}\sigma/\sigma_\delta)^\rho$ or, using Eq. (1.17),

$$\Pr\{\text{fiber failure at distance } s\} = \left(\frac{1}{1+\pi(s-1)}\right)^{\rho/2} \left(\frac{K_r\sigma}{\sigma_\delta}\right)^\rho . \tag{1.98}$$

This result holds approximately for $1 \le s \le \epsilon D$ where ϵ is about 1/10, and

$D = 2\sqrt{r/\pi}$ is the cluster diameter. This is roughly the range of influence of the cluster "tip" (analogous to the K-field in linear elastic fracture mechanics). Clearly the first factor in Eq. (1.98) increases with decreasing ρ and leads to an increased number of fiber failures away from the cluster edge as compared to fibers right at the edge ($s = 1$). Beyond this range the stress is close to the far field value, σ. In the present case $r = 239$, $D \approx 18$, and the range is $1 \leq s \leq 2$ covering just two fibers from the edge. Nevertheless one can see increasing numbers of breaks near the edge in the sub-adjacent neighbors as ρ decreases.

We can use Eq. (1.98) to illustrate a more subtle aspect of the effect of ρ as suggested in Figure 1.19. Suppose that as ρ is decreased, the applied stress σ is chosen such that $(K_r\sigma/\sigma_\delta)^\rho = C \ll 1$, where C is independent of ρ. We may estimate the number of fibers that immediately fail due to the introduction of the penny-shaped r-cluster where r is large. This requires evaluating the integral

$$\left(\frac{K_r\sigma}{\sigma_\delta}\right)^\rho \int_1^{\epsilon 2\sqrt{r/\pi}} \frac{2\pi(s+\sqrt{r/\pi})}{(1+\pi(s-1))^{\rho/2}} ds,$$

where $2\pi(s+\sqrt{r/\pi})$ is the number of fibers in a ring of radius $s+\sqrt{r/\pi}$ outside the cluster and the rest of the integrand is the probability of a fiber failure in that ring. Upon evaluating the integral we notice that the result asymptotically has the factor $r^{1-\rho/4}$. Thus as r increases this integral behaves differently for $\rho > 4$ versus $\rho \leq 4$, converging in the former case and diverging in the latter. This suggests that as ρ decreases below 4, in the vicinity of a large 2D break cluster under HVLLS, new breaks are more likely away from the cluster than around its edge. Repeating this calculation for a 1D cluster of r breaks under HLLS, one finds that $\rho = 2$ is the transition value for divergence.

On the other hand, as a δ-bundle fails when σ is increased, intact fibers will typically have survived previous stress levels. Thus a variant of the above calcula-

tion is to assume that all fibers have been "proof-tested" just enough to support stress σ on the δ-bundle *with* the penny-shaped r-cluster, and that a small stress increment $\Delta\sigma$ is required to induce failures. It can be shown that ρ effectively is replaced by $\rho - 1$ in the result so the threshold for divergence increases to $\rho = 5$ in 2D HVLLS and $\rho = 3$ in 1D HLLS.

[43] conducted an investigation somewhat like the one above, except that he concentrated on the stress transferred from only one break to other fibers over the whole composite. In the plane of the break this overload scales as s^{-2} in the 1D HLLS case and s^{-3} in 2D HVLLS. To this he added the applied stress σ, which the fibers were assumed to have previously survived. Because he integrated the decaying overload along fibers (far outside our δ-bundles) he concluded for all $\rho > 0$ that divergence occurs in the number of flaws broken in all fibers over the whole composite due to one break. However, repeating his calculation over fibers within a δ-bundle leads to convergence for all $\rho > 0$, so little insight into the role of ρ is gained without focusing on large clusters with $1/\sqrt{s}$ fiber stress decay at their edges.

These arguments indicate that during δ-bundle failure under increasing σ, the tendency towards dispersed fiber failures versus cluster growth increases as ρ decreases, but the values of ρ determined above are too high to directly explain the transition. Also, when ρ is small, the probability of finding very weak fibers below strength σ is much more than when ρ is large, and thus many dispersed fiber breaks are to be expected. This aspect appears to be borne out by Figures 1.3 and 1.7, and Figure 1.19 as well as by inspection of many simulations.

In addition to ρ, the number of fibers n in the δ-bundle also plays a role in the occurrence of a dispersed versus a cluster growth failure mode. Smaller composites

tend to be stronger, and thus, show a higher proportion of dispersed fiber breaks caused by the applied stress σ. Also, clusters are smaller when they become unstable. In larger composites, the cluster size required for instability is larger, mainly because the applied stress σ is smaller (i.e., the composite is weaker) and a higher stress concentration at the cluster edge is needed to fail fibers. Nevertheless, it appears that no matter how large the cluster is before instability, the tendency when ρ is small is to form dispersed breaks at the cluster edge as it grows, thus spreading the stress redistribution.

1.7 Conclusions and Relations to Other Results

In Eqs. (1.40) and (1.73) we have the weakest-link, characteristic distribution function $W(\sigma)$ for 1D and 2D δ-bundles under HLLS and HVLLS, respectively. These bundles are links in the chain-of-bundles model for the failure of large 2D and 3D unidirectional composites, respectively. For sufficiently large Weibull modulus ρ, say $\rho > 2$ in 3D composites and $\rho > 1$ in 2D planar composites, the strength distribution of a composite of length $L = m\delta$ and with n fibers is $H_{m,n}(\sigma) \approx 1 - (1 - W(\sigma))^{mn}$. When ρ decreases below these values, however, the details of the load-sharing become increasingly unimportant, and the δ-bundle strength distribution for fixed n is not only increasingly Gaussian up to quite large n but also converges to that for ELS whose analytical form was given. For fixed ρ, however, this Gaussian nature is expected to persist only up to a δ-bundle size of the order of the critical cluster size increased to eliminate the likelihood of stalling. Then the distribution function for δ-bundle strength appears to be that for a chain of Gaussian 'patches' of $\tilde{n}$ fibers in the δ-bundle, particularly under 2D HVLLS.

Thus the composite can be viewed as a weakest-link arrangement of $m\tilde{m}$ such Gaussian patches. As the number of fibers n in the composite increases by orders of magnitude, it is not clear that this Gaussian nature will persist, especially in 1D HLLS.

Simpler versions of the form for $W(\sigma)$, Eq. (1.40), have been derived in related failure models where elements have strength 0 or 1 with probability p and $1-p$, respectively. See for example [13], [20] and [33], where in the latter two works power prefactors were obtained in $W(\sigma)$ as here. Very recent work, carried out by Wu and Leath [44, 45] under similar assumptions, has yielded distribution forms very similar to those here. Earlier versions are also given in [32]. In the time dependent setting, analogous versions, $W(t)$, have been obtained without a power prefactor by [10] and [11], and with a power factor by [31]. In these works hard transitions to Gaussian lifetime behavior were noted when a breakdown parameter decreased below a certain critical value.

Fiber break clusters need not lie in a transverse plane but can wander out of plane since new breaks can form next to old ones anywhere within length δ. However the tendency towards alignment is fairly strong unless the variability in fiber strength is large. Nevertheless, the idea of using a single length-scale δ for fiber load transfer may be unrealistic when large break clusters develop before instability. Thus the chain-of-bundles concept may be too restrictive in certain cases and the load-sharing model may require revision beyond using the fiber load values obtained along a single break plane.

To account for some of these features, simulation results have been generated by [26] for a true 3D model using a modified, square array version of HVLLS with eight matrix shear couplings rather than four. Their results were successfully

modeled by [32] using the Gaussian-link approach of the dispersed failure mode at the end of the last section, but generalized to elastic global load-sharing. Using the $W(\sigma)$ cluster growth approach here [32] were only able to model quite well their results for $\rho = 20$ but not $\rho = 10$ and 5 where misfits similar to those appearing in Figure 1.13 occurred. As here, using Eq. (1.50) for N_r and adjusting γ and η may greatly improve the fit, but nevertheless, the range for ρ corresponding to a dispersed failure mode may have a higher transition value than observed here.

We also mention work by [24] for a lattice-based model similar to HVLLS but with the added features of fiber slip and pullout at breaks causing tractions across the final fracture plane. Their Monte Carlo simulation results for $\rho = 5$ and 10 were successfully modeled using the Gaussian-link approach of the dispersed failure mode described at the end of the previous section, but generalized to global load-sharing as in [8] and [34]). Using a version of the cluster growth model here, which assumes $\gamma = 1/2$ in $W(\sigma)$, [32] were able to model fairly well their results for $\rho = 10$ but not $\rho = 5$ where misfits occurred similar to those appearing in Figure 1.13. Again, using Eq. (1.50) and adjusting γ and η may greatly improve the fit but once more the transition ρ value for a dispersed failure mode may be higher than observed here. In practice there may actually be considerable overlap in the ranges for ρ where the two models may apply.

We have set the length of a δ-bundle to be δ of Eq. (1.9). In reality this definition tends to produce too large a composite failure probability in the chain-of-bundles model because of the stress decay along a fiber from its peak in actual composites. This reduces the probability of finding a flaw. A more realistic definition of δ involves ρ (or one can modify the definition of K_r also involving ρ) as discussed in [32]. Except for a shift in stress scale and change in the value of m,

revising the definition of δ has negligible effect on our results. Although we use the same characteristic length scale, δ, in HLLS and HVLLS, the physical decay length along a fiber is about one-half that in the HLLS case for the same volume fraction of fiber since there are three times as many fiber-to-fiber couplings in HVLLS.

Bibliography

[1] Argon, A.S. (1974). Statistical Aspects of Fracture. *in Fracture and Fatigue, L. J. Broutman, ed., Academic Press, New York*, pp. 153–190

[2] Batdorf, S.B. (1982). Tensile strength of unidirectionally reinforced composites. *International Journal Reinforced Plastics and Composites* **1**, pp. 153–164.

[3] Batdorf, S.B. and Ghaffarian, R. (1982). Tensile strength of unidirectionally reinforced composites II. *International Journal of Reinforced Plastics and Composites* **1**, pp. 165–176.

[4] Beyerlein, I.J. and Phoenix, S.L. (1997a). Statistics of fracture for an elastic notched composite lamina containing Weibull fibres – Part I. Features from Monte-Carlo simulations. *Engineering Fracture Mechanics* **57**, pp. 241–265.

[5] Beyerlein, I.J. and Phoenix, S.L. (1997b). Statistics of fracture for an elastic notched composite lamina containing Weibull fibres – Part II. Probability models of crack growth. *Engineering Fracture Mechanics* **57**, pp. 267–299.

[6] Beyerlein, I.J., Phoenix, S.L., and Sastry, A.M. (1996). Comparison of shear-lag theory and continuum fracture mechanics for modeling fiber and matrix stresses in an elastic cracked composite lamina. *International Journal of Solids and Structures* **33**, pp. 2543–2574.

[7] Coleman, B.D. (1958). On the strength of classical fibres and fibre bundles. *Journal of the Mechanics Physics of Solids* **7**, pp. 60–70.

[8] Curtin, W.A. (1991). Theory of mechanical properties of ceramic matrix composites. *Journal of the American Ceramic Society* **74**, pp. 2837–2845.

[9] Curtin, W.A. (1999). Stochastic damage evolution and failure in fiber-reinforced composites. *Advances in Applied Mechanics* **36**, pp. 163–253.

[10] Curtin, W.A. and Scher, H. (1997). Time-dependent damage evolution and failure in materials. I. Theory. *Physical Review B* **55**, pp. 12038-12050.

[11] Curtin, W.A., Pamel, W., and Scher, H. (1997). Time-dependent damage evolution and failure in materials. II. Simulations. *Physical Review B* **55**, pp. 12051–12061.

[12] Daniels, H.E. (1945). The statistical theory of the strength of bundles of threads I *Proceedings of the Royal Society. London A* **183**, pp. 405–435.

[13] Duxbury, P.M. and Leath, P.L (1987). The failure distribution in percolation models of breakdown. *Journal of Physics A: Mathematical and General* **20**, pp. L411–L415.

[14] Goda, K. and Phoenix, S. L. (1994). Reliability approach to the tensile strength of unidirectional CFRP composites by Monte-Carlo simulation in a shear-lag model. *Composite Science and Technology* **50**, pp. 457–468.

[15] Goda, K. (1999). The role of interfacial debonding in increasing the strength and reliability of unidirectional fibrous composites. *Composite Science and Technology* **59**, pp. 1871–1879.

[16] Gücer D.E. and Gurland, J. (1962). Comparison of the statistics of two fracture modes. *Journal of the Mechanics Physics of Solids* **10**, pp. 365–373.

[17] Harlow, D.G. and Phoenix, S.L. (1978a). The chain-of-bundles probability model for the strength of fibrous materials I : analysis and conjectures. *Journal of Composite Materials* **12**, pp. 195–214.

[18] Harlow, D.G. and Phoenix, S.L. (1978b). The chain-of-bundles probability model for the strength of fibrous materials II: a numerical study of convergence. *Journal of Composite Materials* **12**, pp. 314–334.

[19] Harlow, D.G. and Phoenix, S.L. (1981). Probability distributions for the strength of composite materials II: a convergent sequence of tight bounds. *International Journal of Fracture* **17**, pp. 60l–630.

[20] Harlow, D.G. and Phoenix, S.L. (1991). Approximations for the strength distribution and size effect in an idealized lattice model of material breakdown. *Journal of the Mechanics and Physics of Solids* **39**, pp. 173–200.

[21] Hedgepeth, J.M. (1961). Stress concentrations in filamentary structures. *NASA TND–882*.

[22] Hedgepeth, J.M. and Van Dyke, P. (1967). Local stress concentrations in imperfect filament composites. *Journal of Composite Materials* **1**, pp. 294–309.

[23] Hikami, F. and Chou, T.W. (1990). Explicit crack problem solutions of unidirectional composites: Elastic stress concentrations. *AIAA Journal* **22**, pp. 499–505.

[24] Ibnabdeljalil, M. and Curtin, W.A. (1997). Strength and reliability of fiber reinforced composites: Localized load-sharing and associated size effects. *International Journal of Solids and Structures* **34**, pp. 2649–2668.

[25] Kuo, C.C. and Phoenix, S.L. (1987). Recursions and limit theorems for the strength and lifetime distributions of a fibrous composite. *Journal of Applied Probability* **24**, pp. 137–159.

[26] Landis, C.M., Beyerlein, I.J. and McMeeking, R.M. (2000). Micromechanical simulation of the failure of fiber reinforced composites. *Journal of the Mechanics and Physics of Solids* **48**, pp. 621–648.

[27] Leath, P.L. and Duxbury, P.M. (1994). Fracture of heterogeneous materials with continuous distributions of local breaking strengths. *Physical Review B* **49**, pp. 14905–14917.

[28] Mahesh, S., Beyerlein, I.J. and Phoenix, S.L. (1999). Size and heterogeneity effects on the strength of fiber composites. *Physica D* **133**, pp. 371–389.

[29] Manders, P.W., Bader, M.G. and Chou, T.-W. (1982). Monte Carlo simulation of the strength of composite fibre bundles. *Fibre Science and Technology* **17**, pp. 183–204.

[30] McCartney, L.N. and Smith, R.L. (1983). Statistical theory of the strength of fiber bundles. *ASME Journal of Applied Mechanics* **105**, pp. 601–608.

[31] Newman, W.I. and Phoenix, S.L. (2001). Time-dependent fiber bundles with local load sharing. *Physical Review E* **63**, pp. 021507-1–20.

[32] Phoenix, S.L., and Beyerlein, I.J. (2000a). Statistical Strength Theory for Fibrous Composite Materials, *Chapter 1.19 in Vol. 1 (T.-W. Chou, ed.) of Comprehensive Composite Materials (A. Kelly and C. Zweben, series eds.), Pergamon - Elsevier Science*, pp. 559–639.

[33] Phoenix, S.L., and Beyerlein, I.J. (2000b). Distributions and size scalings for strength in a one-dimensional random lattice with load redistribution to nearest and next-nearest neighbors. *Physical Review E* **62**, pp. 1622–1645.

[34] Phoenix, S.L., Ibnabdeljalil, M. and Hui, C.-Y. (1997). Size effects in the distribution for strength of brittle matrix fibrous composites. *International Journal of Solids and Structures* **34**, pp. 545–568.

[35] Phoenix, S.L. and Smith, R.L. (1983). A comparison of probabilistic techniques for the strength of fibrous materials under local load-sharing among fibers. *International Journal of Solids and Structures* **19**, pp. 479–496.

[36] Rosen, B.W. (1964). Tensile failure of fibrous composites. *AIAA Journal* **2**, pp. 1985–1991.

[37] Scop, P.M. and Argon, A.S. (1967). Statistical theory of strength laminated composites. *Journal of Composite Materials* **1**, pp. 92–99.

[38] Scop, P.M. and Argon, A.S. (1969). Statistical theory of strength laminated composites II. *Journal of Composite Materials* **3**, pp. 30–47.

[39] Smith, R.L. (1980). A probability model for fibrous composites. *Proceedings of the Royal Society, London A* **372**, pp. 539–553.

[40] Smith, R.L. (1982). The asymptotic distribution of the strength of a series-parallel system with equal load sharing. *Annals of Probability* **10**, pp. 137–171.

[41] Smith, R.L. (1983). Limit theorems and approximations for the reliability of load-sharing systems. *Advances in Applied Probability* **15**, pp. 304–330.

[42] Smith, R.L., Phoenix, S.L., Greenfield, M.R., Henstenburg, R.B. and Pitt, R.E. (1983). Lower-tail approximation for the probability of failure of three-dimensional fibrous composites with hexagonal geometry. *Proceedings of the Royal Society, London A* **388**, pp. 353–391.

[43] Suemasu, H. (1982). An analytical study of probabilistic aspects of strength of unidirectional fiber reinforced composites under tensile loads. *Transactions of the Japanese Society for Composite Materials* **8**, pp. 29–36.

[44] Wu, B.Q., and Leath, P.L. (2000a). Fracture strength of one-dimensional systems with continuous disorder: a single-crack approximation. *Physical Review B* **61**, pp. 15028–15034.

[45] Wu, B.Q., and Leath, P.L. (2000b). Similarity of growing cracks in breakdown of heterogeneous planar interfaces. *Physical Review B* **62 no. 13**.

[46] Zhang, S.D., and Ding, E.J. (1996). Failure of fiber-bundles with local load-sharing. *Physical Review B* **53**, pp. 646–654.

[47] Zweben, C. (1968). Tensile failure of fiber composites. *AIAA Journal* **6**, pp. 2325–2331.

[48] Zweben, C. and Rosen, B.W. (1970). A statistical theory of material strength with application to composite materials. *Journal of the Mechanics and Physics of Solids* **18**, pp. 189–206.

Chapter 2

Asymptotic Strength of a Planar Local Load Sharing Composite with Discrete Fiber Strengths

2.1 Introduction

A unidirectional composite tape is a fiber-matrix assemblage in which long aligned continuous fibers made of one material are embedded in a planar matrix made of a different material. Commonly the fibers are stiff and brittle while the matrix is relatively compliant and ductile. When loaded in tension along the fiber direction, most of the applied load is carried by the stiff fibers. Some of these fibers may fail due to the loading. The role of the matrix is to transmit the load dropped at fiber breaks to other intact fibers in their vicinity.

The matrix accomplishes this load transfer mostly by undergoing deformation in shear. Its action of concentrating loads dropped by a broken fiber on fibers in

the near vicinity of the break is known as *local load sharing*. Transverse to the fiber direction in the plane of a fiber break, this produces large stress concentrations on the intact fibers nearest the break and possibly smaller ones on fibers further away. Along the fiber direction, it effects a stress recovery on the broken fiber to the far field applied load over a characteristic length scale δ. δ generally depends upon the geometry of the fiber arrangement in the matrix as well as the constitutive properties of the fiber, matrix and the interface.

Various local load sharing models have been proposed. The simplest model, used in this work is the idealized local load sharing model due to Harlow and Phoenix [1]. In this model, the overload on an intact fiber adjacent to ℓ fiber breaks summing on both sides in a planar tape is assumed to be $K_\ell = 1 + (\ell/2)$. This amounts to assuming that each broken fiber simply transfers half its load to each of its two nearest intact neighbors in the same transverse plane. If the load applied to the composite per fiber is x, an intact fiber adjacent to ℓ broken fibers will carry load $(1 + (\ell/2))x$. A more realistic model for elastic fibers in an elastic matrix is due to Hedgepeth [2]. Hedgepeth uses shear-lag arguments to deduce the stress and displacement fields due to a single break and derives the stress field due to multiple breaks by a weighted superposition of the single break solutions.

Owing to the presence of small crack-like flaws of varying strength present in fibers, fiber strength often tends to show considerable variability. The Weibull distribution is often used to fit experimental fiber strength data.

$$F(x) = \Pr\{X \leq x\} = 1 - \exp\left(-(L/L_0)(x/x_0)^\rho\right), \quad , x \geq 0. \tag{2.1}$$

Here ρ is the shape parameter, x_0 the scale parameter, L the fiber length and L_0 the gauge length of the test. If $x \ll x_0$, the Weibull distribution is well approximated

by the power law distribution

$$F(x) \approx \frac{L}{L_0}\left(\frac{x}{x_0}\right)^{\rho}. \tag{2.2}$$

In this paper, we are concerned with the strength distribution of large idealized local load sharing composite tapes. Following numerous previous studies, we slice the composite longitudinally into *bundles* of length 2δ and make the so called "chain-of-bundles" assumption. Since stress recovery in a broken fiber is nearly complete within length δ on either side of the break, we assume that the bundle strengths are mechanically and statistically independent of each other. Thus we assume that the composite fails when the weakest of its independent bundles fails. More formally, if an L-long n-fiber composite is subjected to tensile strength x per fiber and the strength distribution of each of its $m = L/(2\delta)$ bundles is $G_n(x)$, then composite strength distribution is given by

$$H_{m,n}(x) = 1 - (1 - G_n(x))^m, \quad x \geq 0. \tag{2.3}$$

The problem is therefore reduced to determining $G_n(x)$ under idealized local load sharing given the strength distribution $F(x)$ of the individual fibers.

Harlow and Phoenix [1] first recognized the existence of a weakest link basis to bundle strength by exactly evaluating the strength distribution of small planar bundles under a continuous distribution $F(x)$ for fiber strength. They found numerically that there is a characteristic distribution function $W(x)$ independent of n such that

$$W_n(x) \equiv 1 - (1 - G_n(x))^{1/n} \to W(x), \text{ for } x > 0, \text{ as } n \to \infty$$

and observed that convergence in relative terms was nearly complete for n as small as 9 when the fiber strength variability was typical. However they were

unable to evaluate the error in relative terms as is important in characterizing the lower tail behavior of $G_n(x)$. In [3], Harlow considers a bundle in which fiber strengths are either 0 or 1. He set up a primitive recursion matrix which gave the probability of failure of a $j+1$-fiber composite given the probability of failure of an j-fiber composite and using the Perron-Frobenius theorem proved the existence of the characteristic distribution function and related the speed of convergence of $1-(1-W(x))^n$ to $G_n(x)$ to the relative magnitudes of the largest and second largest eigenvalues of this matrix. This same approach was used by Harlow and Phoenix [4] to determine tight bounds on the probability of occurrence of a k-cluster when composite size, n is large. Kuo and Phoenix [5] considered the more general case in which fiber strengths are continuously distributed and by means of a recursion analysis, obtained the characteristic distribution function as the largest eigenvalue of a sparse infinite matrix. Harlow and Phoenix [6] applied the Chen-Stein method to the composite with 0-1 fiber strength and obtained an expression for the asymptotic strength as composite size increases together with a tight error bound. Leath and Duxbury [7] gave an alternative approach to doing this with similar results.

In this work, we begin with an n-fiber bundle under idealized local load sharing whose fibers can take on one of $r \ll n$ distinct strengths following a prescribed discrete distribution. Specifically we suppose that the fiber strengths $(S_i, i \in \{1,2,\ldots,n\})$ are i.i.d. and distributed according to $\mathbf{P}\{S_1 = \sigma_j\} = \beta_j$, $j = 0,1,\ldots,r$ and $\sigma_0 < \sigma_1 < \cdots < \sigma_r$. Using the idealized local load sharing model we may determine integers ℓ_j, $j = 0,1,\ldots,r$ such that $(1+(\ell_j-1)/2)x < \sigma_j \leq (1+(\ell_j/2))x$. As will be shown in Section 2.3, we may assume that $\ell_0 < \ell_1 < \cdots < \ell_r$ and that $\sigma_0 < x < \sigma_1$ so that $\ell_0 = 0$. All other cases are

either trivial or readily collapsible into this case. Our first main result loosely states that the probability of bundle failure, $\mu_r(n)$ is approximately

$$\mu_r(n) \approx C\ell_1(\ell_2-\ell_1)\cdots(\ell_r-\ell_{r-1})(n-\ell_r)$$
$$\beta_0^{\ell_1}(\beta_0+\beta_1)^{\ell_2-\ell_1}\cdots(\beta_0+\beta_1+\cdots+\beta_{r-1})^{\ell_r-\ell_{r-1}}$$

provided $\min(\ell_1, \ell_2-\ell_1, \ldots, \ell_r-\ell_{r-1}, n-\ell_r)$ is sufficiently large. Here C is a constant that depends only on $\beta_0, \beta_1, \ldots, \beta_r$ and not on any of the ℓ_j's.

Our second main result deals with bounds on bundle failure probability when fiber strengths are continuously distributed according to a power law distribution. This bound is obtained by sandwiching the power law distribution between two discrete strength distributions and applying the first result. It is also found that this bound is tight.

2.2 The Chen-Stein Method

As described by Arratia et al [8], the Chen-Stein method of Poisson approximation is a powerful tool for computing an error bound when approximating probabilities using the Poisson approximation. Let I be an arbitrary index set and suppose $\{Y_i, i \in I\}$ are $0-1$ Bernoulli random variables with $p_i = \mathbf{P}\{Y_i = 1\} > 0$. Then $p_i = \mathbf{E}[Y_i]$ and we let

$$\lambda = \sum_{i\in I} p_i \text{ and } T = \sum_{i\in I} Y_i. \tag{2.4}$$

Also let W be a Poisson random variable with mean $\lambda \in (0,\infty)$. For each $i \in I$ let J_i denote an arbitrarily chosen set of *near neighbors* of i and let

$$V_i = T - \sum_{j=J_i} Y_j \tag{2.5}$$

We think of J_i as the neighborhood of dependence of i such that Y_i is independent or nearly independent of Y_j for $j \notin J_i$. Then for $A \subseteq \mathbb{Z}_+$, the Chen-Stein theorem asserts that

$$\begin{aligned} |\mathbf{P}\{T \in A\} - \mathbf{P}\{W \in A\}| &\leq \Delta f \sum_{i \in I} \sum_{j \in J_i} p_i p_j + \Delta f \sum_{i \in I} \sum_{j \in J_i} \mathbf{E}[Y_i Y_j] \\ &\quad + \left| \sum_{i \in I} \mathbf{E}\left\{ (Y_i - p_i) f(V_i + 1) \right\} \right| \\ &= b_1 + b_2 + b_3 \end{aligned} \tag{2.6}$$

where f is a function for which $\|f\| \leq \min(1, 1.4\lambda^{-1/2})$ and $\Delta f \leq \min(1, 1/\lambda)$. The b_1, b_2, b_3 notation follows from Arratia et al [8]. Loosely b_1 measures the neighborhood size, b_2 the expected number of neighboring occurrences of a given occurrence and b_3 the dependence between an event and the number of occurrences outside its neighborhood of dependence.

2.3 The Discrete Fiber Strength Bundle

Let $I = \{1, 2, \ldots, n\}$ be an index set and let $(Z_i : i \in I)$ be i.i.d. random variables distributed according to $\mathbf{P}\{Z_i = 0\} = \beta_0 \equiv \alpha$, $\mathbf{P}\{Z_i = 1\} = \beta_1$, $\mathbf{P}\{Z_i = 2\} = \beta_2$, $\ldots$, $\mathbf{P}\{Z_i = r\} = \beta_r$ where $\alpha + \beta_1 + \beta_2 + \cdots + \beta_r = 1$, and $\beta_j > 0$ for $j = 0, 1, \ldots, r$. Since we repeatedly discuss the event $\bigcup_{j=q}^{p} \{Z_i = j\}$ where p and q are integers, with $0 \leq q < p \leq r$ in what follows, it is helpful to introduce a shorthand notation for it. We will henceforth take the shorthand $\{Z_i \in p_q\}$ to be synonymous with $\{Z_i \in \{q, q+1, \ldots, p\}\}$. Then $\mathbf{P}\{Z_i = p_q\} = \sum_{j=q}^{p} \beta_j$. For example, if we specify $\{Z_i = 3_1\}$, it implies the event $\{Z_i = 1\} \cup \{Z_i = 2\} \cup \{Z_i = 3\}$. Also let us define

$$\gamma_j := \frac{\alpha}{\alpha + \beta_1 + \cdots + \beta_j} \tag{2.7}$$

for $j = 1, 2, \ldots, r$ and $\gamma_0 = 1$.

Consider an n-fiber bundle whose fibers are indexed by the set I. Let the strength S_i of its i-th fiber be σ_{Z_i} where $0 \leq \sigma_0 < \sigma_1 < \sigma_2 < \cdots < \sigma_r$ are arbitrary but fixed real numbers. Let this composite be subjected to far-field tensile stress nx in the fiber direction so that the normalized stress per fiber is x. If $x < \sigma_0$ or $\sigma_r \leq x$, all the fibers and hence the bundle survive or fail respectively with probability 1. If however $\sigma_0 \leq x < \sigma_r$, the applied stress x causes partial failure of the bundle by breaking those fibers whose strength is smaller than x. To ensure force equilibrium, the failure of these fibers must overload intact fibers. We assume that this overloading occurs according to the local load sharing rule described below. Some of the overloaded fibers may fail and produce even greater overloads on the remaining intact fibers. This process of fiber breaking and intact fiber overloading may possibly lead up to failure of all the fibers in the bundle, which we take to be the same as bundle failure.

Define non-negative integers $(\ell_j \in \mathbb{Z}_+ : j = 0, 1, \ldots, r)$ such that $(1 + (\ell_j - 1)/2)x < \sigma_j \leq (1 + (\ell_j/2))x$ if $\sigma_j \geq x$ and $\ell_j = 0$ if $\sigma_j < x$. That is, ℓ_j is the smallest number of broken neighbors that must surround an intact fiber of strength σ_j in order to overload it to failure. We may assume $\ell_0 < \ell_1 < \ell_2 < \cdots < \ell_r$ for if $\ell_j = \ell_{j+1}$ for some $j \in \{0, 1, 2, \ldots, r-1\}$ then fibers of strength σ_j and σ_{j+1} are indistinguishable in terms of their failure behavior at fixed applied x and we may eliminate one, say ℓ_{j+1} from consideration and set $\mathbf{P}\{Z_i = j\} = \beta_j + \beta_{j+1}$.

Let X_n denote the smallest applied tensile stress x at which the bundle fails; X_n is then called the bundle strength. We seek the distribution function $G_n(x) = \mathbf{P}\{X_n \leq x\}$ for $x \geq 0$. The analysis is readily extended to a network, which we view as a chain of m statistically and structurally independent bundles, each

consisting of n fibers. The distribution of network strength $X_{m,n}$ is readily derived once $G_n(x)$ is known: $H_{m,n}(x) = \mathbf{P}\{X_{m,n} \leq x\} = 1 - (1 - G_n(x))^m$, for $x \geq 0$ due to the serial nature of the network.

The problem of $G_n(x)$ determination is the subject of this paper. For the purpose of a better overview, we give here a short sketch of the arguments made to this end in the following sections. In what follows, a *sub-bundle* will refer to a continuous portion of the n-fiber bundle. We begin in Section 2.4 by evaluating the probability of failure of a sub-bundle within which fibers are restricted to have strengths σ_0 and σ_1 (such a sub-bundle will be called a 0-1 sub-bundle). The approach follows that of Harlow and Phoenix [6] although we pay more attention here to the boundary effects. Then in Section 2.5 we consider all the possible ways in which a sub-bundle whose fibers are allowed strengths σ_0, σ_1 and σ_2 (a 0-1-2 sub-bundle) can fail. By evaluating the probability of each of these so called *failure configurations* we show that two of the configurations dominate the rest in the magnitude of their probability of occurrence. These two dominant 0-1-2 configurations contain a 0-1 sub-bundle in them; to evaluate the failure probability of the 0-1-2 sub-bundle one therefore needs the probability of failure of a 0-1 sub-bundle evaluated in Section 2.4 to arrive at the failure probability of a 0-1-2 sub-bundle. Continuing this process inductively to a 0-1-2-3 sub-bundle we have in that case another set of failure configurations all but two of whose probabilities turn out to be negligible as well. Carrying on in this manner, we finally arrive at (2.77) which is our main result for the strength of a 0-1-2-$\cdots$-r bundle. The error bounds on $\mu_r(n)$ become increasingly small as $\ell_1 \wedge (\ell_2 - \ell_1) \wedge \cdots \wedge (\ell_r - \ell_{r-1}) \wedge (n - \ell_r) \to \infty$.

2.4 Strength of a 0-1 Bundle

Let $I_1 = \{p, p+1, \ldots, p+n_1-1\} \subset I$, $p \leq n - n_1 + 1$ be the index set of a sub-bundle in the n-fiber bundle such that $Z_i = 1_0$ for $i \in I_1$, i.e., all the fibers within the sub-bundle indexed by I_1 have strength either σ_0 or σ_1. Let $Z_i, i \in I_1$ be distributed as stated in Section 2.3 so that the probability of occurrence of a sub-bundle consisting entirely of fibers with $Z_i = 1_0$ is $(\alpha + \beta_1)^{n_1}$ for any p. Let $n_1 \geq \ell_1$. We also define two imaginary fibers at positions $p-1$ and $p-2$ such that $Z_{p-1} = Z_{p-2} = 1$. Observe that the sub-bundle indexed by I_1 fails if and only if the sub-bundle indexed by $I_1 \cup \{p-2, p-1\}$ fails so that their probabilities of occurrence are equal. As will be seen shortly, these imaginary boundary fibers simplify the consideration of failure configurations close to the boundary while leaving the probability of failure of the sub-bundle unchanged.

We wish to approximate the probability of failure of this sub-bundle, which we shall refer to as a 0-1 bundle, using the Chen-Stein method. We begin by defining events associated with fiber $i \in I_1 \cup \{p-2, p-1\}$ that produce $Y_i = 1$ where Y_i is the dependent Bernoulli process defined in section 2.2. Following Harlow and Phoenix [6] we define $Y_i = 1$, $i \in I_1$ if $Z_i = 1$, $Z_{i+\ell_1+1} = 0$, $i + \ell_1 + 1 \in I_1$ and there is exactly one 1 amongst $Z_{i+1}, Z_{i+2}, \ldots, Z_{i+\ell_1}$. Otherwise we set $Y_i = 0$.

It is convenient to express this definition pictorially as

$$\begin{array}{ccccccc} i & & & & \downarrow & & \\ 1 & \underbrace{0 \quad \cdots \quad 0}_{0 \leq s < \ell_1} & & 1 & \underbrace{0 \quad \cdots \quad 0}_{\ell_1 - s} & & \end{array} \tag{2.8}$$

We will henceforth refer to such depictions of the definition of $Y_i = 1$ as failure configurations. Observe that we have not shown the $n_1 - (\ell_1 + 2)$ 1_0-fibers surrounding this configuration in the sub-bundle indexed by I_1. On this configu-

ration, we have marked fiber i and have also labelled the *pressured* element with a $\downarrow$. This pressured fiber is surrounded by at least ℓ_1 broken fibers so that it will fail. Note that the failure of the pressured fiber results in catastrophic failure of the 0-1 bundle since it implies that all other 1's in it will be overloaded as well.

Following the Chen-Stein method, we first evaluate $\mathbf{P}\{Y_i = 1\}$:

$$\mathbf{E}[Y_i] = \mathbf{P}\{Y_i = 1\} = \begin{cases} \alpha^{\ell_1}(\alpha+\beta_1)^{n_1-\ell_1} & \text{if } i = p-2, \\ \ell_1\beta_1\alpha^{\ell_1}(\alpha+\beta_1)^{n_1-(\ell_1+1)} & \text{if } i = p-1, \\ \ell_1\beta_1^2\alpha^{\ell_1}(\alpha+\beta_1)^{n_1-(\ell_1+2)} & \text{if } p \le i < p+n_1-\ell_1-1, \\ 0 & \text{if } i \ge p+n_1-\ell_1-1. \end{cases} \tag{2.9}$$

where $Y_{p-2} = 1$ if the event

$$\begin{array}{cccc} p-2 & p-1 & & \\ & \downarrow & & \\ 1 & 1 & \underbrace{0 \quad \cdots \quad 0}_{\ell_1} & \end{array} \tag{2.10}$$

which is a special case of (2.8) occurs and $Y_{p-1} = 1$ if the event (2.8) occurs with $i = p-1$. Also for $i \ge p+n_1-\ell_1$ configurations of the form (2.8) cannot occur since they necessarily specify ℓ_1+1 fibers to the right of the starting fiber of the configuration.

Observe that our special assignments $Z_{p-2} = Z_{p-1} = 1$ enable us to treat the special configurations associated with the left boundary as also being configurations of the form (2.8). If we set $\lambda_1 = \mathbf{E}[T] = \sum_{i=p}^{p+n_1-1} \mathbf{P}\{Y_i = 1\}$,

$$\lambda_1(n_1) = (n_1-\ell_1)(\ell_1\alpha^{\ell_1}\beta_1^2)(\alpha+\beta_1)^{n_1-(\ell_1+2)}\left\{1+O\left(\frac{1}{n_1-\ell_1}\right)\right\} \tag{2.11}$$

Then from (2.6) we approximately have $\mathbf{P}\{T=0\} \approx \exp(-\lambda_1)$ with error $b_1+b_2+b_3$ whose magnitude we presently bound. We first choose $J_i = \{j :$

$|j-i| \le \ell_1 + 1\}$ to be the neighborhood of dependence of fiber i. This choice for J_i gives $b_3 = 0$ because then Y_i and $\{Y_j : j \notin J_i\}$ are independent as there are no common fibers involved between them. Since V_i depends only on $\{Y_j : j \notin J_i\}$, Y_i and V_i are independent and therefore $b_3 = 0$. Also from (2.6) we have for b_1

$$\begin{aligned} b_1 &\le \min(1, 1/\lambda_1) 2(n_1 - \ell_1)(\ell_1 + 1)(\lambda_1/(n_1 - \ell_1))^2 \\ &= \min(1, 1/\lambda_1) 2(\ell_1 + 1) \frac{\lambda_1^2(n_1)}{(n_1 - \ell_1)} \end{aligned} \tag{2.12}$$

Here we have only multiplied by the factor $n_1 - \ell_1$ because $p_i p_j = 0$, when either $i > n_1 - \ell_1$ or $j > n_1 - \ell_1 - 1$ or both.

Bounding b_2 in (2.6) requires finding pairs of failure configurations such that $Y_i Y_j = 1$ for $j \in J_i$. For $0 \le s < \ell_1$, we have $Y_i Y_j = 1$ only for configurations of the form

$$\begin{array}{ccccccccccc} i & & & & j & & & & & & \\ & & & & \downarrow & & & & \downarrow & & \\ 1 & \underbrace{0 \cdots 0}_{0 \le s < \ell_1} & & 1 & \underbrace{0 \cdots 0}_{\ell_1 - s} & & \underbrace{0 \cdots 0}_{0 \le t < s} & 1 & \underbrace{0 \cdots 0}_{s-t} & & \\ \multicolumn{6}{c}{\overbrace{\qquad\qquad\qquad\qquad\qquad\qquad}^{Y_i}} & & & & & \\ & & & & \multicolumn{6}{c}{\overbrace{\qquad\qquad\qquad\qquad\qquad\qquad\qquad\qquad\qquad\qquad}^{Y_j}} \end{array} \tag{2.13}$$

which has, for fixed s, probability $s\beta_1^3 \alpha^{\ell_1 + s} (\alpha + \beta_1)^{n_1 - (\ell_1 + s + 3)}$ so that

$$\begin{aligned} \sum_{s=0}^{\ell_1 - 1} \mathbf{E}[Y_i Y_{i+s+1}] &\le \sum_{s=0}^{\ell_1 - 1} s\beta_1^3 \alpha^{\ell_1 + s} (\alpha + \beta_1)^{n_1 - (\ell_1 + s + 3)} \\ &\le \beta_1^3 \alpha^{\ell_1} (\alpha + \beta_1)^{n_1 - (\ell_1 + 3)} \sum_{s=0}^{\infty} s\gamma_1^s \\ &= \beta_1 \alpha^{\ell_1 + 1} (\alpha + \beta_1)^{n_1 - (\ell_1 + 2)} \end{aligned} \tag{2.14}$$

when $i \le p + n_1 - \ell_1 - 1$ and 0 otherwise. Also when $i = p - 2$ or $i = p - 1$, the

probability of those configurations is $\lambda_1 O(1/n - \ell_1)$. Therefore,

$$\begin{aligned} b_2 &\leq \min(1, 1/\lambda_1)(n_1 - \ell_1)\beta_1\alpha^{\ell_1+1}(\alpha+\beta_1)^{n_1-(\ell_1+2)} \\ &\leq \min(1, 1/\lambda_1)\frac{2\alpha\lambda_1}{\ell_1\beta_1} \end{aligned} \tag{2.15}$$

b_2 is therefore $\lambda_1 O(1/\ell_1)$ as $\lambda_1 \downarrow 0$. For small λ_1, $\exp(-\lambda_1) \approx 1 - \lambda_1$ and we may write the probability of failure of an n_1-fiber bundle, $\mu_1(n_1)$ including the Chen-Stein bound as

$$\begin{aligned} \mu_1(n_1) = (n_1 - \ell_1)(\ell_1\alpha^{\ell_1}\beta_1^2)(\alpha+\beta_1)^{n_1-(\ell_1+2)} \\ \left\{1 \pm O\left(\frac{1}{\ell_1} + \frac{1}{n_1 - \ell_1}\right)\right\} \end{aligned} \tag{2.16}$$

For reasons that will be clear at the end of the next section, we rewrite this as

$$\begin{aligned} \mu_1(n_1) = (n_1 - \ell_1)C_0\ell_1\alpha^{\ell_1}(\alpha+\beta_1)^{n_1-\ell_1} \\ \left\{1 \pm O\left(\frac{1}{\ell_1} + \frac{1}{n_1 - \ell_1}\right)\right\} \end{aligned} \tag{2.17}$$

where

$$C_0 = \frac{\beta_1^2}{(\alpha+\beta_1)^2} = (1-\gamma_1)^2$$

2.5 Strength of a 0-1-2 Bundle

In the previous section we approximated the failure probability of a 0-1 sub-bundle. As a first step towards an approximate formula for the probability of failure of a 0-1-2-$\cdots$-r bundle, for $r \geq 2$, we approximate in this section, the failure probability of the 0-1-2 sub-bundle, i.e., one whose fibers have $Z_i = 2_0$.

As in the previous section, let $I_2 = \{p, p+1, \ldots, p+n_2-1\} \subset I$ index a sub-bundle for some $p \leq n - n_2 + 1$ such that $Z_i = 2_0$ for $i \in I_2$. Let Z_i be distributed as stated in Section 2.3. Similar to the case of the 0-1 bundle, set $Z_{p-2} = Z_{p-1} = 2$

for fictitious fibers at positions $p-2$ and $p-1$ to simplify the consideration of boundary effects. As in the case of the 0-1 bundle, the sub-bundle indexed by I_2 fails if and only if the sub-bundle indexed by $I_2 \cup \{p-2, p-1\}$ fails. Also let $n_2 \geq \ell_2$.

Our procedure for approximating the failure probability of this sub-bundle is similar to that of the 0-1 bundle although it is more complicated. We begin by defining failure configurations in the 0-1-2 sub-bundle in Section 2.5.1 and in Section 2.5.2 we evaluate their probabilities. Section 2.5.3 is concerned with bounding the Poisson approximation error $b_1 + b_2 + b_3$.

2.5.1 Failure Configurations

The simplest failure configurations of the 0-1-2 sub-bundle are direct extensions of (2.8)

$$\begin{array}{cccc} i & & \downarrow & \\ 2_1 & \underbrace{0 \quad \cdots \quad 0}_{0 \leq s < \ell_1} & 2 & \underbrace{0 \quad \cdots \quad 0}_{\ell_2 - s} \end{array} \tag{2.18}$$

and

$$\begin{array}{cccc} i & & \downarrow & \\ 2 & \underbrace{0 \quad \cdots \quad 0}_{\ell_1 \leq s < \ell_2} & 2 & \underbrace{0 \quad \cdots \quad 0}_{\ell_2 - s}. \end{array} \tag{2.19}$$

In scanning the 0-1-2 sub-bundle from left to right if either of these configurations is found, we set $Y_i = 1$ and consider the sub-bundle failed. Besides these direct extensions, there are configurations in which a pressured fiber with $Z_i = 2$ is overloaded to failure by the first failure of a nearby 0-1 sub-bundle. In the following configurations,

$$\underbrace{1_0 \cdots 1_0 \, \langle 0\text{-}1 \rangle \, 1_0 \cdots 1_0}_{\ell_2 - s}$$

denotes a failing 0-1 sub-bundle with $\ell_2 - s$ fibers and L is taken as a positive integer such that $L < \ell_1 \wedge \ell_2 - (\ell_1 + 1)$. In this representation, $\langle$0-1$\rangle$ denotes the 0-1 failure configuration (2.8). It turns out later that optimally $L = -\log_{\gamma_1}(\min(\ell_1, \ell_2 - (\ell_1 + 1)))$.

$$\begin{array}{cccc} & i & & \downarrow \\ 2_1 & \underbrace{0 \quad \cdots \quad 0}_{0 \le s < L} & 2 & \underbrace{1_0 \cdots 1_0 \, \langle\text{0-1}\rangle \, 1_0 \cdots 1_0}_{\ell_2 - s} \end{array} \tag{2.20}$$

$$\begin{array}{cccc} & i & & \downarrow \\ 2_1 & \underbrace{0 \quad \cdots \quad 0}_{L \le s < \ell_1 \wedge (\ell_2 - (\ell_1 + 1))} & 2 & \underbrace{1_0 \cdots 1_0 \, \langle\text{0-1}\rangle \, 1_0 \cdots 1_0}_{\ell_2 - s} \end{array} \tag{2.21}$$

$$\begin{array}{cccc} & i & & \downarrow \\ 2 & \underbrace{0 \quad \cdots \quad 0}_{\ell_1 \le s < \ell_2 - (\ell_1 + 1)} & 2 & \underbrace{1_0 \cdots 1_0 \, \langle\text{0-1}\rangle \, 1_0 \cdots 1_0}_{\ell_2 - s} \end{array} \tag{2.22}$$

$$\begin{array}{ccccc} & & i & & \downarrow \\ 2_1 & \underbrace{0 \quad \cdots \quad 0}_{0 \le t < s} & 2 & \underbrace{1_0 \cdots 1_0 \, \langle\text{0-1}\rangle \, 1_0 \cdots 1_0}_{\ell_2 - s} & 2 \quad \underbrace{0 \quad \cdots \quad 0}_{1 \le s < L} \end{array} \tag{2.23}$$

$$\begin{array}{cccc} & i & & \downarrow \\ 2 & \underbrace{1_0 \cdots 1_0 \, \langle\text{0-1}\rangle \, 1_0 \cdots 1_0}_{\ell_2 - s} & 2 & \underbrace{0 \quad \cdots \quad 0}_{L \le s < \ell_2 - (\ell_1 + 1)} \end{array} \tag{2.24}$$

Or, the 0-1-2 sub-bundle can fail by failing a pressured 2 by the failure of two 0-1 sub-bundles:

$$\begin{array}{cccc} & i & & \downarrow \\ 2 & \underbrace{1_0 \cdots 1_0 \, \langle\text{0-1}\rangle \, 1_0 \cdots 1_0}_{\ell_1 + 2 \le s < \ell_2 - (\ell_1 + 1)} & 2 & \underbrace{1_0 \cdots 1_0 \, \langle\text{0-1}\rangle \, 1_0 \cdots 1_0}_{\ell_2 - s} \end{array} \tag{2.25}$$

Failure configurations of a 0-1-2 bundle need not necessarily have a 2 at the pressured position. The following are valid failure configurations in that their presence

signifies 0-1-2 bundle failure, but which are not counted by the failure configurations listed hitherto. In such cases, we take the 0-1 bundle's failure configuration as the pressured element.

$$\begin{array}{ccccc} & & i & & \downarrow \\ \underbrace{0 \ \cdots \ 0}_{\ell_2-\ell_1-s-1} & 2 & \underbrace{1_0 \ \cdots \ 1_0}_{0\vee(\ell_2-2\ell_1)\le s<\ell_2-(\ell_1+2)} & & \underbrace{\langle 0\text{-}1\rangle \ 1_0 \ \cdots \ 1_0}_{\ell_2-s} \end{array} \tag{2.26}$$

$$\begin{array}{ccccc} & & i & & \downarrow \\ 2 & & \underbrace{1_0 \ \cdots \ 1_0}_{\ell_2-(\ell_1+2)\le s<\ell_2} & & \underbrace{\langle 0\text{-}1\rangle}_{\ell_1+2} \end{array} \tag{2.27}$$

and indeed, a sufficiently long failing 0-1 bundle can double as a failing 0-1-2 sub-bundle as well.

$$\begin{array}{ccc} i & & \downarrow \\ \underbrace{1_0 \ \cdots \ 1_0}_{\ell_2} & & \underbrace{\langle 0\text{-}1\rangle}_{\ell_1+2} \end{array} \tag{2.28}$$

A few remarks about these configurations are in order. Firstly, we claim that the above collection of failure configurations is exhaustive in that a failing sub-bundle of $Z_i = 2_0$, $i \in I_2$ fibers must contain at least one of the configurations listed above. Secondly, not all the above listed configurations are possible for arbitrary ℓ_1 and ℓ_2. If, for instance $\ell_1 > \ell_2 - (\ell_1 + 1)$, the configurations (2.22) and (2.25) are impossible. Thirdly, notice that in configurations (2.23) and (2.26) we specify certain fibers to the left of fiber i whereas in the other configurations, we do not do so. This is done to reduce overlap between configurations so that the dominating part of the Poisson approximation error, b_2 can be kept small in comparison to the probability of bundle failure. Without fibers to the left of fiber i in (2.23), we

have the configuration $2\ \ 1_0 \cdots 1_0\ \ 2\ \ 0 \cdots 0$ which may overlap (2.20) as

$$\begin{array}{ccccccccc} i & & j & & & & & & \\ & & \downarrow & & & & \downarrow & & \\ 2_1 & \underbrace{0 \quad \cdots \quad 0}_{0 \le s_1 < L} & 2 & \underbrace{1_0 \ \cdots \ 1_0 \ \langle 0\text{-}1 \rangle \ 1_0 \ \cdots \ 1_0}_{\ell_2 - s_1} & & \underbrace{1_0 \ \cdots \ 1_0}_{\ell_2 - s_2 + s_1} & 2 & \underbrace{0 \quad \cdots \quad 0}_{1 \le s_2 < L} & \end{array}$$

and results in b_2 being of the order of the probability being estimated. Using the methods of the next section, the probability of this event may be seen to be of order comparable to the probability of occurrence of either (2.20) or (2.23) which dominate the probability being estimated. Since a tight error bound is desired, this possibility is to be avoided.

2.5.2 Failure Probability

The probability of occurrence of any of the various failure configurations listed in section 2.5.1 depends on $i \in I_2$. Since each configuration specifies at least $\ell_2 + 2$ fibers to the right of fiber i,

$$Y_i = 0 \quad \text{for } i \ge p + n_2 - \ell_2 - 1$$

Let $L \le i < p + n_2 - \ell_2 - 1$. For this case we now evaluate the probability of configurations (2.20) and (2.23) and show that these are the dominant failure configurations in that their probability of occurrence is of higher order than that of all other failure configurations listed in Section 2.5.1.

From (2.20) and (2.17) we have

$$\begin{aligned}\mathbf{P}\{(2.20)\} &= (\beta_1+\beta_2)\beta_2(\alpha+\beta_1+\beta_2)^{n_2-(\ell_2+2)}\sum_{s=0}^{L-1}\alpha^s\mu_1(\ell_2-s)\\ &= \beta_2(\beta_1+\beta_2)C_0\ell_1\alpha^{\ell_1}(\alpha+\beta_1+\beta_2)^{n_2-(\ell_2+2)}\\ &\quad\sum_{s=0}^{L-1}\alpha^s(\ell_2-\ell_1-s)(\alpha+\beta_1)^{\ell_2-\ell_1-s}\\ &\quad\left\{1\pm O\left(\frac{1}{\ell_1}+\frac{1}{\ell_2-\ell_1-s}\right)\right\}\end{aligned} \tag{2.29}$$

which reduces to

$$\begin{aligned}\mathbf{P}\{(2.20)\} =& \frac{(\alpha+\beta_1)(\beta_1+\beta_2)\beta_2}{\beta_1(\alpha+\beta_1+\beta_2)^2}\ \mu_1(\ell_2)\\ &(\alpha+\beta_1+\beta_2)^{n_2-\ell_2}\left\{1\pm O\left(\gamma_1^L\right)\right\}\end{aligned} \tag{2.30}$$

Also, for configuration (2.23) we have

$$\begin{aligned}\mathbf{P}\{(2.23)\} &= (\beta_1+\beta_2)\beta_2^2\sum_{s=1}^{L-1}\sum_{t=0}^{s-1}\alpha^{s+t}\mu_1(\ell_2-s)(\alpha+\beta_1+\beta_2)^{n_2-(\ell_2+t+3)}\\ &= \beta_2^2(C_0\ell_1\alpha^{\ell_1})(\alpha+\beta_1+\beta_2)^{n_2-(\ell_2+2)}\\ &\quad\sum_{s=1}^{L-1}\alpha^s\left(1-\gamma_2^s\right)(\ell_2-\ell_1-s)(\alpha+\beta_1)^{\ell_2-\ell_1-s}\\ &\quad\left\{1\pm O\left(\frac{1}{\ell_1}+\frac{1}{\ell_2-\ell_1-s}\right)\right\}\end{aligned} \tag{2.31}$$

where γ_2 is defined in (2.7) and which when evaluated gives

$$\begin{aligned}\mathbf{P}\{(2.23)\} =& \frac{\beta_2^2\alpha(\alpha+\beta_1)(\beta_1+\beta_2)}{\beta_1(\alpha+\beta_1+\beta_2)^2\{(\alpha+\beta_1)(\beta_1+\beta_2)+\alpha\beta_1\}}\ \mu_1(\ell_2)\\ &(\alpha+\beta_1+\beta_2)^{n_2-\ell_2}\left\{1\pm O\left(\gamma_1^L\right)\right\}\end{aligned} \tag{2.32}$$

Adding the disjoint probabilities (2.30) and (2.32) we get

$$\begin{aligned}\mathbf{P}\{(2.20)\cup(2.23)\} =& \frac{\beta_2(\alpha+\beta_1)(2\alpha+\beta_1)(\beta_1+\beta_2)^2}{\beta_1(\alpha+\beta_1+\beta_2)^2\{(\alpha+\beta_1)(\beta_1+\beta_2)+\alpha\beta_1\}}\ \mu_1(\ell_2)\\ &(\alpha+\beta_1+\beta_2)^{n_2-\ell_2}\left\{1\pm O\left(\gamma_1^L\right)\right\}\end{aligned} \tag{2.33}$$

It remains to be shown that all other configurations listed in Section 2.5.1 have probability whose order of magnitude is smaller than $\mathbf{P}\{(2.20)\cup(2.23)\}$. We begin with the configurations (2.18) and (2.19). Their union starting at fiber i is a subset of the event

$$\begin{array}{cccc} i & & \downarrow & \\ 2_1 & \underbrace{0 \quad \cdots \quad 0}_{0\le s<\ell_2} & 2 & \underbrace{0 \quad \cdots \quad 0}_{\ell_2-s} \end{array} \tag{2.34}$$

so that

$$\begin{aligned} \mathbf{P}\{(2.18)\cup(2.19)\} &\le \mathbf{P}\{(2.34)\} \\ &= (\beta_1+\beta_2)\beta_2\ell_2\alpha^{\ell_2} \\ &= \mathbf{P}\{(2.20)\cup(2.23)\}O(\gamma_1^L) \end{aligned} \tag{2.35}$$

Next consider the superset of events (2.21) and (2.22):

$$\begin{array}{cccc} i & & \downarrow & \\ 2_1 & \underbrace{0 \quad \cdots \quad 0}_{L\le s<\ell_2-(\ell_1+1)} & 2 & \underbrace{1_0 \cdots 1_0 \,\langle 0\text{-}1\rangle\, 1_0 \cdots 1_0}_{\ell_2-s} \end{array} \tag{2.36}$$

Then

$$\begin{aligned} \mathbf{P}\{(2.21)\cup(2.22)\} &\le \beta_2(\beta_1+\beta_2)(\alpha+\beta_1+\beta_2)^{n_2-(\ell_2+2)} \\ &\qquad \sum_{s=L}^{\ell_2-(\ell_1+2)} \alpha^s\mu_1(\ell_2-s) \\ &= \mathbf{P}\{(2.20)\cup(2.23)\}O(\gamma_1^L) \end{aligned} \tag{2.37}$$

By a similar calculation, it may be seen that the probability of (2.24) is also

$\mathbf{P}\{(2.20) \cup (2.23)\}O(\gamma_1^L)$. Next for (2.25) we have

$$\begin{aligned}
\mathbf{P}\{(2.25)\} =& \beta_2^2(\alpha+\beta_1+\beta_2)^{n_2-(\ell_2+2)} \sum_{s=\ell_1+2}^{\ell_2-(\ell_1+2)} \mu_1(s)\mu_1(\ell_2-s) \\
\leq& \frac{\beta_2^2 C_0}{6(\alpha+\beta_1+\beta_2)^2}(\alpha+\beta_1+\beta_2)^{n_2-\ell_2}\mu_1(\ell_2) \\
& \left(\frac{\ell_1((\ell_2-2\ell_1)\vee 0)^3}{\ell_2-\ell_1}\gamma_1^{\ell_1}\right) \\
=& \mathbf{P}\{(2.20) \cup (2.23)\}\, O\left(\frac{\ell_1((\ell_2-2\ell_1)\vee 0)^3}{\ell_2-\ell_1}\gamma_1^{\ell_1}\right)
\end{aligned} \tag{2.38}$$

Note here that if

$$\frac{\ell_1(\ell_2-2\ell_1)^3}{\ell_2-\ell_1}\gamma_1^L = \Omega(1)$$

the contribution of $\mathbf{P}\{2.25\}$ will be quite substantial in comparison to $\mathbf{P}\{(2.20) \cup (2.23)\}$.

Next

$$\begin{aligned}
\mathbf{P}\{(2.26)\} \leq& \beta_2(C_0\ell_1\alpha^{\ell_1})(\alpha+\beta_1)^{\ell_2-\ell_1} \\
& \sum_{s=0\vee(\ell_2-2\ell_1)}^{\ell_2-(\ell_1+3)} \alpha^{\ell_2-\ell_1-s-1}(\alpha+\beta_1+\beta_2)^{n_2-(\ell_2+1)-(\ell_2-\ell_1-s-1)} \\
\leq& \frac{\beta_2\alpha^2}{(\beta_1+\beta_2)(\alpha+\beta_1+\beta_2)^2}(\alpha+\beta_1+\beta_2)^{n_2-\ell_2}\frac{\mu_1(\ell_2)}{\ell_2-\ell_1} \\
=& \mathbf{P}\{(2.20) \cup (2.23)\}\, O\left(\frac{1}{\ell_2-\ell_1}\right)
\end{aligned}$$

and

$$\begin{aligned}
\mathbf{P}\{(2.27)\} \leq& \beta_2(\ell_1\beta_1^2\alpha^{\ell_1})(\alpha+\beta_1+\beta_2)^{n_2-(\ell_2+1)} \sum_{s=\ell_2-(\ell_1+2)}^{\ell_2-1}(\alpha+\beta_1)^s \\
\leq& \frac{\beta_2(\alpha+\beta_1+\beta_2)}{1-(\alpha+\beta_1)}(\alpha+\beta_1+\beta_2)^{n_2-(\ell_2+2)}\frac{\mu_1(\ell_2)}{\ell_2-\ell_1} \\
=& \mathbf{P}\{(2.20) \cup (2.23)\}O(1/(\ell_2-\ell_1))
\end{aligned}$$

Finally we have

$$\begin{aligned}\mathbf{P}\{(2.28)\} \leq & (\ell_1 \alpha_1^{\ell_1} \beta_1^2)(\alpha+\beta_1)^{\ell_2} \\ \leq & \mu_1(\ell_2) O\left(\frac{(\alpha+\beta_1)^{\ell_1}}{\ell_2-\ell_1}\right) \\ = & \mathbf{P}\{(2.20)\cup(2.23)\} O\left(\frac{(\alpha+\beta_1)^{\ell_1}}{\ell_2-\ell_1}\right)\end{aligned} \tag{2.39}$$

Adding all these probabilities, we have for $p+L \leq i < p+n_2-\ell_2-1$

$$\begin{aligned}\mathbf{P}\{Y_i=1\} = & \frac{\beta_2(\alpha+\beta_1)(2\alpha+\beta_1)(\beta_1+\beta_2)^2}{\beta_1(\alpha+\beta_1+\beta_2)^2\{(\alpha+\beta_1)(\beta_1+\beta_2)+\alpha\beta_1\}}\ \mu_1(\ell_2) \\ & (\alpha+\beta_1+\beta_2)^{n_2-\ell_2} \\ & \left\{1 \pm O\left(\gamma_1^L + \frac{\ell_1\{(\ell_2-2\ell_1)\vee 0\}^3}{\ell_2-\ell_1}\gamma_1^{\ell_1}\right)\right\}\end{aligned} \tag{2.40}$$

Next consider i such that $p \leq i < p+L$ and evaluate the probabilities of the configurations listed in Section 2.5.1. (2.30) continues to hold for $\mathbf{P}\{(2.20)\}$. However, the event (2.23) maybe decomposed according to whether $i \leq s$ or not.

$$\begin{array}{lll} i & & \downarrow \\ 2 & \underbrace{1_0 \cdots 1_0\ \langle 0\text{-}1\rangle\ 1_0 \cdots 1_0}_{\ell_2-s} & 2\quad \underbrace{0\quad \cdots\quad 0}_{i\leq s<L} \quad \text{if } i \leq s \end{array} \tag{2.41}$$

If $i > s$, the configuration remains (2.23) with s constrained to lie in the range $1 \leq s < i$. $\mathbf{P}\{(2.23)\}$ is now given by

$$\begin{aligned}\mathbf{P}\{(2.23)\} = & (\beta_1+\beta_2)\beta_2^2 \sum_{s=i-p+1}^{L-1}\sum_{t=0}^{s-1} \alpha^{s+t}\mu_1(\ell_2-s)(\alpha+\beta_1+\beta_2)^{n_2-(\ell_2+t+3)} \\ & + \beta_2^2 \sum_{s=1}^{i-p} \alpha^s \mu_1(\ell_2-s)(\alpha+\beta_1+\beta_2)^{n_2-(\ell_2+2)} \\ = & (\beta_1+\beta_2)\beta_2^2 \sum_{s=1}^{L-1}\sum_{t=0}^{s-1} \alpha^{s+t}\mu_1(\ell_2-s)(\alpha+\beta_1+\beta_2)^{n_2-(\ell_2+t+3)} \\ & + \beta_2^2 \sum_{s=1}^{i-p+1} (\alpha\gamma_2)^s \mu_1(\ell_2-s)(\alpha+\beta_1+\beta_2)^{n_2-(\ell_2+2)}\end{aligned} \tag{2.42}$$

The first term in (2.42) reduces to (2.32). The second term when simplified becomes

$$\{\text{second term of (2.42)}\} = \frac{\alpha^2\beta_2^2}{(\alpha+\beta_1)(\beta_1+\beta_2)+\alpha\beta_1}\ \mu_1(\ell_2)(\alpha+\beta_1+\beta_2)^{n_2-(\ell_2+2)} (1-(\gamma_1\gamma_2)^{i-p+1}) \left\{1 \pm O\left(\frac{1}{\ell_1}+\frac{1}{\ell_2-\ell_1}\right)\right\} \tag{2.43}$$

That the probability of all the other configurations is dominated by $\mathbf{P}\{(2.20) \cup (2.23)\}$ may be seen in the same way as before.

Next consider the case $i = p-1$. Then

$$\mathbf{P}\{(2.20)\} = \frac{(\alpha+\beta_1)\beta_2}{\beta_1}\ \mu_1(\ell_2)(\alpha+\beta_1+\beta_2)^{n_2-(\ell_2+1)} \tag{2.44}$$

and

$$\mathbf{P}\{(2.23)\} = \frac{\alpha\beta_2}{\beta_1}\ \mu_1(\ell_2)(\alpha+\beta_1+\beta_2)^{n_2-(\ell_2+1)} \tag{2.45}$$

Again all other configurations' probabilities are dominated by these two. Finally, when $i = p-2$, $\mathbf{P}\{(2.23)\} = 0$. However, $\mathbf{P}\{(2.20)\} = \mu_1(\ell_2)(\alpha+\beta_1+\beta_2)^{n_2-\ell_2}$ which once again dominates all other probabilities.

Setting $\lambda_2 = \mathbf{E}[T] = \sum_{i=p}^{p+n_2-1} \mathbf{P}\{Y_i = 1\}$, we have

$$\lambda_2(n_2) = (n_2-\ell_2)C_1\mu_1(\ell_2)(\alpha+\beta_1+\beta_2)^{n_2-\ell_2} \left\{1 \pm O\left(\gamma_1^L + \frac{\ell_1\{(\ell_2-2\ell_1)\vee 0\}^3}{\ell_2-\ell_1}\gamma_1^{\ell_1} + \frac{L}{n_2-\ell_2}\right)\right\} \tag{2.46}$$

where

$$C_1 = \frac{(\gamma_1-\gamma_2)(1+\gamma_1)(1-\gamma_2)^2}{\gamma_1(1-\gamma_1)(1-\gamma_1\gamma_2)}$$

Choosing $L = \lceil -\log_{\gamma_1}(\ell_1 \wedge (\ell_2-\ell_1))\rceil$, we have the error term close to its smallest

value and

$$\lambda_2(n_2) = (n_2-\ell_2)C_1\mu_1(\ell_2)(\alpha+\beta_1+\beta_2)^{n_2-\ell_2} \left\{1 \pm O\left(\frac{\ell_1\{(\ell_2-2\ell_1)\vee 0\}^3}{\ell_2-\ell_1}\gamma_1^{\ell_1} + \frac{\lceil -\log_{\gamma_1}(\ell_1\wedge(\ell_2-\ell_1))\rceil}{n_2-\ell_2}\right)\right\} \tag{2.47}$$

2.5.3 Poisson Approximation Error

We now bound the Chen-Stein error $b_1+b_2+b_3$ arising from the Poisson approximation of the dependent process Y_i. We begin by defining $J_i = \{j : |j-i| \le \ell_2+L+1\}$ so that random variables Y_i and $\{Y_j : j \notin J_i\}$ are independent and consequently, $b_3 = 0$. As before,

$$\begin{aligned} b_1 &\le \min(1,1/\lambda_2)2(n_2-\ell_2-1)(\ell_2+L+1)(\lambda_2/(n_2-\ell_2-1))^2 \\ &= \min(1,1/\lambda_2)2(\ell_2+L+1)\lambda_2^2/(n_2-\ell_2-1) \end{aligned} \tag{2.48}$$

Bounding b_2 requires finding pairs of failure configurations such that $Y_iY_j = 1$, $j \in J_i$. If one or both of Y_i and Y_j arise from a configuration different from (2.20) and (2.23), we know that the probability of the resulting overlapped configuration is $\mathbf{P}\{(2.20)\cup(2.23)\}O(\ell_1^{-1}+(\ell_2-\ell_1)^{-1})$. Therefore we only need consider overlaps of (2.20) and (2.23).

Configurations of the form (2.20) may overlap themselves to produce $Y_iY_j = 1$, for $j \in J_i$ as

$$\begin{array}{cccccccc} i & & \downarrow & & & j & & \\ 2_1 & \underbrace{0\cdots 0}_{0\le s_1<L} & 2 & \underbrace{1_0\cdots 1_0\ \langle 0\text{-}1\rangle\ 1_0\cdots 1_0}_{\ell_2-s_1-w-1} & 1 & \underbrace{0\cdots 0}_{w\le s_2<L} & \cdots & \\ & & & \downarrow & & & & \\ & & \cdots & 2 & \underbrace{1_0\cdots 1_0\ \langle 0\text{-}1\rangle\ 1_0\cdots 1_0}_{\ell_2-s_2} & & & \end{array} \tag{2.49}$$

and

$$\begin{array}{ccccccccccc} & & i & & \downarrow & & & & & & j & & \\ 2_1 & \underbrace{0\ \cdots\ 0}_{0\le s_1<L} & 2 & \underbrace{1_0\ \cdots\ 1_0\ \langle 0\text{-}1\rangle\ 1_0 \cdots\ 1_0}_{\ell_2-s_1} & & \underbrace{2_0\ \cdots\ 2_0}_{0\le w<L-1} & 2_1 & \ldots & & & \\ & & & & & & & & \downarrow & & \\ \ldots & & \underbrace{0\ \ldots\ 0}_{0\le s_2<L} & 2 & \underbrace{1_0\ \cdots\ 1_0\ \langle 0\text{-}1\rangle\ 1_0\ \cdots\ 1_0}_{\ell_2-s_2} & & & & & & & & \end{array} \tag{2.50}$$

or they may overlap configurations (2.23) as:

$$\begin{array}{ccccccccccc} & & i & & \downarrow & & & & & & & & \\ 2_1 & \underbrace{0\ \cdots\ 0}_{0\le s_1<L} & 2 & \underbrace{1_0\ \cdots\ 1_0\ \langle 0\text{-}1\rangle\ 1_0 \cdots\ 1_0}_{\ell_2-s_1-w-1} & 1 & \underbrace{0\ \cdots\ 0}_{w\le t<s_2} & \ldots & & & & & \\ & & & & j & & & & \downarrow & & & & \\ & \ldots & 2 & \underbrace{1_0\ \cdots\ 1_0\ \langle 0\text{-}1\rangle\ 1_0\ \cdots\ 1_0}_{\ell_2-s_2} & & 2 & \underbrace{0\ \ldots\ 0}_{0\le s_2<L} & & & & & & \end{array} \tag{2.51}$$

and

$$\begin{array}{ccccccccccc} & & i & & \downarrow & & & & & & & & \\ 2_1 & \underbrace{0\ \cdots\ 0}_{0\le s_1<L} & 2 & \underbrace{1_0\ \cdots\ 1_0\ \langle 0\text{-}1\rangle\ 1_0 \cdots\ 1_0}_{\ell_2-s_1} & & \underbrace{2_0\ \cdots\ 2_0}_{0\le w<L-1} & \ldots & & & & & \\ & & & & j & & & & \downarrow & & & & \\ & \ldots & 2 & \underbrace{1_0\ \cdots\ 1_0\ \langle 0\text{-}1\rangle\ 1_0\ \cdots\ 1_0}_{\ell_2-s_2} & & 2 & \underbrace{0\ \ldots\ 0}_{0\le s_2<L} & & & & & & \end{array} \tag{2.52}$$

Turning next to configurations in which (2.23) overlaps itself, we have $Y_iY_j =$

$1, j \in J_i$ when

$$\begin{array}{ccccccccc} & & & & i & & & & \downarrow j & & \\ 2_1 & \underbrace{0 \cdots 0}_{0\le t<s_1} & 2 & \underbrace{1_0 \cdots 1_0 \langle 0\text{-}1\rangle 1_0 \cdots 1_0}_{\ell_2-s_1} & & 2 & \underbrace{0 \cdots 0}_{1\le s_1<L} & \cdots & \\ & & & & \downarrow & & & & \\ \cdots & & \underbrace{0 \cdots 0}_{0\le s_2-s_1<L-s_1} & 2 & \underbrace{1_0 \cdots 1_0 \langle 0\text{-}1\rangle 1_0 \cdots 1_0}_{\ell_2-s_2} & 2 & \underbrace{0 \ldots 0}_{0\le s_2<L} & & \end{array} \tag{2.53}$$

and

$$\begin{array}{ccccccccc} & & & & i & & & & \downarrow j & & \\ 2_1 & \underbrace{0 \cdots 0}_{0\le t<s_1} & 2 & \underbrace{1_0 \cdots 1_0 \langle 0\text{-}1\rangle 1_0 \cdots 1_0}_{\ell_2-s_1} & & 2 & \underbrace{0 \cdots 0}_{1\le s_1<L} & \cdots & \\ & & & & \downarrow & & & & \\ \cdots & \underbrace{2_0 \cdots 2_0\, 2_1\, 0 \ldots 0}_{0\le w<s_2} & 2 & \underbrace{1_0 \cdots 1_0 \langle 0\text{-}1\rangle 1_0 \cdots 1_0}_{\ell_2-s_2} & 2 & \underbrace{0 \ldots 0}_{0\le s_2<L} & & & \end{array} \tag{2.54}$$

and finally for configurations in which (2.23) overlaps (2.20) to produce $Y_iY_j =$ $1, j \in J_i$, we have

$$\begin{array}{ccccccccc} & & & & i & & & & \downarrow & & \\ 2_1 & \underbrace{0 \cdots 0}_{0\le t<s_1} & 2 & \underbrace{1_0 \cdots 1_0 \langle 0\text{-}1\rangle 1_0 \cdots 1_0}_{\ell_2-s_1} & & 2 & \underbrace{0 \cdots 0}_{1\le s_1<L} & \cdots & \\ & & & & j & & \downarrow & & \\ \cdots & \underbrace{2_0 \cdots 2_0}_{0\le w<L} & 2_1 & \underbrace{0 \ldots 0}_{0\le s_2<L} & 2 & \underbrace{1_0 \cdots 1_0 \langle 0\text{-}1\rangle 1_0 \cdots 1_0}_{\ell_2-s_2} & & & \end{array} \tag{2.55}$$

In bounding the probability of these configurations the configuration

$$2 \quad \underbrace{1_0 \cdots 1_0 \langle 0\text{-}1\rangle 1_0 \cdots 1_0}_{\ell_2-L+1\le \ell_2-s_2<\ell_2} \tag{2.56}$$

arises repeatedly and has probability

$$\begin{aligned}\mathbf{P}\{(2.56)\} \leq & \beta_2 \sum_{s_2=0}^{L-1} (\alpha+\beta_1)^{\ell_2-s_2-(\ell_1+2)}(\ell_2-s_2-\ell_1-1) \\ = & \lambda_2 O\left(\frac{1}{(\alpha+\beta_1)^L}\right)\end{aligned} \tag{2.57}$$

With this result in hand, it is readily seen that $\mathbf{P}\{(2.49)\} = \lambda_2^2 O((\alpha+\beta_1)^{-L})$. For, the probability of the fiber arrangement to the left of the second pressured element 2 is bounded from above by λ_2, the arrangement to the right of the second pressured element has probability bounded from above by $\lambda_2 O((\alpha+\beta_1)^{-L})$ and these two events are independent.

Similar arguments for the other configurations establish that the Poisson approximation error is $\lambda_2 O(\lambda_2/(\alpha+\beta_1)^L)$. Since $\lambda_2 = o(\alpha^L)$, the Poisson error is bounded more loosely by $\lambda_2 O(\alpha^L/(\alpha+\beta_1)^L) = \lambda_2 O(\gamma_1^L)$.

Thus, the probability of failure of a 0-1-2 sub-bundle accounting for both boundary and Poisson approximation error is

$$\begin{aligned}\mu_2(n_2) = & (n_2-\ell_2)C_1\mu_1(\ell_2)(\alpha+\beta_1+\beta_2)^{n_2-\ell_2} \\ & \left\{1 \pm O\left(\frac{\ell_1\{(\ell_2-2\ell_1)\vee 0\}^3}{\ell_2-\ell_1}\gamma_1^{\ell_1} + \frac{1}{\ell_1} + \frac{1}{\ell_2-\ell_1} + \right.\right. \\ & \left.\left. \frac{\lceil -\log_{\gamma_1}(\ell_1 \wedge (\ell_2-\ell_1))\rceil}{n_2-\ell_2}\right)\right\}\end{aligned} \tag{2.58}$$

where

$$\begin{aligned}C_1 = & \frac{\beta_2(\alpha+\beta_1)(2\alpha+\beta_1)(\beta_1+\beta_2)^2}{\beta_1(\alpha+\beta_1+\beta_2)^2\{(\alpha+\beta_1)(\beta_1+\beta_2)+\alpha\beta_1\}} \\ = & \frac{(\gamma_1-\gamma_2)(1+\gamma_1)(1-\gamma_2)^2}{\gamma_1(1-\gamma_1)(1-\gamma_1\gamma_2)}\end{aligned}$$

2.6 Strength of a 0-1-2-3 Bundle

Let, as before $I_3 = \{p-2, p-1, p, p+1, \ldots, p+n_3-1\} \subset I$ for some $p \leq n-n_3+1$ such that $Z_i = 3_0$ for $i \in I_3$. Let Z_i be distributed as described in Section 2.3

except that $Z_{p-2} = Z_{p-1} = 2 = 1$. Also let $n_3 \geq \ell_3$.

The generalization from the 0-1-2 bundle to the 0-1-2-3 bundle proceeds on much the same lines as the generalization from the 0-1 bundle to the 0-1-2 bundle. Let L be as defined in Section 2.5.1 and let us denote a $\ell_3 - s$ fiber long failing 0-1-2 sub-bundle with

$$\underbrace{2_0 \cdots 2_0 \langle\text{0-1-2}\rangle\ 2_0 \cdots 2_0}_{\ell_3 - s}.$$

Configuration (2.20) generalizes to

$$\begin{array}{cccc} & i & & \downarrow \\ 3_1 & \underbrace{0 \cdots 0}_{0 \leq s < L} & 3 & \underbrace{2_0 \cdots 2_0 \langle\text{0-1-2}\rangle\ 2_0 \cdots 2_0}_{\ell_3 - s} \end{array} \tag{2.59}$$

and

$$\begin{array}{cccc} & i & & \downarrow \\ 3_1 & \underbrace{0 \cdots 0}_{0 \leq s < L} & 3 & \underbrace{1_0 \cdots 1_0 \langle\text{0-1}\rangle\ 1_0 \cdots 1_0}_{\ell_3 - s} \end{array} \tag{2.60}$$

and configuration (2.23) generalizes to

$$\begin{array}{ccccccc} & & i & & & \downarrow & \\ 3_1 & \underbrace{0 \cdots 0}_{0 \leq t < s} & 3 & \underbrace{2_0 \cdots 2_0 \langle\text{0-1-2}\rangle\ 2_0 \cdots 2_0}_{\ell_3 - s} & 3 & \underbrace{0 \cdots 0}_{1 \leq s < L} \end{array} \tag{2.61}$$

and

$$\begin{array}{ccccccc} & & i & & & \downarrow & \\ 3_1 & \underbrace{0 \cdots 0}_{0 \leq t < s} & 3 & \underbrace{1_0 \cdots 1_0 \langle\text{0-1}\rangle\ 1_0 \cdots 1_0}_{\ell_3 - s} & 3 & \underbrace{0 \cdots 0}_{1 \leq s < L} \end{array} \tag{2.62}$$

Then,

$$\begin{aligned}\mathbf{P}\{(2.59)\} &= (\beta_1+\beta_2+\beta_3)\beta_3(\alpha+\beta_1+\beta_2+\beta_3)^{n_3-(\ell_3+2)}\sum_{s=0}^{L-1}\alpha^s\mu_2(\ell_3-s)\\ &= (\beta_1+\beta_2+\beta_3)\beta_3(C_1\mu_1(\ell_2))(\alpha+\beta_1+\beta_2+\beta_3)^{n_3-(\ell_3+2)}\\ &\quad \sum_{s=0}^{L-1}\alpha^s(\ell_3-\ell_2-s)(\alpha+\beta_1+\beta_2)^{\ell_3-\ell_2-s}\\ &\quad \left\{1\pm O\left(\frac{\ell_1\{(\ell_2-2\ell_1)\vee 0\}^3}{\ell_2-\ell_1}\gamma_1^{\ell_1}+\frac{L}{\ell_3-\ell_2-s}\right)\right\}\end{aligned} \tag{2.63}$$

which reduces to

$$\mathbf{P}\{2.59\} = \frac{(\alpha+\beta_1+\beta_2)(\beta_1+\beta_2+\beta_3)\beta_3}{(\beta_1+\beta_2)(\alpha+\beta_1+\beta_2+\beta_3)^2}\mu_2(\ell_3)(\alpha+\beta_1+\beta_2+\beta_3)^{n_3-\ell_3} \tag{2.64}$$

Similarly,

$$\begin{aligned}\mathbf{P}\{(2.60)\} &= (\beta_1+\beta_2+\beta_3)\beta_3(\alpha+\beta_1+\beta_2)^{n_3-(\ell_3+2)}\sum_{s=0}^{L-1}\alpha^s\mu_1(\ell_3-s)\\ &= \frac{(\alpha+\beta_1)(\beta_1+\beta_2+\beta_3)\beta_3}{\beta_1(\alpha+\beta_1+\beta_2+\beta_3)^2}\mu_1(\ell_3)(\alpha+\beta_1+\beta_2+\beta_3)^{n_3-\ell_3}\end{aligned} \tag{2.65}$$

Since

$$\begin{aligned}\frac{\mu_1(\ell_3)}{\mu_2(\ell_3)} &= O\left\{\frac{\ell_3-\ell_1}{(\ell_3-\ell_2)(\ell_2-\ell_1)}\left(\frac{\alpha+\beta_1}{\alpha+\beta_1+\beta_2}\right)^{\ell_3-\ell_2}\right\}\\ &= O\left\{\left(\frac{1}{\ell_3-\ell_2}+\frac{1}{\ell_2-\ell_1}\right)\left(\frac{\gamma_2}{\gamma_1}\right)^{\ell_3-\ell_2}\right\}\end{aligned}$$

(2.64) dominates (2.65). Next,

$$\begin{aligned}\mathbf{P}\{(2.61)\} &= (\beta_1+\beta_2+\beta_3)\beta_3^2\sum_{s=1}^{L-1}\sum_{t=0}^{s-1}\alpha^{s+t}\mu_2(\ell_2-s)(\alpha+\beta_1+\beta_2+\beta_3)^{n_3-(\ell_3+3+t)}\\ &= \beta_3^2(C_1\mu_1(\ell_2))(\alpha+\beta_1+\beta_2+\beta_3)^{n_3-(\ell_3+2)}\\ &\quad \sum_{s=1}^{L-1}\alpha^s\left(1-\gamma_3^s\right)(\ell_3-\ell_2-s)(\alpha+\beta_1+\beta_2)^{\ell_3-\ell_2-s}\\ &\quad \left\{1\pm O\left(\frac{\ell_1\{(\ell_2-2\ell_1)\vee 0\}^3}{\ell_2-\ell_1}\gamma_1^{\ell_1}+\frac{L}{\ell_3-\ell_2-s}\right)\right\}\end{aligned} \tag{2.66}$$

which upon reduction becomes

$$\mathbf{P}\{(2.61)\} = \frac{\beta_3^2\alpha(\beta_1+\beta_2+\beta_3)(\alpha+\beta_1+\beta_2)}{(\beta_1+\beta_2)\{(\alpha+\beta_1+\beta_2)(\beta_1+\beta_2+\beta_3)+\alpha(\beta_1+\beta_2)\}} \quad \mu_2(\ell_3)$$
$$(\alpha+\beta_1+\beta_2+\beta_3)^{n_3-(\ell_3+2)} \tag{2.67}$$

and

$$\mathbf{P}\{(2.62)\} = (\beta_1+\beta_2+\beta_3)\beta_3^2 \sum_{s=1}^{\ell-1}\sum_{t=0}^{s-1} \alpha^{s+t}\mu_1(\ell_3-s)(\alpha+\beta_1+\beta_2+\beta_3)^{n_3-(\ell_3+3+t)} \tag{2.68}$$

which when simplified gives

$$\mathbf{P}\{(2.62)\} = \frac{\beta_3^2\alpha(\beta_1+\beta_2+\beta_3)(\alpha+\beta_1)}{\beta_1\{(\alpha+\beta_1)(\beta_1+\beta_2+\beta_3)+\alpha\beta_1\}} \quad \mu_1(\ell_3)$$
$$(\alpha+\beta_1+\beta_2+\beta_3)^{n_3-(\ell_2+2)} \tag{2.69}$$

(2.69) maybe seen to be of smaller order of magnitude than (2.67) exactly as (2.64) is seen to dominate (2.65). Also, adding (2.64) and (2.67) gives

$$\mathbf{P}\{(2.59)\cup(2.61)\} = \frac{\beta_3(\alpha+\beta_1+\beta_2)(2\alpha+\beta_1+\beta_2)(\beta_1+\beta_2+\beta_3)^2}{(\beta_1+\beta_2)\{(\alpha+\beta_1+\beta_2)(\beta_1+\beta_2+\beta_3)+\alpha(\beta_1+\beta_2)\}}$$
$$\mu_2(\ell_3) \quad (\alpha+\beta_1+\beta_2+\beta_3)^{n_3-(\ell_3+2)} \tag{2.70}$$

We must also consider the configuration of the form

$$\begin{array}{lll} i & & \downarrow \\ 3 & \underbrace{2_0\ \cdots\ 2_0\ \langle\text{0-1-2}\rangle\ 2_0\ \cdots\ 2_0}_{\ell_2+2\le s<\ell_3-(\ell_2+1)} & 3\ \ \underbrace{2_0\ \cdots\ 2_0\ \langle\text{0-1-2}\rangle\ 2_0\ \cdots\ 2_0}_{\ell_3-s} \end{array} \tag{2.71}$$

which has probability

$$\mathbf{P}\{(2.71)\} = \beta_3^2 \sum_{s=\ell_2+2}^{\ell_3-(\ell_2+2)} \mu_2(s)\mu_2(\ell_3-s)$$
$$= \mathbf{P}\{2.59\cup(2.61)\}\ O\left(\frac{\ell_1(\ell_2-\ell_1)\{(\ell_3-2\ell_2)\vee 0\}^3}{\ell_3-\ell_2}\gamma_1^{\ell_1}\left(\frac{\gamma_2}{\gamma_1}\right)^{\ell_2}\right) \tag{2.72}$$

In a manner similar to the 0-1-2 case, we may show that all other failure configurations of a 0-1-2-3 bundle are dominated by the configurations (2.20) and (2.23). Accounting for the discrepancy in the probability of (2.23) when $p \leq i < p+L$ exactly as in the 0-1-2 bundle, we finally have for $\lambda_3 = \mathbf{E}[T] = \sum_{i=p}^{p+n_3-1} \mathbf{P}\{Y_i = 1\}$

$$\begin{aligned}\lambda_3(n_3) = (n_3-\ell_3)(C_2\mu_2(\ell_3))(\alpha+\beta_1+\beta_2+\beta_3)^{n_3-\ell_3} \\ \left\{1 \pm O\left(\frac{1}{\ell_1}+\frac{1}{\ell_2-\ell_1}+\frac{L}{\ell_3-\ell_2}+\frac{L}{n_3-\ell_3}+\right.\right. \\ \frac{\ell_1\{(\ell_2-2\ell_1)\vee 0\}^3}{\ell_2-\ell_1}\gamma_1^{\ell_1}+ \\ \left.\left.\frac{\ell_1(\ell_2-\ell_1)\{(\ell_3-2\ell_2)\vee 0\}^3}{\ell_3-\ell_2}\gamma_1^{\ell_1}\left(\frac{\gamma_2}{\gamma_1}\right)^{\ell_2}\right)\right\}\end{aligned} \tag{2.73}$$

where

$$\begin{aligned}C_2 &= \frac{\beta_3(\alpha+\beta_1+\beta_2)(2\alpha+\beta_1+\beta_2)(\beta_1+\beta_2+\beta_3)^2}{(\beta_1+\beta_2)(\alpha+\beta_1+\beta_2+\beta_3)^2\{(\alpha+\beta_1+\beta_2)(\beta_1+\beta_2+\beta_3)+\alpha(\beta_1+\beta_2)\}} \\ &= \frac{(\gamma_2-\gamma_3)(1+\gamma_2)(1-\gamma_3)^2}{\gamma_2(1-\gamma_2)(1-\gamma_2\gamma_3)}\end{aligned}$$

The Poisson approximation error can be bounded exactly as in the 0-1-2 case. It turns out to be of the order of the error term in (2.73) and including that as well, we have $\mu_3(n_3) = \lambda_3(n_3)$ for the probability of failure of the 0-1-2-3 sub-bundle.

2.7 Strength of a 0-1-2-$\cdots$-r Bundle

The above steps of generalization from a 0-1-2-$\cdots$-$j-1$ sub-bundle to a 0-1-2-$\cdots$-j sub-bundle can be carried out indefinitely. For the 0-1-2-$\cdots$-j, $j \geq 2$ sub-bundle

which is n_j fibers long, the dominant failure configurations are

$$\begin{array}{cccc} & & i & \downarrow \\ j_1 & \underbrace{0 \quad \cdots \quad 0}_{0\le s<L} & j & \underbrace{(j-1)_0 \cdots (j-1)_0 \,\langle \text{0-1-2-}\cdots\text{-}(j-1)\rangle\, (j-1)_0 \cdots (j-1)_0}_{\ell_j - s} \end{array} \tag{2.74}$$

and

$$\begin{array}{cccccc} & & & i & & \\ j_1 & \underbrace{0 \cdots 0}_{0\le t<s} & j & \underbrace{(j-1)_0 \cdots (j-1)_0 \,\langle \text{0-1-}\cdots\text{-}(j-1)\rangle\, (j-1)_0 \cdots (j-1)_0}_{\ell_j - s} & & \\ & & & & \downarrow & \\ & & \cdots & j & \underbrace{0 \quad \cdots \quad 0}_{1\le s<L} & \end{array} \tag{2.75}$$

and evaluating their probabilities as before, we have

$$\begin{aligned} \mu_j(n_j) = (n_j - \ell_j)\,(C_{j-1}\mu_{j-1}(\ell_j))\,(\alpha+\beta_1+\cdots+\beta_j)^{n_j-\ell_j} \\ \left\{1 \pm O\left(\frac{\lceil -\log_{\gamma_1}(\ell_1 \wedge (\ell_2-\ell_1))\rceil}{n_j-\ell_j} + \right.\right. \\ \frac{\ell_1(\ell_2-\ell_1)\cdots(\ell_{j-1}-\ell_{j-2})\{(\ell_j-2\ell_{j-1})\vee 0\}^3}{\ell_j-\ell_{j-1}} \\ \left.\left. \times\gamma_1^{\ell_1}\left(\frac{\gamma_2}{\gamma_1}\right)^{\ell_2}\cdots\left(\frac{\gamma_{j-1}}{\gamma_{j-2}}\right)^{\ell_{j-1}}\right)\right\} \end{aligned} \tag{2.76}$$

where

$$C_{j-1} = \frac{(\gamma_{j-1}-\gamma_j)(1+\gamma_{j-1})(1-\gamma_j)^2}{\gamma_{j-1}(1-\gamma_{j-1})(1-\gamma_j\gamma_{j-1})}$$

This is the relation between the probability of failure of a 0-1-2-$\cdots$-j and a 0-1-2-$\cdots$-$j-1$ bundle and it brings out the hierarchical nature of the failure process. Explicitly, by substituting for μ_j, $j = 1, 2, \ldots, r-1$ and replacing n_r by n we

obtain

$$\begin{aligned}\mu_r(n) &= C_0C_1C_2\cdots C_{r-1}\\ &\quad \ell_1(\ell_2-\ell_1)(\ell_3-\ell_2)\cdots(\ell_r-\ell_{r-1})(n-\ell_r)\\ &\quad \alpha^{\ell_1}(\alpha+\beta_1)^{\ell_2-\ell_1}\ \cdots\ (\alpha+\beta_1+\cdots\beta_{r-1})^{\ell_r-\ell_{r-1}}(1\pm\varepsilon)\end{aligned} \tag{2.77}$$

where we have used $\alpha+\beta_1+\cdots+\beta_r=1$. Here,

$$\begin{aligned}\varepsilon = O\Bigg(&\frac{\lceil -\log_{\gamma_1}(\ell_1\wedge(\ell_2-\ell_1))\rceil}{(n-\ell_r)\wedge(\wedge_{j=1}^{r}(\ell_j-\ell_{j-1}))}+\\ &\bigvee_{j=2}^{r}\frac{\prod_{m=2}^{j}\left\{(\ell_{m-1}-\ell_{m-2})(\gamma_{m-1}/\gamma_{m-2})^{\ell_{m-1}}\right\}\left\{(\ell_j-2\ell_{j-1})\vee 0\right\}^3}{\ell_j-\ell_{j-1}}\Bigg)\end{aligned} \tag{2.78}$$

where terms involving ℓ_p, $p\le 0$ must be dropped. Also note that

$$\prod_{j=1}^{r}C_{j-1}=(1-\gamma_1)(1-\gamma_r)\prod_{j=2}^{r}\frac{(\gamma_{j-1}-\gamma_j)(1+\gamma_{j-1})(1-\gamma_j)}{\gamma_{j-1}(1-\gamma_j\gamma_{j-1})} \tag{2.79}$$

2.8 Power Law Fiber Strength

We now use (2.77) to estimate the strength distribution of a local load sharing n-fiber bundle whose fiber strengths are distributed according to the power law

$$F(y)=\begin{cases}0, & y\le 0\\ y^{\rho}, & 0\le y\le 1\\ 1 & y>1,\end{cases} \tag{2.80}$$

where ρ is the shape parameter of the distribution. To do so we must discretize $F(y)$ sufficiently coarsely. For simplicity, we will restrict the applied load per fiber to take on one of the discrete values

$$x_k=\frac{1}{K(k^2c)}=\frac{1}{1+(k^2c/2)},\quad k=0,1,2,\ldots \tag{2.81}$$

where c is a sufficiently large integral constant so chosen that the discretization of $F(y)$ is suitably coarse. For each k and x_k we consider the bounding distributions $\underline{F}_k(y)$ and $\overline{F}_k(y)$ of $F(y)$ defined as follows:

$$\underline{F}_k(y) = \begin{cases} 0, & y \leq x_k \\ F\left(K((j-1)^2 c)x_k\right), & K((j-1)^2 c)x_k < y \leq K(j^2 c)x_k, \\ & j = 1, 2, \ldots, k, \\ 1, & y > 1 \end{cases} \tag{2.82}$$

and

$$\overline{F}_k(y) = \begin{cases} 0, & y \leq 0 \\ F\left(K(c)x_k\right), & 0 \leq y < K(c)x_k \\ F\left(K(j^2 c)x_k\right), & K((j-1)^2 c)x_k \leq y < K(j^2 c)x_k,\ j = 2, 3, \ldots, k \\ 1, & y > 1. \end{cases} \tag{2.83}$$

Figure 2.1 shows a sketch of such discretization with $k = 3$, and $c = 2$. Thus, for all y,

$$\underline{F}_k(y) \leq F(y) \leq \overline{F}_k(y). \tag{2.84}$$

Let $G_n(x_k)$, $\overline{G}_n(x_k)$ and $\underline{G}_n(x_k)$ be the bundle strength distributions corresponding to fiber strength distributions $F_k(y)$, $\overline{F}_k(y)$ and $\underline{F}_k(y)$ respectively. Then,

$$\overline{G}_n(x_k) \geq G_n(x_k) \geq \underline{G}_n(x_k) \tag{2.85}$$

This can be seen by investigating the realizations of fiber strength. For any set of realizations S_F of n-fiber bundles drawn from the distribution $F(y)$, a set of equal probability $S_{\underline{F}}$ drawn from $\underline{F}_k(y)$ can be constructed by horizontally projecting

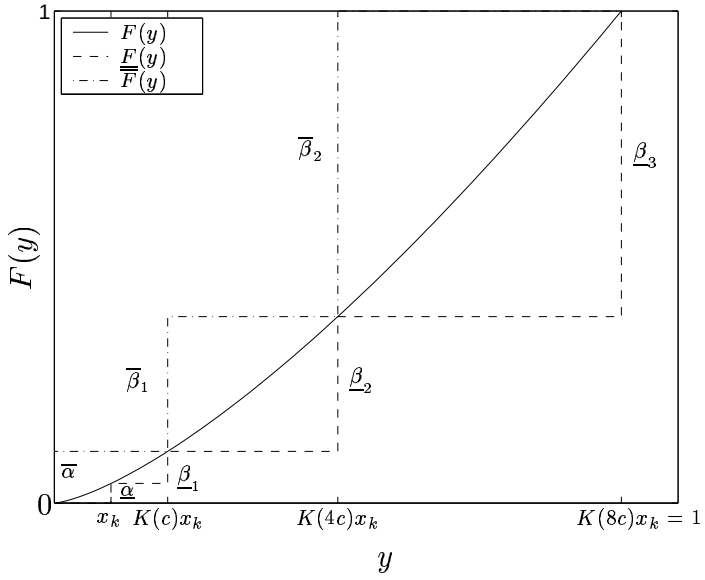

Figure 2.1: Schematic of the discretization of a continuous power law distribution using $k = 3$, and $c = 2$.

fiber strengths in S_F onto the distribution $\underline{F}_k$. More specifically, suppose $\omega_F = \{s_1, s_2, \ldots, s_n\} \in S_F$ is a realization of an n-fiber bundle drawn from $F(y)$. From it we may then construct the realization $\omega_{\underline{F}} = \{\underline{s}_1, \underline{s}_2, \ldots, \underline{s}_n\} \in S_{\underline{F}}$ according to

$$\underline{s}_i = 1 + \frac{c}{2}\left\lceil \frac{2}{c}\sqrt{\frac{s_i}{x_k} - 1} \right\rceil^2 \tag{2.86}$$

For the discretised distribution function (2.82) we note that the error term in (2.77) is $O(1/c)$. Also, we have $\ell_j = cj^2$, for $j = 1, 2, \ldots, k$. It turns out that this choice of ℓ_j maximizes $\underline{G}_n(x_k)$; i.e., $\ell_j = cj^2$ approximately satisfies $\partial\mu_k/\partial\ell_j = 0$, for $j = 1, \ldots, k$. Similarly, $\ell_j = cj^2$, $j = 1, \ldots, k-1$ minimizes $\overline{G}_n(x_k)$ thereby supplying tight bounds on $G_n(x_k)$.

Corresponding to the discrete distribution function $\underline{F}_k(y)$ we have the proba-

bility masses

$$\begin{aligned} \underline{\alpha} &= x_k^\rho \\ \underline{\beta}_j &= (K(j^2c)x_k)^\rho - (K((j-1)^2c)x_k)^\rho, \text{ for } j = 1, 2, \ldots, k \end{aligned} \tag{2.87}$$

where we have identified the masses with underlined versions of $\alpha, \beta_1, \ldots$ defined in Section 2.3. Similarly, corresponding to $\overline{F}_k(y)$ we have

$$\begin{aligned} \overline{\alpha} &= (K(c)x_k)^\rho \\ \overline{\beta}_j &= (K((j+1)^2c)x_k)^\rho - (K(j^2c)x_k)^\rho, \text{ for } j = 1, 2, \ldots, k-1 \end{aligned} \tag{2.88}$$

We now apply (2.77) to compute the probability of failure of a 0-1-2-$\cdots$-k bundle, $\underline{G}_n(x_k)$ whose fiber strengths are distributed according to $\underline{F}_k(y)$ under applied load x_k per fiber. Observe that in this case

$$\gamma_j = \frac{1}{\{K(j^2c)\}^\rho}.$$

The first product in (2.77) becomes

$$\begin{aligned} \prod_{j=1}^{k} C_{j-1} &= \left(1 - \frac{1}{K_1^\rho}\right)\left(1 - \frac{1}{K_r^\rho}\right) \prod_{j=2}^{k} \frac{\left(\frac{1}{K_{j-1}^\rho} - \frac{1}{K_j^\rho}\right)\left(1 + \frac{1}{K_{j-1}^\rho}\right)\left(1 - \frac{1}{K_j^\rho}\right)}{\frac{1}{K_{j-1}^\rho}\left(1 - \frac{1}{K_{j-1}^\rho K_j^\rho}\right)} \\ &\approx \prod_{j=1}^{k}\left(1 - \left(\frac{c(j-1)^2+2}{cj^2+2}\right)^\rho\right) \approx \prod_{j=1}^{k}\left(1 - \left(1 - \frac{1}{j}\right)^{2\rho}\right) \end{aligned} \tag{2.89}$$

To further simplify (2.89) we note that

$$1 - \left(1 - \frac{1}{j}\right)^{2\rho} \approx \begin{cases} 2\rho/j, & \text{for } j > \lceil 3\rho \rceil \\ \exp\left(-e^{-2\rho/j}\right), & \text{for } j \le \lceil 3\rho \rceil \end{cases} \tag{2.90}$$

where we have picked the transition point from one form to the other by comparing the numerical values of each form on the right side with the form on the left side. Then,

$$\prod_{j=1}^{k} C_{j-1} \approx \prod_{j=1}^{r}\left(1 - \left(1 - \frac{1}{j}\right)^{2\rho}\right) \approx \Phi(\rho)\frac{(2\rho)^k}{k!} \tag{2.91}$$

where

$$\begin{aligned}\Phi(\rho) &= \prod_{j=1}^{\lceil 3\rho\rceil} \frac{\exp(-e^{-2\rho/j})}{2\rho/j} \\ &\approx \frac{\lceil 3\rho\rceil!}{(2\rho)^{\lceil 3\rho\rceil}} \exp\left(-\int_0^{\lceil 3\rho\rceil} e^{-\frac{2\rho}{t}} dt\right) \\ &\approx \frac{\lceil 3\rho\rceil!}{(2\rho)^{\lceil 3\rho\rceil-1}} \exp\left\{-\lceil 3\rho\rceil \exp(-2\rho/\lceil 3\rho\rceil) + 2\rho \mathrm{Ei}(-2\rho/\lceil 3\rho\rceil) + e^{-2\rho}\right\}\end{aligned} \tag{2.92}$$

where Ei denotes the exponential integral

$$\mathrm{Ei}(x) = \int_{-\infty}^{x} \frac{e^t}{t} dt, \qquad x \neq 0$$

The second product in (2.77) may be reduced as

$$\prod_{j=1}^{k} (\ell_j - \ell_{j-1}) = \prod_{j=0}^{k-1} \{c(j+1)^2 - cj^2\} = \left(\frac{c}{2}\right)^k \frac{(2k)!}{k!} \tag{2.93}$$

Finally, the third product in (2.77) becomes

$$\begin{aligned}\prod_{j=0}^{k-1} \left\{\left(1 + \frac{j^2 c}{2}\right) x_k\right\}^{\rho c(2j+1)} &= {x_k}^{\rho c} \prod_{j=1}^{k-1} \left(\frac{j^2 c x_k}{2}\right)^{\rho c(2j+1)} \left(1 + \frac{2}{j^2 c}\right)^{\rho c(2j+1)} \\ &\approx (k^2 e)^{2\rho} (2/c)^{\rho c} \exp\left(-\frac{2\rho}{x_k}\right) \left(\frac{(k!)^2}{k^{2(k+1)}}\right)^{\rho c}\end{aligned} \tag{2.94}$$

Upon applying Stirling's formula $k! \approx \sqrt{2\pi} e^{-k} k^{k+0.5}$ and making the substitution $k^2 c/2 \approx 1/x_k$ for large k, we have

$$\begin{aligned}\prod_{j=0}^{k-1} \left\{\left(1 + \frac{j^2 c}{2}\right) x\right\}^{\rho c(2j+1)} &\approx \left(\frac{4\pi}{c}\right)^{\rho c} \left(\frac{2e}{c x_k}\right)^{2\rho} \left(\frac{c x_k}{2}\right)^{\rho c/2} \\ &\qquad \exp\left(-\frac{2\rho}{x_k} - 2\rho c \sqrt{\frac{2}{c x_k}}\right)\end{aligned} \tag{2.95}$$

Multiplying (2.91), (2.93) and (2.95), we have for $\underline{G}_n(x_k)$

$$\underline{G}_n(x_k) = \mu_k(n) = (n - 2/x_k)\, \underline{\aleph}(c, \rho) \left(\frac{c x_k}{2}\right)^{\frac{\rho}{2}(c-4)+\frac{1}{4}} \exp\left(-\underline{B}\frac{2\rho}{x_k}\right) \tag{2.96}$$

where

$$\underline{\aleph}(c,\rho) = \Phi(\rho)\left(\frac{4\pi}{c}\right)^{\rho c}\frac{e^{2\rho}}{\sqrt{\pi}} \tag{2.97}$$

and

$$\underline{B} = 1 + (2c - \frac{\log(4\rho c)}{\rho})\sqrt{\frac{x_k}{2c}} \tag{2.98}$$

A similar calculation may be carried out for $\overline{G}_n(x_k)$ which is the probability of failure of a bundle with fiber strengths distributed according to the law $\overline{F}_k(y)$. Manipulating the expression for $\mu_r(n)$ in (2.77) as before, we get

$$\overline{G}_n(x_k) = \mu(n) = (n - 2/x_k)\,\overline{\aleph}(c,\rho)\left(\frac{cx_k}{2}\right)^{\frac{\rho}{2}(c-4)+\frac{3}{4}}\exp\left(-\overline{B}\frac{2\rho}{x_k}\right) \tag{2.99}$$

where

$$\overline{\aleph}(c,\rho) = \Phi(\rho)\left(\frac{1}{2\pi}\right)^{\rho c}\frac{e^{-2\rho}}{\sqrt{\pi}}\frac{1}{2c} \tag{2.100}$$

and

$$\overline{B} = 1 - (2c + \frac{\log(4\rho c)}{\rho})\sqrt{\frac{x_k}{2c}} \tag{2.101}$$

The bounds $\overline{G}_n(x_k)$ and $\underline{G}_n(x_k)$ are hardly asymptotically convergent as $x_k \downarrow 0$. In fact,

$$\frac{\overline{G}_n(x_k)}{\underline{G}_n(x_k)} \sim \sqrt{x_k}\exp\left(\sqrt{\frac{32\rho^2 c}{x_k}}\right) \tag{2.102}$$

which blows up as $x_k \downarrow 0$.

2.9 Discussion and Conclusion

Despite their not being tight bounds, the forms of $\overline{G}_n(x_k)$ and $\underline{G}_n(x_k)$ suggest the following form for the strength distribution of n-fiber bundles with power law distributed fibers:

$$\tilde{G}_n(x_k) = (n - 2/x_k)\aleph(c,\rho)\left(\frac{cx_k}{2}\right)^{\frac{\rho}{2}(c-4)+\varphi_1}\exp\left(-B\frac{2\rho}{x_k}\right) \tag{2.103}$$

where $B = 1+(\varphi_2-\log(4\rho c)/\rho))\sqrt{x_k/2c}$ with $-2c \leq \varphi_2 \leq 2c$ and $1/4 \leq \varphi_1 \leq 3/4$. Also $\aleph$ must be bounded between $\underline{\aleph}$ and $\overline{\aleph}$.

The question arises as to the choice of c. Clearly, choosing $c = 1$ or close to one in (2.82) and (2.83) results in the finest possible discretization, one which will capture the true fiber strength distribution. However if such a choice were made the error bounds in (2.78) will become $O(1)$. Thus c should be chosen large enough that the errors in (2.78) are well bounded, while not so large that it is an extremely coarse discretization of the given power law distribution.

It is interesting to note that a form for $\tilde{G}_n(x)$ similar to (2.103) was arrived at by Phoenix and Beyerlein [9] using heuristic arguments for growth of clusters of breaks in a composite with fibers of continuously distributed random strengths. For the n-fiber bundle distribution they obtain

$$\begin{aligned} \tilde{G}_n(x) &= n\aleph(\rho)\left(\frac{x}{2}\right)^{-\frac{3\rho}{2}} \exp\left(-B\frac{2\rho}{x}\right) \\ &= 1 - \exp\left[-n\aleph(\rho)\left(\frac{x}{2}\right)^{-\frac{3\rho}{2}} \exp\left(-B\frac{2\rho}{x}\right)\right] \end{aligned} \tag{2.104}$$

where

$$B = 2^{-\frac{1}{\rho}}\left[1 + \frac{1}{\rho^2}\left(\Gamma(1/\rho, 1) + \frac{\rho}{2(\rho+1)}\right)\right] \tag{2.105}$$

where $\Gamma(1/\rho, 1)$ refers to the incomplete gamma function. Also, for $\aleph$ they have

$$\aleph(\rho) = \frac{2^\rho e^{3\rho}}{2^{5/2}3^{5\rho/2}} \tag{2.106}$$

This formula has been verified against Monte Carlo simulations and found to be very accurate when ρ is large, say $\rho \geq 5$. It will be observed that although the scale factor $\aleph$ does not match, the other dominant terms including the power of $(x/2)$ and the argument of the exponential functions in (2.103) and (2.104) match very closely by setting $c = 1$ in (2.103). This suggests that the error bound (2.78) is much too conservative when ρ is large when c is taken to be small.

Bibliography

[1] Harlow, D. G., and Phoenix, S. L., (1978) The chain-of-bundles probability model for the strength of fibrous materials I: analysis and conjectures. *J. Comp. Mater.*, **12** 195–214.

[2] Hedgepeth, J.M., (1961) Stress concentrations in filamentary structures. *NASA TND–882*.

[3] Harlow D. G., (1985), The pure flaw model for chopped fiber composites , *Proc. R. Soc. Lond. A* **397**, 211–232.

[4] Harlow D. G., Phoenix, S. L., (1981).Probability distributions for the strength of composite materials, Parts I and II. *Int. J. Fract.*, **17**, 4. 347–371 and 601–629.

[5] C-C Kuo and S. L. Phoenix (1987) Recursions and limit theorems for the strength and lifetime distributions of a fibrous composite, *J. App. Probab.*, **24** No. 1, 137–159.

[6] D.G. Harlow and S. L. Phoenix (1991) Approximations for the strength distribution and size effect in an idealized lattice model of material breakdown, *J. Mech. Phys. Solids*, **39** No. 2, 173–200.

[7] Leath, P.L. and Duxbury, P.M., Exactly solvable models of material breakdown, *Phys. Rev. B*, **49**, 12676

[8] Arratia, R., Goldstein, L., and Gordon, L. (1990), Poisson approximation and the Chen-Stein method, *Stat. Sci.*, **5** No. 4, 403–434.

[9] Phoenix, S. L., and Beyerlein, I. J., (2000) Statistical strength theory for fibrous composite materials, in *Comprehensive Composite Materials*, Edited by A. Kelly and C. Zweben.

Chapter 3

Theoretical and Monte Carlo Study of Lifetime Distribution for Fibrous Composites in Creep-Rupture Loading

3.1 Introduction

This work considers the lifetime statistics for unidirectional fiber-reinforced composite materials in which aligned elastic creeping fibers are embedded in a viscoelastic matrix and which fail by stress- or creep-rupture under tensile creep loading (sustained load over long durations). The failure process involves both random time dependent fiber failure and matrix viscoelastic creep. If the fibers are much stiffer than the matrix, as is commonly the case, the bulk of the tensile load applied in the fiber direction is borne by the fibers. Accordingly composite

lifetime is for the most part determined by stochastic fiber failures which introduce considerable statistical variability in composite lifetime itself. In this work we construct probabilistic failure models of such materials under creep loading, derive composite lifetime distributions from these models and validate them against empirical distributions obtained from Monte Carlo simulations of their failure.

Common examples of fiber-matrix systems which undergo creep rupture when subjected to creep loading include polymer matrix composites such as aramid, graphite, S-glass, or kevlar fibers embedded in a polymer matrix such as epoxy or polyester resin or metal matrix composites such as silicon carbide fibers in an aluminum matrix. Pressure vessels, engine components, flywheels, and reusable rocket motor casings are some of the structures in which these fiber-matrix systems find application and in which they may fail by creep rupture. In life safety applications, structures must be designed so that their probability of failure is extremely low (smaller than say 10^{-6}) and for this reason accurate knowledge of their lower tail lifetime distribution is valuable.

Fiber creep-rupture originates at the molecular level in the form of intermolecular slipping and bond breaking due to thermal activation especially in kevlar fibers and to a lesser extent also in graphite fibers. In time, these microstructural defects are thought to overload other neighboring molecular bonds eventually forming microcracks or flaws of random strength at random locations in the fiber which grow in time and eventually travel across the fiber, thereby failing it. Conceptually, fiber failure models capture the growth of defects within small fiber segments by accounting for the time taken by some defect in a small fiber segment to reach a critical size. This time depends on its load history and the inherent variability of the material.

Damage accumulation within a unidirectional composite under creep loading begins with the failure of the weakest fiber flaws some time after load application. Fiber failure may be accompanied by one or more of fiber-matrix interfacial debonding, matrix yielding, fiber pull-out and frictional sliding of the fiber in relation to the matrix. In all cases, stress dropped at a broken fiber gets transferred primarily by means of matrix shear to neighboring intact fibers whose failure it then proceeds to hasten. This in turn may lead to successive failure of nearby fibers culminating in the formation of a propagating catastrophic crack which will fail the entire composite. While the complex phenomena accompanying fiber failure undoubtedly affect composite lifetime statistics, they are secondary in that they merely modify the composite lifetime determined by fiber breaking and the interaction between fiber breaks.

A comprehensive study of the composite failure process including all the details of the failure mechanisms is yet impossible both from a mechanics and from a stochastic process standpoint. We will therefore first describe an idealization of composite structure and failure processes in terms of successive fiber failure and load redistribution by means of matrix shear which, while still preserving its key physical aspects and capturing the dominant statistics of its lifetime, will render its consideration tractable.

3.1.1 The Idealized Unidirectional Composite

Our idealized composite consists of a parallel array of n stiff, brittle, elastic fibers of cross sectional area A_f and length L, embedded in a flexible, perfectly bonded, elastic or viscoelastic matrix. Two fiber arrays are considered: a linear array forming a 2D planar composite ("2D Array") and a hexagonal array forming a

3D composite ("3D Array"), as shown in Figure 3.1. As shown in the figure, fibers in the 2D array are indexed from left to right by a single integral coordinate ℓ whereas in the 3D array, each fiber is identified by its ℓ and m coordinates. We assume a high fiber-matrix stiffness ratio so that the fibers carry virtually all the tensile load. The composite is loaded by applying a far-field, tensile load p_∞ to the fibers so that total tensile load is approximately np_∞. The matrix acts primarily to transfer load locally from broken to intact fibers through shear. This is idealized in terms of specific fiber load-sharing models in Section 3.2.

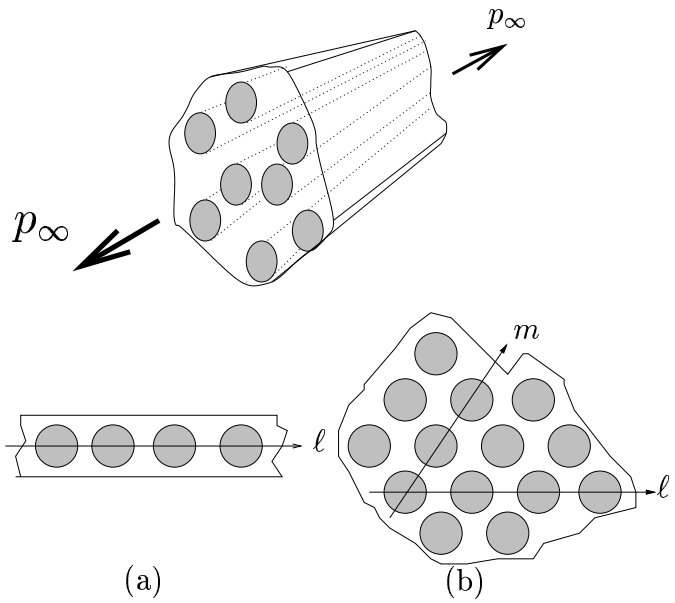

Figure 3.1: The two fiber arrays considered: (a) planar array and (b) hexagonal array. The far-field stress applied to the fibers is p_∞. Fibers in the 2D array are indexed by a single integer ℓ whereas in the 3D array, they are indexed by the ordered pair (ℓ, m).

Fibers typically have random flaws distributed along them which are formed during their manufacture or processing. In Section 3.3 we adapt a fiber lifetime

model due to Coleman to our particular situation wherein the lifetime of a fiber is determined by the breakdown of its weakest flaw which depends on its load history. As would be expected, for fixed weakest flaw strength the lifetime decreases with increasing fiber load and for fixed load history, the lifetime decreases with decreasing flaw strength. As the strength of the weakest flaw tends to be random, so also is the fiber lifetime for a given load history.

When a constant tensile load of p_∞ per fiber is applied to a composite specimen, the first few weakest fibers successively fail and the matrix surrounding each fiber break serves to transfer the lost fiber load to neighboring fibers through shear deformation. This stress transfer occurs over a length scale, which in general is time-dependent, and of the order of a few fiber diameters. The resulting local stress concentrations may cause neighboring fibers to fail earlier than the next weakest fiber in the composite under far field load of p_∞, thereby possibly diverting the fiber break path from that which follows the weakest flaw strengths to that which follows the highest stress concentrations. In turn, as time progresses, these new breaks will cause even more fiber failures in their vicinity, and so on. Elsewhere in the composite, removed from this growing cluster of breaks other fiber failures continue to occur; these may merge and become part of the cluster as it grows. As the size of a cluster of breaks grows, the stress concentration on the fibers ahead of the cluster tip steadily increases and the time between the formation of breaks extending the cluster decreases. In other words as time progresses, cluster growth accelerates and effectively forms a running crack which propagates until it fails all the fibers in the composite. The lifetime of a specimen is defined as the time to complete failure of the composite since the time of application of a far-field load.

3.1.2 Results from Previous Literature

We may classify previous literature pertinent to the present study into two categories. The first category consists of work on fiber lifetime model formulation and the determination of asymptotic lifetime of equal load sharing bundles by Coleman [1, 2, 3, 4, 5], and Phoenix [6]. Equal load sharing is the manner of load redistribution in a partially failed composite wherein the load dropped by broken fibers is equally divided amongst all the surviving fibers. We detail Coleman's fiber lifetime formulation in Section 3.3 and Phoenix's conclusion that the lifetime of an equal load sharing bundle of Coleman fibers is asymptotically normally distributed in Section 3.4.1 and will therefore not go into them here. Ibnabdeljalil and Phoenix [7] study the lifetime distribution of composites by means of Monte Carlo simulations where global load sharing, a more continuous version of equal load sharing in which stresses dropped by a break is regained a certain characteristic distance away from the break, applies and find that under certain conditions, their empirical distributions have a weakest link structure in terms of links with log-normal lifetime.

The second category of work relates to local load sharing composites. Here, unlike in equal load sharing bundles, stress concentration ahead of a transverse array of fiber breaks (a discrete crack) in the composite is concentrated at the crack tip and fibers further away feel little overload due to the crack. The asymptotic lifetime in such a case is not normal. Instead it has a weakest link basis in terms of a certain characteristic lifetime distribution as Tierney[8, 9] and Phoenix and Tierney[10] have shown. These authors consider idealized load sharing rules, which in the case of a planar array of fibers translates to the stress concentration on the two fibers adjacent to an r-cluster of breaks being equal to $1 + r/2$. While this

idealization captures the important characteristic of crack formation and propagation in the composite, it is far too severe. Hedgepeth [11] and Hedgepeth and Van Dyke [12] give a mechanically consistent means of calculating the stress state in a partially damaged composite by their shear-lag analysis which results in more realistic stresses in the composite. Their analysis is restricted to the case where both the fiber and matrix are elastic. It was extended by Lagoudas et al [13] to the case when the matrix may be viscoelastic and all the fiber breaks in the composite lie in a single plane perpendicular to the fiber direction. Beyerlein and Phoenix [14] however give a shear-lag methodology to compute the stress state in the composite under arbitrary arrangements of breaks. To our knowledge, lifetime studies of Hedgepeth composites with fibers undergoing time-dependent breakdown and an elastic or viscoelastic matrix have not been done and we address that question here.

A class of problems closely related to the lifetime problem of composites is the strength problem where fibers have random strengths according to some prescribed distribution function and the composite is loaded quasistatically under increasing tension. The strength distribution of the composite is usually sought. The strength problem can be viewed as a limiting case of the lifetime problem and affords insights into the dominant composite failure modes near the limit. In this connection we note the works of Beyerlein and Phoenix [15, 16], Landis et al [17], Wu and Leath [18], Newman and Phoenix [19], and Mahesh et al [20].

3.2 Load Sharing in Unidirectional Arrays

In this section we extend the method of Beyerlein and Phoenix [14] and Landis et al [17] to calculate the stress state in a finite partially failed arbitrary array of fibers embedded in an elastic or a viscoelastic matrix. In addition we provide for the application of periodic boundary conditions in all directions which will enable us to consider a periodically repeating *unit cell* and determine stresses in it in the presence of fiber breaks.

3.2.1 Governing Equations and Boundary Conditions

We consider a collection of $n < \infty$ fibers aligned parallel to the x-axis and embedded arbitrarily in a matrix. According to Hedgepeth's shear-lag assumptions, fibers deform in pure tension and the matrix deforms in pure shear. The fibers are loaded uniformly in the far field at $x = \pm\infty$ in simple tension under load p_∞ per fiber (i.e., the entire composite carries load np_∞), where x is the coordinate along the fiber direction. We will frequently refer to the fiber direction as longitudinal and to the planes perpendicular to it as transverse. We assume that fibers are linear elastic and let E_f be the fiber tensile modulus and A_f its cross sectional area. Let $p_i(x,t)$ and $u_i(z,t)$ be the tensile load and displacement respectively in fiber i, $1 \le i \le n$ at position x and time t. Clearly $p_i(x,t) = p_\infty$ for all x and t when all the fibers are intact. However if some fibers break, loads redistribute from broken to intact fibers through shear stresses in the matrix. Let the shear force per unit length transmitted from fiber j to fiber i through the matrix at (x,t) be $q_{ij}(x,t)$. Then for force equilibrium of a fiber element of length dx, we need

$$A_\mathrm{f}\frac{\partial p_i}{\partial x}dx + \left(\sum_{j=1}^{n} q_{ij}\right) dx = 0, \qquad i = 1, 2, \ldots, n. \tag{3.1}$$

Hooke's law for the fiber gives

$$p_i(x,t) = E_{\rm f} A_{\rm f} \frac{\partial u_i(x,t)}{\partial x}. \tag{3.2}$$

To relate q_{ij} to the relative displacement of fibers we must assume a matrix constitutive law. Here we assume a matrix with power-law viscoelastic creep compliance in shear,

$$J_{\rm m} = J_{\rm e} \left(\frac{t}{t_{\rm cm}} \right)^{\alpha} \tag{3.3}$$

and limit ourselves to $0 \leq \alpha \leq 1$. If $G_m(t)$ is the corresponding relaxation modulus, it can be shown using Laplace transforms and the fact $s^2 \bar{J}_{\rm m}(s) \bar{G}_{\rm m}(s) = 1$ that

$$G_{\rm m}(t) = G_{\rm e} \left(\frac{t_{\rm cm}}{t} \right)^{\alpha} \tag{3.4}$$

where $G_{\rm e}$ and $J_{\rm e}$ are related according to

$$G_{\rm e} = 1/(J_{\rm e}\Gamma(1+\alpha)\Gamma(1-\alpha)). \tag{3.5}$$

Then

$$q_{ij}(x,t) = \int_{-\infty}^{t} G_{\rm m}(t-v)\varphi_{ij} \frac{\partial}{\partial v}(u_j(x,v) - u_i(x,v))dv \tag{3.6}$$

The form (3.3) assumed for creep compliance is a reduction of the form

$$J'_{\rm m}(t) = J_{\rm e}(1 + t/t_{\rm cm})^{\alpha} \tag{3.7}$$

which, unlike (3.3) also accounts for instantaneous elastic shear response of the matrix. Form (3.3) is used because it is more amenable to algebraic manipulations than (3.7). Asymptotically as $t/t_{\rm cm} \to \infty$, the two forms converge but differ in the initial response at smaller times. It turns out that the instantaneous stress and displacement response of (3.7) is well approximated by (3.3) by setting $t = t_{\rm cm}$.

In (3.6), $\varphi_{ij}(u_j(x,v) - u_i(x,v))$ is the matrix displacement in shear and q_{ij} represents the shear force on fiber i due to fiber j as a hereditary integral. φ_{ij},

$i \neq j$ is a non-negative non-dimensional geometric parameter that may quantify the proximity of fibers i and j.

In simulating 2D arrays, we impose periodic boundary conditions on the string of n fibers so that fibers $\ell = 1$ and $\ell = n$ are adjacent. In this case φ_{ij} is readily expressible in terms of composite geometric parameters. Let the effective matrix width between the fibers be w, and the matrix thickness (perpendicular to the plane of the fibers) be h. A simple case is to assume h is also the main fiber cross-sectional dimension. In the matrix bay between adjacent fibers $\ell = i$ and $\ell = i + 1$, we take the effective shear force per unit length $q_{i,i+1}(z)$ to be

$$q_{ij}(x,t) = \int_{-\infty}^{t} G_{\mathrm{m}}(t-v)\frac{h}{w}\frac{\partial}{\partial v}(u_j(x,v) - u_i(x,v))dv, \quad \text{if } |i-j| = 1 \tag{3.8}$$

and $q_{ij}(x,t) = 0$ otherwise. Thus for the 2D array, we take

$$\varphi_{ij} = \begin{cases} h/w & \text{if } |i-j| \mod n = 1, \\ 0 & \text{otherwise} \end{cases} \tag{3.9}$$

when $i \neq j$. In our 3D array simulations of n fiber unit cells we assume they have rhombus shaped transverse sections of side length $\sqrt{n}$ with periodic boundary conditions imposed upon them so that each edge of the rhombus cross section is contiguous with the edge opposite to it. We label the fiber at $(\ell, m) = (0,0)$ as 1, then we label the remaining fibers in the composite with integers in sequence first proceeding along the $m = 0$ row, then the $m = 1$ row and so on until the $m = \sqrt{n} - 1$-th row. Thus, the fiber with label i is located at $\ell = i \mod \sqrt{n}$ and $m = \lfloor i/\sqrt{n} \rfloor$. Conversely, the fiber at (ℓ, m) is indexed by $\ell\sqrt{n} + m + 1$.

In such an array, a similar argument for φ_{ij} as in the 2D array can be carried

through with w representing an effective matrix thickness.

$$\varphi_{(\ell_1,m_1),(\ell_2,m_2)} = \begin{cases} h/w & \text{if } \max((\ell_1-\ell_2) \bmod \sqrt{n}, (m_1-m_2) \bmod \sqrt{n}) = 1, \\ 0 & \text{otherwise} \end{cases} \tag{3.10}$$

where (ℓ_1, m_1) are the coordinates of fiber i and (ℓ_2, m_2) are the coordinates of fiber j and $i \neq j$. We will specify φ_{ii} later. While we have delved into the consideration of these two arrays owing to their relevance in the following sections, the shear-lag methodology presented in the remainder of this section is applicable to arbitrary fiber arrays as long as their φ_{ij} is chosen appropriately.

Combining (3.1), (3.2), and (3.6) we have for the governing differential equation

$$\begin{aligned} E_{\mathrm{f}}A_{\mathrm{f}}\frac{\partial^2 u_i(x,t)}{\partial x^2} + \int_{-\infty}^{t} G_{\mathrm{m}}(t-v)\frac{\partial}{\partial v}\left(\sum_{\substack{j=1 \\ j\neq i}}^{n} \varphi_{ij}u_j(x,v) - \left(\sum_{j=1}^{n}\varphi_{ij}\right)u_i(x,v)\right) dv \\ = 0 \qquad i = 1, 2, \ldots, n \end{aligned} \tag{3.11}$$

Defining

$$\varphi_{ii} = -\sum_{j=1 i\neq j}^{n} \varphi_{ij}, \tag{3.12}$$

(3.11) can be shortened to

$$E_{\mathrm{f}}A_{\mathrm{f}}\frac{\partial^2 u_i(x,t)}{\partial x^2} + \int_{-\infty}^{t} G_{\mathrm{m}}(t-v)\left(\sum_{j=1}^{n}\varphi_{ij}\frac{\partial u_j(x,v)}{\partial v}\right) dv = 0 \tag{3.13}$$

We now turn to the boundary conditions in conjunction with which this system of differential equations must be solved. Let B be the set of r breaks in the periodic patch at time t. We locate each break by the fiber on which it occurs and its x coordinate in the fiber direction. That is, let

$$B = \{(i_1, x_1), (i_2, x_2), \ldots, (i_r, x_r)\}. \tag{3.14}$$

Also let us consider a composite in which these breaks occur periodically along the fiber direction with periodicity L. That is, if $x_k < L$, $k = 1, \ldots, r$, fiber breaks repeat at $x_k \pm jL$, $j = 0, 1, 2, \ldots$. This is actually a generalization of the case wherein infinite boundary conditions are considered; the case of infinite boundary conditions is retrieved by letting $L \to \infty$. If L is finite, periodicity demands that for $i = 1, 2, \ldots, n$

$$p_i(x = 0, t) = p_i(x = L, t), \qquad t \geq 0, \tag{3.15}$$

for traction continuity in the fiber direction across unit cells and if $c(t)$ denotes some arbitrary function continuous in t

$$u_i(0, t) = u_i(L, t) + c(t), \quad t \geq 0, \quad (i, 0) \notin B \tag{3.16}$$

for displacement continuity in the absence of boundary cracks. $c(t)$ is independent of i but in general must depend on the position and number of fibers in the array. By way of the traction free boundary condition at fiber breaks, we have

$$p_{i_k}(x_k) = E_{\mathrm{f}} A_{\mathrm{f}} \frac{\partial u_{i_k}(x_j)}{dx} = 0, \qquad (i_k, x_k) \in B, \quad k = 1, \ldots, r. \tag{3.17}$$

And finally in order that the applied load be carried by all the fibers, we must have

$$\sum_{i=1}^{n} p_i(x, t) = n p_\infty, \quad t \geq 0, \quad 0 \leq x \leq L. \tag{3.18}$$

In Section 3.2.3, we solve the problem of determining stresses in a periodic patch in the presence of a single break and in Section 3.2.4, we detail the approach to superpose single break solutions in order to handle multiple interacting breaks which may or may all form at once. But first in Section 3.2.2, we express the boundary value problem in non-dimensional terms by suitable change of variables.

3.2.2 Normalized Governing Equations and Boundary Conditions

We define the quantities φ and δ_{v} as

$$\varphi = \max_{\substack{1\le i,j\le n \\ i\neq j}} \varphi_{ij}, \tag{3.19}$$

and

$$\delta_{\mathrm{v}} = \sqrt{\frac{E_{\mathrm{f}} A_{\mathrm{f}} J_{\mathrm{e}}}{\varphi}}. \tag{3.20}$$

δ_{v} is a viscoelastic characteristic length and is approximately the length of the unload zone around a fiber break after time t_{cm} of its formation. Correspondence can be made between the elastic and the viscoelastic matrix problems by choosing the parameters of the creep compliance such that $\delta_{\mathrm{v}} \approx \delta_{\mathrm{e}} \approx \sqrt{EA/G\varphi}$ where G is the shear modulus of the elastic matrix.

In terms of φ and δ_{v}, we define ϕ_{ij}, ξ, p_i and U_i, for $1 \le i, j \le n$ as

$$\phi_{ij} = \frac{\varphi_{ij}}{\varphi} \tag{3.21}$$

$$\xi = \frac{x}{\delta_{\mathrm{v}}} \tag{3.22}$$

$$\tau = \frac{t}{t_{cm}} \tag{3.23}$$

$$\mathscr{G}_{\mathrm{m}}(\tau) = \frac{G(\tau t_{\mathrm{cm}})}{G_{\mathrm{e}}} \tag{3.24}$$

$$\sigma_i(\xi,\tau) = \frac{p_i(\xi\delta_{\mathrm{v}}, \tau t_{\mathrm{cm}})}{p_\infty} \tag{3.25}$$

$$U_i(\xi,\tau) = u_i(\xi\delta_{\mathrm{v}}, \tau t_{\mathrm{cm}}) \frac{E_{\mathrm{f}} A_{\mathrm{f}}}{p_\infty \delta_{\mathrm{v}}} \tag{3.26}$$

The normalization of u_i is such that Hooke's law takes on the form

$$\frac{\partial U_i}{\partial \xi} = \sigma_i. \tag{3.27}$$

In accordance with (3.22), the normalized composite unit cell length becomes

$$\mathfrak{L} = \frac{L}{\delta_{\mathrm{v}}}. \tag{3.28}$$

Also from (3.9), (3.12), and (3.21) it follows that for 2D arrays,

$$\phi_{ij} = \begin{cases} -2 & \text{if } i = j, \\ 1 & \text{if } |i-j| \mod n = 1, \\ 0 & \text{otherwise} \end{cases} \tag{3.29}$$

Similarly, for 3D arrays, we have from (3.10), (3.12), and (3.21) that

$$\varphi_{(\ell_1,m_1),(\ell_2,m_2)} = \begin{cases} -6 & \text{if } \ell_1 = \ell_2 \text{ and } m_1 = m_2, \\ 1 & \text{if } \max((\ell_1-\ell_2) \mod \sqrt{n}, (m_1-m_2) \mod \sqrt{n}) = 1, \\ 0 & \text{otherwise.} \end{cases} \tag{3.30}$$

With these normalizations, the governing equation (3.11) becomes

$$\frac{\partial^2 U_i(\xi,\tau)}{\partial \xi^2} + \int_{-\infty}^{\tau} \mathscr{G}_{\mathrm{m}}(\tau - v) \left(\sum_{j=1}^{n} \phi_{ij} \frac{\partial U_j(\xi, v)}{\partial v} \right) dv = 0 \qquad i = 1, 2, \ldots, n \tag{3.31}$$

As for the normalized version of the boundary conditions (3.15)–(3.18), we have

$$\sigma_i(\xi = 0, \tau) = \sigma_i(\xi = \mathfrak{L}, \tau), \quad \tau \geq 0, \quad i = 1, \ldots, n \tag{3.32}$$

$$\sigma_{i_k} = \frac{\partial U_{i_k}(\xi_j)}{\partial \xi} = 0, \quad (i_k, \xi_k) \in B, \quad k = 1, \ldots, r \tag{3.33}$$

$$U_i(\xi = 0, \tau) = U_i(\xi = \mathfrak{L}, \tau) + c(\tau) \quad (i, 0) \notin B \tag{3.34}$$

and

$$\sum_{i=1}^{n} \sigma_i(\xi, \tau) = n, \quad 0 \leq \xi \leq \mathfrak{L}, \quad \tau \geq 0. \tag{3.35}$$

$c(\tau)$ in the third boundary condition is the normalized version of $c(t)$ in (3.16).

The problem can be cast in influence function terms by effecting the change of variables

$$U_i'(\xi,\tau) = U_i(\xi,\tau) - \xi \tag{3.36}$$

so that if $\sigma_i' = \partial U_i'/\partial\xi$,

$$\sigma_i'(\xi) = \sigma_i(\xi) - 1. \tag{3.37}$$

Primes here do not denote differentiation. To obtain U_i', we must solve the system of differential equations

$$\frac{\partial^2 U_i'(\xi,\tau)}{\partial\xi^2} + \int_{-\infty}^{\tau} \mathscr{G}_{\mathrm{m}}(\tau - v)\left(\sum_{j=1}^{n}\phi_{ij}\frac{\partial U_j'(\xi,v)}{\partial v}\right)dv = 0 \qquad i = 1,2,\ldots,n \tag{3.38}$$

subject to the boundary conditions

$$\sigma_i'(\xi=0,\tau) = \sigma_i'(\xi=\mathfrak{L},\tau), \quad \tau \geq 0, \quad (i,0)\notin B \tag{3.39}$$

$$U_i'(\xi=0,\tau) = U_i'(\xi=\mathfrak{L},\tau) + c'(\tau), \quad (i,0)\notin B \tag{3.40}$$

$$\sigma_{i_k}' = \frac{\partial U_{i_k}'(\xi_j)}{\partial\xi} = -1, \quad (i_k,\xi_k)\in B, \quad k = 1,\ldots,r \tag{3.41}$$

and

$$\sum_{i=1}^{n}\sigma_i'(\xi,\tau) = 0, \quad \tau \geq 0, \quad 0 \leq \xi \leq \mathfrak{L} \tag{3.42}$$

The stress field $\sigma_i'(\xi,\tau)$ is therefore the stress in a periodic patch due to a unit normalized *compressive* load at each of the fiber breaks; i.e., σ_i so determined corresponds to the influence of the compressive force applied at the break on the rest of the composite. If we solve for U_i', it is simple to obtain the displacement field due to the far-field unit normalized tensile load using (3.36) and (3.37). In the next section, we give the solution for a single break and in Section 3.2.4 we extend the solution to multiple breaks by linear superposition.

3.2.3 Single Break Solution

Let $\bar{U}_i(\xi, s)$ be the Laplace transform of $U_i'(\xi, \tau)$, $i = 1, \ldots, n$.

$$\bar{U}_i(\xi, s) = \int_0^\infty U_i'(\xi, \tau) e^{-s\tau} d\tau. \tag{3.43}$$

In terms of $\bar{U}_i(\xi, s)$, (3.31) becomes

$$\begin{gathered} \frac{\partial^2 \bar{U}_i(\xi, s)}{\partial \xi^2} + s\bar{\mathscr{G}}_{\mathrm{m}}(s) \left(\sum_{j=1}^{n} \phi_{ij} \bar{U}_j(\xi, s) \right) = 0 \\ i = 1, \ldots, n \end{gathered} \tag{3.44}$$

Corresponding to the presence of a single break at $(i_0, 0)$, the boundary conditions (3.39)–(3.42) become

$$\frac{\partial \bar{U}_i}{\partial \xi}(0, s) = \frac{\partial \bar{U}_i}{\partial \xi}(\mathfrak{L}, s), \quad s \geq 0, \quad i = 1, 2, \ldots, n \tag{3.45}$$

$$\bar{U}_i(0, s) = \bar{U}_i(\mathfrak{L}, s) + \bar{c}'(s), \quad s \geq 0, \quad i \neq i_0 \tag{3.46}$$

$$\frac{\partial \bar{U}_i}{\partial \xi}(0, s) = -\frac{1}{s}, \quad s \geq 0, \quad i = i_0 \tag{3.47}$$

and

$$\sum_{i=1}^{n} \frac{\partial \bar{U}_i}{\partial \xi}(\xi, s) = 0, \quad 0 \leq \xi \leq \mathfrak{L}, \quad s \geq 0 \tag{3.48}$$

For the power law matrix creep function, we have

$$s\bar{\mathscr{G}}(s) = \frac{s^\alpha}{\Gamma(1+\alpha)}, \quad \alpha \geq 0 \tag{3.49}$$

In terms of the vector $\bar{\mathbf{U}} = \{\bar{U}_1 \bar{U}_2 \cdots \bar{U}_n\}^T$, and the matrix $\Phi = [\phi_{ij}]$, (3.44) can be rewritten as

$$\left(\frac{\sqrt{\Gamma(1+\alpha)}}{s^{\alpha/2}} \right)^2 \frac{\partial^2}{\partial \xi^2} \{\bar{\mathbf{U}}\} - [\mathbf{\Phi}]\{\bar{\mathbf{U}}\} = \{\mathbf{0}\} \tag{3.50}$$

To solve this equation, we need the eigenvalues and eigenvectors of Φ. Φ is a symmetric diagonal dominant matrix with zero row (and column) sums. This implies

that the eigenvalues $\lambda_i^2, i = 1, \ldots, n$ are real and according to Gershgorin's theorem, $\lambda_i^2 \in [0, 2\max_{1\le i\le n} |\phi_{ii}|), i = 1, 2, \ldots, n$. We make the additional assumption that the system of differential equations is semi-connected, that is, given any distinct integers p, and q, there is a sequence of integers $p = k_1,\ k_2,\ k_3,\ \ldots,\ k_m = q$, such that the matrix entries $\phi_{k_1k_2},\ \phi_{k_2k_3},\ \ldots,\ \phi_{k_{m-1}k_m}$ are non-zero. Since $\lambda_1 = 0$ lies on the boundary of the Gershgorin disk, to it corresponds the eigenvector $c\mathbf{1} = \{11\ldots1\}^T$, unique up to the multiplicative constant c. Thus, the null space of Φ is one-dimensional and has the basis $\mathbf{1}$. Also, since the remaining $n-1$ eigenvectors are orthogonal to $\mathbf{1}$, their rows must sum identically to zero.

Let the normalized right eigenvectors of $[-\Phi]$ be $\mathbf{E}_j$, $j = 1, 2, \ldots, n$ corresponding to the eigenvalues λ_j^2, $j = 1, 2, \ldots, n$ where the normalization can, for example, be done so that $\sum_{i=1}^n |E_{ij}| = n$ for each i. As noted above, $\lambda_1 = 0$, and $\mathbf{E}_1 = \mathbf{1}$. The solution to the system of equations (3.50) is

$$\begin{aligned}\bar{\mathbf{U}}(\xi, s) =& \frac{1}{s^{1+\alpha/2}} \{e_1\mathbf{E}_1 + \\ & \sum_{j=2}^{n} e_j\mathbf{E}_j \left[\exp\left(-\frac{\lambda_j s^{\alpha/2}\xi}{\sqrt{\Gamma(1+\alpha)}}\right) - \exp\left(\frac{\lambda_j s^{\alpha/2}(\xi - \mathfrak{L})}{\sqrt{\Gamma(1+\alpha)}}\right)\right]\}\end{aligned} \tag{3.51}$$

where $e_j \equiv e_j(s)$, $j = 1, 2, \ldots, n$ are scalar multiples of the eigenvectors which must be chosen appropriately. Then

$$\begin{aligned}\frac{\partial \bar{\mathbf{U}}}{\partial \xi}(\xi, s) =& \frac{1}{s}\left\{\sum_{j=2}^{n} e_j\mathbf{E}_j \frac{\lambda_i}{\sqrt{\Gamma(1+\alpha)}}\right. \\ & \left.\left[-\exp\left(-\frac{\lambda_i s^{\alpha/2}\xi}{\sqrt{\Gamma(1+\alpha)}}\right) - \exp\left(\frac{\lambda_j s^{\alpha/2}(\xi - \mathfrak{L})}{\sqrt{\Gamma(1+\alpha)}}\right)\right]\right\}\end{aligned} \tag{3.52}$$

Boundary conditions (3.45) and (3.48) are already satisfied by this solution, the former being obvious by substitution and the reason for latter being that the row sum of each eigenvector other than the first is zero. To satisfy the remaining two conditions (3.46) and (3.47), we must scale the eigenvectors $\mathbf{E}_i, i = 1, 2, \ldots, n$ by

choosing e_i appropriately. (3.46) is satisfied if for $i \neq i_0$

$$e_1 E_{i1} + \sum_{j=2}^{n} e_j E_{ij} \left[1 - \exp\left(-\frac{\lambda_j s^{\alpha/2} \mathfrak{L}}{\sqrt{\Gamma(1+\alpha)}} \right) \right] = 0, \quad 0 \leq s < \infty \tag{3.53}$$

and (3.48) is satisfied if

$$\sum_{j=2}^{n} \frac{\lambda_j}{\sqrt{\Gamma(1+\alpha)}} e_j E_{i_0 j} \left[-1 - \exp\left(-\frac{\lambda_j s^{\alpha/2} \mathfrak{L}}{\sqrt{\Gamma(1+\alpha)}} \right) \right] = -1, \quad 0 \leq s < \infty. \tag{3.54}$$

(3.53) and (3.54) together give n linear equations to solve for n unknowns e_j, $j = 1, \ldots, n$ at any s. To obtain normalized stresses and displacements in the time domain, we must invert (3.51) and (3.52). Exact inversion is intractable. However according to Schapery's direct method for approximate Laplace inversion,

$$f(t) = s\, \bar{f}(s)\big|_{s=e^{-\gamma}/t} \tag{3.55}$$

where $\gamma \approx 0.577$ is Euler's constant. Beyerlein et al discuss the regime of accurate validity of Schapery's approximate inverse formula. In terms of the approximate inverse, the solution becomes

$$\begin{aligned} \mathbf{U}'(\xi,\tau) = & \frac{\tau^{\alpha/2}}{\mu} \{ e_1 \mathbf{E}_1 + \\ & \sum_{j=2}^{n} e_j \mathbf{E}_j \left[\exp\left(-\frac{\lambda_j \mu \xi}{\tau^{\alpha/2} \sqrt{\Gamma(1+\alpha)}} \right) - \exp\left(\frac{\lambda_j \mu (\xi - \mathfrak{L})}{\tau^{\alpha/2} \sqrt{\Gamma(1+\alpha)}} \right) \right] \Bigg\} \end{aligned} \tag{3.56}$$

and

$$\begin{aligned} \frac{\partial \mathbf{U}'}{\partial \xi}(\xi,\tau) = & \left\{ \sum_{j=2}^{n} e_j \mathbf{E}_j \frac{\lambda_j}{\sqrt{\Gamma(1+\alpha)}} \times \right. \\ & \left. \left[-\exp\left(-\frac{\lambda_j \mu \xi}{\tau^{\alpha/2} \sqrt{\Gamma(1+\alpha)}} \right) - \exp\left(\frac{\lambda_j \mu (\xi - \mathfrak{L})}{\tau^{\alpha/2} \sqrt{\Gamma(1+\alpha)}} \right) \right] \right\} \end{aligned} \tag{3.57}$$

where

$$\mu = e^{-\gamma \alpha/2} \tag{3.58}$$

and $\mathbf{E}_j$, $j = 1, 2, \ldots, n$ are scaled so that

$$e_1 E_{i1} + \sum_{j=2}^{n} e_j E_{ij} \left[1 - \exp\left(-\frac{\lambda_j \mu \mathfrak{L}}{\tau^{\alpha/2}\sqrt{\Gamma(1+\alpha)}} \right) \right] = 0, \quad 0 \leq \tau < \infty \tag{3.59}$$

and

$$\sum_{j=2}^{n} \frac{\lambda_j}{\sqrt{\Gamma(1+\alpha)}} e_j E_{i_0 j} \left[-1 - \exp\left(-\frac{\lambda_j \mu \mathfrak{L}}{\tau^{\alpha/2}\sqrt{\Gamma(1+\alpha)}} \right) \right] = -1, \quad 0 \leq \tau < \infty \tag{3.60}$$

We reiterate that $e_j \equiv e_j(\tau)$ represent time varying scales for the eigenvectors $\mathbf{E}_j$.

At this point it is worth making explicit the tacit assumption in the notation so far that

$$U_j(\xi, \tau) = U_j(\xi, \tau; i_0, \xi_0 = 0) \tag{3.61}$$

, i.e., the displacement at a certain point indexed by j in the unit cell is determined by the location (i_0, ξ_0) of the fiber break in the unit cell. The displacement field $U_i(\xi, \tau; i_0, \xi^\sharp)$ due to a single break on fiber i_0 at $\xi = \xi^\sharp$ for arbitrary $0 \leq \xi^\sharp \leq \mathfrak{L}$ is obtained by translating $U_j(\xi, \tau; i_0, \xi_0 = 0)$ as

$$U_j^\sharp(\xi, \tau; i_0, \xi^\sharp) = U_j((\xi - \xi^\sharp) \bmod \mathfrak{L}, \tau; i_0, \xi_0 = 0). \tag{3.62}$$

If we wish to obtain the displacement field due to a break on fiber $i_1 \neq i_0$, simple solution shifting is inadequate in general and the entire procedure described above may have to be carried out for fiber i_1. However a computationally attractive feature of the 2D and 3D arrays of Section 3.1.1 is that for these arrays translational invariance holds in the transverse direction also. In 2D arrays it suffices to carry out the above analysis for a fiber break at $\ell = 0$, $\xi = 0$ and determine $U_j(\xi, \tau; 0, 0)$. Then the displacement of fiber ℓ, $U^\sharp(\ell, \xi, \tau; \ell^\sharp, \xi^\sharp)$ due to a break at $\ell = \ell^\sharp$, and $\xi = \xi^\sharp$ is given by

$$U^\sharp(\ell, \xi, \tau; \ell^\sharp, \xi^\sharp) = U((\ell - \ell^\sharp) \bmod n, (\xi - \xi^\sharp) \bmod \mathfrak{L}, \tau; 0, 0) \tag{3.63}$$

Similarly in 3D arrays, the displacement of a fiber (ℓ, m), $U^\sharp(\ell, m, \xi, \tau; \ell^\sharp, \xi^\sharp)$ due to a break at $\ell = \ell^\sharp$, $m = m^\sharp$, and $\xi = \xi^\sharp$ is given by

$$U^\sharp(\ell, m, \xi, \tau; \ell^\sharp, \xi^\sharp) = U((\ell - \ell^\sharp) \bmod \sqrt{n}, (m - m^\sharp) \bmod \sqrt{n}, \\ (\xi - \xi^\sharp) \bmod \mathfrak{L}, \tau; 0, 0) \tag{3.64}$$

That completes the solution of the single fiber break problem. Next in Section 3.2.4 we consider the linear superposition of single break solutions to determine the stress state due to r fiber breaks formed at different times.

3.2.4 Multiple Break Solution

As briefly discussed in Section 3.2.1, the single break solution can be superposed to obtain the multiple break solution. We wish to determine the displacement and stress state in a periodic composite cell at normalized time $\tau \geq \tau_r$ due to r breaks formed at normalized times $\tau_1 \leq \tau_2 \leq \ldots \leq \tau_r$ and located at (i_1, ξ_1), (i_2, ξ_2), ..., and (i_r, ξ_r) where the first coordinate identifies the fiber and the second coordinate the normalized position of the fiber break within the periodic cell.

For $1 \leq i, j \leq r$, let $\Lambda_{ij}(\tau)$ denote the normalized stress at the location of fiber break j due to a unit compressive load applied at fiber break i after normalized time τ of application of the load. That is, let

$$\Lambda_{ij}(\tau) = \frac{\partial U'_j}{\partial \xi}(\xi_j, \tau; i, \xi_i) \tag{3.65}$$

be the influence at (j, ξ_j) due to a fiber break at (i, ξ_i) as determined by (3.57) in the notation of (3.61). We need to find weighting functions $w_i(\zeta), i = 1, 2, \ldots, r$ such that

$$-1 = \sum_{\substack{i=1 \\ \tau_i \leq \tau}}^{r} \left[\Lambda_{ij}(\tau - \tau_i) w_i(\tau_i) + \int_{\tau_i}^{\tau} \Lambda_{ij}(\tau - \zeta) \frac{\partial w_i(\zeta)}{\partial \zeta} d\zeta \right], \quad j = 1, 2, \ldots, r \tag{3.66}$$

Analytical solution for $w_i(\zeta),\ i \in \{1, 2, \ldots, r\}$ and $0 \leq \zeta \leq \tau$ is generally intractable. A numerical procedure consists of stepping though normalized time from $\zeta = 0$ to $\zeta = \tau$ as follows. Define $0 = \zeta_0 < \zeta_1 < \ldots < \zeta_k = \tau$, as a partition of the time interval $[0, \tau]$ such that for each τ_i, $i = 1, \ldots, r$, there is a ζ_{p_i} such that $\tau_i = \zeta_{p_i}$. Then, we may approximately express condition (3.66) in terms of the ζ_i's as

$$-1 = \sum_{\substack{i=1 \\ \tau_i \leq \tau}}^{r} \left[\Lambda_{ij}(\tau - \tau_i) w_i(\tau_i) + \sum_{m=p_i+1}^{k} \Lambda_{ij}(\tau - \zeta_m) \left(w_i(\zeta_m) - w_i(\zeta_{m-1}) \right) \right], \qquad (3.67)$$

$$j = 1, 2, \ldots, r$$

Clearly, the choice of $\zeta_i,\ i = 1, \ldots, k$ determines the accuracy and speed of the numerical approximation. We discuss these aspects further below. Beyerlein and Phoenix [14] discuss alternative methods of solution, and their merits and demerits.

In terms of

$$C_j(\tau) = -1 - \sum_{\substack{i=1 \\ \tau_i \leq \tau}}^{r} \left[\Lambda_{ij}(\tau - \tau_i) w_i(\tau_i) - \Lambda_{ij}(0^+) w_i(\zeta_{k-1}) + \sum_{m=p_i+1}^{k-1} \Lambda_{ij}(\tau - \zeta_m) \left(w_i(\zeta_m) - w_i(\zeta_{m-1}) \right) \right], \qquad (3.68)$$

$$j = 1, 2, \ldots, r$$

(3.67) can be rewritten as a matrix equation

$$[\Lambda(0^+)]\{w(\tau)\} = \{\mathbf{C}(\tau)\} \qquad (3.69)$$

where $\Lambda(0^+)$ is the matrix of instantaneous influences of the r breaks on each other and $\mathbf{C} = \{C_1, C_2, \ldots, C_r\}^T$. This system of equations can then be solved for the weights $w_j(\tau),\ j = 1, \ldots, r$. It can be shown that $[\Lambda(0^+)]$ is negative definite.

3.2.5 Results and Approximations

The shear-lag approach described in previous sections is applicable to arbitrary arrays of aligned fibers. Here forward however, we focus solely on the 2D and 3D arrays discussed in Section 3.1.1 subjected to periodic boundary conditions both in the fiber direction and in the transverse plane. For these arrays, we will examine composite stresses in the presence of certain special configurations of breaks that will be of utility in the course of probabilistic modeling in Section 3.4.

In terms of the similarity variables

$$z = \frac{\xi}{\tau^{\alpha/2}} \qquad \text{and} \qquad z' = \frac{\mathfrak{L} - \xi}{\tau^{\alpha/2}} \tag{3.70}$$

(3.57) becomes

$$\frac{\partial \mathbf{U}'}{\partial \xi}(z, z') = \left\{ \sum_{i=2}^{n} \mathbf{C}_i \frac{\lambda_i}{\sqrt{\Gamma(1+\alpha)}} \times \left[-\exp\left(-\frac{\lambda_i \mu z}{\sqrt{\Gamma(1+\alpha)}} \right) - \exp\left(\frac{\lambda_i \mu z'}{\sqrt{\Gamma(1+\alpha)}} \right) \right] \right\} \tag{3.71}$$

Setting $\mathfrak{L} \to \infty$ in this expression, we see that the dependence of stress state on ξ and τ enters exclusively through the similarity variable z. Also, in this case, as n is increased, the stress solution quickly approaches that of Beyerlein and Phoenix's[16] $n = \infty$ solution obtained using an influence function approach. In the results presented in the rest of this section, this condition will be met. In fact, convergence to the $n = \infty$ solution is numerically complete if we take $n = 400$ in the presence of fewer than 20 fiber breaks even when contiguous in both arrays. Under these conditions, the transverse interaction of fiber breaks across unit cells can be neglected.

Figure 3.2 pertains to the stress profile in the fiber adjacent to a transverse cluster of breaks in a 2D array with $\mathfrak{L} = \infty$. $K_k(z)$ is the stress concentration in

the fiber adjacent to the k-cluster at $\xi = 0$ formed at $\tau = 0$ in adjacent fibers. An approximation of the form

$$K_k(z) \approx \check{K}_k(z) = 1 + (\check{K}_k(0) - 1)(1 - z/\sqrt{k}) \exp(-z) \tag{3.72}$$

accurate for small k where

$$K_k(0) \approx \check{K}_k(0) = \sqrt{\frac{\pi k}{4} + 1} \tag{3.73}$$

is also plotted in this figure. Throughout, we will use $\check{}$ to denote approximations. If we let ω_k be the "overload length" on the fiber adjacent to a cluster of k breaks, that is, the length over which its stress concentration exceeds 1, then in 2D with $\mathfrak{L} = \infty$ we can approximately take

$$\omega_k \approx \check{\omega}_k = \sqrt{k}\tau^{\alpha/2}. \tag{3.74}$$

A more convenient expression which becomes a better approximation than (3.72) for larger k is

$$K_k(z) \approx \check{K}_k(z) = 1 + (\check{K}_k(0) - 1) \exp(-z(1 + 1/\sqrt{k})) \tag{3.75}$$

Unlike (3.72), (3.75) however results in $K_k(z) > 1$, for all z.

A similar observation also holds for the 3D array if we identify the *tight cluster* as the 3D counterpart of the cluster of k contiguous breaks in 2D. A tight cluster of breaks in a 3D array is an ordered collection of fiber breaks in a transverse plane wherein each successive fiber to break occurs on an intact fiber facing the greatest overload due to the previous set of breaks. Figure 3.3 depicts the ordered 10-break tight cluster together with the peak stress concentrations faced by the intact fiber on the periphery of the pre-existing cluster that faces the highest stress concentration. This sequence of stress concentrations is not monotonic.

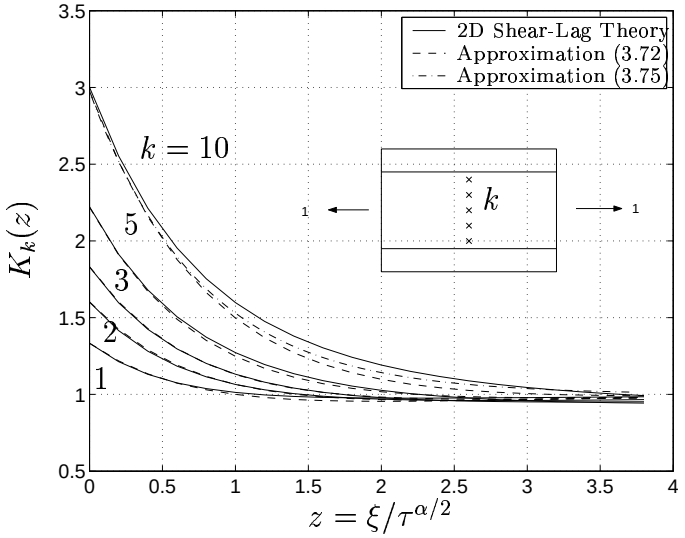

Figure 3.2: Stress decay in 2D on the fiber adjacent to a cluster of k breaks in the $\xi = 0$ plane. $\mathfrak{L}$ is set to ∞ so there are no longitudinal images of the cluster. The number of fibers is taken large enough that the transverse interaction of clusters is negligible.

$k = 6$ for instance fails at a higher stress concentration than $k = 7$. This is due to the jaggedness of the tight cluster as it grows. The $k = 7$ fiber is for instance, surrounded by three broken fibers when it fails as opposed to the $k = 8$ fiber which has two broken neighbors. Aspects of these irregularities are discussed in further detail in Mahesh et al [21] and accounting for them will be key to probabilistic modeling of the lifetime distribution in 3D arrays.

For the fiber under the greatest overload from the critical cluster (which may therefore break and thereby extend it), it can be seen in Figure 3.4 that

$$K_k(z) \approx \check{K}_k(z) = 1 + (\check{K}_k(0) - 1)(1 - 2z/\sqrt[4]{k}) \exp(-2z) \tag{3.76}$$

is a reasonable approximation for the stress decay on the fiber adjacent to the cluster away from the cluster plane. The overload length in 3D with $\mathfrak{L} = \infty$

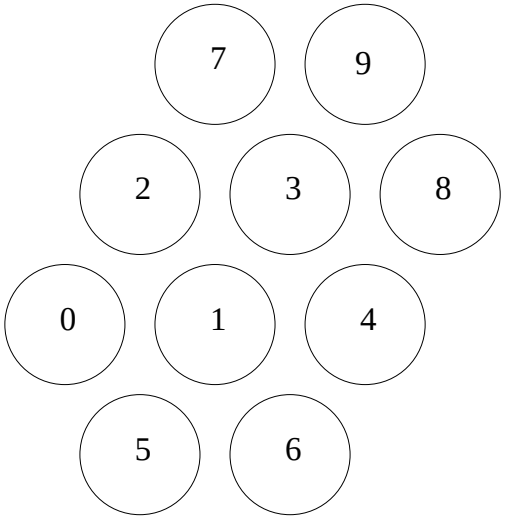

k	$K_k(0)$	$\check{K}_k(0)$
0	1.0000	1.0000
1	1.1046	1.1658
2	1.2337	1.2280
3	1.2828	1.2736
4	1.3205	1.3109
5	1.3644	1.3428
6	1.5889	1.3711
7	1.4107	1.3965
8	1.4596	1.4198
9	1.6163	1.4414

Figure 3.3: One possible sequence for tight cluster growth to 10 fiber breaks in a hexagonal fiber array. The numbers $(0, 1, 2, \ldots, 9)$ denote the order of fiber breaking. Also included are the associated stress concentrations in the $\xi = 0$ plane if $\mathfrak{L} = \infty$ and their estimates according to (3.78).

approximately is

$$\omega_k \approx \check{\omega}_k = \tau^{\alpha/2} \sqrt[4]{k}/2 \tag{3.77}$$

As indicated before, the edge jaggedness of a tight cluster is reflected in the fluctuations of the stress concentrations experienced by its neighbors and hence in $K_k(0)$. An accurate approximation for the peak stress concentration around a *smooth* k-cluster, none of whose neighbors is adjacent to three or more fiber breaks is given by

$$K_k(0) \approx \check{K}_k(0) = \sqrt{\frac{2\sqrt{k}}{\pi^{3/2}} + 1} \tag{3.78}$$

Among clusters of fewer than 20 breaks, $k = 6$, 9, 11, 13, 15, 17 and 18 are not smooth clusters; all the others are. The actual $K_k(0)$ for clusters that are not smooth is always somewhat greater than that given by (3.78). As in the 2D case,

for larger k, $K_k(z)$ is better approximated by

$$K_k(z) \approx \check{K}_k(z) = 1 + (\check{K}_k(0) - 1)\exp(-2z(1 + 1/\sqrt[4]{k})). \tag{3.79}$$

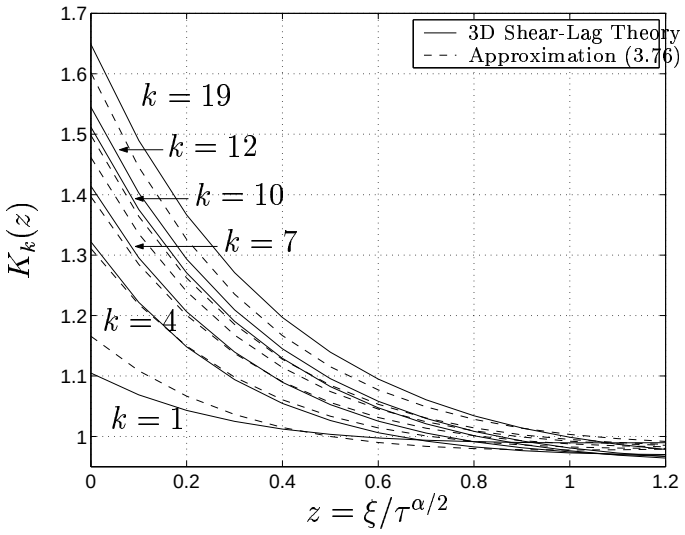

Figure 3.4: Stress decay in 3D on the fiber adjacent to a cluster of k breaks in the $\xi = 0$ plane. $\mathfrak{L}$ is set to ∞ so there are no longitudinal images of the cluster. The number of fibers in the unit cell is taken large enough that the transverse interaction of clusters is negligible.

The approximations heretofore were derived for the case $z' = \infty$. However they are also accurate when $z \ll z'$. This is especially true for small α since $\mu/\sqrt{\Gamma(1+\alpha)}$ in (3.71) decreases very slowly with increasing α from its peak value of 1 at $\alpha = 0$. In fact, even for $\alpha = 0.5$, $\mu/\sqrt{\Gamma(1+\alpha)} \approx 0.92$. While the stress still decays away from a break in 2D and 3D according to (3.75) and (3.79) respectively, the approximations can be improved by modifying the expression for $\check{K}_k(0)$ to take into account the longitudinal interaction between breaks and their images which finite z' entails. The following modified forms of (3.75) and (3.79)

are good approximations if $\mathfrak{L} < \infty$ but $z \ll z'$; in 2D in terms of

$$z_L = \frac{\mathfrak{L}}{\tau^{\alpha/2}}$$

we have approximately

$$K_{k,L} \approx \check{K}_{k,L}(0) = \sqrt{\frac{\pi k}{4}\left(1 - \exp(-z_L\psi_1/k)\right) + 1} \tag{3.80}$$

and in 3D,

$$K_{k,L}(0) \approx \check{K}_{k,L}(0) = \sqrt{\frac{2\sqrt{k}}{\pi^{3/2}}\left(1 - \exp(-z_L\pi\psi_1/\sqrt{k})\right) + 1}. \tag{3.81}$$

If the matrix is viscoelastic with a small power α, then too these approximations hold with reasonable accuracy if $\mathfrak{L}$ is replaced by $e^{-\gamma\alpha/2}\mathfrak{L}/(\tau^{\alpha/2}\Gamma(1+\alpha))$ so long as $e^{-\gamma\alpha/2}\mathfrak{L}/(\tau^{\alpha/2}\Gamma(1+\alpha)) \gg 1$. Figures 3.5 and 3.6 compare these approximations against stress concentrations obtained by the shear-lag procedure. Here $\psi_1(\mathfrak{L})$ is a fitting parameter such that as $k \to \infty$, $\check{K}_{k,L}(0) \to \sqrt{\pi\mathfrak{L}\psi_1/4 + 1}$.

When z and z' become comparable however, the simple approximations for $K_k(0)$ in 2D and 3D break down. Figure 3.7 shows the stress concentration on the fiber next to a single break in an $\alpha = 0.5$ bundle. For comparison, the time invariant stress concentration in an elastic matrix composite is also shown. At small times, when $\mathfrak{L}/\tau^{\alpha/2}$ is large, the influence between a break and its longitudinal periodic images is negligible and stresses in the vicinity of a break are entirely driven by the break and not by its periodic images. However at larger $\tau^{\alpha/2}$, interactions between the breaks becomes larger causing the weights (which equal the opening displacement of the breaks) to decrease from their value at smaller times. This in turn prompts a decrease in the overload on the fibers adjacent to the break as evidenced in Figure 3.7. However since the stress dropped by the broken fiber must be picked up by the surviving fibers in its transverse plane so

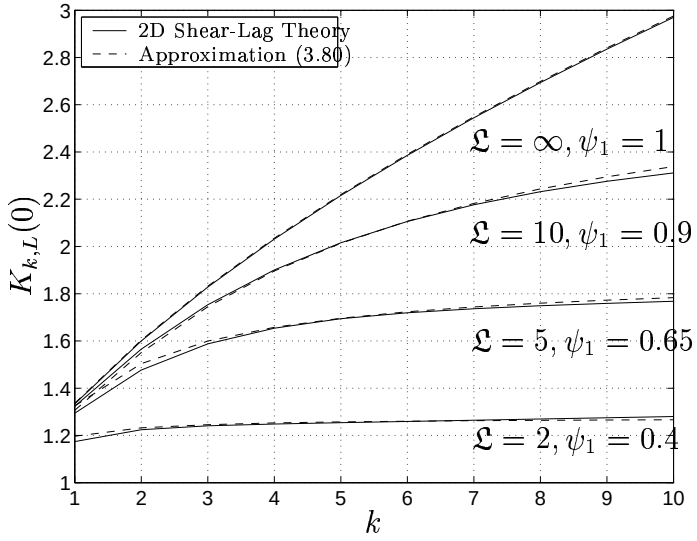

Figure 3.5: Stress concentration ahead of a k-crack in a periodic 2D bundle of $n = 100$ fibers of length $\mathfrak{L}$. ψ_1 is a fitting parameter in (3.80).

that equilibrium can be maintained, the overload on fibers further out from the break will increase. Thus, stresses tend to equalize throughout the unit cell with increasing time if $\alpha \neq 0$ with the speed of equalization increasing with α. The influence of periodic boundaries is enhanced by the presence of a large number of breaks in each unit cell since then breaks interact with the images of their neighboring breaks in addition to their own. This in turn causes a further decrease in opening displacements at fiber breaks and the process of stress equalization in the unit cell proceeds faster.

Finally we consider the stress ahead of a configuration of k staggered fiber breaks on adjacent fibers which comprises of two limbs of equal length $k/2$. The two limbs are staggered longitudinally through ξ_s. That is, the configuration consists of fiber breaks on adjacent fibers $1, 2, \ldots, k/2$ at $\xi = 0$ and breaks on

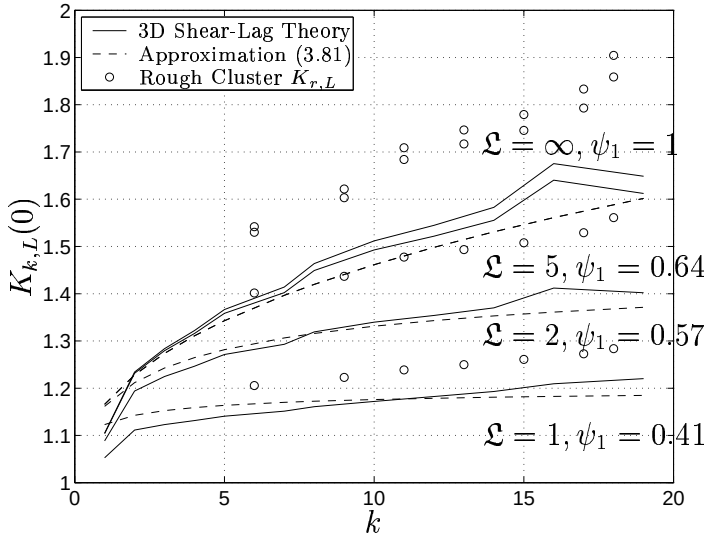

Figure 3.6: Stress concentration ahead of a k-crack in a periodic 3D bundle of $n = 100$ fibers of length $\mathfrak{L}$. $\psi_1 = \psi_1(\mathfrak{L})$ is the fitting parameter in (3.81). Peak stress ceoncentration ahead of rough clusters are shown separately and labeled with $\circ$.

fibers $k/2+1, k/2+2, \ldots, k$ at ξ_s. In 2D, letting $z_s = \xi_s/\tau^{\alpha/2}$ and $\mathfrak{L} = \infty$ we have

$$\check{K}_{k,z_s} \approx \sqrt{\frac{\pi k}{8}\left(1 + \exp(-\psi_2 z_s/\sqrt{k})\right) + 1}, \tag{3.82}$$

an accurate approximation as seen from Figure 3.8. The corresponding formula for 3D is approximately

$$\check{K}_{k,z_s} \approx \sqrt{\frac{\sqrt{k}}{\pi^{3/2}}\left(1 + \exp(-\psi_2 z_s/\sqrt[4]{k})\right) + 1}. \tag{3.83}$$

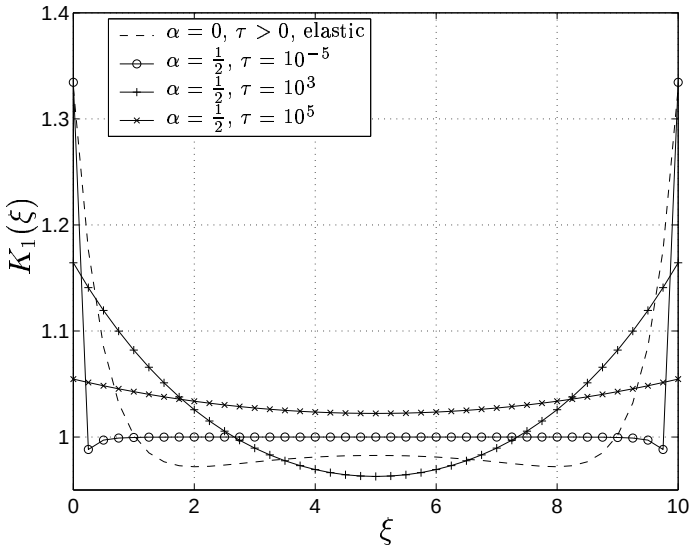

Figure 3.7: Time variation of the stress profile in the fiber adjacent to a single break in a 2D array of length $\mathfrak{L} = 10$ when $\alpha = 0.5$. For comparison the time-invariant stress profile corresponding to an elastic matrix ($\alpha = 0$) is also shown.

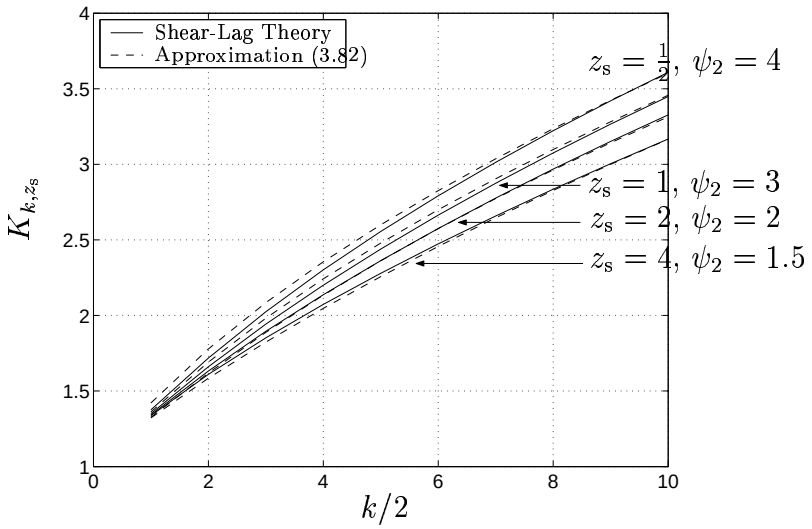

Figure 3.8: Stress concentration ahead of two adjacent $k/2$-long clusters staggered by $z = \xi_0/\tau^{\alpha/2}$ when $\mathfrak{L} = \infty$. ψ_2 is a fitting parameter used in (3.82).

3.3 Fiber Strength Distribution

Coleman [4] introduced a lifetime model whereby the probability that a fiber of length l fails before time t when subjected to the load program $p_u(s)$, $0 \leq s \leq t$, uniformly along its length (i.e., $p_u(s)$ is independent of position within the fiber) is given by

$$F_u(t; p_u(\cdot)) = 1 - \exp\left\{-\Psi\left(l; \int_0^t \kappa(p_u(s))ds\right)\right\} \tag{3.84}$$

with the functional forms

$$\Psi(l; y) = \frac{l}{l_0} y^\beta \tag{3.85}$$

and

$$\kappa(p_u(s)) = \frac{(p_u(s)/p_0)^\rho}{t_{\text{cf}}} \tag{3.86}$$

for Ψ and κ. Here l_0 is the gage length with respect to which other scale quantities are given and t_{cf} is a characteristic fiber time scale. Incorporating (3.85) and (3.86) in (3.84) we get

$$F_u(t; p_u(\cdot)) = 1 - \exp\left\{-\frac{l}{l_0}\left(\frac{1}{t_{\text{cf}}}\int_0^t \left(\frac{p_u(s)}{p_0}\right)^\rho ds\right)^\beta\right\}. \tag{3.87}$$

If however the load $p(x,t)$ in a fiber is non-uniform, i.e., both position and time dependent as is the case in the vicinity of fiber breaks in a composite, a natural generalization of (3.87) is

$$F(t, p(\cdot)) = 1 - \exp\left\{-\frac{1}{l_0}\int_0^l dy\left[\frac{1}{t_{\text{cf}}}\int_0^t \left(\frac{p(y,s)}{p_0}\right)^\rho ds\right]^\beta\right\}. \tag{3.88}$$

Normalizing the fiber load according to

$$\pi(\xi, \tau) = \frac{p(\xi\delta_{\text{v}}, \tau t_{\text{cm}})}{p_{\text{cf}}} = \frac{p(x,t)}{p_{\text{cf}}} \tag{3.89}$$

where

$$p_{\text{cf}} = p_0 \left(\frac{l_0}{\delta_{\text{v}}}\right)^{\frac{1}{\rho\beta}} \left(\frac{t_{\text{cf}}}{t_{\text{cm}}}\right)^{\frac{1}{\rho}} \tag{3.90}$$

the distribution (3.88) can be rewritten in terms of normalized quantities as

$$\mathscr{F}(\tau, \pi(\cdot)) = 1 - \exp\left(- \int_0^{\lambda} d\xi \left[\int_0^{\tau} (\pi(\zeta))^{\rho} d\zeta \right]^{\beta} \right). \tag{3.91}$$

where $\lambda = l/\delta_{\mathrm{v}}$ is the normalized length of a fiber element. Restricting (3.91) to the case where loading on a fiber is uniform, we get the normalized form of (3.87)

$$\mathscr{F}_u(\tau, \pi(\cdot)) = 1 - \exp\left(-\lambda \left[\int_0^{\tau} (\pi_u(\zeta))^{\rho} d\zeta \right]^{\beta} \right) \tag{3.92}$$

where $\pi_u(\tau) = p_u(t)/p_{\mathrm{cf}}$. According to (3.92) we have that a fiber element of unit normalized length ($\lambda = 1$) loaded uniformly for unit normalized time ($\tau = 1$) under unit normalized load ($\pi_u = 1$) has probability $1 - 1/e$ of failure. Also, if we denote the normalized far field applied load by $\pi_\infty = p_\infty/p_{\mathrm{cf}}$, then

$$\pi_i(\xi, \tau) = \sigma_i(\xi, \tau)\pi_\infty \tag{3.93}$$

relates the normalized fiber load $\pi(\xi, \tau)$ to the fiber stress concentration $\sigma_i(\xi, \tau)$ defined in (3.25). For a fiber element of normalized length λ,

$$H(\lambda, \tau, \pi(\cdot)) = \int_0^{\lambda} d\xi \left[\int_0^{\tau} (\pi(\xi, \zeta))^{\rho} d\zeta \right]^{\beta} \tag{3.94}$$

is called the *cumulative hazard* of fiber failure. Let Z be an exponentially distributed random variable

$$\Pr\{Z \leq z\} = 1 - \exp(-z). \tag{3.95}$$

The time to failure of a fiber has distribution given by (3.91) if the failure criterion is taken to be

$$Z \geq H(\lambda, \tau, \pi(\cdot)). \tag{3.96}$$

Stated otherwise, a fiber segment loaded (not necessarily uniformly) along its length is broken if its cumulative hazard exceeds its exponentially distributed

standard representative random variable Z. In the case of uniform loading, the cumulative hazard becomes

$$H(\lambda, \tau, \pi_u(\cdot)) = \lambda \left[\int_0^\tau (\pi_u(\zeta))^\rho d\zeta \right]^\beta .$$

in terms of which the fiber failure criterion (3.96) holds.

As a simple example let us consider the constant load program

$$\pi_u(\tau) = \mathscr{R}, \quad \zeta \geq 0. \tag{3.97}$$

applied uniformly to a fiber of normalized length λ. Then its lifetime distribution in terms of the normalized variable calculated from (3.92) is

$$\mathscr{F}_u(\tau) = 1 - \exp\left(-\lambda \mathscr{R}^{\rho\beta} \tau^\beta\right). \tag{3.98}$$

Another example from which an interesting interpretation of fiber "strength" emerges is the loading

$$\pi_u(\tau) = \mathscr{R}\tau, \quad \tau \geq 0 \tag{3.99}$$

linear in time with loading rate $\mathscr{R}$ and uniform along the fiber. Then in terms of the new parameters $s = \mathscr{R}\tau$, the strength and $\varrho = (\rho + 1)\beta$, its effective Weibull modulus, the distribution function for strength (3.92) becomes

$$\mathscr{F}_u(s) = 1 - \exp\left(-\frac{\lambda}{(\rho+1)^\beta \mathscr{R}^\beta} s^\varrho\right). \tag{3.100}$$

If we let $\rho \uparrow \infty$ and $\beta \downarrow 0$ such that ϱ is fixed, then,

$$[(\rho + 1)\mathscr{R}]^\beta = \frac{(\varrho \mathscr{R})^\beta}{\beta^\beta} \longrightarrow 1$$

as $\beta \downarrow 0$. That is, the strength distribution becomes increasingly independent of the loading rate.

3.4 Probabilistic Analysis of Composite Fracture

3.4.1 Equal Load Sharing Arrays

An asymptotic result for the lifetime distribution of a loose bundle of n fibers (no matrix) loaded under tension has been obtained by Phoenix [6]. The load sharing in such a bundle is termed equal load sharing, when the stress concentration in each of $n-k$ remaining intact fibers in a bundle is given by

$$K_k = \frac{n}{n-k} \tag{3.101}$$

According to Phoenix [6] the lifetime of an ELS bundle of n initially intact fibers each of length λ is asymptotically normally distributed as $n \to \infty$. That is,

$$G_n(\tau) \Longrightarrow \Phi\left(\frac{\tau - \mu}{\sigma/\sqrt{n}}\right) \tag{3.102}$$

where

$$\mu = \pi_\infty^{-\rho} \lambda^{-1/\beta} \rho^{1/\beta} \Gamma(1 + 1/\beta), \tag{3.103}$$

$$\sigma^2 = 2(\rho \lambda^{-1/\beta} \pi_\infty^{-\rho})^2 [I_1(\rho, \beta) - I_2(\rho, \beta)] \tag{3.104}$$

and

$$\Phi(z) = \frac{1}{\sqrt{2\pi}} \int_{-\infty}^{z} e^{-z^2/2} dz. \tag{3.105}$$

Here

$$I_1(\rho, \beta) = \int_0^\infty \int_0^{w_2} e^{(1-\rho)w_1^\beta} e^{-\rho w_2^\beta} dw_1 dw_2 \tag{3.106}$$

which is given by the series

$$I_1(\rho, \beta) = \frac{(n+1)!(n+1)}{\rho^{n+1}(2\rho - 1)^{n+1}} \sum_{k=0}^{n} \frac{(k+n)! \rho^k}{k!(2\rho - 1)^k} \tag{3.107}$$

when $1/\beta = n + 1$ where n is an integer and if not, by

$$I_1(\rho, \beta) = \frac{1}{\beta^2 (2\rho - 1)^{2/\beta}} \sum_{k=0}^{\infty} \frac{(\rho - 1)^k \Gamma(2/\beta + k)}{(2\rho - 1)^k (1/\beta)(1/\beta + 1) \cdots (1/\beta + k)}. \tag{3.108}$$

Also, I_2 is given by

$$I_2(\rho,\beta) = \int_0^\infty \int_0^{w_2} e^{-\rho(w_1^\beta + w_2^\beta)} dw_1 dw_2 = \frac{\Gamma^2(1+1/\beta)}{2\rho^{2/3}} \tag{3.109}$$

The equal load sharing assumption is not generally valid in the presence of a matrix which tends to concentrate stress on survivors near fiber breaks rather than equally distribute them across the composite. We will find however that normality of the lifetime distribution seen in large equal load sharing bundles appears also for large local load sharing bundles in which fiber breaking is highly dispersed.

3.4.2 Chain of Bundles Model

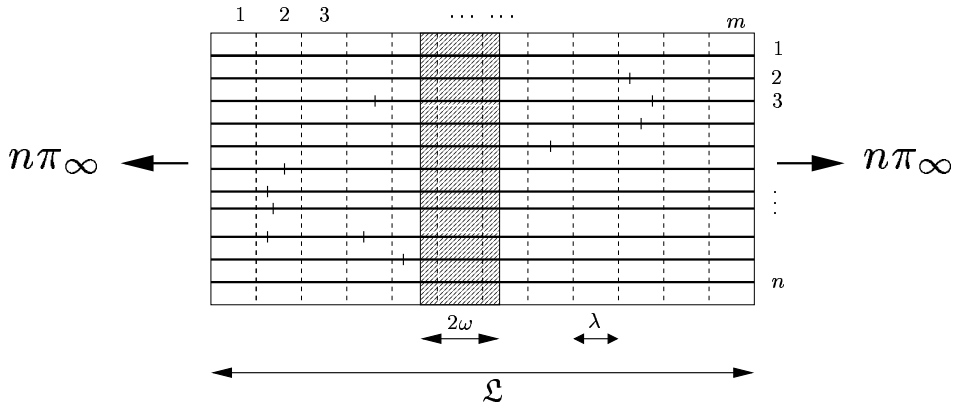

Figure 3.9: Chain of bundles subdivision of a composite of normalized length $\mathfrak{L}$ into m smaller λ-bundles each of whose failure is statistically and mechanically almost independent of the others. $\lambda = \mathfrak{L}/m$. 2ω is the longitudinal length scale of transverse cracking which we will later take to be the overload length ahead of critical cluster of breaks (defined in Section 3.4.4).

Composite failure typically corresponds to the formation of a transverse crack sufficiently long to become unstable. It has been common in the literature to

idealize the failure process in terms of a longitudinal partition of the composite of normalized length $\mathfrak{L}$ into m transverse slabs or short bundles as shown in Figure 3.9 and to regard composite failure as the failure of the weakest of these bundles. The failure process within a given bundle is treated as statistically weakly dependent on that in neighboring bundles.

$\mathfrak{L}/m$ need not correspond to the longitudinal length scale of catastrophic transverse failure initiation and propagation in the composite. Let ω be the time dependent stress overload length of a single break or a cluster of transverse breaks. Approximations for ω when fiber breaks are arranged transversely in 2D and 3D are given respectively in (3.74) and (3.77). Then 2ω and not $\mathfrak{L}/m$ determines the longitudinal length scale of transverse stress distribution and cracking. We will refer to each of the m bundles of real length λ and effective length 2ω as λ-bundles. Typically, $2\omega > \lambda$ and therefore, overload lengths of adjacent bundles may overlap causing their failure events to be dependent. However, this dependence is only local owing to the relatively short range of the overload region and many of the results of the fully independent case are excellent approximations. In particular, if $G_n(\tau)$ is the lifetime distribution of a single λ-bundle, and $H_{m,n}(\tau)$, that of the entire composite, to an excellent approximation,

$$H_{m,n}(\tau) = 1 - [1 - G_n(\tau)]^m \tag{3.110}$$

3.4.3 k-Crack Formation Probability

We will now focus on the failure of a single λ-bundle of n-fibers. First, we recognize the failure of k adjacent fibers in the λ-bundle as a likely precursor to the failure of the λ-bundle for any $k \leq n$ and call the event of its formation k-cracking.

Let $Z_1, \ldots, Z_k$ be independent unit exponentially distributed standard repre-

sentative random variables as described in Section 3.3. Let $T(Z_1, \ldots, Z_k; \lambda')$ be the normalized time required to fail a parallel arrangement of fiber elements of length λ where fiber i has standard representative random variable Z_i, for $1 \leq i \leq k$ and

$$\lambda' = \max(\lambda, 2\omega) \tag{3.111}$$

where 2ω is the longitudinal length scale of transverse cracking shown in Figure 3.9. Also let each fiber element be loaded at each instant of time such that the normalized load profile along its length is determined by two constants – $\mathfrak{K}$ and c according to

$$\pi(\xi, \tau) = \pi_\infty \left[1 + (\mathfrak{K} - 1) \exp\left(-|\xi| c/\tau^{\alpha/2}\right)\right], \tag{3.112}$$

for $-\lambda'/2 \leq \xi \leq \lambda'/2$. The notational distinction we make between $\mathfrak{K}$ and K is that K is always thought of as the stress concentration ahead of a cluster of breaks, whereas $\mathfrak{K}$ more generally refers to the stress concentration due to a set of arbitrarily located breaks. This choice of the functional form for $\pi(\xi, \tau)$ is motivated by the approximate stress profiles (3.75) and (3.79) in 2D and 3D respectively. $\mathfrak{K}$ and c may themselves be time-dependent quantities. It must be understood that the form (3.112) is chosen for the stress profile because it is a good approximation for the stress concentration ahead of a tight cluster of breaks the formation of which is the dominant mode of composite fracture under certain conditions to be discussed shortly. Configurations of fiber breaks other than a tight cluster may result in stress profiles considerably different from that of (3.112). We ignore such configurations owing to their small probability of occurrence. Also the form (3.112), accurate for a cluster of breaks that form simultaneously may not be so good when breaks in the tight cluster form at different times. However we disregard these minor differences.

The first scaling relation is an adaptation of Tierney's [8, 9] to load profile (3.112). It is independent of the far-field applied load π_∞. For $\tau > 0$, we have

$$\tau T(Z_1, \ldots, Z_n; \lambda') = T(\tau^{\beta+\alpha/2} Z_1, \ldots, \tau^{\beta+\alpha/2} Z_n; \lambda' \tau^{\alpha/2}) \tag{3.113}$$

or equivalently,

$$T(Z_1, \ldots, Z_n; \lambda') = \tau T(\tau^{-\beta-\alpha/2} Z_1, \ldots, \tau^{-\beta-\alpha/2} Z_n; \lambda'/\tau^{\alpha/2}). \tag{3.114}$$

This relation can be established inductively. When some l of the k fibers under consideration are broken (not necessarily in a tight cluster), let I be the set of $k-l$ fibers still intact and let $\mathfrak{K}_i(\tau)$ and $c_i(\tau)$ determine the stress concentration in fiber i, $i \in I$ according to (3.112). The variation of $\mathfrak{K}_i$ and c_i with time is mainly due to the formation of fiber breaks elsewhere in the bundle. Let $T_{l+1} \equiv T_{l+1}(Z_1, \ldots, Z_n; \lambda')$ be the time to failure of the next fiber. Then, for any $x > 0$, if $\mathfrak{K}_i > 1$, for $i \in I$,

$$\begin{aligned}
xT_{l+1} &\equiv xT_{l+1}(Z_1, \ldots, Z_n; \lambda') \\
&= \inf_{i \in I} \left\{ x\tau_i : Z_i \le \int_0^{\lambda'} d\xi \left[\int_0^{\tau_i} [1 + (\mathfrak{K}_i - 1) e^{-\frac{\xi c_i}{\zeta^{\alpha/2}}}]^\rho d\zeta \right]^\beta \right\} \\
&= \inf_{i \in I} \left\{ \tau_i : x^\beta Z_i \le \int_0^{\lambda'} d\xi \left[\int_0^{\tau_i} [1 + (\mathfrak{K}_i - 1) e^{-\frac{\xi c_i x^{\alpha/2}}{\zeta^{\alpha/2}}}]^\rho d\zeta \right]^\beta \right\} \\
&= \inf_{i \in I} \left\{ \tau_i : x^{\beta+\alpha/2} Z_i \le \int_0^{\lambda' x^{\alpha/2}} d\xi \left[\int_0^{\tau_i} [1 + (\mathfrak{K}_i - 1) e^{-\frac{\xi c_i x^{\alpha/2}}{\zeta^{\alpha/2}}}]^\rho d\zeta \right]^\beta \right\} \\
&= T_{l+1}(x^{\beta+\alpha/2} Z_1, \ldots, x^{\beta+\alpha/2} Z_n; \lambda' x^{\alpha/2})
\end{aligned} \tag{3.115}$$

where intermediate steps involve no more than appropriate change of variables.

Similarly, a load scaling relationship can be established as follows. Let $T(Z_1, \ldots, Z_n; \lambda'; \pi_\infty)$

be the time to failure as before, but under external load π_∞. Then,

$$\begin{aligned} T(Z_1,\ldots,Z_n;\lambda';\pi_\infty) &= T(Z_1/\pi_\infty^{\rho\beta},\ldots,Z_n/\pi_\infty^{\rho\beta};\lambda';1) \\ &= \pi_\infty^{-\frac{\rho\beta}{\beta+\alpha/2}} T(Z_1,\ldots,Z_n;\lambda'\pi_\infty^{\frac{\rho\beta\alpha/2}{\beta+\alpha/2}};1) \end{aligned} \tag{3.116}$$

where we have used (3.113) to obtain the second expression on the right hand side. Equivalenty we have

$$\pi_\infty^{\frac{\rho\beta}{\beta+\alpha/2}} T(Z_1,\ldots,Z_n;\lambda'/\pi_\infty^{\frac{\rho\beta\alpha/2}{\beta+\alpha/2}};\pi_\infty) = T(Z_1,\ldots,Z_n;\lambda';1). \tag{3.117}$$

Owing to their dependence on (3.113), the scaling laws (3.116) and (3.117) too require that at each step $\mathfrak{K}_i > 1$, $i \in I$ in order to be valid. In the case that $\mathfrak{K}_i = 1$, for $i \in I$, (i.e., the each successive break forms under the far-field load, and is completely uninfluenced by any other break), we have the scaling relation

$$T(Z_1,\ldots,Z_n;\lambda';\pi_\infty) = \pi_\infty^{-\rho} T(Z_1,\ldots,Z_n;\lambda';1). \tag{3.118}$$

In actuality, in Section 3.6.1 we will find that composites pass through an initial phase of disperse fiber breaking under far-field load when (3.118) is applicable and then a phase of clustered fiber failure wherein the form (3.112) with $\mathfrak{K}_i > 1$ is a good approximation for the stress concentration on fibers under risk of failure. Hence the actual scaling rule between load and lifetime can be expected to follow an load exponent in between ρ and $\rho\beta/(\beta+\alpha/2)$. That this is the case will be shown in Section 3.6.1.

If $W_k(\tau)$ is the distribution function of $T(Z_1,\ldots,Z_k;\lambda';\pi_\infty)$, then

$$\begin{aligned}
W_k(\tau) &= \Pr\{T(Z_1,\ldots,Z_k;\lambda';\pi_\infty)\le\tau\}\\
&= \Pr\{\tau^{-1}\pi_\infty^{-\frac{\rho\beta}{\beta+\alpha/2}}T(Z_1,\ldots,Z_k;\lambda'\pi_\infty^{\frac{\rho\beta\alpha/2}{\beta+\alpha/2}};1)\le 1\}\\
&= \Pr\{T(\tau_1^{-\beta-\alpha/2}Z_1,\ldots,\tau_1^{-\beta-\alpha/2}Z_k;\lambda'/\tau^{\alpha/2};1)\le 1\}\\
&\qquad \text{letting } \tau_1=\tau\pi_\infty^{\frac{\rho\beta}{\beta+\alpha/2}} \text{ and using (3.114)}\\
&= \int_{\mathbb{R}^k} 1_{[0,1]}(T(y_1,\ldots,y_k;\lambda'/\tau^{\alpha/2};1))\tau^{k(\beta+\alpha/2)}\pi_\infty^{k\rho\beta}\times\\
&\qquad\qquad \exp\left(-\tau^{\beta+\alpha/2}\sum_{i=1}^k y_i\right)dy_1\ldots dy_k\\
&\qquad\qquad \text{upon setting } y_i=\tau_1^{-\beta-\alpha/2}z_i\\
&\longrightarrow \lambda^*\{y\in\mathbb{R}_k^+ : T(y_1,\ldots,y_k;\lambda'/\tau^{\alpha/2})\le 1\}\tau^{k(\beta+\alpha/2)}\pi_\infty^{k\rho\beta}\\
&\qquad\qquad \text{as } \tau\downarrow 0 \text{ by monotone convergence}
\end{aligned} \tag{3.119}$$

Here λ^* denotes the Lebesgue measure. Tierney provides an approximation for $\lambda^*\{y\in\mathbb{R}_k^+ : T(y_1,\ldots,y_k;\lambda'/\tau^{\alpha/2})\le 1\}$. Adapted to the load profile (3.112), it becomes,

$$\begin{aligned}
&\lambda^*\{y\in\mathbb{R}_k^+ : T(y_1,\ldots,y_k;\lambda'/\tau^{\alpha/2})\le 1\} = \Gamma(1+\beta)^k\Gamma(k\beta+1)^{-1}\times\\
&\prod_{j=0}^{k-1}\left[2N_j\int_0^{\frac{\lambda'}{2\tau^{\alpha/2}}}d\xi\left\{\int_0^1[1+(K_j(0)-1)\exp(-\xi c_j/\zeta^{\alpha/2})]^\rho d\zeta\right\}^\beta\right]
\end{aligned} \tag{3.120}$$

where we will take $c_j = 1+1/\sqrt{j}$ for 2D arrays and $c_j = 2(1+1/\sqrt[4]{j})$ for 3D arrays. N_j, the number of neighbors around a tight j-cluster is

$$N_j = \begin{cases} 1, & \text{if } j=0\\ 2, & \text{if } j=1,2,\ldots,k\end{cases} \tag{3.121}$$

in 2D and

$$N_j \approx \pi D = 2\sqrt{\pi j} \tag{3.122}$$

in 3D. Here D is the tight j-cluster diameter determined by $\pi D^2/4 = j$. The above approximation is accurate only for large ρ. In that case we have by combining (3.119) and (3.120):

$$W_k(\tau) = 2^k\Gamma(1+\beta)^k\Gamma(1+k\beta)^{-1}\pi_\infty^{k\rho\beta}\tau^{k(\beta+\alpha/2)} \prod_{j=0}^{k-1}\left[N_j\int_0^{\frac{\lambda'}{2\tau^{\alpha/2}}}d\xi\left\{\int_0^1[1+(K_j(0)-1)\exp(-\xi c_j/\zeta^{\alpha/2})]^\rho d\zeta\right\}^\beta\right] \tag{3.123}$$

If $\alpha = 0$, the double integral collapses trivially into the single integral:

$$P_j = \int_0^{\frac{\lambda'}{2}} d\xi[1+(K_j(0)-1)\exp(-\xi c_j)]^{\rho\beta} \tag{3.124}$$

The integral in the product above may be approximated as follows for $\alpha \neq 0$:

$$\begin{aligned} P_j &= \int_0^{\frac{\lambda'}{2\tau^{\alpha/2}}} d\xi\left\{\int_0^1[1+(K_j(0)-1)\exp(-\xi c_j/\zeta^{\alpha/2})]^\rho d\zeta\right\}^\beta \\ &= (\theta-1)^\beta\int_0^{\frac{\lambda'}{2\tau^{\alpha/2}}} d\xi\left\{\int_0^\infty\frac{[1+(K_j(0)-1)\exp(-\xi c_j(w+1))]^\rho}{w^\theta}dw\right\}^\beta \\ &= \frac{(\theta-1)^\beta}{c_j}\int_0^{\frac{\lambda' c_j}{2\tau^{\alpha/2}}} d\mu_j\left\{\int_0^\infty\frac{[1+\mathfrak{C}_j\exp(-\mu_j w)]^\rho}{(w+1)^\theta}dw\right\}^\beta \end{aligned} \tag{3.125}$$

upon making the change of variable $w = \zeta^{-\alpha/2} - 1$ where $\theta = 2/\alpha + 1$ in the first step and $\xi c_j = \mu_j$ in the second and abbreviating $(K_j(0)-1)\exp(-\mu_j) = \mathfrak{C}_j$. We have an accurate approximation for the inner integral when ρ is large

$$\begin{aligned} \int_0^\infty\frac{[1+\mathfrak{C}_j\exp(-\mu_j w)]^\rho}{(w+1)^\theta}dw &= (1+\mathfrak{C}_j)^\rho\int_0^\infty\frac{\left[1-\frac{\mathfrak{C}_j}{\mathfrak{C}_j+1}(1-e^{-\mu_j w})\right]^\rho}{(w+1)^\theta}dw \\ &\approx (1+\mathfrak{C}_j)^\rho\int_0^\infty\frac{\exp(-\mathfrak{C}_j\mu_j\rho w/(\mathfrak{C}_j+1))}{(w+1)^\theta}dw \\ &\approx (1+\mathfrak{C}_j)^\rho\int_0^\infty\exp\left(-\frac{\mathfrak{C}_j\mu_j\rho w}{\mathfrak{C}_j+1}-\theta\log(w+1)\right)dw \\ &\approx (1+\mathfrak{C}_j)^\rho\int_0^\infty\exp\left(-\frac{\mathfrak{C}_j\mu_j\rho w}{\mathfrak{C}_j+1}-\theta w\right)dw \\ &= \frac{(1+\mathfrak{C}_j)^{\rho+1}}{\theta+\mathfrak{C}_j(\theta+\rho\mu_j)}. \end{aligned} \tag{3.126}$$

Whereas $[1+\mathfrak{C}_j \exp(-\mu_j w)]^\rho > 1$ for all $w \geq 0$, our exponential approximation in the second step including $(1+\mathfrak{C}_j)^{\rho+1}$ tends to zero for large w. To account for this disparity, we notice that the exponential factor dips below one at $w_1 = (1/\mu_j)(1+1/\mathfrak{C}_j)\log(1+\mathfrak{C}_j)$ so that the error is bounded by $\int_{w_1}^{\infty}(w+1)^{-\theta}dw = (\theta-1)^{-1}(w_1+1)^{-(\theta-1)}$. In view of this correction term, we take our inner integral to be of the following form which, in addition to being an improvement of the approximation (as determined numerically) is exact when $\mathfrak{C}_j = 0$.

$$\int_0^{\infty} \frac{[1+\mathfrak{C}_j \exp(-\mu_j w)]^\rho}{(w+1)^\theta} dw \approx \frac{(1+\mathfrak{C}_j)^{\rho+1}}{(\theta-1)+\mathfrak{C}_j((\theta-1)+\rho\mu_j)} \tag{3.127}$$

Substituting this expression into (3.125) yields

$$P_j \approx \frac{1}{c_j}\int_0^{\frac{\lambda' c_j}{2\tau^{\alpha/2}}} \frac{[1+(K_j-1)e^{-\mu}]^{(\rho+1)\beta}}{1+(K_j-1)e^{-\mu}(1+\frac{\rho\mu\alpha}{2})} d\mu \tag{3.128}$$

in terms of the original variables. This formula is very accurate when ρ is large (≥ 15 say) and θ is moderate(≥ 5 say). Although the above analysis was done for the case $\alpha \neq 0$, (3.128) is well defined even if $\alpha = 0$. Indeed, it collapses to the integral for $\alpha = 0$, (3.124) when that is so. Furthermore, we can approximate (3.128) in a manner similar to the approach used to evaluate the inner integral above if $\lambda' \geq \lambda$ to obtain

$$P_j \approx \frac{1}{c_j}\frac{K_j^{\rho\beta+1}}{(K_j-1)}\chi \tag{3.129}$$

where

$$\chi = \frac{1}{\beta(\rho+1)}\left[1+\frac{1+\rho\alpha/2}{\rho+1}\right] \tag{3.130}$$

The error involved in the approximation of the outer integral is larger than that in the approximation of the inner integral since the rate of decay $(\rho+1)\beta$ of the dominant term, $[1+(K_j-1)e^{-\mu}]^{(\rho+1)\beta}$ is typically much smaller than ρ which was the decay rate in the inner integral. This leaves asymptotic approximations such

as the ones above focusing near the origin somewhat less accurate [22]. Therefore in our numerical calculations, we numerically integrate (3.127) instead of using (3.129). However the value of (3.129) lies in that it captures in closed form the cumulative hazard ahead of a cluster of j breaks except perhaps for a scale constant and can be used in a closed form evaluation of the $W_k(\tau)$ in Section 3.7.

In simplified form we finally have

$$\begin{aligned} W_k(\tau) &\approx 2^{k-1}\Gamma(1+\beta)^k\Gamma(1+k\beta)^{-1}\pi_\infty^{k\rho\beta}\tau^{k(\beta+\alpha/2)}\prod_{j=0}^{k-1}N_jP_j \\ &\approx (2\chi)^{k-1}\Gamma(1+\beta)^k\Gamma(1+k\beta)^{-1}\pi_\infty^{k\rho\beta}\tau^{k(\beta+\alpha/2)}\frac{\lambda}{\tau^{\alpha/2}}\prod_{j=1}^{k-1}\frac{N_j}{c_j}\frac{K_j^{\rho\beta+1}}{K_j-1} \end{aligned} \tag{3.131}$$

where in the second step, we have extracted the anomalous $j = 0$ factor $\lambda/\tau^{\alpha/2}$ from the product series. Unlike the other factors, this factor corresponds to the initial break or the *seed* of the k-cluster, the probability of its formation, given by (3.98) is therefore independent of α.

3.4.4 k^*-Crack and Composite Lifetime

Let $G_n^{[k]}(\tau)$ be the probability of occurrence of at least one k-crack originating in a λ-long n-fiber bundle. Then,

$$G_n^{[k]} = 1 - [1 - W_k(\tau)]^n \tag{3.132}$$

If we treat the composite as a serial arrangement of m such bundles which are mechanically and statistically independent then, the probability of occurrence of at least one k-crack in the composite, $H_{mn}^{[k]}(\tau)$ is

$$H_{mn}^{[k]}(\tau) = 1 - [1 - W_k(\tau)]^{mn} \tag{3.133}$$

Now, in cases where composite failure is driven by the formation and catastrophic propagation of a single cluster of breaks, composite failure may be regarded

as a proper subevent of the formation of a k-crack. Consequently, the distribution function for composite lifetime, $H_{mn}(\tau)$ may be bounded as follows

$$\begin{aligned} H_{mn}(\tau) &\leq \min_{1\leq k\leq n} H_{mn}^{[k]}(\tau) \\ &= \min_{1\leq k\leq n} 1-[1-W_k(\tau)]^{mn} \\ &= 1-[1-\min_{1\leq k\leq n} W_k(\tau)]^{mn} \\ &= 1-[1-W_{k^*}(\tau)]^{mn} \end{aligned} \tag{3.134}$$

where $k^*(\tau)$ is the crack size that minimizes $W_k(\tau)$ for each τ and is called the *critical cluster size*. In Section 3.6, when comparing to Monte Carlo simulations we will find the above upper bound to be especially tight when ρ is large so as to serve as a good approximation of the distribution function itself.

3.5 Monte Carlo Failure Simulation

3.5.1 Simulation Procedure

We will now describe the construction of a Monte Carlo composite model, which while somewhat discretized for computational reasons reasonably approximates the geometry of the flaw arrangement in the idealized unidirectional composite described in Section 3.1.1. The discretizations described below are essential in making the composite failure simulation algorithm reasonably fast. However, the extent of these idealizations is much smaller than in the construction of the analytical model described in the next section.

We begin by conceptually partitioning the n-fiber 2D or 3D array of normalized length $\mathfrak{L}$ into m bundles each of length $\lambda = \mathfrak{L}/m$ as in the chain-of-bundles model. We will term the part of a fiber belonging to a bundle as a fiber *segment*. Each

segment is then further subdivided into $2f+1$ ($\gg 1$) *fragments*. Thus there are m bundles, n fibers, mn fiber segments and $n_f = mn(2f+1)$ fragments in the simulation cell. Fragment lengths are geometrically proportioned with the central fragment being the shortest in the bundle and each fragment going away from the center longer than the previous fragment by a constant multiple. Let us denote the length of the i-th fragment by l_i, $i = 1, \ldots, n_f$. Each fragment is then assigned an independent standard representative random variable Z_i which is exponentially distributed with rate l_i. This is accomplished by producing uniform $U(0,1)$ random variables $U_i, i = 1, \ldots, n_f$, from which $Z_i, i = 1, \ldots, n_f$, the desired standard representative random variables are obtained according to

$$Z_i = -\frac{\log U_i}{l_i}, \quad i = 1, \ldots, n_f. \tag{3.135}$$

The corresponding flaw is treated as though located at the mid-point of the fragment.

Far field load of π_∞ is then applied to the virtual composite and the first task is to determine the time to failure τ_1 of the weakest fragment. This time is determined using (3.92) as

$$\tau_1^\beta = \min_{i=1,\ldots,n_f} \frac{Z_i}{\pi_\infty^{\rho\beta}}. \tag{3.136}$$

The next step consists of transferring the break from the fragment where it occurs to the center of the segment in which the fragment resides. This simplification effectively renders the assumed flaw distribution more akin to the chain of bundles model of Section 3.4.2 than to the idealized unidirectional composite of Section 3.1.1. However this step is necessary for computational tractability of the simulation algorithm, and we will shortly investigate its impact on the simulated composite lifetime distribution. Fragments belonging to the fiber segment in

which the break occurs are then eliminated from future consideration by setting their Z_i to ∞. This is done because the fragments within the broken segment will be unloaded due to the fiber break and their failure probability in the future is very small. Also, even if such a break did form within the broken segment, it will be have minimal influence on the stress state in the composite. Eliminating the broken segment from future consideration ensures that each segment fails at most once.

Since every fiber break is transported to the mid-point of its segment, the peak overload on its neighboring fibers occurs at the mid-points of the corresponding segments and decays roughly exponentially along their length down to the far-field value. For the purpose of determining the residual lifetime of each fragment in these overloaded segments, we assume constant stress along the length of the fragment at the same value as at its center. Fragments closer to the segment mid-point were chosen earlier to be shorter so as to better capture the rapidly varying stresses there.

Successive segments are broken in a recursive manner. Let the stress concentration and the standard representative random variables at the end of the $(k-1)$-th recursive step be $\mathfrak{K}_i(k-1)$ and $Z_i(k-1)$, $i = 1, 2, \ldots, n_f$ respectively. The k-th recursive step consists of determining the time to failure of the k-th break starting with a system of $k-1$ breaks and updating the quantities $\mathfrak{K}_i(k)$ and $Z_i(k)$ to reflect the presence of the new break. We begin the k-th recursive step by determining the smallest residual fragment lifetime using

$$\tau_{\text{res}}(k-1) = \min_{i=i,\ldots,n_f} \frac{Z_i^{\frac{1}{\beta}}(k-1)}{(\mathfrak{K}_i(k-1)\pi_\infty)^\rho}. \tag{3.137}$$

Global time is then advanced by $\tau_{\text{res}}(k-1)$ and the time of the k-th fragment failure, $\tau_k = \tau_{k-1} + \tau_{\text{res}}(k-1)$ is recorded. The break is then repositioned at the

center of its segment. The standard representative random variable of each of the surviving fragments is then updated as

$$Z_i(k) = Z_i(k-1) - (\mathfrak{K}_i'(k-1)\pi_\infty)^{\rho\beta}\tau_{\text{res}}^{\beta}, \quad i = 1, 2, \ldots, n_f$$

to reflect the elapsing of time τ_{res}. Here $\mathfrak{K}_i'(k-1) = \max(\mathfrak{K}_i(k-1), 0)$. In order to speed up the computations, $\mathfrak{K}_i(k)$ is determined from shear-lag calculations only at segment centers and is interpolated to fragment centers according to

$$\mathfrak{K}_i(\xi) = A + B\exp(-c\xi/\tau^{\alpha/2}) \tag{3.138}$$

where A and B are chosen so as to fit the stress concentrations determined by shear-lag calculations at segment centers. τ is taken to be τ_k, the time of formation of the k-th break. That is, interpolation assumes that all k breaks were formed at once at time 0. In keeping with (3.75) and (3.79) c is taken to be $1 + 1/\sqrt{k}$ in 2D and $2(1 + 1/\sqrt[4]{k})$ in 3D. where k is the number of fiber breaks in the same bundle as the fiber segments between which interpolation is done. These steps are repeated until the failure criterion described in the next section is satisfied.

As may be expected, the most time consuming operation in the above recursion by far is the computation of stress concentrations due to a set of pre-existing breaks. It involves implementing the procedures of sections 3.2.3 and 3.2.4. Efficient implementation of this step is therefore critical. Recall that as breaks are formed in succession, their weights are determined using (3.69). $[\Lambda(0^+)]_{(r\times r)}$ for the fixed set of breaks is the northwest corner of the $[\Lambda(0^+)]_{(r+1\times r+1)}$ matrix with a new break appended to this preexisting set. It would be imperative to exploit this structure to efficiently compute weights using (3.69). To this end, we observe that since $-[\Lambda(0^+)]_{(r\times r)}$ is symmetric and positive definite, it permits Cholesky

factorization of the form

$$-[\Lambda(0^+)]_{r\times r} = L_{r\times r}L_{r\times r}^T \tag{3.139}$$

where L is the lower triangular Cholesky factor (see Horn and Johnson [23]). We make the solution for weights efficient by storing, updating and using the Cholesky factor of the $-[\Lambda(0^+)]_{r\times r}$ as we step through fiber breaks. The procedure to update L to account for the formation of break $r+1$ in the presence of r breaks is as follows. Let $B_{r\times 1}$ be the vector of influences of the previous r breaks on the $(r+1)$-th break. Then,

$$L_{r+1\times r+1} = \begin{bmatrix} L_{r\times r} & 0_{r\times 1} \\ X_{1\times r} & P_{1\times 1} \end{bmatrix} \tag{3.140}$$

where X is obtained by solving

$$L_{r\times r}X^T = B$$

by forward substitution and

$$P = \sqrt{1 - XX^T}.$$

We now turn to the key difference which lies in the arrangement of fiber flaws between the Monte Carlo model and the idealized unidirectional composite of Section 3.1.1. In the Monte Carlo model, flaws are assumed to occur in a uniform grid that passes through the centers of the fiber bundles. This has the effect of unrealistically aligning fiber breaks perpendicular to the fiber direction and thereby facilitating the extension of clusters of breaks since the configuration of aligned fiber breaks produces the greatest stress concentration ahead of the cluster tip. However such a restriction on fiber break arrangement is indispensable from a computation time standpoint since the determination of influences in a uniform

grid of break sites due to fiber breaks occurring at other sites in the uniform grid can be done by translating the influences of a single break anywhere in the grid according to (3.63) and (3.64). On the other hand, if the potential break sites were situated arbitrarily, the entire influence field of each fiber break on all other potential break sites would have to be evaluated anew using the shear lag methodology. Alternatively stresses could be interpolated from a regular grid to the locations of arbitrarily occurring break sites, but this approach tends to be unsatisfactory because stresses can vary exponentially in the array.

Alignment of fiber breaks is not much of an issue when the length of a segment λ is much smaller than the overload length ahead of the cluster tip. Indeed, it would be best to choose λ as small as possible in order to reduce the effects of such alignment. In our simulations, we take $\lambda = 0.5$, since this is the smallest value of λ within our computational capability. Using a smaller λ increases the number of segments in the composite which in turn increases simulation time.

We simulate the failure of $n = 100$ fiber 2D and 3D arrays of fibers of normalized length $\mathfrak{L} = L/\delta_{\mathrm{v}} = 10$ under periodic boundary conditions. Fiber statistics are determined by the parameters β and ρ in (3.92). In this study, we consider three combinations of (β, ρ): $(0.1, 75)$, $(0.3, 25)$, and $(0.5, 15)$. In all cases, we have $\rho\beta = 7.5$ which is at a value far exceeding the transition to dispersed breakdown as observed by Curtin and Scher [24] and Curtin et al [25]. We investigate the role of matrix viscoelasticity by considering three powers for the power law compliance: $\alpha = 0$, 0.1 and 0.5. $\alpha = 0$ corresponds to the elastic case. Failure is studied under three applied loads as well: $\pi_\infty = 0.3$, 0.5 and 0.7. For each set of parameter values we test $n_{\mathrm{sim}} = 1024$ virtual specimens. The simulations were performed on a cluster computer of Intel 500 MHz processors. Depending on the parameters of

the model, computations took anywhere between 0.5 and 1500 processor-hours.

3.5.2 Composite Failure Criterion

We now turn to the criterion which, when met, signals composite failure in the simulation algorithm above. Several reasonable possibilities exist for such a criterion three of which we consider here. The first possibility is that failure is taken to occur with the exceedance of composite strain rate ($\dot{\varepsilon}$) over a fixed threshold, $\dot{\varepsilon} > \varepsilon_c$. Composite strain, proportional to the sum of fiber break opening displacements, or, their weights in (3.69) is easily determined. However,

A second approach is to consider the composite failed if a bundle of some appropriately chosen length (say the characteristic length or the overload length for some fixed k) has all the fibers in it failed. k is to be chosen large enough that it represents a critical cluster, i.e., one which will continue to propagate with a high probability.

A third approach of a purely numerical nature is to identify composite failure with the speed of occurrence of successive fiber breaks by considering the composite failed if

$$\frac{\tau_{i+1} - \tau_i}{\tau_{i+1}} < \epsilon \tag{3.141}$$

where τ_i is the time of formation of the i-th break and ϵ is a suitably chosen small constant.

We use (3.141) as our failure criterion with ϵ taken to be the computer's machine precision (about 10^{-16}). This choice turns out to be the most conservative failure criterion in that its satisfaction occurs only after the satisfaction of the other two criteria discussed above. It is to be remarked however that the first two criteria have a mechanical basis, while the third does not. It is based on the

observation that the time between successive fiber failures becomes progressively small after the composite goes unstable. Consequently, the satisfaction of the first two criteria (which occur more or less at the same time) signal composite instability and the continued simulation up to the satisfaction of the third criterion often results in post-critical fiber breaking often removed from the cluster of breaks that went unstable. These post-critical breaks however are of no concern since they are formed well after the failure process in the composite has gone catastrophic and they take negligible time to form, thereby hardly affecting the empirical lifetime distribution obtained from the simulations.

3.5.3 Failure Configurations

We will now argue that depending on the fiber and matrix parameters and the applied load π_∞, composite failure is dominated by one or the other of two qualitatively distinct modes of failure — a clustered failure mode which loosely accompanies high fiber failure probability sensitivity to load, high applied load and small overload length and a dispersed global failure mode which goes with reduced fiber failure sensitivity to load, small applied loads and large overload lengths.

We first examine a case wherein the clustered failure mode dominates. Figure 3.10 shows the arrangement of fiber failures in the vicinity of the composite failure plane in the median specimen among $n_{\text{sim}} = 1024$ simulations of $n = 100$ fiber, $\beta = 0.1$, $\rho = 75$, elastic matrix composite with $\alpha = 0$ under applied load $\pi_\infty = 0.7$. Longitudinally this composite is divided into $m = 20$ bundles so the length of each segment is $\lambda = 0.5$. In Figure 3.11 we have shown the evolution of composite strain with time for this same specimen. On the one hand the strain blows up after the failure of 44 fibers at time $\tau_{44} = 0.5615 \times 10^{-5}$ while on the

other as is evident from Figure 3.10 the incremental times between fiber failures after the formation of 44 breaks become negligible in sum suggesting that this particular specimen goes unstable after the formation of 44 fiber breaks. Fiber breaks before the 45-th are denoted in Figure 3.10 by a $\circ$ while the 45-th break and those after are marked with a $\times$. Also observe that the number of contiguous fiber breaks in the failure plane which propagates catastrophically is $k^* = 4$. We will return to this observation in Section 3.6.

The clustered failure mode transitions to the dispersed mode smoothly. Loosely speaking, the transition occurs because the stress concentration ahead of a cluster of breaks does not propagate it with sufficiently high probability (compared to break formation under the far field stress) as we vary fiber and matrix parameters appropriately. For example, keeping all else fixed, decreasing ρ in (3.92) reduces the probability of a fiber failure with increasing fiber load. Such a variation of the parameters causes the clustering mode to be suppressed by increasing the degree of out of plane breaking ahead of the cluster tip. As an example of a case wherein out of plane break staggering is prevalent while the composite still fails by the formation of a cluster of breaks spanning several planes perpendicular to the fiber direction, consider the median among $n_{\text{sim}} = 1024$ specimen of $\beta = 0.5$, $\rho = 15$ composites under applied load $\pi_\infty = 0.3$. Figure 3.12 shows the evolution of strain with time for this specimen. In contrast to Figure 3.11 here strain increments occur rather continuously owing to the large number of initial dispersed breaks that form, seemingly in an uncorrelated manner, before a cluster is initiated. While no sharp point is identifiable where strain blow-up begins, we take this number to be 101 breaks, where the strain rate (not shown) shows a first large acceleration. We show the configuration of fiber breaks at that time in Figure 3.13. Observe that

a cluster of breaks straddling $\xi = 8$ to $\xi = 9.5$ forms and frequently switches from one plane to the next.

At the other end of the failure mode spectrum we have composites that fail by dispersed fiber failure almost entirely. Whereas, here too, by continuing simulations well past the strain instability criterion we induce cluster formation, it represents localization in a global load sharing like system eventually. Figure 3.14 shows the break configuration in the entire composite with $\beta = 0.5$, $\rho = 15$ at applied load $\pi_\infty = 0.3$ with matrix $\alpha = 0.5$ when the strain instability criterion is satisfied and almost the entire lifetime of the composite has elapsed. The difference between this and the previous case lies in the length of the overload zone. Whereas in the previous case, since the matrix was elastic, the overload zone is confined to it its time independent value of approximately $2\delta_v$, in the present case of Figure 3.14, the overload zone expands to almost the total length of the composite, increasing the opportunity for staggering of a crack many-fold. This increasingly becomes an issue as α increases. Also an important point to note is that since normalized time τ spans many decades, the overload length $\omega \propto \tau^{\alpha/2}$ varies considerably. Since staggered cracks propagate with less probability than aligned cracks, owing to the smaller stress concentration ahead of them, this in turn feeds into the general propensity towards dispersed breaking.

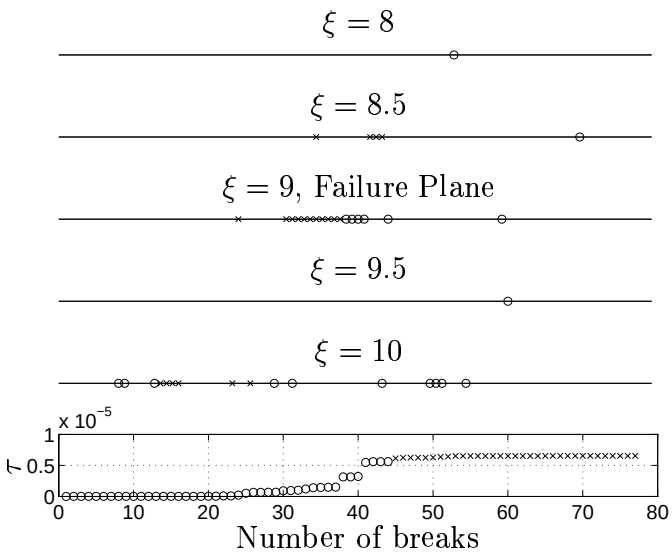

Figure 3.10: Snapshot of damage near the failure plane in the median $\beta = 0.1$, $\rho = 75$, $\alpha = 0$ specimen under load $\pi_\infty = 0.7$ among $n_{\text{sim}} = 1024$ simulations at time $\tau = 6.536 \times 10^{-6}$ when the failure criterion (3.141) is satisfied after the formation of 77 breaks. Each of the horizontal lines denotes a bundle of $n = 100$ fibers and successive bundle centers are spaced $\lambda = 0.5$ apart. Only five out of the twenty bundles simulated are shown. Each $\circ$ denotes a fiber broken before the composite goes unstable according to the strain criterion (which is satisfied after the formation of 44 fiber breaks) and each $\times$ denotes a post-critical broken fiber. Notice that the critical cluster size $k^* = 4$ and that staggering of breaks in the catastrophic cluster occurs between planes $\xi = 8.5$ and $\xi = 9$. At the bottom of the figure we plot the times at which fiber breaks occur in the composite.

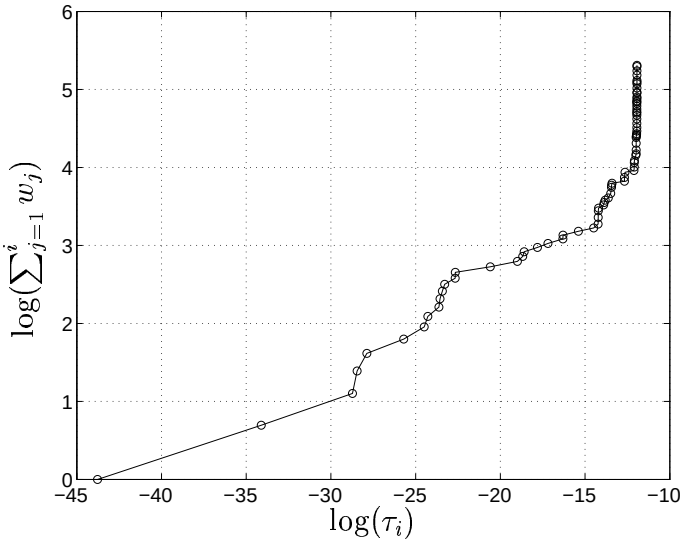

Figure 3.11: Plot of strain versus time in the median $\beta = 0.1$, $\rho = 75$, $\alpha = 0$, specimen under applied load $\pi_\infty = 0.7$. Each $\circ$ denotes the time of formation of a fiber break. Initially the strain increases rapidly as breaks accumulate randomly in the composite, then a cluster forms and takes time to extend. Finally the cluster growth goes critical causing cluster extension to proceed rapidly prompting the blow-up of composite strain. Here composite strain blows up starting at break number 45.

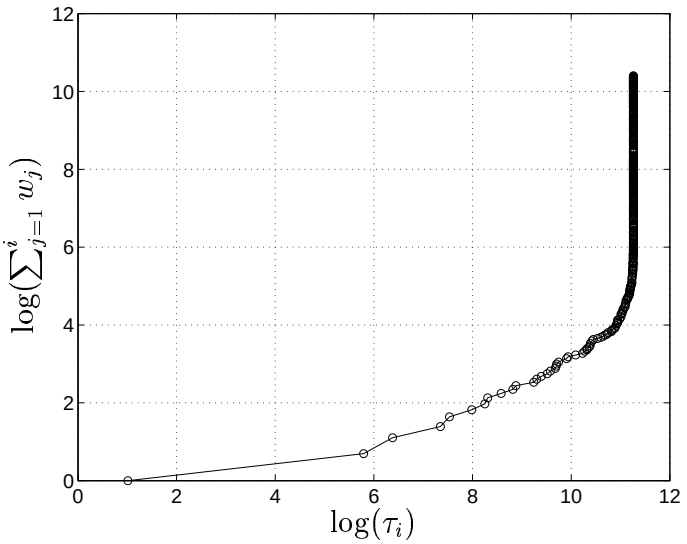

Figure 3.12: Plot of strain versus time in the median $\beta = 0.5$, $\rho = 15$, $\alpha = 0$, under applied load $\pi_\infty = 0.3$. Each $\circ$ denotes the formation of a new break. Dispersed initial breaks take up much of the lifetime of this composite with criticality apparently reached when the disperse failures have reached a certain concentration. This happens in this specimen when the number of breaks equals 94.

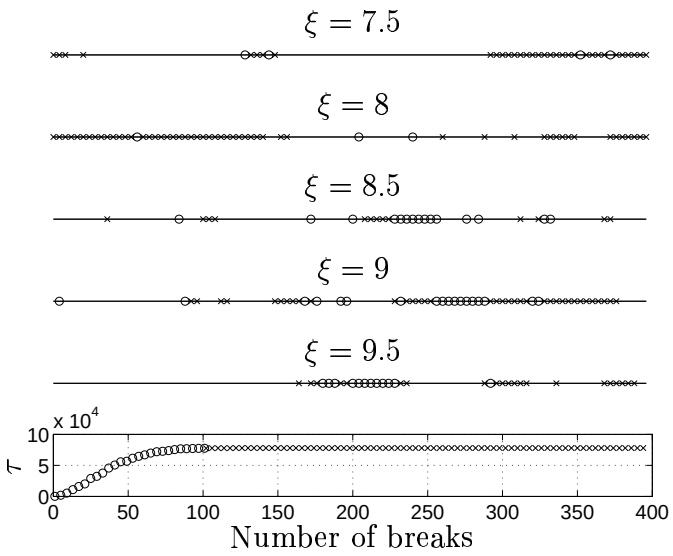

Figure 3.13: Snapshot of the damage near the failure volume of a median $\beta = 0.5$, $\rho = 15$, $\alpha = 0$, specimen among $n_{\text{sim}} = 1024$ under applied load $\pi_\infty = 0.3$, at $\tau = 7.788 \times 10^4$ when the failure criterion (3.141) is satisfied. The meanings of the horizontal line, $\circ$, and $\times$ are identical to those in Figure 3.10. Notice the extensive stagger between bundles centered at $\xi = 8.5$, $\xi = 9$ and $\xi = 9.5$. The failure plane is not identifiable; instead the bundles centered about these three planes maybe be thought as a failure volume. After the critical cluster has formed, failure progresses in the plane $\xi = 8$ to a large extent. In the bottom most plot showing the times of formation of breaks, only every fourth break has been marked for legibility.

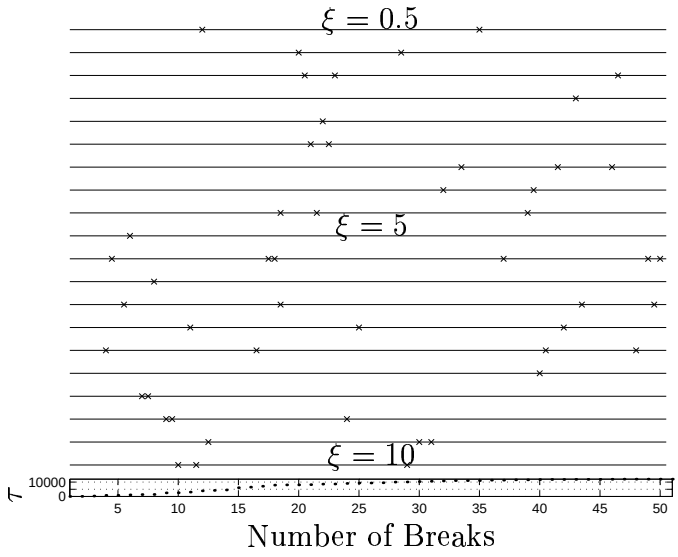

Figure 3.14: Completely dispersed failure snapshot of the median $\beta = 0.5$, $\rho = 15$, $\alpha = 0.5$, composite under applied load $\pi_\infty = 0.3$, at time $\tau = 1.21 \times 10^4$ when it goes critical as per the strain criterion. The overload length of a single break at this time almost encompasses the whole of the composite.

3.6 Comparison of Monte Carlo Empirical and Analytical Lifetime Distributions

In this section, we will compare the empirical lifetime distributions obtained from the Monte Carlo simulations just described and the analytical model developed in Section 3.4. We will find that the gradual transition from a localized failure mode to a global failure mode seen in the failure patterns of Section 3.5.3 is reflected in their lifetime distribution going from a weakest-link form with a characteristic distribution function in the cluster formation and growth case to a log-normal or normal distribution in the dispersed failure case. Since the size of the unit cell in the simulations is necessarily small, we must pay particular attention to the role of boundary effects (here manifested as the effects of periodic boundary conditions) on the failure mode of the composite and will find that periodic boundary conditions impel small composites to a dispersed failure mode.

All empirical distributions discussed are those of $n = 100$ fiber composites of normalized length $\mathfrak{L} = 10$ divided into $m = 20$ bundles longitudinally. According to this division in each fiber there are two fiber segments per characteristic length δ_{v}. Therefore, the empirical weakest link distribution $\hat{W}(\tau)$ is derived from the empirical composite lifetime distribution $\hat{H}_{mn}(\tau)$ according to

$$\hat{W}(\tau) = 1 - (1 - \hat{H}_{mn}(\tau))^{1/mn} \tag{3.142}$$

$mn = 20 \times 100 = 2000$ in the remainder of this discussion.

3.6.1 2D Arrays

A key quantity affecting the lifetime distribution function $H_{mn}(\tau)$ is the stress concentration ahead of a cluster of k fiber breaks. As seen in the failure configurations of Section 3.5.3 the typical propagating cluster of k breaks tends to be somewhat staggered. In view of this fact and our observations in Section 3.2.5 regarding the effect of periodic boundary conditions and staggering ahead of a cluster of k breaks in (3.80) and (3.82) respectively, we take the form of the stress concentration ahead of a cluster of k breaks in 2D arrays to be

$$K_k(\tau) = \sqrt{\frac{\pi k}{8}\psi_k(1 + \exp(-\mathfrak{L}/(k\tau^{\alpha/2}))) + 1} \tag{3.143}$$

where we provisionally let ψ_k be a free parameter. The dependence of $K_k(\tau)$ on τ is weak and τ may be varied considerably without significantly affecting $K_k(\tau)$. We therefore can let τ in (3.143) be the normalized time since the formation of the first break in the k-cluster without affecting the approximation much.

This form for K_k, in addition to accounting for the influence of interaction between periodic unit cells also accounts for the staggering of fiber breaks through the parameter ψ_k. We find that it is suffices to let

$$\psi_k = \begin{cases} 1 & \text{if } k < k_0 \\ \psi & \text{if } k \geq k_0 \end{cases} \tag{3.144}$$

where k_0 is appropriately chosen and ψ is maintained as a free parameter which is fit so as to produce the tightest bound in the lower tail of the empirical lifetime distribution produced by the simulations. We only allow $1 \leq \psi \leq 2$; $\psi = 1$ corresponds to the k-cluster comprised of two equal limbs (as defined before (3.82)) infinitely apart while $\psi = 2$ corresponds to the case the two limbs are aligned transversely.

It is to be emphasized that the form (3.143) with the restriction (3.144) at best represents an attempt to capture the dominant effect of the stress concentration ahead of a staggered cluster of k-breaks using the fewest number of fitting parameters. As will be seen, the chosen form results in predicted lifetime distributions which accurately capture the form of the empirical distributions.

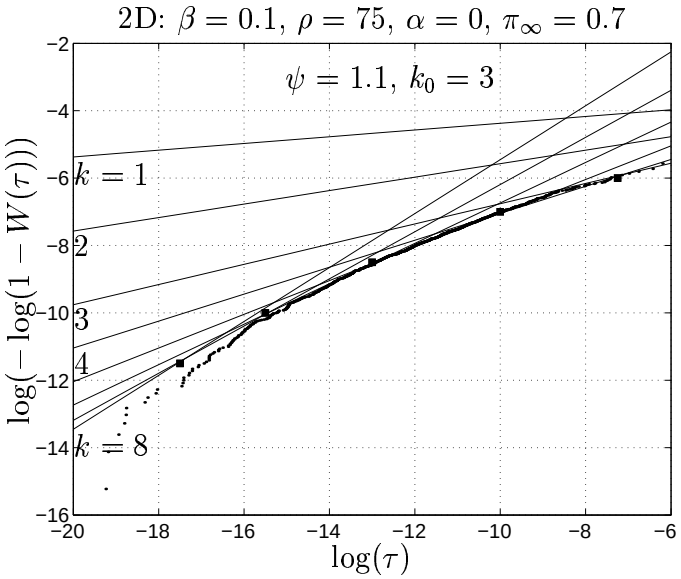

Figure 3.15: Comparison of the empirical weakest link distribution with the k-envelope given by (3.131) in a $\beta = 0.1$, $\rho = 75$ elastic matrix ($\alpha = 0$) composite on Weibull paper under applied load $\sigma = 0.7$. To get good agreement between the two, we set the parameters $\psi = 1.1$ and $k_0 = 3$. Points of intersection of the k-lines are marked with squares.

Figure 3.15 shows the comparison between empirical $\hat{W}(\tau)$ obtained from Monte Carlo simulations and $W_k(\tau)$, $k = 1, \ldots, 8$, from (3.123) for the case of a fiber matrix system under applied load $\pi_\infty = 0.7$ wherein the matrix is elastic and fiber statistics are determined by the parameters $\beta = 0.1$ and $\rho = 75$. According to (3.134), the model predicts an upper bound which is the minimum envelope

of the shown $W_k(\tau)$. To obtain good agreement between $\min_k W_k(\tau)$ and $\hat{W}(\tau)$, we have set the free parameters $\psi = 1.1$ and $k_0 = 3$. As is evident, the minimum envelope of $W_k(\tau)$ approximates the shape of $\hat{W}(\tau)$ well but divergence is seen in the lower tail. Decreasing ψ for larger k would amend this divergence. Doing so is physically justifiable since larger k corresponds in general to a greater degree of staggering to correct for which ψ must be made smaller.

The empirical median lifetime of this composite is found to be $\tau_{\frac{1}{2}} \approx 6.5 \times 10^{-6}$ at which time $k^* = 4$ in the Weibull lower envelope. From Figure 3.10 it can be seen that the critical cluster size k^* in the failure plane of the median specimen is indeed 4.

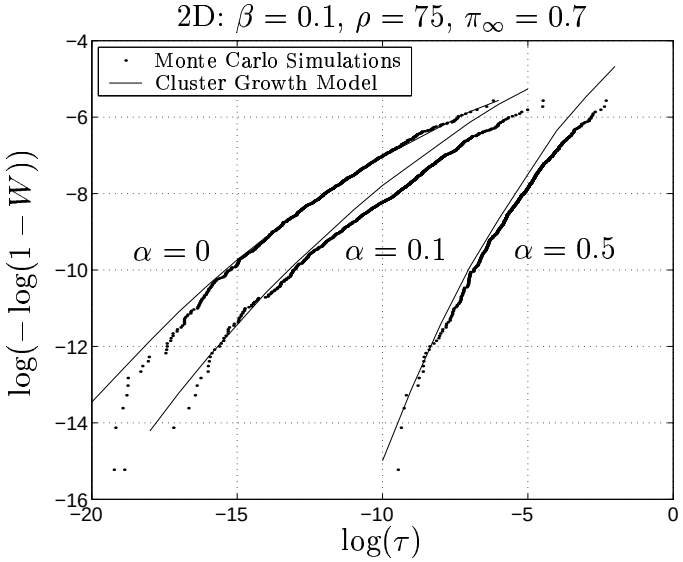

Figure 3.16: Comparison on Weibull paper of the empirical weakest link distribution with the minimum of the k-envelope in $\beta = 0.1$, $\rho = 75$ fiber composites with matrix of three different α: $\alpha = 0$, 0.1, and 0.5 under stress $\pi_\infty = 0.7$. The (ψ, k_0) pairs for these three α are respectively, $(1.1, 3)$, $(1.4, 3)$ and $(1.75, 3)$.

Figure 3.16 shows the Weibull lower envelope of the $\beta = 0.1$ and $\rho = 75$

composites when $\alpha = 0$, 0.1 and 0.5 the first of which we just discussed. The applied normalized load is $\pi_\infty = 0.7$. Observe that the median lifetime of the three cases varies in the reverse order of their overload lengths ω_k at the failure time. The median lifetime of the $\alpha = 0$, $\alpha = 0.1$, and $\alpha = 0.5$ composites are respectively $\tau_{1/2} = 6.5 \times 10^{-6}$, 7.7×10^{-6} and 6.0×10^{-3}. In all three cases, the median lies in the range of $k^* = 4$. This implies that the approximate normalized overload lengths in the three cases calculated using (3.74) are $\breve{\omega}_4 = 2$, 1.11, and 0.56 respectively. Since the elastic ($\alpha = 0$) composite has an overload zone next to a fiber break which instantaneously extends to $\omega_4 = 2$, a break in it subjects a greater length of its neighboring segment to overload than it would in an $\alpha = 0.1$ or $\alpha = 0.5$ viscoelastic composite. This qualitatively explains the observed trend in the median lifetime. In computing the model lines for the three different cases, we have substituted $\tau = \tau_{1/2}$ in (3.143) without appreciable error. While $k_0 = 3$ is fixed in all three cases, $\psi = 1.1$, 1.4, and 1.75 when $\alpha = 0$, 0.1, and 0.5 respectively. This is in keeping with the overload length argument suggested above; correction necessary to account for staggering is smaller if the overload length is shorter. This in turn results in ψ closer to 2 as α increases.

Also observe that the disagreement in the lower tail between the predicted and empirical weakest link distributions seen for $\alpha = 0$ decreases and almost disappears as α is increased up to 0.5. Viewed in conjunction with the increased possibility of staggering that accompanies increased overload length ω_k as α decreases according to $\omega_k \propto \tau^{\alpha/2}$, this bolsters our earlier suggestion that the assumed forms (3.143) and (3.144) for K_k are imperfect and break down as fiber break staggering ahead of a cluster becomes pronounced.

As indicated earlier, the cluster growth failure mode gives way to a dispersed

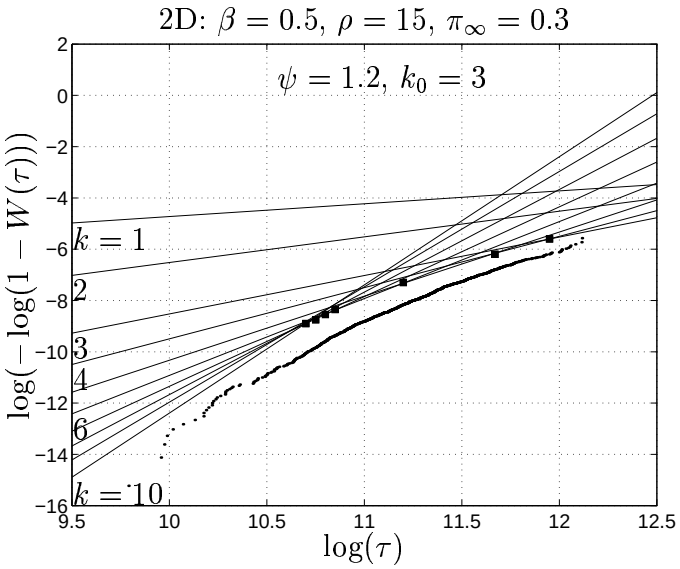

Figure 3.17: The inability of the k-envelope model to fit the empirical weakest-link distribution of $\beta = 0.5$, $\rho = 15$ fiber elastic matrix $\alpha = 0$ composites under $\pi_\infty = 0.7$. Lines of $k > 5$ appear to intersect almost at a single point. For the parameters we have taken $\psi = 1.2$ and $k_0 = 3$ here. Points of intersection of the k-lines are marked with squares.

failure mode as cluster extension probability is decreased. In Figure 3.17, in attempting to fit $W_k(\tau)$ to the weak-linked lifetime distribution of an elastic matrix composite with fiber parameters $\beta = 0.5$ and $\rho = 15$, we find that the lines of $W_k(\tau)$ intersect each other almost at a point when k exceeds about 5. An explanation follows from the boundedness of stress concentrations ahead of a k-cluster of breaks in a unit cell under periodic boundary conditions in accordance with (3.80). Let K_L be this upper bound for a unit cell of height $\mathfrak{L}$. That is, let $K_{k,L} < K_L$,

for $k = 1, 2, \ldots$. Then for sufficiently large k, the ratio W_{k+1}/W_k becomes

$$\frac{W_{k+1}(\tau)}{W_k(\tau)} = \frac{2\chi\Gamma(1+\beta)}{c_k}\frac{\Gamma(1+(k+1)\beta)}{\Gamma(1+k\beta)}\left(1-\frac{1}{K_{k,L}}\right)^{-1}(K_{k,L}\pi_\infty)^{\rho\beta}\tau^{\beta+\alpha/2}$$
$$\approx 2\chi\Gamma(1+\beta)\beta^\beta\gamma(k)(K_L\pi_\infty)^{\rho\beta}\tau^{\beta+\alpha/2}. \tag{3.145}$$

where $\gamma(k) = O((k+1)^\beta)$ is a slowly increasing function of k when β is small. From this we may define an *accumulation time*

$$\tau_{\mathrm{a}} = (2\chi\Gamma(1+\beta)\beta^\beta\gamma(k)(K_L\pi_\infty)^{\rho\beta})^{-\frac{2}{\alpha+2\beta}}. \tag{3.146}$$

$W_{k+1}(\tau) < W_k(\tau)$, for $\tau < \tau_{\mathrm{a}}$ and all $k > k_0$ for some k_0. For $\tau \geq \tau_{\mathrm{a}}$ however, there is a unique k^* such that $W_{k^*}(\tau) \leq W_k(\tau)$, for all k at each τ where $k^* = k^*(\tau)$. By this argument, accumulation of W_k of the above described nature should occur for all values of β and ρ for sufficiently high k.

After the stress concentration ahead of a cluster of breaks fails to substantially increase with the size of the cluster, cluster extension must proceed at the same speed irrespective of cluster length. In this condition a global damage mode appears to take over and fail fibers in a dispersed manner until they link up and fail the composite.

Disperse failure is characteristic of equal load sharing bundles which as discussed in Section 3.4.1 have Gaussian lifetime distributions asymptotically as $n \to \infty$. That gives us reason to expect the same distribution even in local load sharing composites when fiber failure has a disperse nature. However we do not find obvious normal tendency for any of our simulated lifetime distributions. A second possibility suggested by the longitudinal localization of disperse fiber breaks within bands smaller than the composite length is that the empirical

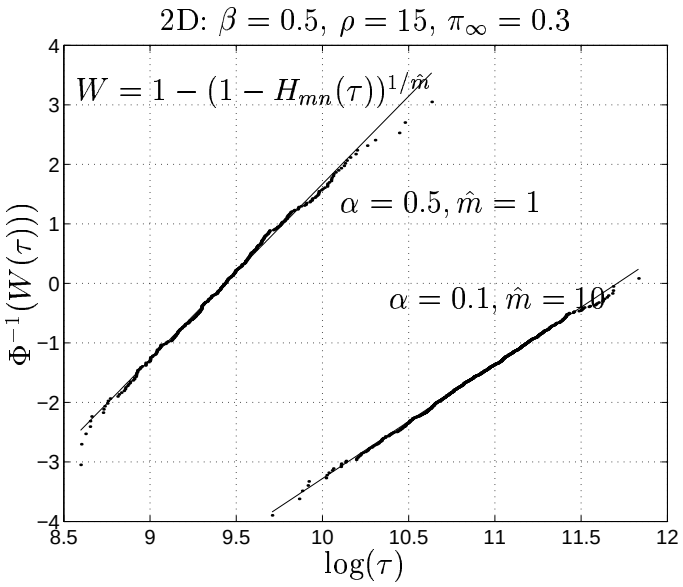

Figure 3.18: Plots of the weak linked empirical distribution of $\beta = 0.5$, $\rho = 15$ composites under applied stress $\pi_\infty = 0.3$ on log-normal paper. The linearity of the plots suggests that the weak linked distributions are log-normal.

lifetime distribution follows

$$\hat{H}_{mn}(\tau) = 1 - (1 - \hat{W}(\tau))^{\hat{m}} \tag{3.147}$$

where $\hat{W}(\tau)$ is normally distributed and the composite may be thought of as a weakest link arrangement of $\hat{m}$ equal load sharing bundles. However again, $\hat{W}(\tau)$ determined from (3.147) fails to be Gaussian for all $\hat{m}$ as determined from our simulation $\hat{H}_{mn}$ data.

However it turns out, and this is curious, that $\hat{W}(\tau)$ is very linear on log-normal coordinates which differs from the normal coordinates in that the horizontal axis is $\log\tau$ instead of τ. Figure 3.18 shows the weak linked lifetime distributions of $\beta = 0.5$, $\rho = 15$ composite specimens with matrix of $\alpha = 0.1$ and $\alpha = 0.5$ on log-normal probability paper together with straight lines which are least squares

fits of them. Here $\hat{m}$ is chosen in each case to be the integer which minimizes the standard error of both the slope and intercept estimates of the fitting straight lines. The line corresponding to $\alpha = 0$ is excluded from this figure since the standard error corresponding to it does not achieve a minimum at any reasonable $\hat{m}$ and continually decreases as $\hat{m}$ is increased and the concept fails to work, i.e., the form (3.147) does not capture the distribution of $\hat{H}_{mn}$ for $\alpha = 0$. This observation is in agreement with Figure 3.17 which shows that the k-cluster growth model is a reasonable assumption until it is superseded by non-accelerating crack growth due to the influence of its periodic images. $\alpha = 0$ thus appears to be in between the clustered and disperse failure modes in behavior for this limited unit cell size.

We follow the argument of Ibnabdeljalil and Phoenix [7] to explain the observed log-normal link $W(\tau)$ of $H_{m,n}(\tau)$. It hinges on the connection between the lifetime problem and the static strength problems established through (3.100). It is found from Monte Carlo simulations of the strength of equal load sharing strength bundles that their strength distribution converges rapidly to the normal distribution even when the bundles are as small as $n = 5$. This is in contrast to the equal load sharing lifetime bundles whose convergence to their asymptotic normal distribution is much slower so that convergence is not complete even for $n = 500$. Since our weakest link bundles are quite small, their lifetime distribution is non-normal in feature.

To see the log-normality of our lifetime distribution we must determine the lifetime distribution corresponding to a normal strength distribution. Following Ibnabdeljalil and Phoenix [7] and Phoenix [6] the standardized lifetime of an equal

load sharing bundle has the scaling

$$\mathscr{T} = \begin{cases} \int_0^T \pi^\rho(s)ds = T\pi_\infty^\rho, & \text{if } \pi(s) = \pi_\infty \\ \int_0^{T'} \pi^\rho(s)ds = \frac{\mathscr{R}^\rho T'}{\rho+1}, & \text{if } \pi(s) = \mathscr{R}s \end{cases} \tag{3.148}$$

where T and T' are the actual failure times under the two kinds of loadings - constant and linearly increasing. $\mathscr{R}$ is the loading rate and $\mathscr{T}$ is a standard time assuming $\pi_\infty = 1$. This remarkable result for both the fiber and the bundle emerges from the factorization property of the power law breakdown rule in integrals [6]. Equating the two right hand sides and substituting the strength-time relationship $\Sigma = \mathscr{R}T'$ in the linearly increasing load case gives

$$T\pi_\infty^\rho = \frac{\mathscr{R}^\rho T'}{\rho+1} = \frac{\Sigma^{\rho+1}}{(\rho+1)\mathscr{R}} \tag{3.149}$$

which implies that

$$\Sigma \propto \mathscr{T}^{\frac{1}{\rho+1}} \approx \frac{1}{\rho+1}\log(\mathscr{T}) + 1 \tag{3.150}$$

where the latter approximation is accurate for large ρ ($\rho \geq 10$, say) and $\mathscr{T}$ close to one. Since Σ is normal, this suggests that $\mathscr{T}$ must be log-normal.

A scaling relation between the applied load and lifetime which holds in a bundle wherein each fiber is subjected to the load profile (3.112) was derived in (3.116) and the scaling relation in the absence of stress concentrations in (3.118). The actual stress state in a partially failed composite lies in between these extremes and we now look into the actual scaling relationship seen in our Monte-Carlo simulations.

Figure 3.19 shows the variation of the median composite lifetime with applied load when fiber $\beta = 0.1$ and $\rho = 75$ and matrix $\alpha = 0$, 0.1, and 0.5. When $\alpha = 0$, the load-lifetime scaling relation (3.116) collapses into (3.118) which appears to hold. Thus, the median lifetime $\tau_{1/2}$ scales exactly as $\pi_\infty^{-\rho}$. However

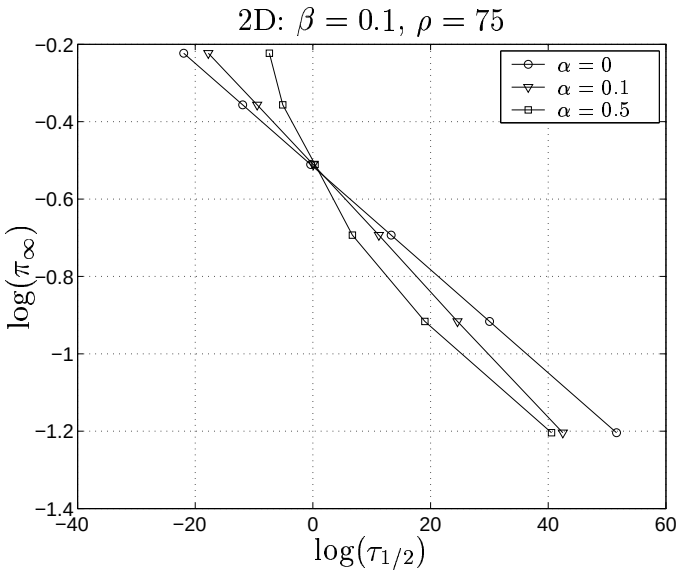

Figure 3.19: Scaling of the median lifetime($\tau_{1/2}$) with applied load(π_∞) for composites with $\beta = 0.1$, and $\rho = 75$ and different α. In the case of the elastic matrix, $\alpha = 0$, the scaling relation exactly is $\pi_\infty^{75}\tau_{1/2} = c$ where c is a constant. When $\alpha = 0.1$, the scaling $\pi_\infty^{58}\tau_{1/2} = c$ is a good approximation. When $\alpha = 0.5$, the simple power law scaling fails to hold.

when $\alpha \neq 0$, the situation is more complicated. While (3.116) suggests the form $\pi_\infty^{\rho\beta/(\beta+\alpha/2)}\tau_{1/2} =$ constant, for the load-lifetime scaling in this case and which, for $\alpha = 0.1$ becomes $\pi_\infty^{50}\tau_{1/2} =$ constant it turns out that the actual scaling relation for $\alpha = 0.1$ goes as $\pi_\infty^{58}\tau_{1/2} =$ constant. Thus the actual load scaling power(58) lies in between the exponents given by (3.118) and (3.116). A possible reason for this deviation is that while form (3.118) is written for the case wherein fiber failures occur independently of each other and (3.116) for case wherein they form in a way so as to extend a crack, in reality, the composite failure starts with disperse breaking wherein (3.118) is more applicable and terminates with the growth of a cluster of breaks when (3.116) is more applicable. Therefore it seems quite rea-

sonable that the actual scaling exponent be in between the exponents given by either extreme case. Furthermore, (3.131) provides us a way to approximate the actual load scaling exponent. It is readily seen from here that the dependence of the characteristic lifetime distribution on load goes as

$$W_k(\tau) \sim \pi_\infty^{\frac{\rho\beta}{\beta+((k-1)/k)\alpha/2}}\tau \tag{3.151}$$

so it would be reasonable to expect

$$\pi_\infty^{\rho\beta/(\beta+((k-1)/k)\alpha/2}\tau_{1/2} = \text{constant} \tag{3.152}$$

so long as the composite fails by cluster formation and growth. Setting $k = 3$ which is the observed critical cluster size in this expression for the median range, we find that the load-lifetime scaling exponent is 56.25 which is very close to the observed scaling exponent, 58.

Figure 3.20 shows the comparison of a single specimen under three different applied loads. The scaled time of occurrence of fiber failures is plotted here against the fiber break number with scaling done according to (3.118). The initial fiber breaks, formed mostly due to the applied load and independent of other breaks in the composite collapse into one under this scaling. However after about $\mathfrak{N} = 8$ breaks form, divergence is noticed among the different load levels as fiber breaks begin to interact.

Figure 3.21 shows the same plot except that scaling is done according to the relation (3.116). This scaling fails to collapse the three curves into one master curve towards the end of the failure process. Instead, the order of the scaled lifetimes under the different load levels is reversed in this case from that in Figure (3.20) suggesting an over-correction by the scaling exponent.

In Figure 3.22, scaling is done according to (3.152) and a closer approach although not collapse of the scaled failure times in the different cases to each other is seen. k for each specimen is chosen to be the critical cluster size k^* for that specimen. It must be recognized that the sequence of breaks leading upto composite failure is different in the different specimen owing to the different applied loads although they have identical standard representative random variables. The scaling (3.152) is derived by statistical arguments, not deteministic ones, unlike (3.118) and (3.116). This makes the lack of collapse of the three curves unsurpising. Another contributor to the disagreement between the three scaled lifetimes in this figure is that length scale correction as suggested by (3.116) has not been incorporated here.

Figure 3.23 shows the same scaling but of the median specimen under the three loads. Since the scaling relation is statistical in nature, it is reasonable to compare the statistically similar median specimen although they are not the same realization in that they have different standard representative random variables. As is seen, the failure times are close to each other; however this collapse is only approximate suggesting that the somewhat non-linearity of the $\alpha = 0.1$ line in Figure 3.19. However the observed mismatch of the failure times is much smaller than the lifetime variability in the three specimens.

When $\alpha = 0.5$, as is evident from Figure 3.19, the power-law load lifetime scaling breaks down especially for smaller loads. This is to be expected, for as α increases, so does the overload length ahead of a crack prompting the dispersion of breaks in the fiber direction as often observed above. This causes the breakdown of the cluster-driven mode of composite failure, which in turn results in breakdown of the power-law load-lifetime scaling relationship.

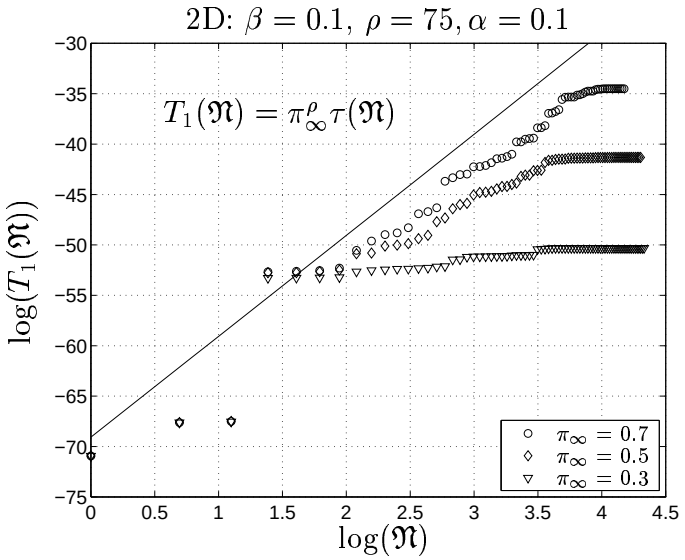

Figure 3.20: Damage evolution by way of fiber failures in time in a single $\beta = 0.1$, $\rho = 75$ specimen (same standard representative random variables) under three different loads: $\pi_\infty = 0.3$, 0.5, and 0.7. The time $\tau(\mathfrak{N})$ of occurrence of break $\mathfrak{N}$ for each applied load π_∞ is scaled to unit applied load using $T_1(\mathfrak{N}) = \pi_\infty^\rho \tau(\mathfrak{N})$ which would be the scaling of composite lifetime is the breaks formed solely on account of the far-field load as in (3.118). As this figure shows this scaling is valid in the initial stages of failure when the fiber breaks are few and far apart but breaks down after the formation of about $\mathfrak{N} = 8$ breaks at which point cluster growth takes over.

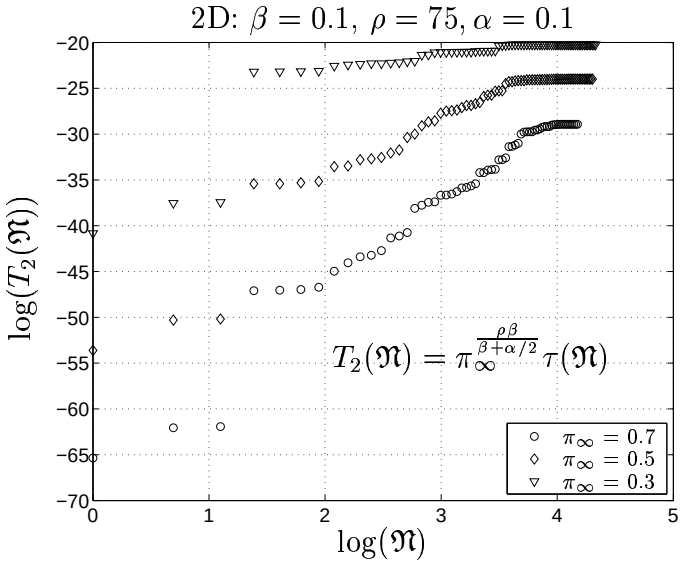

Figure 3.21: Figure 3.20 plotted with the scaling $T_2(\mathfrak{N}) = \pi_\infty^{\rho\beta/(\beta+\alpha/2)}\tau(\mathfrak{N})$ as would be expected in a load sharing bundle according to (3.116).

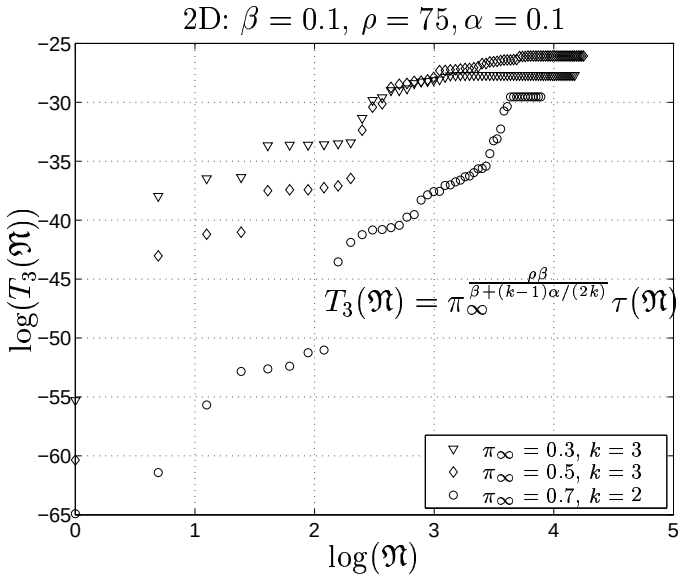

Figure 3.22: Figure 3.20 plotted with the scaling $T_3(\mathfrak{N}) = \pi_\infty^{\rho\beta/(\beta+(k-1)\alpha/(2k))}\tau(\mathfrak{N})$ as would be expected in a load sharing bundle according to (3.152). The three specimen have identical standard representative random variables.

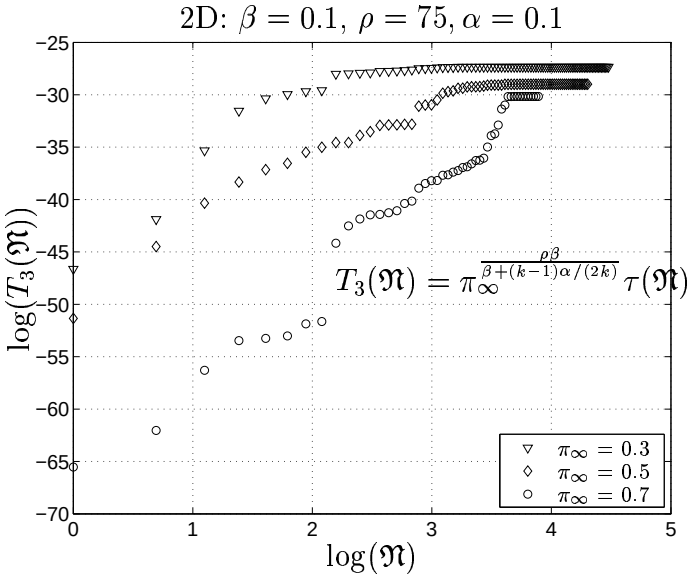

Figure 3.23: Figure 3.20 plotted with the scaling $T_3(\mathfrak{N}) = \pi_\infty^{\rho\beta/(\beta+(k-1)\alpha/(2k))}\tau(\mathfrak{N})$ as would be expected in a load sharing bundle according to (3.152). The three specimen shown are the three median specimen among 1024 simulations and do not have the same standard representative random variables.

3.6.2 3D Arrays

In 3D, the effect of periodic images of a cluster of breaks in the fiber direction is considerably smaller than that in 2D. For this reason, we assume the form for the stress ahead of a k-cluster to be

$$K_k = \sqrt{\frac{\sqrt{k}}{\pi^{3/2}}\psi_k + 1} \tag{3.153}$$

where we have absorbed the smaller correction for periodicity

$$1 + \exp(-\mathfrak{L}\pi\psi_1/\sqrt{k})$$

into the factor ψ_k itself. (3.153) is derived from the form (3.83) for the stress concentration ahead of a staggered cluster of breaks. Also, we find that it suffices to take ψ_k of the form

$$\psi_k = \begin{cases} 1, & \text{if } k = 1 \\ \psi & \text{if } k > 1. \end{cases} \tag{3.154}$$

as in 2D where ψ is left as a free fitting parameter albeit subject to the bounds $1 \leq \psi \leq 2$. In (3.122) we noted that the number of neighbors surrounding a j-cluster of fiber breaks is $N_j \approx (4\pi)^{1/2} j^{1/2}$. However the stress concentration varies considerably from fiber to fiber among the neighbors of a cluster of breaks and in a previous work [20] we have found it essential to accommodate this variability by letting

$$N_j = \eta j^{\nu} \tag{3.155}$$

where both η and ν are fitting parameters. N_j may be viewed as the number of fibers surrounding a cluster that are effectively at high risk of failure.

Figure 3.24 shows the comparison of the cluster growth model against the empirical weakest link distribution obtained from simulations of a $\beta = 0.1$, $\rho = 75$

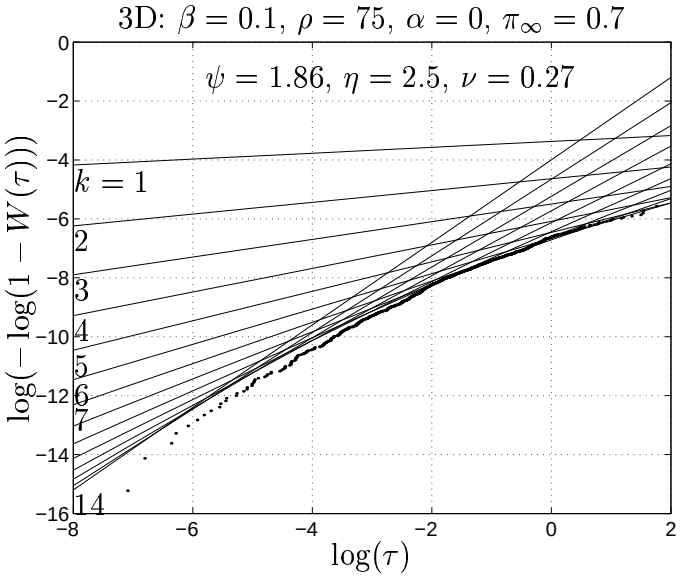

Figure 3.24: Comparison of the empirical weakest link distribution with the k-envelope given by (3.131) in a $\beta = 0.1$, $\rho = 75$ 3D elastic matrix composite under applied load $\pi_\infty = 0.7$ on Weibull probability paper. To get good agreement between the two, we set the parameters $\psi = 1.86$, $\eta = 1.25$, and $\nu = 0.27$.

elastic matrix composite under load $\pi_\infty = 0.7$. To fit the data we have taken $N_j = 1.25j^{0.27}$ and $\psi = 1.86$. The closeness of the fitting parameter ψ to 2 suggests that out of plane staggering of fiber breaks is minimal for this set of parameters. Owing to the smaller stress concentrations ahead of a k-cluster in 3D than in 2D, the probability range of the simulations encompasses more k^* regimes in 3D than in 2D. Figure 3.25 similarly compares the cluster growth model with the empirical weakest link distribution in a $\beta = 0.5$, $\rho = 15$ composite in an $\alpha = 0.1$ matrix under applied load $\pi_\infty = 0.3$ per fiber. As seen, the fit is exceptionally good in the lower tail using the fitting parameters shown in the figure. Even though the times are large in this case, the approximate normalized overload length $\breve{\omega}_k \approx \sqrt[4]{k}\tau^{\alpha/2}/2$ here is much smaller than the normalized composite length $\mathfrak{L}$.

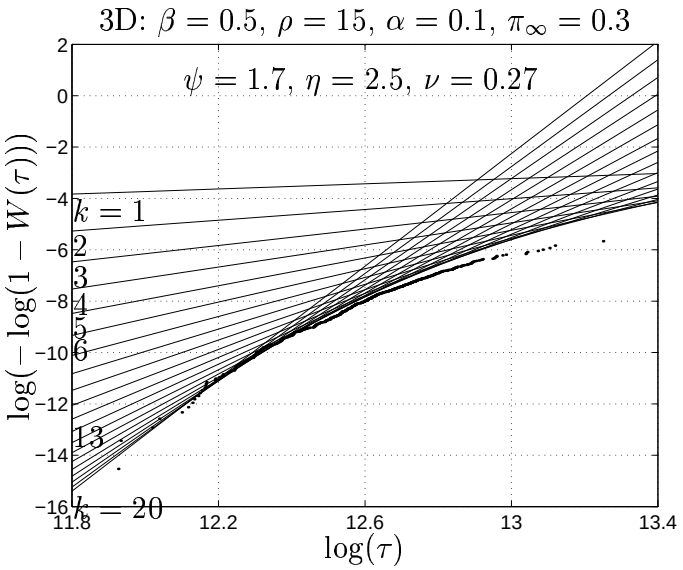

Figure 3.25: Comparison of the empirical weakest link distribution with the k-envelope given by (3.131) in a $\beta = 0.5$, $\rho = 15$ fiber, $\alpha = 0.1$ matrix 3D composite under applied load $\pi_\infty = 0.3$ on Weibull probability paper. To get good agreement between the two, we set the parameters $\psi = 1.7$, $\eta = 1.25$, and $\nu = 0.27$.

Stalling of clusters due to the interaction between breaks and their periodic images is much less of an issue in 3D than in 2D since these interactions, generally speaking, are much smaller in 3D than in 2D arrays. As seen in Figure 3.6, stress concentration ahead of a cluster of breaks is very mildly affected as $\mathfrak{L}$ is decreased from ∞ to 5. The $\mathfrak{L} = 10$ line is almost indistinguishable from the $\mathfrak{L} = \infty$ line and is not shown in that figure.

Figure 3.26 shows the lower envelope of the k-lines for $\beta = 0.1$ and $\rho = 75$ composites with matrices of different α. The observation and explanation in 2D regarding the order of the median lifetimes is also applicable here.

As in 2D, we find that the weak linked lifetime distribution is log-normal as shown in Figure 3.27 when $\pi_\infty = 0.3$. (The simulation of $\alpha = 0.5$, $\pi_\infty = 0.3$

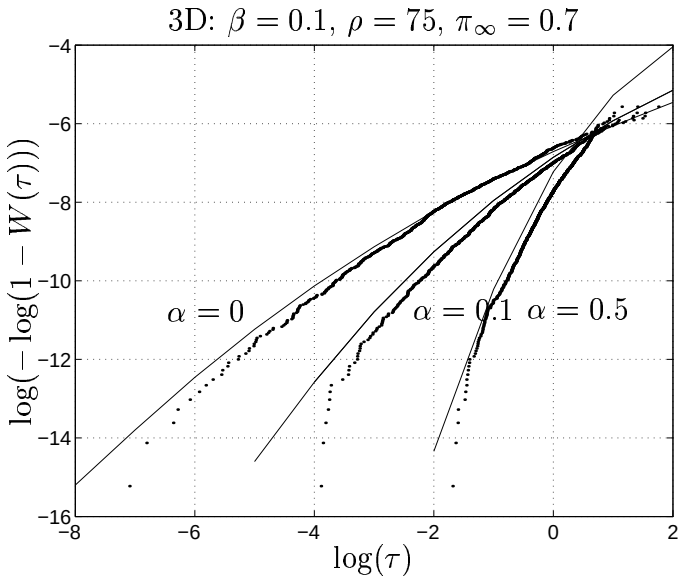

Figure 3.26: Comparison on Weibull paper of the empirical weakest link distribution with the minimum of the k-envelope in $\beta = 0.1$, $\rho = 75$ fiber composites with matrix of three different α: $\alpha = 0$, 0.1, and 0.5 under stress $\pi_\infty = 0.7$. In all three cases we have set $\psi = 1.86$, $\eta = 1.25$, and $\nu = 0.27$.

is beyond our computational capabilities and is not shown here.) Unlike in 2D, log-normality of the weak-linked lifetime distribution in 3D is not tied to cluster stalling owing to interactions between breaks and their images. This suggests that the tendency toward log-normality of the weak-linked lifetime distribution may not be an artifact of our limited simulation unit cell size. But what is surprising here is that $\hat{H}_{mn}$ is itself normally distributed as shown in Figure 3.28 although its mean and standard deviation are far removed from the mean of 6.19×10^3 and standard deviation of 2.76×10^3 predicted by the equal load sharing model for both $\alpha = 0$ and $\alpha = 0.1$ (since matrix characteristics are irrelevant to equal load sharing). We however suspect that normality of $\hat{H}_m n(\tau)$ is coincidental and that it will breakdown in the lower tail. Indications of such a breakdown are already

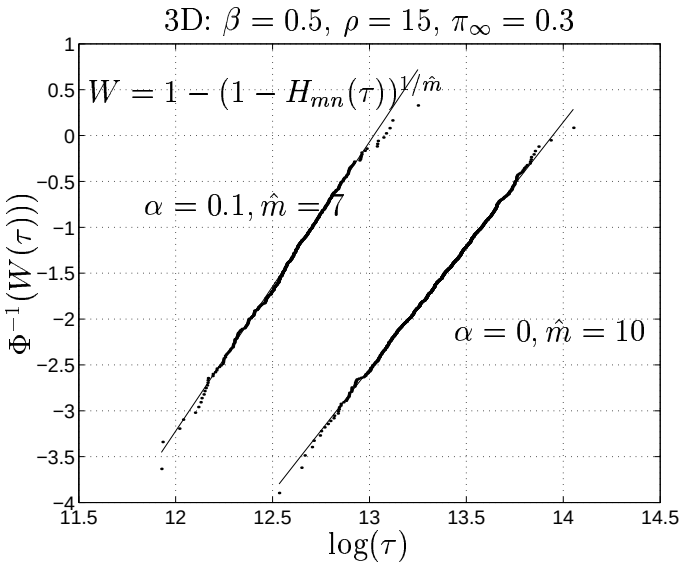

Figure 3.27: Plots of the weak linked empirical distribution $W(\tau)$ of $\beta = 0.5$, $\rho = 15$ composites under applied stress $\pi_\infty = 0.3$ on log-normal paper. The linearity of the plots suggests that the weak linked distributions are log-normal.

seen among the last few specimens in Figure 3.28.

In the next section, we will speculate on the form of the weakest link distribution in large composites.

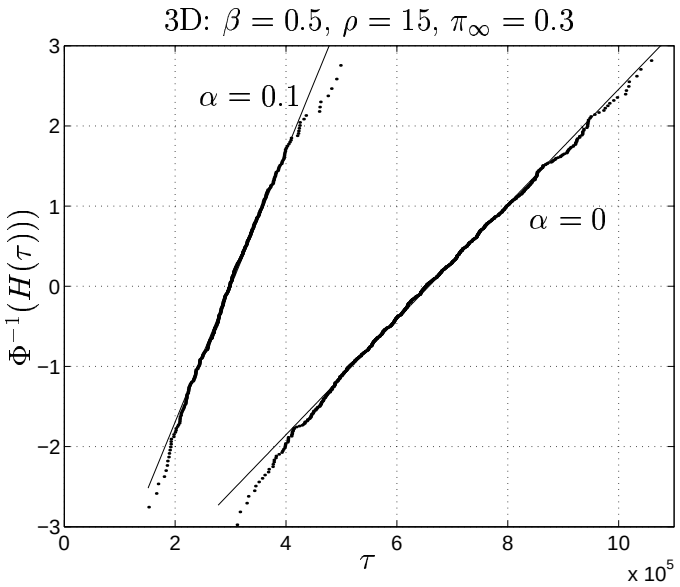

Figure 3.28: Plots of the empirical distribution $H_{mn}(\tau)$ of $\beta = 0.5$, $\rho = 15$ composites under applied stress $\pi_\infty = 0.3$ on normal probability paper. The linearity of the plot suggests normality of the distribution. However the parameters of the normal distribution do not agree with those predicted by equal load sharing theory.

3.7 Large Composites

Hitherto we have confined ourselves to composites with $n = 100$ fibers and of height $L = 10\delta_{\rm v}$, or, $mn = 1000$ fiber segments which is very small compared to real composites which typically have more than $mn = 10^7$ fiber segments of length of the order of $\delta_{\rm v}$. On our small composite we imposed periodic boundary conditions which prevented stress leakage from the unit cell as would occur had we imposed patch boundary conditions which would in turn result in longer composite lifetimes. However periodic boundary conditions resulted in spurious accumulation times owing to the interaction of breaks with their images located in close proximity. Furthermore, under the chain of bundles framework, we recentered the breaks

appearing in each λ-bundle both in the simulations and effectively in the modeling of cluster growth. To reduce the artificial effect of recentering we set $\lambda = 0.5$ which is the smallest value given our computational constraints. While this turned out adequate for large β composites, its effects were clearly discernable when β was smaller resulting in shorter overload lengths. Now we will consider large composites without these artificial restrictions which were imposed in order that failure can be efficiently simulated.

3.7.1 2D Arrays

If $\mathfrak{L} = \infty$, (3.73) and (3.74) express the stress concentration and overload length ahead of a k-cluster. Out of plane staggering of fiber breaks during cluster growth will still need to be accounted for and let us do so by introducing the parameter ψ

$$K_j(0) = \sqrt{\frac{\pi j}{4}\psi + 1}, \quad 0 \le \psi \le 1. \tag{3.156}$$

We will now determine a closed form approximation for the weak-linked lifetime distribution function $W(\tau)$. The composite lifetime distribution can be extracted from it as usual according to

$$H_{mn}(\tau) = 1 - (1 - W(\tau))^{mn} \tag{3.157}$$

We begin with (3.131) with $N_j = 2$, $j = 1, 2, \ldots, k-1$.

$$\begin{aligned} W_k(\tau) =& \tau^{k(\beta+\alpha/2)} \frac{\Gamma^k(\beta+1)}{\Gamma(k\beta+1)} (4\chi)^{k-1} \pi_\infty^{k\rho\beta} \frac{\lambda}{\tau^{\alpha/2}} \\ & \prod_{j=1}^{k-1} \left[\frac{1}{1+\frac{1}{\sqrt{j}}} \frac{K_j^{\rho\beta+1}}{K_j - 1} \right] \end{aligned} \tag{3.158}$$

Let $a = \pi\psi/4$ so that $K_j = \sqrt{1 + aj}$. In terms of a we may express excellent

approximations for the different factors as

$$\prod_{j=1}^{k-1} \frac{1}{1+\frac{1}{\sqrt{j}}} \approx \frac{k^{k/2}}{(\sqrt{k}+1)^{k-1}} e^{-(\sqrt{k}-1)} \tag{3.159}$$

$$\prod_{j=1}^{k-1} K_j \approx \left[\frac{(ak+1)^{k+\frac{1}{a}-\frac{1}{2}}}{(a+1)^{\frac{1}{a}+\frac{1}{2}}} e^{-(k-1)} \right]^{\frac{1}{2}} \tag{3.160}$$

and

$$\begin{aligned} \prod_{j=1}^{k-1} (K_j - 1) \approx & a^{\frac{k-1}{2}} \frac{\left(\sqrt{k+\frac{1}{a}} - \sqrt{1+\frac{1}{a}}\right)^{k-\frac{1}{2}}}{\sqrt{1+\frac{1}{a}} - \sqrt{1+\frac{1}{a}}} e^{-\frac{1}{2}(k-1)} \\ & e^{-\sqrt{\frac{1}{a}}\left\{\sqrt{k+\frac{1}{a}} - \sqrt{1+\frac{1}{a}}\right\}} \end{aligned} \tag{3.161}$$

Setting

$$W_k(\tau) = W_{k+1}(\tau) \tag{3.162}$$

now yields the intersection time of the W_k and W_{k+1} lines:

$$\tau^{\beta+\alpha/2} = \left(1 + \frac{1}{\sqrt{k}}\right) \frac{1}{4\chi} \frac{K_k - 1}{K_k^{\rho\beta+1}} \frac{\Gamma((k+1)\beta+1)}{\Gamma(\beta+1)\Gamma(k\beta+1)} \frac{1}{\pi_\infty^{\rho\beta}} \tag{3.163}$$

Algebraic manipulations following the substitution of (3.159), (3.160), (3.161), and (3.163) in (3.158) result in

$$W_k = \frac{\theta_1}{\tau^{\alpha/2}} \left(k + \frac{1}{a}\right)^{\theta_2} \exp\left\{ -\left(\frac{\rho}{2} - 1\right) \beta \left(k + \frac{1}{a}\right) (1 - \Theta_k) \right\} \tag{3.164}$$

where

$$\begin{aligned} \theta_1 = & \frac{\lambda}{4\chi} \frac{\sqrt[4]{a}\left[\sqrt{1+a} - 1\right]^{1/2}}{(1+a)^{\frac{\rho\beta+1}{2}}} \left(\frac{a}{1+a}\right)^{\theta_2} \\ & \exp\left\{ \left(\frac{\rho}{2} - 1\right) \beta(1 + \frac{1}{a}) + \sqrt{\frac{1}{a}}\sqrt{1+\frac{1}{a}} + 2 \right\}, \end{aligned} \tag{3.165}$$

$$\theta_2 = \left(\frac{1}{a} - \frac{1}{2}\right) \frac{\rho\beta + 1}{2}, \tag{3.166}$$

and

$$\Theta_k = \frac{\sqrt{1/a}-1}{\beta(\rho/2-1)}\left(k+\frac{1}{a}\right)^{-\frac{1}{2}}. \tag{3.167}$$

Inverting (3.163), we get an expression for k in terms of τ

$$k+\frac{1}{a} \approx \frac{\theta_3}{\tau^{\theta_4}} \tag{3.168}$$

where

$$\theta_3 = \left(\frac{3\beta^\beta \pi_\infty^{-\rho\beta}}{16\chi a^{\rho\beta/2}\Gamma(1+\beta)}\right)^{\frac{2}{(\rho-2)\beta}},$$

and

$$\theta_4 = \frac{2}{(\rho-2)\beta}(\beta+\alpha/2)$$

Substituting (3.168) into (3.164) we finally have

$$W(\tau) = \frac{\theta_1\theta_3^{\theta_2}}{\tau^{\theta_5}}\exp\left\{-\left(\frac{\rho}{2}-1\right)\beta\frac{\theta_3}{\tau^{\theta_4}}(1-\Theta(\tau))\right\} \tag{3.169}$$

where

$$\theta_5 = \theta_2\theta_4 - \alpha/2$$

and

$$\Theta(\tau) = \frac{\sqrt{1/a}-1}{(\rho/2-1)\beta}\frac{\tau^{\theta_4/2}}{\sqrt{\theta_3}}.$$

$W(\tau)$ will not be a distribution function unless it is non-decreasing in τ. Setting $dW(\tau)/d\tau > 0$, we have a condition for its regime of validity, viz.,

$$(\rho/2-1)\beta\theta_3\theta_4/\tau^{\theta_4} > \theta_5. \tag{3.170}$$

This condition is obviously not satisfied if $\rho \leq 2$ assuming all the θ constants are positive.

In Figure 3.29 we have compared (3.169) against empirical weak-linked lifetime distributions obtained from Monte-Carlo simulations. It is notable that a good fit

in the case of the $\alpha = 0.5$ composite requires a ψ value slightly in excess of 2, the supposed upper bound on ψ. This is likely due to slight errors introduced during the approximations. For, the effect of small changes in stress concentration on lifetime is large, since lifetime scales as $K^{\rho\beta}$. Although the lower tail of the $\alpha = 0$, $W(\tau)$ distribution is a poor fit of the empirical distribution, we find that the fit improves as α is increased (and the corresponding overload length is decreased). This trend suggests that the failure of the $\alpha = 0$, and $\alpha = 0.1$ lower tail stem largely from the inability of the form (3.156) to capture the periodicity of boundary conditions when the overload length is sizable. In Figure 3.16 where more elaborate correction for periodicity conditions were made by assuming the form (3.143) for the stress concentrations, the fit is much better.

An alternative form for the stress concentration which is likely to be more successful in accounting for periodic boundary conditions while still amenable to closed form $W(\tau)$ determination is

$$K_j(0) = \sqrt{\frac{\pi j^\nu}{4}\psi + 1}. \tag{3.171}$$

assigning as it does an effective crack length of ψj^ν to the j-crack, where both ψ and ν are fitting parameters to be determined in a way that results in $W(\tau)$ being a good fit to the empirical distributions.

Based on our experience with the simulations, we expect that with β and α fixed, composites with large ρ will have $\psi \approx 2$. When ρ is decreased, the cluster growth will be less stress driven, prompting ψ to decrease. Similarly, ψ will decrease with increasing $\omega \propto \tau^{\alpha/2}$ for fixed ρ and β and for fixed ρ and α decrease with increasing β.

We imagine a cutoff ψ_c such that when $\psi < \psi_c$, failure switches from a clustered to a dispersed mode owing to insufficient hazard ahead of a cluster. The

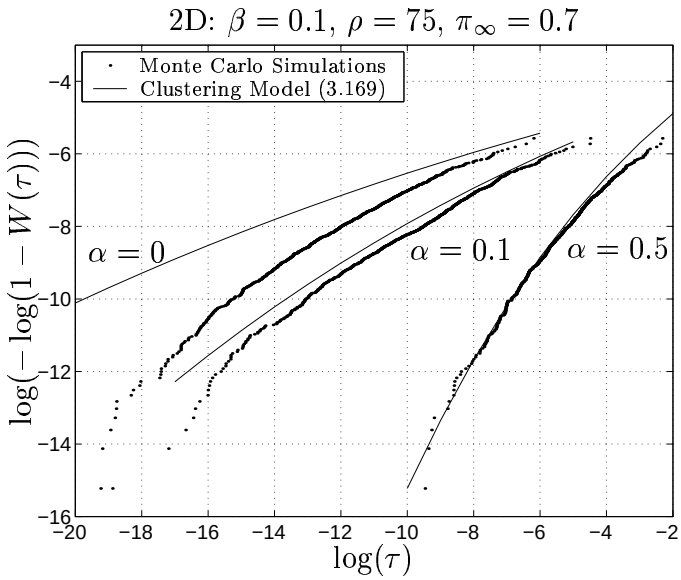

Figure 3.29: Comparison on Weibull paper of the empirical weakest link distribution with the 2D weakest link distribution given by (3.169) in $\beta = 0.1$, $\rho = 75$ fiber composites with matrix of three different α: $\alpha = 0$, 0.1, and 0.5 under stress $\pi_\infty = 0.7$. The values of ψ used in (3.156) in the three cases are 1.8, 1.84, and 2.1 respectively.

simulations suggest that the weakest link in this case is driven by the lower tail of a log-normal distribution of mean μ_1 and standard deviation σ_1 is given by

$$\tilde{\Phi}(z(\tau)) \approx \frac{\exp\left(-z^2(\tau)/2\right)}{\sqrt{2\pi}|z(\tau)|} \tag{3.172}$$

where

$$z(\tau) = \frac{1}{\sigma_1} \log\left(\frac{\tau}{\exp(\mu_1)}\right)$$

and the lifetime distribution $H(\tau)$ is given by

$$H(z(\tau)) = 1 - \left[1 - \tilde{\Phi}(z(\tau))\right]^{\hat{m}} \tag{3.173}$$

As the composite size gets large, so will $\hat{m}$. For large $\hat{m}$, from Leadbetter et al [26,

Theorem 1.5.3] followed by algebraic manipulations we have

$$H(z(\tau)) = 1 - \exp\left(-\exp\{-a_{\hat{m}}(e^{-b_{\hat{m}}+z(\tau)} - 1)\}\right) \tag{3.174}$$

with

$$a_{\hat{m}} = (2\log\hat{m})^{1/2}$$

and

$$b_{\hat{m}} = (2\log\hat{m})^{1/2} - \frac{1}{2}(2\log\hat{m})^{-1/2}(\log\log\hat{m} + \log 4\pi)$$

3.7.2 3D Arrays

Proceeding as in 2D we start by specializing (3.131) for 3D:

$$\begin{aligned} W_k(\tau) = \tau^{k(\beta+\alpha/2)}\frac{\Gamma^k(\beta+1)}{\Gamma(k\beta+1)}\chi^{k-1}\pi_\infty^{k\rho\beta}\frac{\lambda}{\tau^{\alpha/2}} \\ \prod_{j=1}^{k-1}\left[\frac{\eta j^\nu}{1+\frac{1}{\sqrt[4]{j}}}\frac{K_j^{\rho\beta+1}}{K_j-1}\right] \end{aligned} \tag{3.175}$$

Let $a = 2\psi/\pi^{3/2}$ so that $K_j = \sqrt{a\sqrt{j}+1}$. As before, we first approximate the different products in (3.175).

$$\prod_{j=1}^{k-1}\eta j^\nu \approx (2\pi)^{\frac{\nu}{2}}\eta^{k-1}e^{-\nu k}k^{\nu(k-\frac{1}{2})} \tag{3.176}$$

$$\prod_{j=1}^{k-1}\frac{1}{1+\frac{1}{\sqrt[4]{j}}} \approx \frac{k^{k/4}}{(\sqrt[4]{k}+1)^{k-1}}\exp\left\{-\frac{k^{3/4}}{3}+\frac{k^{1/2}}{2}-k^{1/4}+\frac{2}{3}\right\} \tag{3.177}$$

$$\prod_{j=1}^{k-1}K_j \approx \left[\frac{(a\sqrt{k}+1)^{k-\frac{1}{a^2}-\frac{1}{2}}}{(a+1)^{\frac{1}{2}-\frac{1}{a^2}}}\exp\left\{-\frac{k}{4}+\frac{\sqrt{k}}{2a}+\frac{1}{2}\left[\frac{1}{2}-\frac{1}{a}\right]\right\}\right]^{\frac{1}{2}} \tag{3.178}$$

and

$$\begin{aligned} \prod_{j=1}^{k-1}K_j - 1 \approx \frac{(\sqrt{a\sqrt{k}+1}-1)^{k-\frac{1}{2}}}{(\sqrt{a+1}-1)^{\frac{1}{2}}}\exp\left\{-\frac{k-1}{4}+\right. \\ \left.\frac{2}{3a^2}\left[\sqrt{a\sqrt{k}+1}-\sqrt{a+1}\right]-\frac{1}{3a}\left[\sqrt{k}\sqrt{a\sqrt{k}+1}-\sqrt{a+1}\right]\right\} \end{aligned} \tag{3.179}$$

Setting

$$W_k(\tau) = W_{k+1}(\tau) \tag{3.180}$$

as before gives τ in terms of k as

$$\tau^{\beta+\alpha/2} = \left(1 + \frac{1}{\sqrt[4]{k}}\right) \frac{1}{\eta\chi k^{\nu}} \frac{K_k - 1}{K_k^{\rho\beta+1}} \frac{\Gamma((k+1)\beta+1)}{\Gamma(\beta+1)\Gamma(k\beta+1)} \frac{1}{\pi_\infty^{\rho\beta}} \tag{3.181}$$

Substituting (3.176 – 3.181) into (3.175) and simplifying yields

$$W_k \approx \frac{\theta_1}{\tau^{\alpha/2}} \left[\sqrt{k} + \frac{1}{a}\right]^{-\theta_2} \exp\left\{-\left(\frac{\rho\beta}{4} - \beta + \nu\right)\left[\sqrt{k} + \frac{1}{a}\right]^2 (1 - \Theta_k)\right\} \tag{3.182}$$

where

$$\begin{aligned} \theta_1 = \frac{\lambda(2\pi)^{\frac{\nu-1}{2}}}{\eta\chi} \frac{e^{\beta+\frac{1}{2}}}{\sqrt{\beta}} (\sqrt{a+1} - 1)^{\frac{1}{2}} \frac{a^{-\frac{\rho\beta+1}{2}\left(\frac{1}{a^2}+\frac{1}{2}\right)+\frac{1}{4}}}{(a+1)^{\frac{\rho\beta+1}{2}\left(\frac{1}{2}-\frac{1}{a^2}\right)}} \times \\ \exp\left[\frac{\sqrt{a+1}}{3a^2}(2-a) + \frac{\rho\beta}{4a^2}(a-1)^2 + \frac{\beta - \nu + \frac{1}{2}}{a^2} + \frac{2}{3}\right], \end{aligned} \tag{3.183}$$

$$\theta_2 = \frac{\rho\beta+1}{2}\left(\frac{1}{a^2} - \frac{1}{2}\right) + \nu + \frac{1}{4}, \tag{3.184}$$

and

$$\begin{aligned} \Theta_k \approx \frac{4a}{\rho\beta - 4(\beta-\nu)} \left(\sqrt{k} + \frac{1}{a}\right)^{-\frac{1}{2}} - \frac{4(\rho\beta - 2(\beta-\gamma) - \frac{5}{6})}{a(\rho\beta - 4(\beta-\nu))} \left(\sqrt{k} + \frac{1}{a}\right)^{-1} \\ \frac{2(1 - 4/(3a^{3/2}))}{\rho\beta - 4(\beta-\nu)} \left(\sqrt{k} + \frac{1}{a}\right)^{-\frac{3}{2}}. \end{aligned} \tag{3.185}$$

Inverting (3.181) we get

$$\sqrt{k} + \frac{1}{a} \approx \frac{\theta_3}{\tau^{\theta_4}} \tag{3.186}$$

where

$$\theta_3 = \left(\frac{3\beta^\beta \pi_\infty^{-\rho\beta}}{4\eta\chi a^{\rho\beta/2}\Gamma(\beta+1)}\right)^{\frac{2}{\rho\beta - 4(\beta-\nu)}}, \tag{3.187}$$

and

$$\theta_4 = \frac{2\beta + \alpha}{\rho\beta - 4(\beta-\nu)} \tag{3.188}$$

Upon substituting (3.186) into (3.182) we finally get

$$W(\tau) \approx \frac{\theta_1 \tau^{\theta_5}}{\theta_3^{\theta_2}} \exp\left\{ -\left(\frac{\rho\beta}{4} - \beta + \nu \right) \frac{\theta_3^2}{\tau^{2\theta_4}} (1 - \Theta(\tau)) \right\} \tag{3.189}$$

where

$$\theta_5 = \theta_2 \theta_4 + \alpha/2, \tag{3.190}$$

and

$$\begin{aligned} \Theta(\tau) \approx & \frac{4a\theta_3^{-1/2}}{\rho\beta - \beta + \nu} \tau^{\theta_4/2} - \frac{4(\rho\beta - 2(\beta - \gamma) - \frac{5}{6})}{a\theta_3(\rho\beta - 4(\beta - \nu))} \tau^{\theta_4} \\ & \frac{2(1 - 4/(3a^{3/2}))}{\theta_3^{3/2}(\rho\beta - 4(\beta - \nu))} \tau^{3\theta_4/2}. \end{aligned} \tag{3.191}$$

Notice that while the power of the prefactor of the exponential, θ_5 is negative for 2D arrays, it turns positive for 3D arrays.

The transition to the disperse failure mode and the log-normality of the disperse failure mode lifetime weak-linked distribution in 3D can be expected to be identical to that in 2D.

3.8 Conclusion

We have discussed here the failure modes and lifetime distributions of fiber reinforced composites whose fiber lifetimes are random and whose matrix response is viscoelastic. Based on Monte Carlo simulations of small composite unit cells under periodic boundary conditions we find that the failure mode transforms from a model which involves the formation and propagation of a cluster of breaks to one wherein fiber breaks are disperse. This transformation of failure mode occurs as fiber statistical parameters are varied in a manner so as to decrease the hazard ahead of a cluster. The transformation is smooth with the clustered mode under-

going more and more fiber stagger out of the transverse plane before merging with the entirely disperse regime of fiber failure.

Irrespective of the model of failure we expect that when $\varrho = (\rho+1)\beta$ is reasonably large (say more than 4), there will be a weakest link basis to the composite lifetime distribution $H(\tau)$. That is, there will be a critical volume whose failure will signal the rupture of the rest of the composite in arbitrarily small time. If $W(\tau)$ is the lifetime distribution of the critical volume, $H(\tau) = 1 - (1 - W(\tau))^{\hat{m}}$ where $\hat{m}$ is typically larger than the ratio of the composite volume to the critical volume owing to an effective overlap of the critical volumes. The question then is to determine the distribution of the critical volume. As is shown here in the clustered failure mode $W(\tau)$ can be obtained from a simple mode of cluster growth. In the disperse failure mode however, $W(\tau)$ appears to be log-normal at least within the range of our simulations.

Bibliography

[1] Coleman B. D., (1956), Time dependence of mechanical breakdown phenomena, *J. Appl.Phys.*. **27**, 862–866.

[2] Coleman B. D., (1957) A stochastic process model for material breakdown, *Trans. Soc. Rheol.*. **1**, 153–168.

[3] Coleman B. D., (1957) Time dependence of mechanical breakdown of fibers I. Constant total load. *J. Appl. Phys.*. **28**, 1058–1064.

[4] Coleman B.D., (1958) Statistical and time-dependent mechanical breakdown of fibers. *J. Appl. Phys.* . **29**. 968–983.

[5] Coleman B. D., (1958) On the strength of classical fibers and fiber bundles. J. Mech. Phys. Solids **7**. 60–70.

[6] Phoenix S. L., (1978) The asymptotic time to failure of a mechanical system of parallel members. *SIAM J. Appl. Math.*. **34** 227–246.

[7] Ibnabdeljalil M, and Phoenix S. L., (1995) Creep rupture of brittle matrix composites reinforced with time dependent fibers: scalings and Monte Carlo simulations. *J. Mech. Phys. Solids*. **43**, 897–931.

[8] Tierney L., (1980) Limit theorems for the failure time of bundles of fibers under unequal load sharing, Ph.D. Thesis, Cornell University.

[9] Tierney L., (1982) Asymptotic bounds on the time to fatigue failure of bundles of fibers under local load sharing. *Adv. Appl. Probab.*. **56** 95–121.

[10] Phoenix S. L., and Tierney L., (1983) A statistical model for the time dependent failure of unidirectional composite materials under local elastic load-sharing among fibers. *Engng. Fract. Mech.*. **18**, 193–215.

[11] Hedgepeth, J.M., (1961) Stress concentrations in filamentary structures. *NASA TND–882*.

[12] Hedgepeth, J.M. and Van Dyke, P. (1967) Local stress concentrations in imperfect filament composites. *J. Comp. Mater.* **1**, 294–309.

[13] Lagoudas D. C., Hui C-Y, and Phoenix S. L., (1989) Time evolution of overstress profiles near broken fibers in a composite with a viscoelastic matrix. *Int. J. Solids Structures.* **25**, 45–66.

[14] Beyerlein I. J., and Phoenix S. L., (1998) Time evolution of stress redistribution around multiple fiber breaks in a composite with viscous and viscoelastic matrices. *Int J. Solids Structures*. **35**, 3177–3211.

[15] Beyerlein I, J., and Phoenix S. L., (1997a) Statistics of fracture for an elastic notched composite lamina containing Weibull fibers – I: features from Monte Carlo simulation. *Engng. Fract. Mech.*. **57**, 241–265.

[16] Beyerlein I, J., and Phoenix S. L., (1996) Statistics of fracture for an elastic notched composite lamina containing Weibull fibers – II: probability models for crack growth. *Engng. Fract. Mech.*. **57**, 267–299.

[17] Landis C. M., Beyerlein, I.J., and McMeeking R., (1999) Micromechanical simulation of the failure of fiber reinforced composites. *??*. **??**, ??

[18] Wu B. Q., Leath P. L., (2000) Similarity of growing cracks in breakdown of heterogeneous planar surfaces. *Phys. Rev. B*. **62**, 9338

[19] Newman W. I., and Phoenix S. L., (2001) *Phys. Rev. E* **63**, 021507.

[20] Mahesh S., Phoenix S. L., and Beyerlein I. J., Strength distributions and size effects for 2D and 3D composites with Weibull fibers in an elastic matrix. Submitted to *Int. J. Fracture*.

[21] Mahesh S., Beyerlein I. J., and Phoenix S. L., (1999) Size and heterogeneity effects on the strength of fibrous composites. *Physica D: Nonlinear Phenomena*, **133** 371–389

[22] Copson E. T., (1965) Asymptotic Expansions, [Eng.] University Press, Cambridge.

[23] Horn R. A., and Johnson, (1991) Topics in Matrix Analysis, Cambridge University Press, Cambridge.

[24] Curtin W. A., and Scher H., (1997) Time-dependent damage evolution and failure in materials. I. Theory *Phys. Rev. B.*, **55**, 12038–12050.

[25] Curtin W. A., Pamel M., and Scher H., (1997) Time-dependent damage evolution and failure in materials. II. Simulations *Phys. Rev. B.*, **55**, 12051–12061.

[26] Leadbetter M.R., Lindgren G., and Rootzén H., (1983) Extremes and related properties of random sequences and processes. Springer. New York.